/
## Article / Book Information

| ( ) | |
|---|---|
| Title(English) | Study of Ferrite Film Preparation by Facing Targets Sputtering System and Application for Magnetic Disks |
| ( ) | |
| Author(English) | NOBUHIRO MATSUSHITA |
| ( ) | : ( ),<br>: ,<br>: 3233 ,<br>:1998 11 30 ,<br>: ,<br>: |
| Citation(English) | Degree:Doctor of Engineering,<br>Conferring organization: Tokyo Institute of Technology,<br>Report number: 3233 ,<br>Conferred date:1998/11/30,<br>Degree Type:Thesis doctor,<br>Examiner: |
| ( ) | |
| Type(English) | Doctoral Thesis |

# Doctoral Dissertation

# Study of Ferrite Film Preparation by Facing Targets Sputtering System and Application for Magnetic Disks

*Physical Electronics*

*Tokyo Institute of Technology*

## Nobuhiro Matsushita

June 1998

# Study of Ferrite Film Preparation by Facing Targets Sputtering System and Application for Magnetic Disks

## TABLE OF CONTENTS

# Chapter 1

# Overview and Objectives of This Study

After the invention of a sound recording machine *"telegraphone"* after Poulsen[1], the magnetic recording technology has been applied and used everywhere in our life. Sometimes we are using them without being aware of their existence. These days, the development of the data storage system with enormous capacity and high data transfer rate are required for further growing of "Multimedia Society."

Magnetic recording technology has been mainly used as a data storage system for many years, because this technology has several merits superior than those of other technologies. They are non-volatile memory and stable even without outer energy supply, they can achieve extremely high recording density and very high rate random access. Their quite low bit cost is also one of standout merits.

As the amount of information increased, the magnetic recording system had to be developed and there were several innovations in the history of recording media. In the early generation of recording media, needle like particulate magnetic oxides with binder were mainly used as recording layer. However, the amplitude of reproduced signal from recorded bits became smaller with the increase of recording density, and since the sensitivity of head was insufficient at that time, larger remanent magnetization had been required for recording layer. Therefore, the materials of recording layers were changed from oxides to metal alloys, which have larger magnetization.

---

[1] M. Camras: "MAGNETIC RECORDING HANDBOOK," Van Nostrand Reinhold Company, New York, pp.651 (1988)

However, after 1991, the area density of hard disk drive became higher than 1 Gbits/inch$^2$ and the spacing between head and recording layer became quite small of about 50 nm and less. The spacing is getting smaller and smaller year by year, and it would be smaller than 5 nm and finally, head would contact with surface of recording layer in the future. The typical recording layers in rigid disks are Co-Cr-Ta/Cr, and since they are metal alloys with poor chemical stability and low corrosion resistance, the protective layer such as amorphous and/or diamond-like carbon should be deposited on them in addition to the lubricant layer. The thickness of protective layer is about 15 nm in 1997 and its thickness should be also decreased to make the effective spacing between head and recording layer smaller. The development of a recording layer, which is usable even without protective layer, is highly required.

There is a superior candidate applicable as contact type of in-plane recording layer. That is sputtered ferrite film with spinel structure. They have high chemical stability and excellent corrosion resistance. The sputtered Co or Os substituted $\gamma$-Fe$_2$O$_3$ films were investigated and they were applied as recording layer in 1980's[2,3,4,5]. However, their linear recording density was not standout and Co alloy films have been mainly used as recording layers. Since the sensitivity of conventional MIG and thin film type head was not so high at that time, their small remanent magnetization was problem as mentioned before. These days, MR head with extremely high sensitivity are produced commercially and spin valve head with higher sensitivity than that are being developed. As a results of these developments, the requirements for recording layer in recording

---

[2] Y. Ishii et al. : IEEE Trans. Magn., 16[5], pp.646-648 (1980)
[3] K. Tagami, K. Nishimoto, M. Aoyama : IEEE Trans. Magn., 17[6], pp. 3199-3201 (1981)
[4] S. Yoshii et al. : J. Appl. Phys., 53[3], pp. 2556-2560 (1982)

media with ultra high-density is not to be with large magnetization, but to be with low noise level. There is a report that spinel ferrite layer exhibited lower noise than Co-Cr/Cr layer at higher recording density[6].

In addition to noise problem, the appearance of super para-magnetism in recording layer would be crucial problem and should be considered at recording density higher than 10 Gbits/inch$^2$. In longitudinal recording system, since the thickness of recording layer should be decreased at higher recording density for making recorded bit stable to overcome its demagnetizing field. The volume size of recorded bit, therefore, is becoming smaller and smaller with the increase of recording density. It was suggested the application of perpendicular magnetic recording system would be one of superior solutions to these serious problems. As demagnetizing field would be zero at ultimately higher recording density, this system is inherently suitable for high recording density. However, the flux from the bit make small closed loop between neighbored bit one another, the small spacing is necessary to detect their signal at high density. Therefore, the development of a contact type of perpendicular recording layer is also highly required. Ba ferrite film with hexagonal structure seems very suitable for this application, because it has moderately large magnetization and quite large perpendicular anisotropy constant as well as high chemical stability and large corrosion resistance.

As mentioned above, Co ferrite and Ba ferrite films seem to be applicable as contact type of longitudinal and perpendicular magnetic recording layers. Therefore, the deposition of Co ferrite and Ba ferrite films with excellent crystallinity and magnetic

---

[5] O. Ishii et al. : J. Appl. Phys., 61[8], pp. 3825-3828 (1987)
[6] S. Tuboi, T. Korenari, N. Ishiwata, K. Yamada and K. Tagami, J. Mag. Soc. Japan, 18[S1], pp. 95-98 (1994)

characteristics were attempted by using 'damage-free' facing targets sputtering apparatus and their crystallographic and magnetic characteristics as well as the evaluation of their surface smoothness were investigated in this study.

| Chapter 1    Overview and Objectives of This Study |
| --- |

| Chapter 2    Magnetic Recording Systems and Media |
| --- |

| Chapter 3    Preparation Method and Measurements of Specimen Films |
| --- |

| Chapter 4    Co Ferrite Films<br>Chapter 5    Co Ferrite/ZnO Double Layered Films<br>Chapter 6    Co-Zn Ferrite Films |
| --- |

| Chapter 8<br><br>Ba Ferrite/ZnO Double Layered Films |
| --- |

| Chapter 7    Read/Write Characteristics of<br>Co-Zn Ferrite Disks |
| --- |

| Chapter 9    Future Prospects |
| --- |

| Chapter 10    General Conclusions |
| --- |

Fig. 1-1   Out-line of this study.

4

The flowchart of the outline of this thesis is briefly illustrated in Fig. 1-1.

In Chapter 1, i.e. this chapter, the background and overview of this thesis are described.

In Chapter 2, a brief history of recording media and basic theory of longitudinal and perpendicular magnetic recording system are described with short introduction of isotropic recording system.

In Chapter 3, the principle and merits of the 'damage-free' facing targets sputtering system are introduced and they were compared with those of conventional type of another sputtering systems. Measuring methods used in this study are also described in the Chapter 3.

In Chapter 4, the crystallographic and magnetic characteristics of simple Co ferrite films are described. It was also clarified that the oxygen gas pressure $P_{O2}$ affected to the discharge voltage and the deposition rate in reactive sputtering using sintered ferrite targets and gas mixture of Ar and $O_2$.

In Chapter 5, the effects of ZnO underlayer for the epitaxial growth of Co ferrite crystallites and the unique magnetic characteristics of Co ferrite/ZnO film are described.

In Chapter 6, Zn substituted Co ferrite films were deposited and substitution effect for crystallite orientation, magnetic characteristics of the deposited films are described.

In Chapter 7, the read/write characteristics of Co-Zn ferrite disk specimens using a MIG type head and a merged type MR head are described.

In Chapter 8, Ba ferrite films were deposited on ZnO underlayers using Xe mixture gas by changing partial Xe pressure, and the partial Xe pressure dependence of their crystallographic and magnetic characteristics are described for the films deposited from sintered targets with different content. After the optimization of partial Xe pressure, low

substrate temperature deposition of Ba ferrite layers are also described.

In Chapter 9, future prospects of this study which were guided by the obtained results are described

Finally, general conclusions of this thesis are summarized in Chapter 10.

# Chapter 2

# Magnetic Recording Systems and Media

## 2-1 Introduction

Magnetic recording technology is applied and used everywhere in our life and sometimes we are using them without being aware of their existence. There are many applications of them for both professional and consumer level of usage. They are commutation tickets, bankcard, credit card, flexible disk with relatively lower density, and VTR tape and ZIP with relatively higher density, and hard disk drive as data storage system of computers with extremely high density. They are so familiar to us and are used so frequently around us that it is very difficult for us to image our daily life without the existence of magnetic recording technology.

The development of data storage system with enormous capacity and extremely high data transfer rate are required for the arriving "Multimedia Society." Several technologies have been proposed, invented and tried to use as main data storage technology instead of magnetic recording one. They were Bubble memory, magneto-optical disks, flash memory, dynamic random access memory(DRAM), ferroelectric random access memory(FRAM) and so on. However, magnetic recording technology has been mainly used as the storage system for many years, because magnetic recording technology has superior merits than those of other technologies do. They are as follows;

1) Recorded information is non-volatile and stable even without outer energy supply.

2) Possibility of ultra high recording density and enormous capacity of memory storage and extremely high rate random access.

3) Very low bit cost.

It should be noted that magnetic recording system has being developed by not only the improvement of head and recording layer but also that of stable rotation of spin stand, precise servo tracking mechanism, excellent study of tribology between head and media, read/write signal processing with high accuracy and so on. In addition to them, the rapid progress of semiconductors indirectly but greatly contributed to the progress of magnetic recording technology.

In this chapter, longitudinal magnetic recording system which is commonly used in practical applications and perpendicular magnetic recording system which seems to be able to attain recording density higher than 20 Gbits/inch$^2$ will be described briefly. In addition to them, the brief introduction of 'isotropic recording system,' which was proposed by Lemke[1,2] and seems to have potential to attain high density, will be also described.

## 2-2 Brief history of magnetic recording system

All of many applications using magnetic recording system utilize the same basic technology, which has been developed over the last 100 years. The basic style of magnetic recording system is to memorize the analog and digital information signal in recording medium as a size or a direction of magnetization by applying external magnetic field to it, and detect the magnetic flux from it by using sensing element, i.e. called 'head.' This type of magnetic recording system was first proposed by O. Smith in

---

[1] J. U. Lemke: IEEE Trans. Magn., 15, pp.1561 (1979)
[2] J. U. Lemke: J. Appl. Phys., 53, pp.2561 (1982)

1888[3], and invented by Valdemar Poulsen in 1898. The schematic illustration of

"*telegraphone*" invented by Poulsen is shown in Fig. 2-1. It drew a great attention at a

world's fair in Paris in 1900 as 'a most interesting of recent inventions[4]. In this system,

a piano wire winding spirally on dram surface was magnetized partially by using electric

magnet. However, at first, since the magnetic field was applied to a diameter

direction(so we can say it was perpendicular magnetic recording !?) as shown in Fig.

2-2(a), it was difficult to magnetize due to low coercivity and large demagnetizing field.

Then he changed the configuration of poles as shown in Fig. 2-2(b), which looks like a

longitudinal recording system.
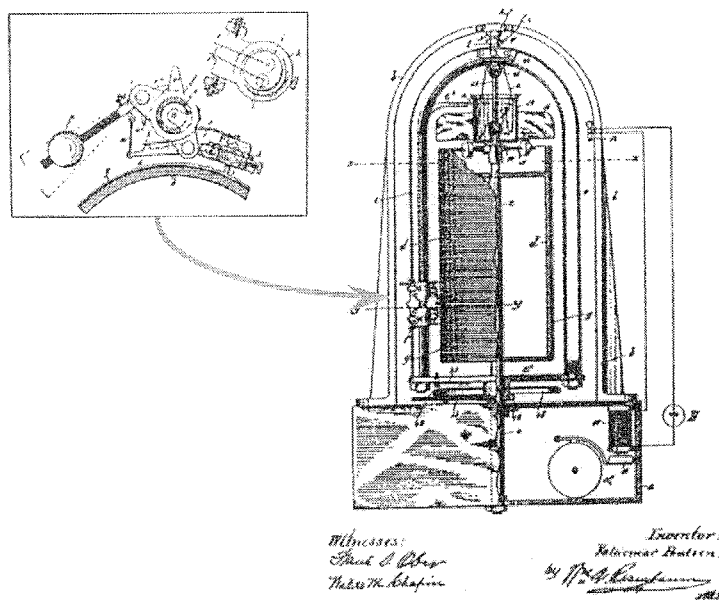
Fig. 2-1   Schematic   illustration   of   sound   recording   machine
"*telegraphone*" invented by Poulsen.

---

[3] O. Smith: "Electric World," pp.116 (1888)
[4] M. Camras: "MAGENTIC RECORDING HANDBOOK," Van Nostrand Reinhold
   Company, New York, pp.651 (1988)

(a)　　　　　　　　　　　　　　　(b)
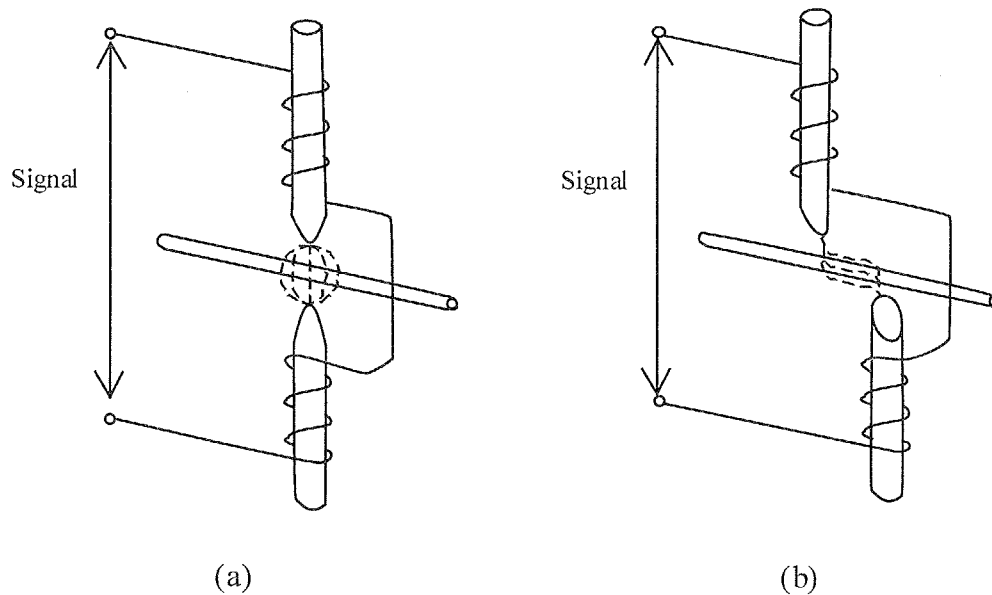
Fig. 2-2　Reconfiguration of recording method in *"telegraphone."*

Finally, he could detect very small signal. After his invention, various improvements have been subjected to magnetic recording system by our seniors to attain higher recording density. Now, it is one of very important key technologies to sustain our life.

Table 2-1 shows the development of magnetic recording technologies. There was drastic progress in magnetic recording technology from the latter part of 1920s to 1940s and the voice information was recorded magnetically. During this term, E. Pfleumer from Germany proposed particulated tape media in 1927 and prepared it in 1936, in which fine particles of iron oxide deposited on plastic film substrate.

At almost the same time, Shüller from Germany proposed and fabricated the ring type head and Prof. Nagai and his group members of Tohoku University proposed and developed the AC bias field recording system.

Table 2-1    Developments of magnetic recording technology.

| Years | Events | Person, Company etc. |
|---|---|---|
| 1888 | Initial idea of magnetic recording (Basic structure of recording tape) | O. Smith |
| 1898 | Invention of magnetic recording machine *"telegraphone"* | V. Poulsen |
| **1900** | | |
| (1906) | Invention of triode vacuum tube | L. de Forest |
| 1907 | DC bias recording method | V. Poulsen et al. |
| **1910** | | |
| (1912) | Amplifier using triode vacuum tube | L. de Forest |
| | Practical use of magnetic recording machine | |
| **1920** | | |
| 1927 | Invention of particulate tape media | F. Pfleumer |
| | Mass production of magnetic recorder | Germany and England |
| **1930** | | |
| 1932 | Invention of ring type head | E. Schüller |
| 1936 | Practical use of particulate paper tape | AEG |
| **1940** | | |
| 1940 | AC biased recording | K. Nagai et al. |
| | Compact magnetic recorder for military use | |
| 1947 | Invention of particulate $\gamma\text{-}Fe_2O_3$ | M. Camras |
| 1948 | Invention of transistor | W. B. Shockley |
| 1949 | Practical application of magnetic tape media | 3M |
| **1950** | | |
| 1953 | Application of tape recorder for external recording machine of calculator | |
| 1954 | Analysis of head field distribution | O. Karlqvist |
| 1956 | Development of VTR | Ampex |
| 1957 | Application of rigid disk for external recording machine of calculator | IBM |
| 1959 | 1 head helical scan system | Toshiba |
| | 2 heads system | JVC |

| 1960 | | |
|------|--------------------------------------------------------------------------|----------------------|
| 1960 | Preparation of metallic powder | F. E. Luorusky et al. |
| 1961 | Idea of multi-turn thin film head | D. P. Gregg |
| 1961 | Co-P, Co-Ni-P thin films using electroplating | J. C. Sallo et al. |
| 1961 | Development of $CrO_2$ powders | T. J. Swobata et al. |
| 1962 | Compact cassette tape | Philips |
| 1964 | Co modified $\gamma$-$Fe_2O_3$ film | D. E. Speliotis et al. |
| 1964 | Multi-track thin film head | J. C. Barton et al. |
| 1965 | Study of magnetic recording media deposited by using obliquely evaporation | D. E. Speliotis et al. |
| | Co-P, Co-Ni-P films using electrode-less plating | J. S. Judge et al. |
| 1967 | Application of $CrO_2$ tape | Du pont |
| 1969 | Multi-turn thin film head | E. P. Valsyn et al. |
| 1970 | | |
| 1971 | MR head | R. P. Hunt |
| 1975 | Co-Cr perpendicular recording film | Iwasaki et al. |
| 1977 | Propose of perpendicular magnetic recording system | Iwasaki et al. |
| 1978 | Practical use of metallic powder tape | 3M |
| 1979 | Computer IBM3370(mounting thin film head) | A. D. Rizzi |
| | Practical usage of Co-Ni evaporated tape | Iizima |
| 1980 | | |
| 1985 | Perpendicular magnetic recording system with linear recording density of 267 kfrpi | M. Watanabe et al. |
| | Detection of signal recorded at 620 kfrpi in perpendicular magnetic recording system | S. Yamamoto et al. |
| 1990 | | |
| 1991 | Attainment of recording density of 1 Gbits/inch$^2$ | IBM |
| 1992 | 2 Gbits/inch$^2$ | Hitachi, Fujitsu |
| 1996 | 3 Gibts/inch$^2$ | IBM |
| 1996 | 5 Gibts/inch$^2$ | Fujitsu |
| 2000 | | |
| 2002? | 20 Gibts/inch$^2$ | *U.S.A. ?　Japan ? The other ?* |
| ???? | 100 Gibts/inch$^2$ and above | *????* |

All of them were very effective to improve the magnetic recording system. The spacing loss was successfully reduced by using flexible substrate and it enabled to decrease the magnetic layer thickness and as a result, the demagnetizing field became smaller. A closed magnetic circuit could be constructed by using a ring type head, and it enabled to "write" and "read" the signal with high efficiency, and AC bias field attained the linearity in read/write process, so that they could be used in analog audio recording systems.

The system established at that time has been a prototype of magnetic recording system and it has not been changed intrinsically for more than 60 years to these days. It should be noted that some important inventions in semiconductor technology, i.e. triode electric tube invented by L.De Forest in 1906 and Transistor by W. B. Shockley et al. in 1948 and so on, contributed to the progress of magnetic recording technology.

After World War II, the magnetic recording system was applied for external memory of computer system and audio-visual recording system. Tape apparatus and rigid disk system were used as external data storage of computer system in 1953 and 1957, respectively. Head technology has also been improved. It was sensational when Ampex(U.S.A) developed four head VTR for broad casting in 1956. Toshiba Corp. and JVC developed one head helical scan system and two heads system, respectively[5,6].

After 1960s, there had been great advancements in technologies to make magnetic powder smaller and to distribute these powder more uniform for recording medium, and those to make gap narrower and to collect leaked flux more efficiently for head.

---

[5] 中川靖造 :"日本の磁気記録開発," ダイヤモンド社, 11 (1984) (in Japanese)
[6] 澤崎憲一 :"電子工学進歩シリーズ 4 VTR," コロナ社 (1971) (in Japanese)

Therefore, areal recording density in commercial products became higher ten times per ten years to the end of 1980s. The increase of areal density had drastically accelerated by the appearance of magneto-resistive (MR) head as shown in Fig. 2-3, and its increase ratio became 100 times per 10 years. Since the increase ratio of areal density increased too fast and its recording density of commercial products would be almost the same that of laboratory level around 1998 as shown in Fig. 2-3 and 'thermal relaxation' seems to be serious problem for longitudinal recording system at higher than 5 Gbits/inch$^2$, several researchers predicted the deceleration of the increase ratio would cause just before 21$^{st}$ century.

However, it has not been clearly observed to date(in June 1998). The technology innovation beyond their prediction was attained by the development of signal processing such as the PRML, servo tracking technology, and the appearance of spin valve head with higher sensitivity than MR head.

The appearance of this type of head with very high sensitivity gave an impact to the researchers and engineers engaged in magnetic recording industry, and it changed the required conditions for the recording layer. In order to attain higher recording density in longitudinal recording system, it is necessary for recording layer to exhibit lower noise level and higher coercivity but not to possess larger magnetization. The transition noise, which increase drastically with increase of recording density is a serious problem for longitudinal recording layer, and it with zero or quite small transition noise level is highly required. In addition to them the availability in a contact type of recording system is necessary because of rapid decrease of the spacing between head and recording layer. This topic will be mentioned again in next section, 2-3 'Magnetic recording media.
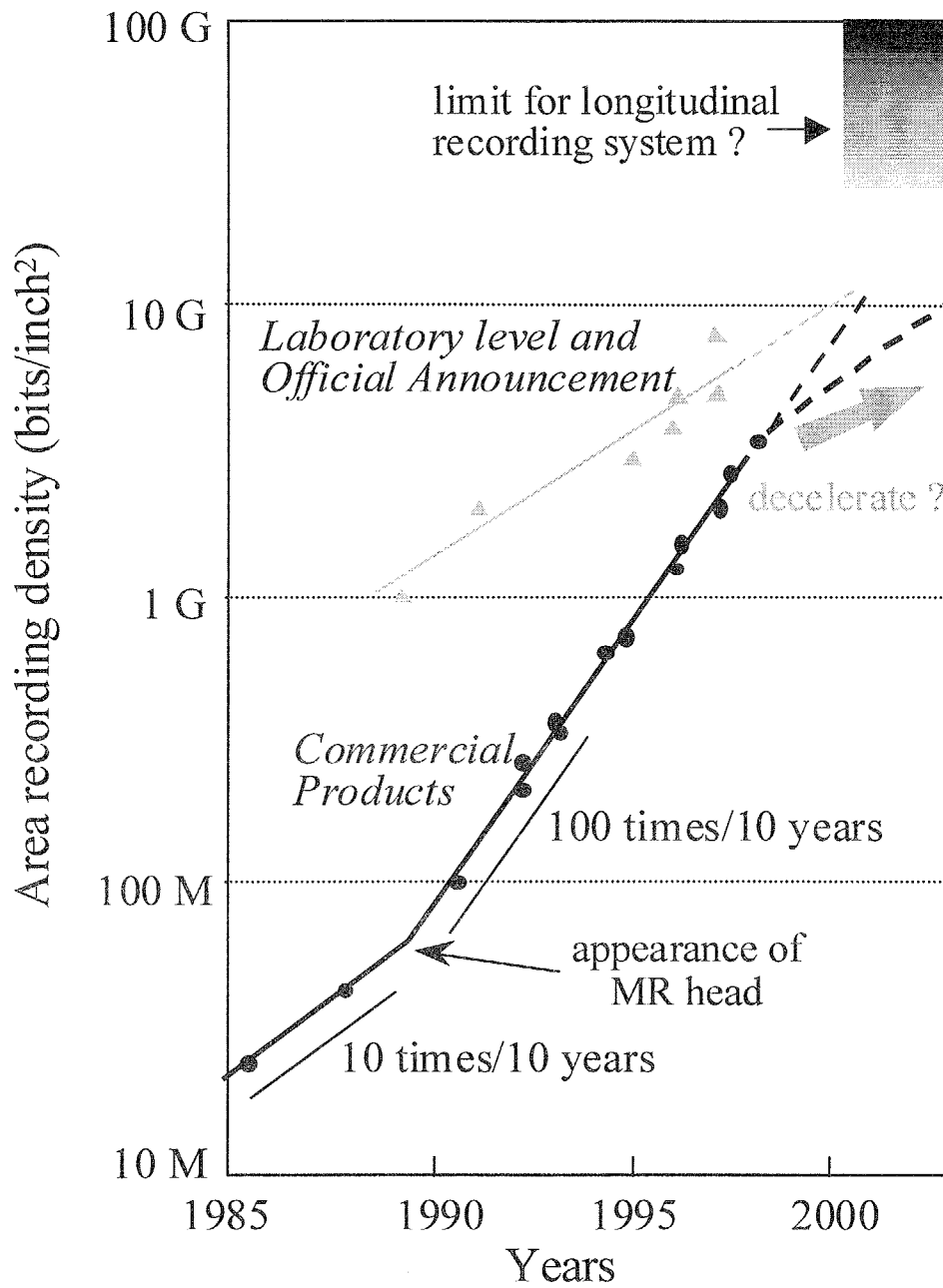
14

Fig. 2-3   Increase of areal recording density year by year.

## 2-3 Magnetic recording media

The recording medium with various type, thickness and magnetic characteristics were shown in Table 2-2. It had been required for recording medium to high S/N ratio for higher recording density and. In other words, to 1980s, it was a history to find a magnetic material with larger remanent magnetization and higher coercivity as shown in Fig. 2-4.

At first, needle like particulate of oxide materials such as $Fe_3O_4$ and $\gamma$-$Fe_2O_3$(1947) were coated with binder in recording layer of tape media. Then $\gamma$-$Fe_2O_3$:Co(1964) and $CrO_2$(1967) were investigated and produced commercially for recording layers of tapes. After a few ten years, the magnetic tapes in which fine Fe alloy powders coated were used instead of oxides tapes. Then metal alloys thin films, such as Co-Cr, Co-Ni-P, deposited by electric plating(1960), evaporation(1964) and sputtering(1972) methods were investigated as recording layer for both tape media and rigid disks. After the latter half of 1980s, Co-Cr based alloy thin films with Cr underlayers, such as Co-Cr/Cr, Co-Cr-Ta/Cr-M and so on, are commercial produced as recording layers in rigid disks.

These days, however, it is clearly recognized that the recording layer, which enables the high recording density at high S/N ratio, should be composed of fine grains.[7] Therefore, they are facing new problem of 'thermal relaxation.' Although the decrease of film thickness $\delta$ and the remanent magnetization $M_r$ should be necessary for longitudinal recording layer as well as the increase of coercivity to achieve higher recording density. It is nonsense to make coercivity higher than head field and the another two conditions are concerned with the decrease of magnetic volume of grain.

---

[7] T. Yogi, T. A. Nguyen : IEEE Trans. Magn., 29, pp.307 (1993)

Table 2-2        Specifications of magnetic recording media.

| Recording Layer | | Application | Thickness (μm) | Remanence $B_r$ (Gauss) | Coercivity $H_c$ (Oe) |
|---|---|---|---|---|---|
| **Particulate media** | $\gamma$-Fe$_2$O$_3$ | Cassette | 4~6 | 1,000~1,500 | 300~380 |
| | // | Tape for calculator | 5~10 | 1,000 | 260~360 |
| | // | Rigid disk | 0.5~1.2 | 500~850 | 300~360 |
| | // | Flexible disk | 2~3 | 700~1,000 | 270~300 |
| | CrO$_2$ | Cassette tape | 4~6 | 1,500~1,600 | 450~550 |
| | // | Video tape | 4~6 | 1.300~1,500 | 600~650 |
| | Co-$\gamma$-Fe$_2$O$_3$ | Cassette tape | 4~6 | 1,450~1,700 | 500~670 |
| | // | Video tape | 4~6 | 1,300~1,500 | 600~650 |
| | Fe | Cassette tape | 2~4 | 2,500~3,500 | 1,000~1,500 |
| | // | Master tape | ? | ? | 1,500~2,000 |
| **Thin film media** | Co-Ni (evaporation) | Cassette tape | 0.3 | 11,000 | 600 |
| | Co-Ni-P (plating) | Rigid disk | 0.05~0.1 | 7,000 ~10,000 | 600~700 |
| | $\gamma$-Fe$_2$O$_3$ (reactive sputtering) | Rigid disk | 0.1~0.2 | 2,500 | 600~700 |
| | Co-Cr-Ta/Cr (sputtering) | Rigid disk | <0.05 | ~400 | ~2,200 |
| | Co-Cr-Pt-Ta/Cr (sputtering) | Rigid disk | <0.05 | ~300 | ~3,000 |
| | Co-Cr-Ta * (sputtering) | Rigid disk | ~0.1 | ~450 | ~2,200 |

* for perpendicular recording system
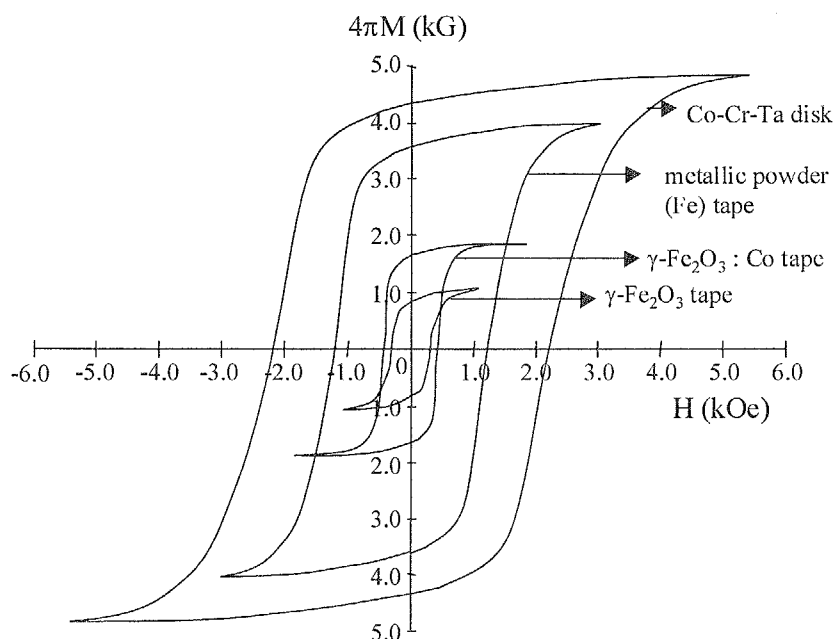
Fig. 2-4   Hysteresis loops of various recording media.

The magnetic domains can not sustain their magnetization stable owing to thermal relaxation when their size become smaller than its critical one, which might be about 10 nm for Co-Cr-Ta alloy film.

The application of the perpendicular recording system would be one of solutions to solve these critical problems for longitudinal recording one as would be mentioned later.

There is another important point to be considered for recording layers with ultra-high density. That is the spacing between head and recording layer. This spacing cause various losses in writing and reading process as would be mentioned in later sections. Therefore, it has been rapidly decreased with the increase of recording density.

Fig. 2-5 shows the decrease of spacing between head and top surface of recording layer. It seems that the spacing will be in the range of 'near-contact' just before 21st century and after that, a perfect contact recording system with the flying height of zero should be achieved as seen in this figure. Although Co-Cr/Cr[8] films are mainly used as the recording layer in rigid disks, the protective layer such as normal and diamond-like carbon is necessary on such alloy films due to poor chemical stability and corrosion resistance. The existence of this layer is a bottleneck to decrease the effective spacing. For example, although flying height of head was only about 25 nm for 5 Gbits/inch$^2$
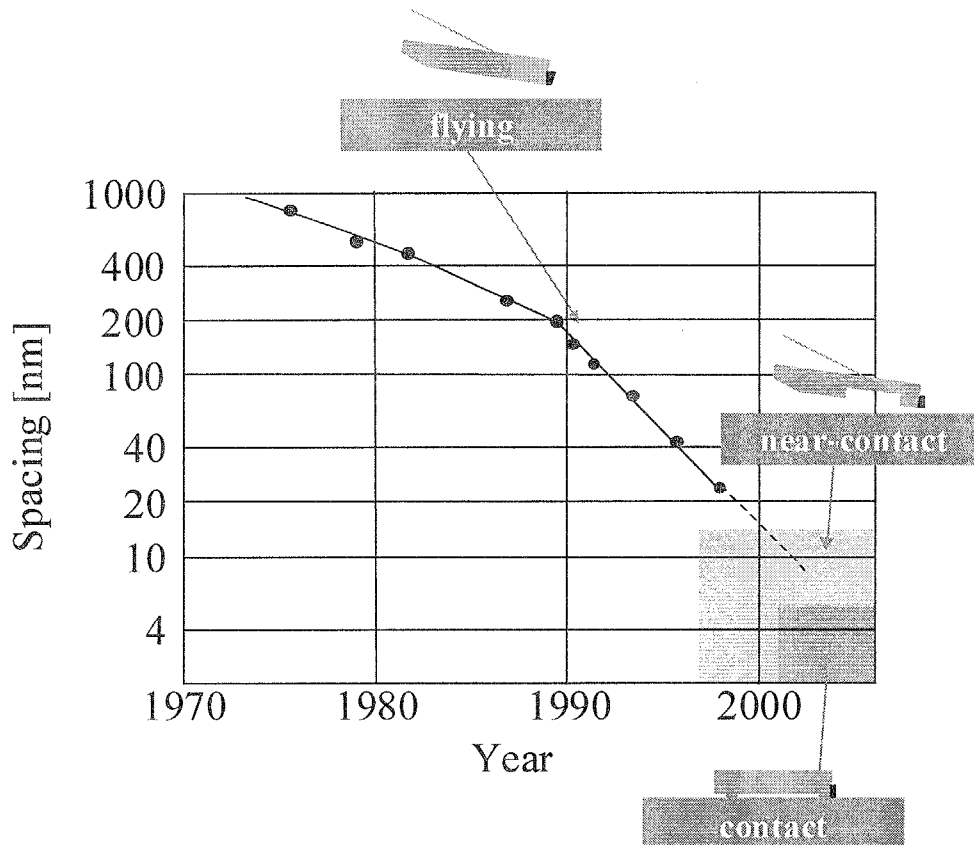


Fig. 2-5 Decrease of spacing year by year.

[8] H.Suzuki, N.Goda, S.Nagaike, Y.Shiroishi, N.Shige and N.Tsumita, IEEE Trans. Magn., 27[6], 4718-4720 (1991)

rigid disks presented by IBM in 1997, the effective spacing was 45 nm due to the existence of protective and lubricant layers.

Therefore, it seems difficult to use Co-Cr alloy film for contact type of recording layer. On the contrary, since the sputtered films of ferrimagnetic oxide such as a spinel type of Co ferrite($CoFe_2O_4$) and a magnetoplumbite type of Ba ferrite($BaFe_{12}O_{19}$) exhibit moderate saturation magnetization $4\pi M_s$ and high coercivity $H_c$ as well as a remarkable chemical stability and high corrosion resistivity, they are also expected as high density recording layer[9,10]. In this thesis therefore, these types of ferrite films with smooth surface were prepared and the read/write characteristics of Co-Zn ferrite disks were investigated later Chapters.

## 2-4 Longitudinal Magnetic Recording System

The recording system commonly used in these days is called "Longitudinal" recording one. The basic writing and reading processes of longitudinal recording system are schematically illustrated in Fig. 2-6(a) and (b), respectively[11]. This system is a combination of a recording medium, which has their magnetic easy axes in in-plane direction and the ring type head, which can produce magnetic field in in-plane direction efficiently between poles. This combination has been the one used traditionally, and is still dominates all major analog and digital applications.

---

[9] H.Torii, E.Fujii and M.Hattori, IEEE Transl. J. Mag. Japan, 6, 765 (1991)
[10] M.Matsuoka, Y.Hoshi, M.Naoe and S.Yamanaka, IEEE Trans. Magn., 18, 1119(1982)
[11] C.D. Mee : "Magnetic Recording Handbook," McGraw-Hill (1990)
  J. C. Mallinson : "The Foundations of Magnetic Recording," Academic Press (1987)

If the magnetic field from head was the square wave with a frequency $f$, and the medium moves with velocity $V$, the recorded pattern can be characterized by the wavelength

$$\lambda = \frac{V}{f} \qquad (2.1)$$

by the bit length $b$

$$b = \frac{\lambda}{2} \qquad (2.2)$$

or by the linear density

$$D = 25.4 \times \frac{2f}{V} \qquad (2.3)$$

measured in flux reversal per inch, i.e. expressed as "frpi" or "FRPI."

Normally the reading process was proceeded by detecting the change of flux which are generate from the remanence in the recording layer by using the electromagnetic induction as shown in Fig. 2-6(b). If this type of head is perfectly contact with the recording layer, and all the available flux $\phi$ could be collected, the voltage induced in a coil with turn number $N$ is expressed as follows.

$$e = -N\frac{d\phi}{dt} = -N\frac{d\phi}{dx} \times \frac{dx}{dt} = -NV\frac{d\phi}{dx} \qquad (2.4)$$

This equation means that the reproduced voltage is proportion to the head coil turn number $N$, relative velocity between head and medium, and the derivative of fulx $\phi$ with respect to position $x$.

**(a) Writing**

Write
Current

Coil

Ring Core

Ring Head

Medium
Motion

Recording
Medium

Track Width

Magnetic
Field

Substrate

Magnetization

Bit Length

**(b) Reading**

Induced
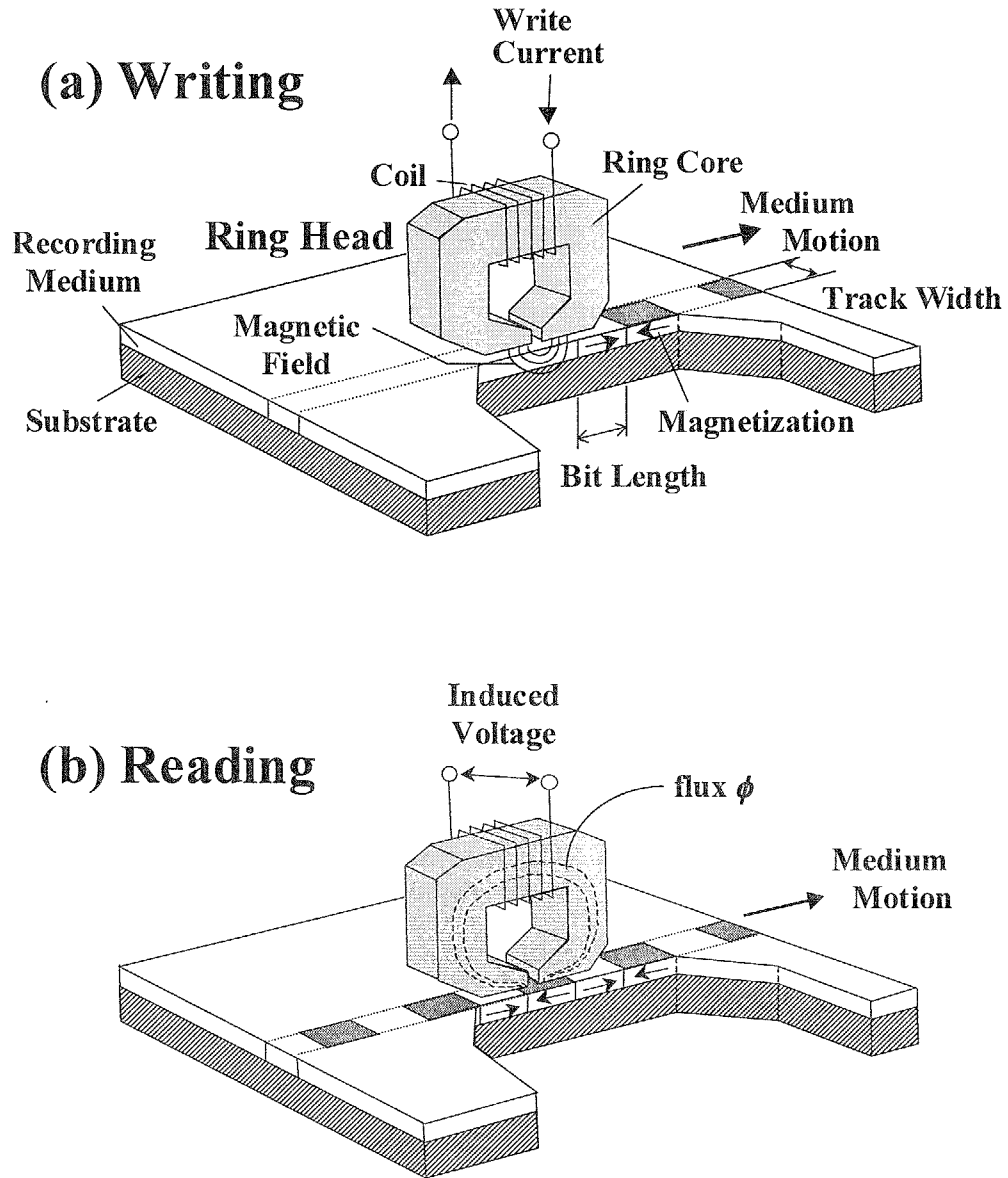Voltage

flux $\phi$

Medium
Motion

Fig. 2-6   Longitudinal recording system using ring type head and recording layer with in-plane anisotropy; (a) writing and (b) reading processes.

Assuming that the total flux in the head coil is constant even for the change of the signal frequency, the reproduced voltage is expressed as

$$e = -N \frac{d\phi}{dt} = 2\pi N B_r W \delta \cos 2\pi f t \qquad (2.5)$$

where $\delta$ is thickness of recording layer, $B_r$ is the remanent magnetization and $W$ is a track width of recorded bit. Finally, the reproduced voltage $e$ is proportional to the frequency $f$, the remanent magnetization $B_r$ and the recording track width $W$.

This equation suggests that the amplitude of reproduced signal becomes small at high density, because the magnetic volume for a recorded bit also becomes small. As a result, it is difficult to detect the signal by using this ring type head. Therefore, a merged type MR heads, which is a combination of a ring type writing head and magneto resistive reading one, are mainly used in rigid disks with high density above 1 Gbits/inch$^2$ after 1996.

This small size of recorded bit causes another problems, which are critical ones for longitudinal recording system. One of them is the increasing of the 'demagnetizing field' in recorded bit.

Recording bit length become smaller with the increase of linear recording density and it causes the increase of the demagnetizing field $H_d$. Fig. 2-7(a) and (b) represent the schematic illustration of the recorded magnetization longitudinally at a low and a high recording density. The bulk of the flux created by the magnetization reversal returns outside the medium, and the demagnetizing field is smaller in Fig. 2-7(a). On the other hand, the recording bit length become smaller and the demagnetizing field $H_d$ and the loss of magnetization associated with it became progressively larger for higher linear recording density as shown in Fig. 2-7(b).

In the plane of the recording layer, the demagnetizing factor at high densities approaches the limiting value $N = 1$, and the value of $H_d$ approaches $-M_0$, where $M_0$ is the value of the demagnetized magnetization at transitions.

In longitudinal recording system, the recorded bits are opposing and are interfered each other. This interference increased wit increase of linear recording density and the demagnetizing field in the recorded bit also drastically increased. In order to decrease the $H_d$, there exists zigzag domain region, in which different magnetic poles are overlapping each other. For attaining high recording density, it is key point to decrease the width of this "zigzag" region, because the transition noise, which causes major noise for longitudinal recording layer, originates from this region. In order to decrease $H_d$, the necessity of higher coercivity and thinner layer thickness for recording layer were pointed by many researchers using their mathematical analysis and simulations as well as experimental results. One of them is a Potter's analysis, which is relatively simple but has relatively better agreement with experimental results.
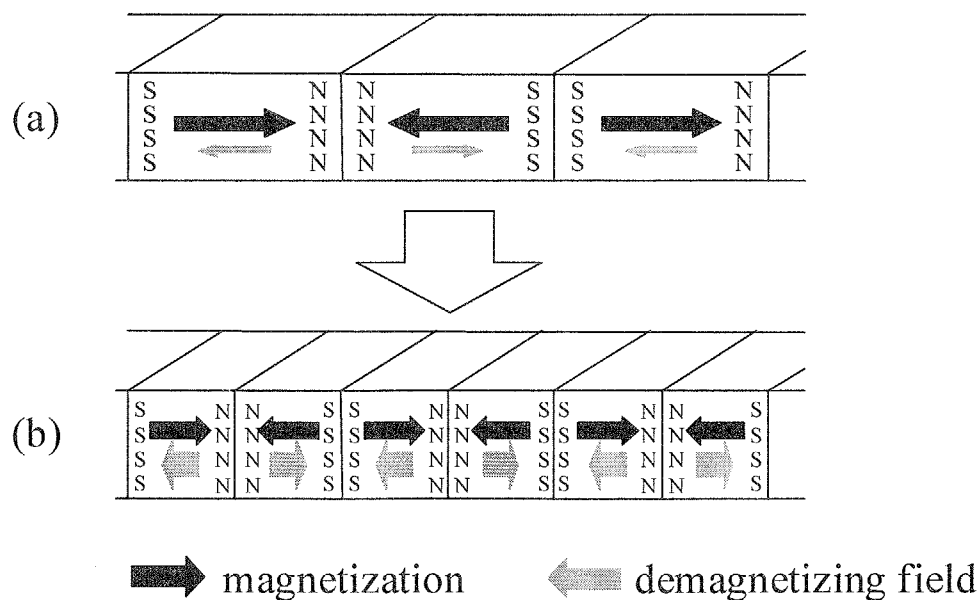


Fig. 2-7  Longitudinally recorded magnetization at (a) a low and (b) a high density.

Magnetized states of longitudinal recording layer are illustrated schematically in Fig. 2-8(a)-(f). Fig. 2-8(a) shows a partial cross section, assuming that there is no magnetization component in $y$ direction, which is correspond to the film thickness direction. Here, $z$ direction, which is perpendicular to this paper, is assumed to be infinite. At first, think about two domain with the saturation magnetization $\pm M_s$ are opposing each other at $x = 0$. There are demagnetizing fields $H_d$ at $x = 0$, where $H_d$ is a function of position $x$ and expressed by $M_s$ and film thickness $\delta$. At $x = 0$, $H_d$ has very large value of $\pm M_r/\mu_0$ ($\pm 4\pi M_r$ in cgs unit) and it much exceeded the value of $H_c$. Since $H_d < H_c$ was necessary for the stability of magnetization, the strength of magnetization should be decreased drastically around $x = 0$. For decreasing $H_d$, so that it would be smaller than $H_c$, zigzag domain structure, which looks like a saw edge, appear between the opposing domains as shown in Fig. 2-8 (d). The strength of magnetization is expressed as an arctangent function of position $x$ as follows[12],

$$M(x) = \frac{2M_r}{\pi} \times \tan^{-1}\left(\frac{x}{a_j}\right) \qquad (2.6)$$

where $a_j$ is a parameter of the gradient of $M(x)$ at $x = 0$ and expresses the transition reverse is constant. From the condition of $H_d < H_c$, transition reverse constant $a_j$ is to be

$$a_j = \frac{1}{2\pi} \times \frac{\delta M_r}{H_c} \qquad (2.7)$$

---

[12] 西川正明: "磁気記録の理論," 朝倉出版, pp.138 (1987) (in Japanese)

(a)

(d)

(b)

(e)

(c)

(f)

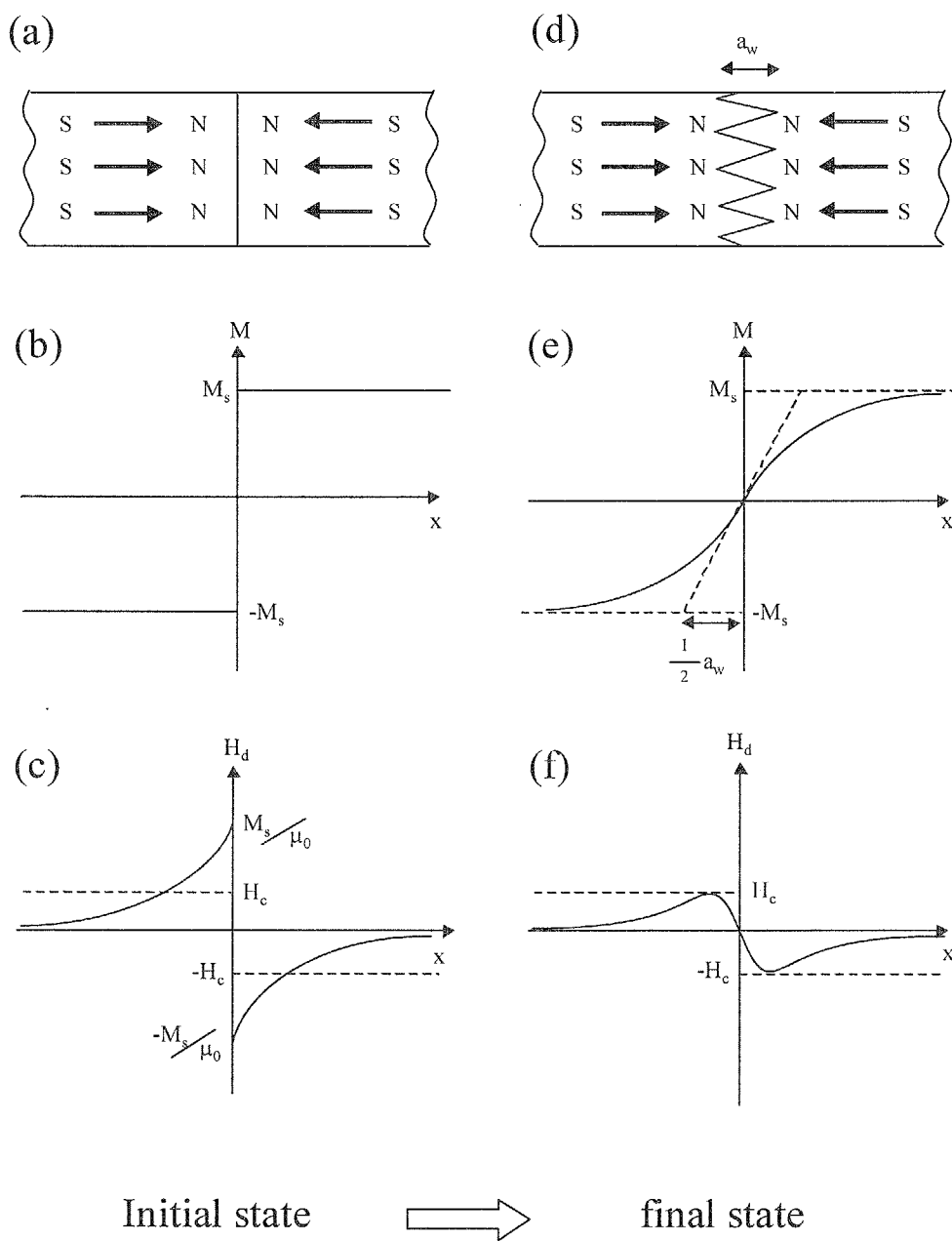Initial state $\Longrightarrow$ final state

Fig. 2-8   Schematic illustration of magnetization state of longitudinal recording media.

Substituting the relationship between the transition reverse constant $a_j$ and transition length $a_w$ of

$$a_w = \pi \times a_j \qquad\qquad (2.8)$$

to (2.7) and therefore, the transition length $a_w$ is expressed as

$$a_w = \frac{1}{2} \times \frac{\delta M_r}{H_c} \qquad\qquad (2.9)$$

Since smaller $a_w$ attributes to higher recording density, the conditions required for recording layer with higher density are 1)smaller recording layer thickness, 2)smaller remanent magnetization and 3)higher coercivity.

Here, it should be considered that it was assumed in this calculation that the head gap is perfectly contact with recording layer so that spacing loss would be zero.

Actually, they had been important guidelines for the recording media used commonly in conventional rigid disks, tapes and floppies. However, in the actual magnetic recording process, there is wide distribution of recorded magnetization in medium due to the head gap and spacing between head and recording layer. Since this makes transition length $a_w$ wider, the real value of $a_w$ becomes larger than that of Potter's approximation. A more strict solution can be obtained by considering coercivity squareness $S^*$ and head field distribution. There is a model of William-Comstock's equation, which has better agreement with actual recorded magnetization pattern and Talke-Tseng's equation, which is modified to recording media with large thickness. For example, it was reported that the calculated $a_w$ by William-Comstock's equation is a

few times larger than that calculated by Potter's equation[13]. From these calculations, it supposed to be clear that the head field distribution caused by the spacing with just only 0.1 μm and below is very effective for the transition length.

There is another way to calculate the reasonable recording density of recording layer, which is independent of reproduce conditions. They can be evaluated by $B_{n,max}$, which is the largest magnetic flux density generated on the recording layer surface just recorded at low density, and $D_{50}$, which is the linear recording density at which the output falls down to 50 %. From the experimental approximation in metallic powder, $\gamma$-Fe$_2$O$_3$ and Co-Ni thin film tape media, they are expressed as follows[14].

$$B_{n,\max} \propto E_p \propto \left(\delta M_r H_c\right)^{0.5} \qquad\qquad (2.10)$$

$$D_{50} \propto \frac{1}{W_{50}} \propto \left(\frac{\delta M_r}{H_c}\right)^{-0.5} \qquad\qquad (2.11)$$

where $E_p$ and $W_{50}$ are the peak value of reproduced wave form and the full width at half maximum of isolated wave form, respectively. There are a lot of another experimental data concerning on $E_p$ and $W_{50}$, where $\delta$ distributed in a wide range from 0.15 to 0.85, and it was recognized that these values significantly depend on each experimental conditions.

Recently, computational simulation for the approximation of these parameters have been actively investigated[15], and in this paper $B_{n,max}$ and $D_{50}$ are expressed as equation (2.12) and (2.13), respectively and their dependence on magnetic characteristics and

[13] 吉田和悦: 東京工業大学学位論文, pp.5-13 (1989) (in Japanese)
[14] 横山克哉: "磁気記録工学入門," 総合電子出版社, pp.346 (1980) (in Japanese)
[15] Y. Nakamura et al.: IEEE Trans. Magn., 25, pp.4159 (1989)

thickness of longitudinal recording media are shown in Fig. 2-9(a) and (b), respectively. They have good agreement with experimental results reported previously[16,17,18].

$$B_{n,\max} \propto \left( \delta M_r H_c \right)^{0.6} \qquad\qquad (2.12)$$

$$D_{50} \propto \left( \frac{\delta M_r}{H_c} \right)^{-0.4} \qquad\qquad (2.13)$$

Combining equation (2.12) and (2.13), we can obtain equation (2.14) as follows,

$$B_{n,\max} \cdot D_{50} \propto \left( \delta M_r \right)^{0.2} \left( H_c \right)^{1.0} \qquad\qquad (2.14)$$

Finally, from this equation, the required conditions for a recording layer with high density are listed as follows;

　　　1) smaller recording layer thickness

　　　2) smaller remanent magnetization

　　　3) higher coercivity

It is clear that the increase of coercivity, condition 3), is the most effective for attaining higher recording density, while too high coercivity is not practical because of magnetic head saturation. Although 1) and 2) are effective to decrease the demagnetizing field effects, they cause the decrease of reproduced signal and therefore, signal detection will become difficult with the increase of recording density. In addition to them, if both of head field distribution and coercive force distribution in recording layer could be narrower, higher recording density would be attained.

---

[16] 横山克哉: "磁気記録技術入門," 総合電子出版社, pp.345 (1980) (in Japanese)
[17] 岩崎俊一 : "高度磁気記録," 電子情報通信学会誌, 52, pp.1241 (1969) (in Japanese)
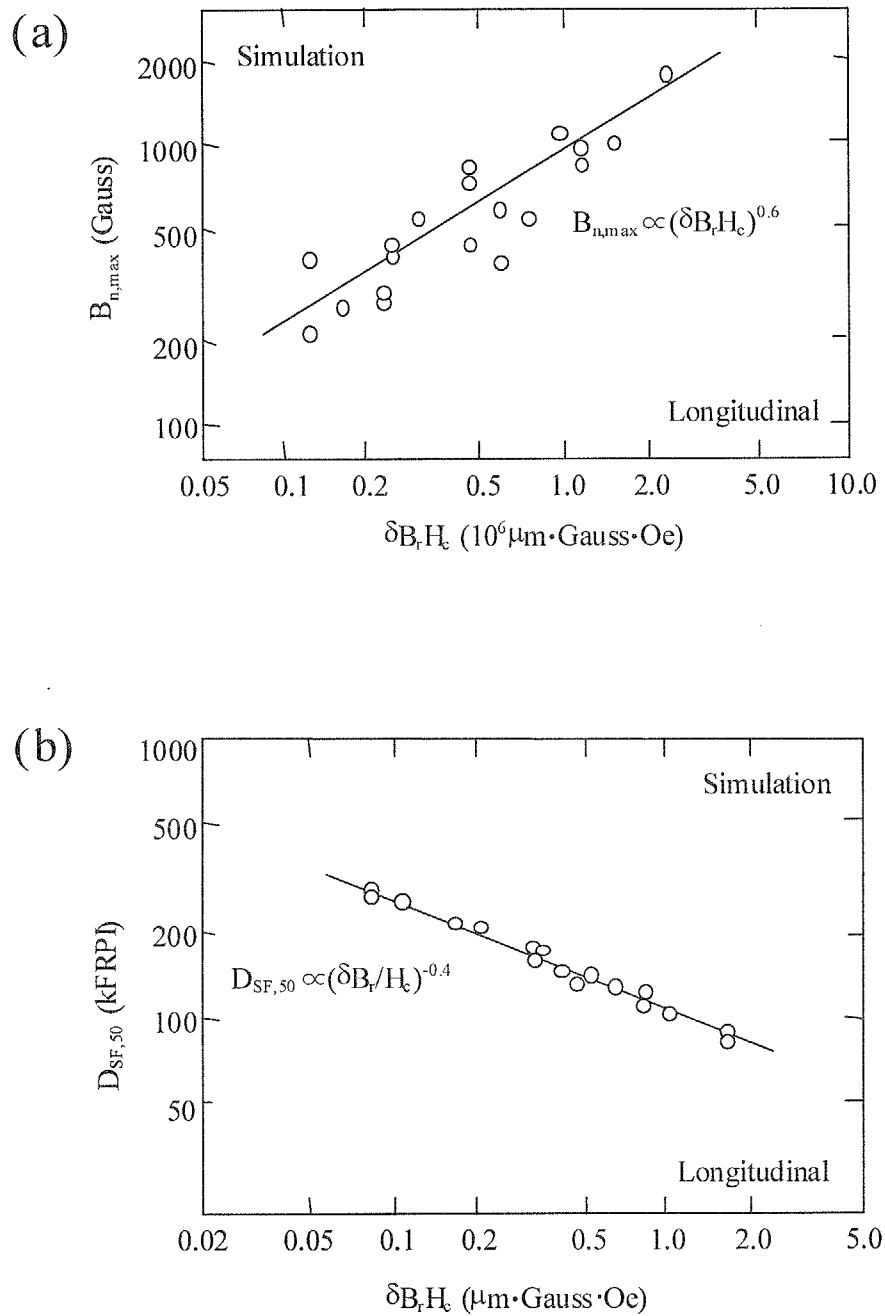[18] D. E. Speliotis et al.: IEEE Trans. Magn., 1, pp.348 (1965)

Fig. 2-9   Dependences   of   (a)$B_{n,max}$   and   (b)$D_{50}$   on   magnetic characteristics   and   thicknesses   of   longitudinal   recording media.

It is easy to attain very high linear recording density of 425 kfrpi in the calculation even for the particulate recording media, which corresponds to 17,000 bits/mm, i.e. the bit length smaller than 60 nm. However, small layer thickness of 10 nm and high coercivity of about 3 kOe are necessary and fine magnetic particles with the same size and shape have to be aligned in order and densely in in-plane direction. It is not so easy to realize such a high recording density because magnetic characteristics of each grains are degraded for the grain smaller than 10 nm in diameter, and the head which can generate the field several times as high as the medium coercivity of 3 kOe are necessary. Even if high linear density recording were attained, the reproduced voltage become small at high recording density and various losses on read-out process make it further smaller. Therefore, the practical reproduced voltage and recording density become much smaller than those of inherent values of recording media. Since protective layer is necessary on Co-Cr alloy recording layer, which is mainly used as recording one, it is a bottleneck to decrease the effective spacing. Therefore, smaller head-media spacing and higher sensitivity of head are conditions necessary for attaining ultra-high linear density. The developments of media with low noise, MR head with high sensitivity and signal process, which can sustain low error late even at low S/N, are enthusiastically investigating by many researchers to achieve ultra-high density above 5 Gbits/inch$^2$.

## 2-5 Perpendicular Magnetic Recording System

The first recording system that Poulsen attempted was a perpendicular recording one. Since the recorded bit length in those days was much larger than that of the present day, the demagnetizing filed in perpendicular direction was larger than that in in-plane

direction and it was difficult to magnetized the recording layer in perpendicular direction as mentioned in 2.2. Therefore longitudinal magnetic recording system has been used for about 100 years in real application and has been improved to adapt for the requirement of higher recording density. However, the improvement of longitudinal recording system has an intrinsic limitation due to its 'self-demagnetization' as well as thermal relaxation at higher than 20 Gbits/inch$^2$. Although these problems are serious for longitudinal recording media, it will not be so serious for the perpendicular magnetic recording system.

In perpendicular recording system, the demagnetization conditions in the central plane of the medium are perfectly different from that in longitudinal recording system.

Fig. 2-10(a) and (b) represent the schematic illustration of perpendicularly recorded magnetization at a low and a high recording density. At the low density in (a), the demagnetizing factor in the perpendicular direction approaches the maximum value $N = 1.0$, corresponding to $H_d = -M_0$. At a high density, as shown in (b), the demagnetization factor and the demagnetizing field approach zero. From this central-plane analysis, it seems that perpendicular recording system is in the ideal mode for high density recording.

The demagnetizing field, occurred in the ferromagnetic thin film perpendicularly to the film plane, is

$$H_d = \frac{M_r}{\mu_0} \qquad (2.15)$$

and the anisotropy energy per unit volume is

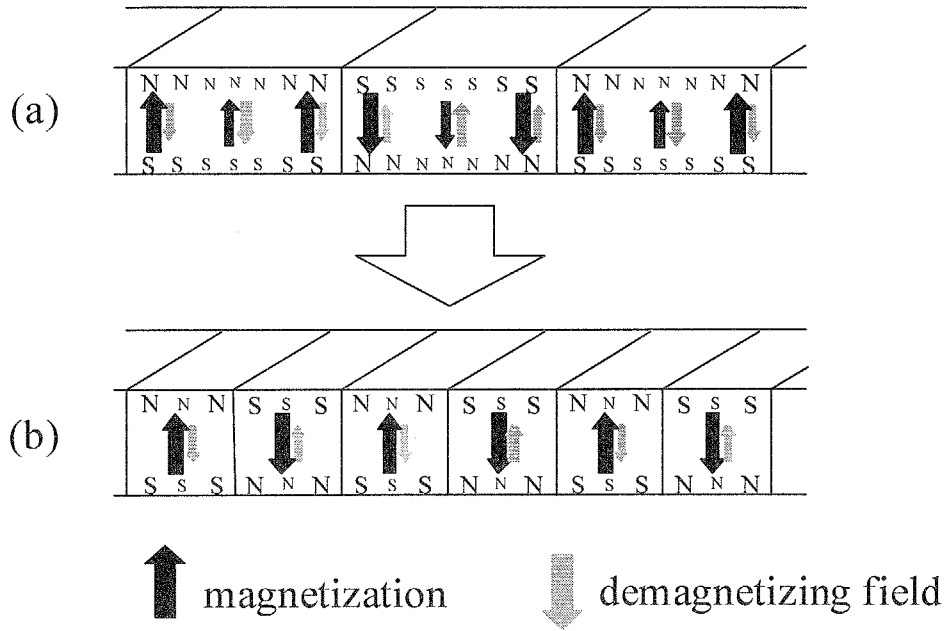$$H_d \times \frac{M_r}{2} = \frac{M_r^2}{2\mu_0} \qquad (2.16)$$

32

**magnetization**    **demagnetizing field**

Fig. 2-10  Perpendicularly recorded magnetization at (a) a low and (b) a high density.

therefore, that per unit area is

$$U_a = \frac{\delta M_r^{\,2}}{2\mu_0} \tag{2.17}$$

On the other hand, the anisotropy energy of the media with magnetocrystalline anisotropy $K_u$ is

$$U_c = \delta \times K_u \tag{2.18}$$

Using (2.17) and (2.18), the basic conditions required for perpendicular recording layer is

$$K_u > \frac{M_r^{\,2}}{2\mu_0} \tag{2.19}$$

Unfortunately, there are not so many kinds of magnetic materials which can satisfy the condition (2.19). Some of them are Co based alloy which are alloyed with Cr, Mo, W, Ru, V and so on. The most representative one is Co-Cr and it was proposed in 1978 by Professor Iwasaki and his stuffs of Research Institute of Electrical Communication of Tohoku

University[19]. They possess h.c.p. structure and magnetic easy axis corresponds to its c-axis. The thin film of Fe-Cr[20], Fe-Ti[21], Fe-Zr[22, 23], Fe:N[24] are also possess perpendicular anisotropy.

Since Ba ferrite film with h.c.p. structure possess very large magnetocrystalline anisotropy field perpendicular to film plane as well as excellent chemical stability and high corrosion resistance[25,26], they are one of promising candidates as contact type of perpendicular magnetic recording layer with ultra-high density. However, high substrate temperature about 600°C was the neck point for the application as recording media. In this study, the low substrate temperature deposition of Ba ferrite film was investigated and would be mentioned in Chapter 8.

The magnetization state of perpendicular recording media is schematically illustrated in Fig. 2-11(a)-(f). Think about the two domains with magnetization $\pm M_r$ whose magnetization vector are directed perpendicular to film plane and reversed at position $x$ = $0$ as shown in Fig. 2-11(a) and (b). The clear difference between longitudinal recording layers and perpendicular one is the distribution of demagnetizing field $H_d$. $H_d$ is zero at $x = 0$ and it decrease gradually with the increase of x for perpendicular recording layer as shown in Fig. 2-11(c), while $H_d$ took the maximum value at $x = 0$ for longitudinal recording layer as shown in Fig. 2-8(c).

[19] S. Iwasaki and K. Ouchi : IEEE Trans. Magn., MAG-14, pp.849 (1978)
[20] Saiki et al. : J Magn. Soc. Jpn, 9, pp.61-64 (1985)
[21] H. Tamai et al.: IEEE Trans. Magn., 23, pp.2737-2739 (1987)
[22] S. Nakagawa, H. Tanaka, M. Naoe : J. Magn. Soc. Japan, 15, pp.605-608 (1991)
[23] S. Nakagawa, H. Tanaka, M. Naoe : J. Appl. Phys., 69[8], pp.5181-5183 (1991)
[24] S. Takahashi, D. Kishimoto, T. Tsujioka, M. Kume and K. Matsuura: J. Magn. Soc. Jpn., 13[S1], pp.829-832 (1989)
[25] M. Matsuoka, Y. Hoshi, M. Naoe and S. Yamanaka : IEEE Trans. on Magn., MAG-18[6], pp. 1119-1122 (1982)
[26] M. Matsuoka, Y. Hoshi and M. Naoe : J. Appl. Phys., 57[8], pp.4040-4042 (1985)

(a)

(d)

(b)

(e)
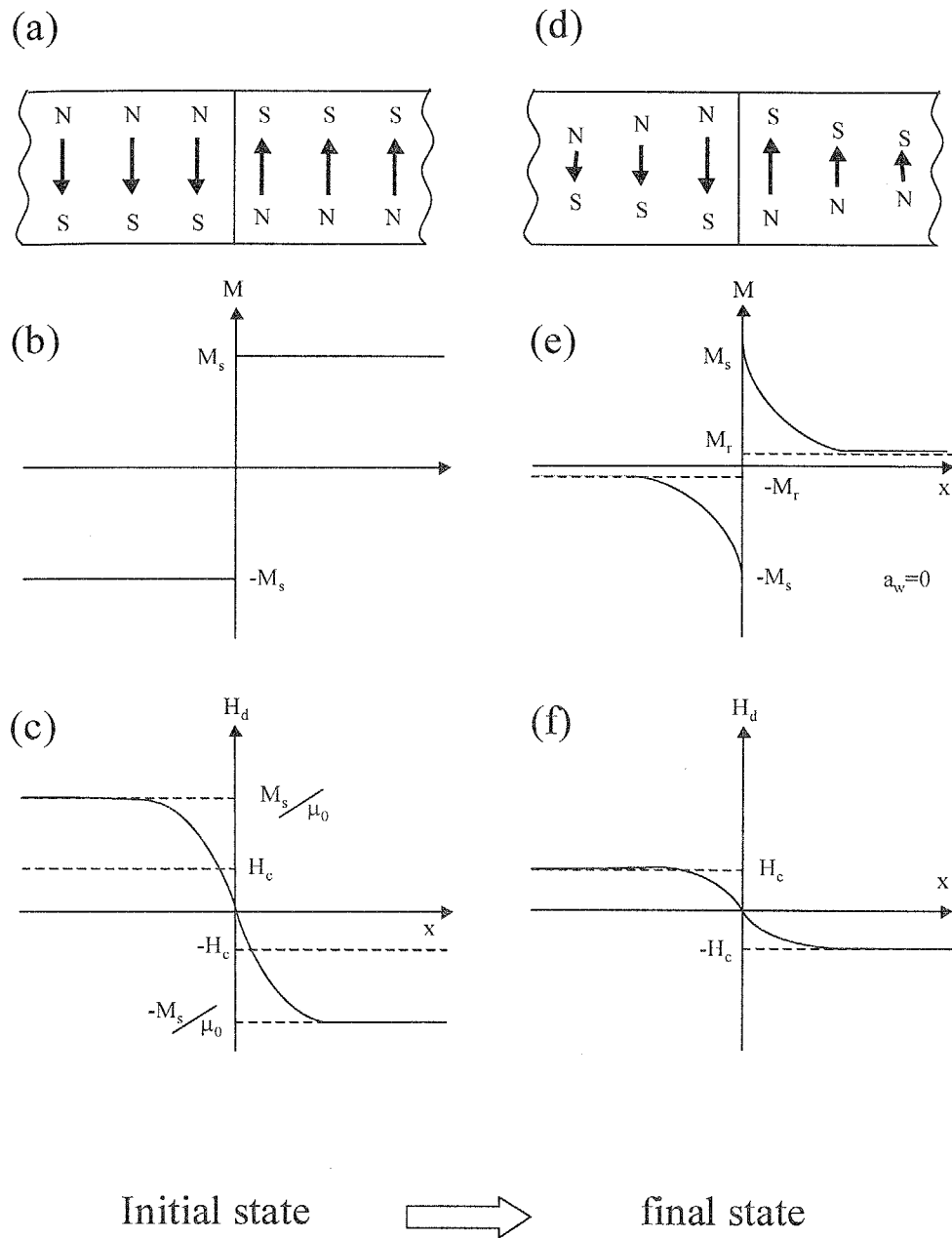
(c)

(f)

Initial state $\Longrightarrow$ final state

Fig. 2-11 Schematic illustration of magnetization state of perpendicular recording media.

Here $H_d$ is expressed as a function of position $x$ using remanence $M_r$ and film thickness $\delta$. There would be magnetic reversal if $H_d > H_c$ and so that $H_d > H_c$ was condition necessary for the stability of magnetization. The magnetizations which are opposing at boundary are emphasized each other. The distribution of magnetization and demagnetizing field are schematically illustrated in Fig. 2-11(d), (e) and (f). The transition length $a_w$ of perpendicular recording media is theoretically 0, while that of longitudinal recording media increases with the increase of recording density. Assuming the ideal conditions in which the loss of head field gradient is zero, the demagnetizing field of perpendicular recording medium is smaller than that of longitudinal magnetic recording medium at high density recording in which wave length $\lambda$ is shorter than $3.94 \times \delta$. Therefore, at enough high recording density, recording layer possess their saturation magnetization $\pm M_s$ that is larger than $\pm M_r$ measured in B-H hysteresis loop. From this simple analysis it is suggested that infinitesimal recording domain can exist in perpendicular magnetic recording layer and its recording limit is independent of $M_s$, $H_c$ and $\delta$ which are closely related to the recording limitation of longitudinal recording system in this assumption.

Perpendicular recording medium seems to attain high recording density above 20 Gbits/inch$^2$, in which one bit will be recorded in 56 nm(Bit size)$\times 0.56$ μm(Track pitch). However, it is not easy to attain such high recording density, because, the transition length $a_w$ is not really zero and the decrease of bit size cause the instability of recorded magnetization.

Professor Nakamura and his group members investigated the computed analysis of perpendicular magnetic recording system[27], in which the approximated magnetization is

---

[27] I. Tagawa and Y. Nakamura : J. Magn. Soc. Jpn., 13[S1], pp.97 (1989)

calculated each time considering their self-consistent conditions[28]. In their calculation Co-Cr/Fe-Ni doublelayered medium and single pole head were used. They reported that the ability of recording media which is independent of reproduce conditions can be evaluated by the maximum surface magnetic flux density generated on the recording layer surface just recorded at low density and the linear recording density at which the output falls 50%, $D_{50}$ are expressed as follows;

$$B_{n,\text{max}} \propto \left(H_c^2 \delta H_c\right)^{0.55} \tag{2.20}$$

$$D_{50} \propto \left(\frac{\delta \sigma_{hc}}{M_s}\right)^{-0.55} \tag{2.21}$$

where $\sigma_{hc}$ is the standard deviation in the distribution of coercive force and expressed as follows;

$$\sigma_{hc} = \frac{\Delta H_c}{1.35k} \times \frac{H_k}{H_c} \tag{2.22}$$

where $H_k$ is anisotropy field measured for bulk film and k is coefficient number of distribution of oriented magnetization. Smaller $\Delta H_c/H_c$ means the closer coercivity squareness $S^*$ to 1.0 and smaller full width at half maximum of switching field distribution SFD. The $\sigma_{hc}$ is strongly correlated with the crystallinity of crystalline-particles of a Co-Cr layer, that is the peak intensity of X-ray diffraction pattern measured for hcp(002), and it can be also simply estimated from hysteresis loops of media[29].

Their dependence on magnetic characteristics and thickness of perpendicularly oriented media are shown in Fig. 2-12.

---

[28]   横山克哉: "磁気記録技術入門," 総合電子出版社, pp.68-70 (1980) (in Japanese)

(a)

Simulation

$B_{n,max} \propto (\delta H_c^2 / \sigma_{hc})^{0.55}$

Perpendicular

$\delta H_c^2 / \sigma_{hc}$ ($10^3 \mu m \cdot Oe$)

(b)

Simulation

$D_{SF,50} \propto (\delta \cdot \sigma_{hc} / B_s)^{-0.55}$

Perpendicular

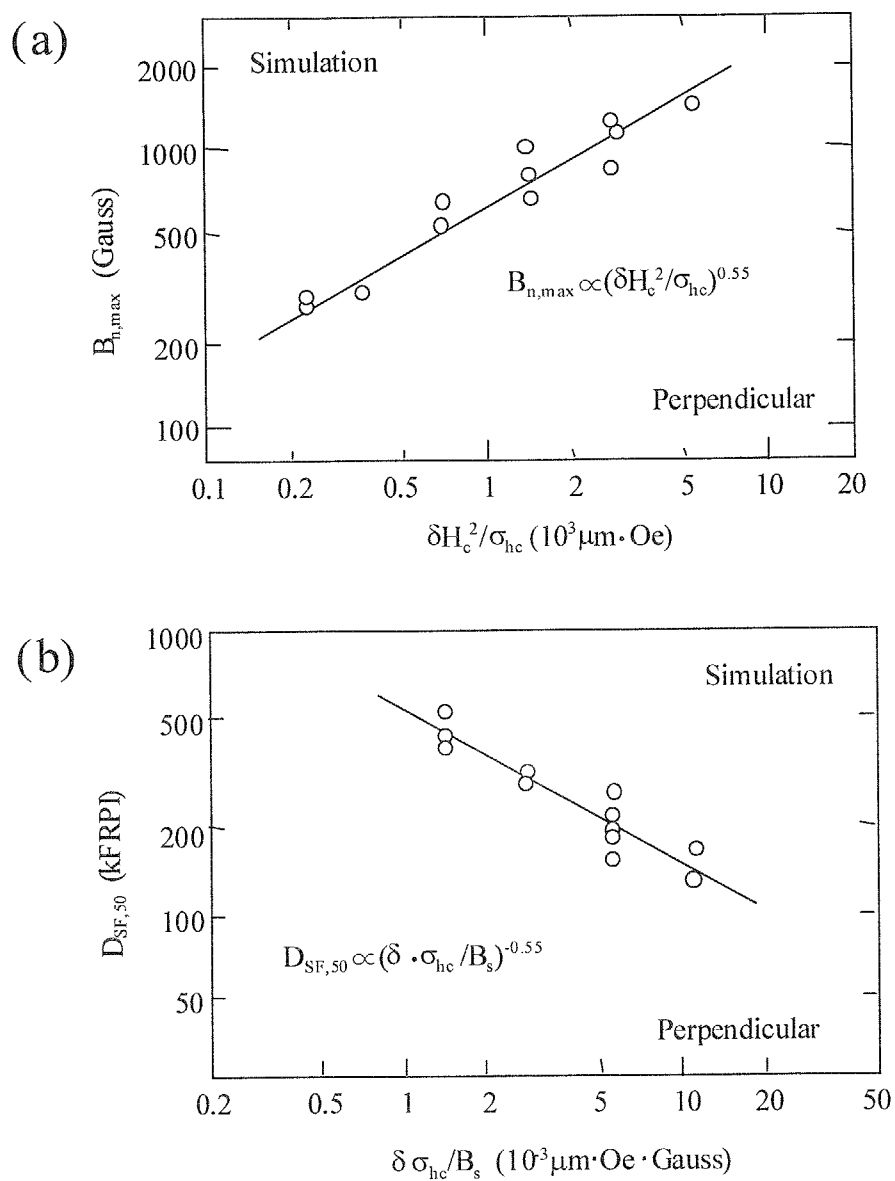$\delta \sigma_{hc} / B_s$ ($10^{-3} \mu m \cdot Oe \cdot Gauss$)

Fig. 2-12 Dependences of (a)$B_{n,max}$ and (b)$D_{50}$ on magnetic characteristics and thicknesses of perpendicular recording media.

[29] I. Tagawa and Y. Nakamura : J. Magn. Soc. Jpn., 15, pp.155 (1991)

Increasing coercivity $H_c$ measured in the direction perpendicular to the surface increases the surface flux density $B_{n,max}$ after recording, but it has no effect on the linear recording bit density $D_{50}$. On the other hand,, narrowing the standard deviation $\sigma_{hc}$ in the distribution of coercivity of crystalline-particles dominantly achieve both $B_{n,max}$ and $D_{50}$ instead of $H_c$. This point should be recognized for the conditions of the perpendicular recording layer with high density.

Moreover, it is also important for perpendicular magnetic recording layer to be applied magnetic field perpendicular to its film plane. Professor Nakamura of Tohoku University confirmed that a recording layer with perpendicular magnetic anisotropy was mainly magnetized perpendicularly by perpendicular field component even if a ring type head was used, perpendicular component of a ring head field is considerably weak as compared with the in-plane one[30]. Therefore, the recording layer was hard to magnetize through the whole thickness as compared with longitudinal recording one in spite of the same recording level. To generate the field perpendicularly to the film plane, various type of single pole type(SPT) heads were proposed and attempted in laboratory level. They were auxiliary-pole driven type SPT head, main-pole driven type one and that with soft underlayers. Theses days, although a main-pole excited type SPT head with soft ferrite side pole is a superior candidate that with ultra high density, further studies and experiments are necessary to be applied practically.

Therefore, it is one of solutions for attaining high density to develop a recording layer, which can utilize the magnetic field generated from conventional type of ring head. In this thesis therefore, spinel type of Co-Zn ferrite disks with isotropic orientation of

magnetization and moderate magnetic characteristics were deposited and their read/write characteristics were investigated in *Chapter 7*.

It should be also noticed that small spacing is necessary even for perpendicular recording system. Fig. 2-13 shows the schematic illustration of small flying height of perpendicular recording system(in case of double-layered film). The leaked flux from recorded bit is closed just around recording layer surface in this case, a small flying height compared with longitudinal system is necessary to detect recorded signal as shown in Fig. 2-13. Since the protective layer, such as diamond-like carbon, about 15 nm thick will be necessary at least for Co-Cr-Ta layer, the flying height of head will have to be about 15 nm to decrease the effective spacing down to 30 nm, which would be necessary at areal density of 10 Gbits/inch$^2$. As mentioned above, the decrease of
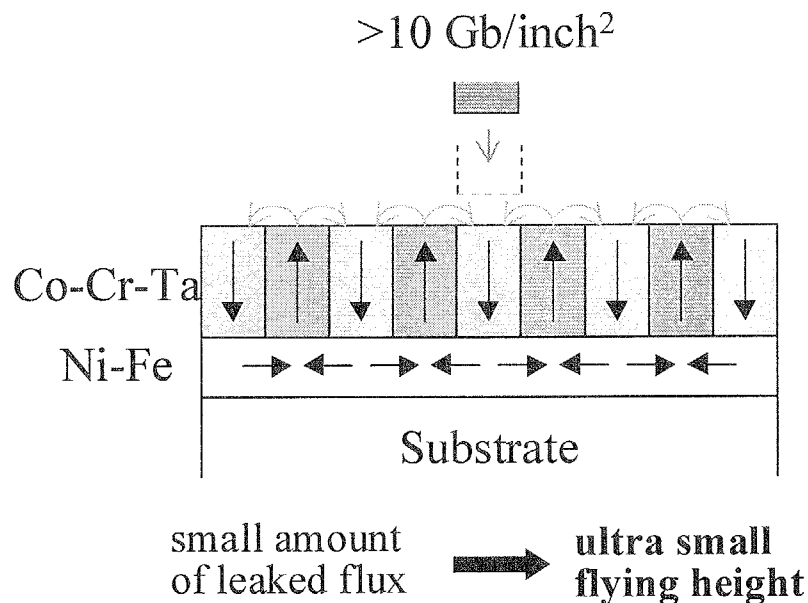


Fig. 2-13    Necessity of small flying height for perpendicular recording system. (in case of double layers)

[30] Y. Nakamura : J. Magn. Soc. Jpn., 13[S1], pp.33-42 (1989)

spacing between head and recording layer will be problem for the perpendicular recording system at ultra-high density, and the development of the contact type of perpendicular recording layer are highly required. In this thesis therefore, Ba ferrite films with excellent perpendicular anisotropy and moderate magnetic characteristics were deposited by the facing targets sputtering system and the low substrate temperature process for it was attempted by using Xe mixture in *Chapter 8*.

## 2-6 Isotropic Magnetic Recording System

This system was proposed by Lemke and he reported that high linear recording density up to 120 kfrpi was possible by using recording medium without anisotropy, i.e. isotropic orientation of magnetization, and a ring type head with narrow gas width of 0.2 $\mu m$[31]. In this media, large perpendicular anisotropy contributed such a high recording density and it could be increased by changing the aspect ratio of aciculated particles. He succeeded to achieve an extremely high linear recording density of 250 kfrpi by using Co:$\gamma$-Fe$_2$O$_3$ tape media and ring type head with narrow gap[32]. This recording density was quite high at that time. These results suggests that the isotropic magnetic recording system has potential to achieve ultra-high density, while it is not as high as that of the maximum value of real perpendicular recording system.

The isotropic magnetic orientation is very suitable for the head field distribution of ring type head and the demagnetizing field seems to be fairly decreased than that of magnetization recorded in-plane direction. The large reproduced signal is also one of merits

---

[31] J. U. Lemke : IEEE Trans. on Magn., 15[6], pp.1561-1563 (1979)
[32] J. U. Lemke : J. Appl. Phys., 53, pp.2561-2563 (1982)

of this system when ring type head is used. There is a simulation result that the recorded

magnetization at angle of 30 degree from film plane generated largest signal amplitude[33].

Fig. 2-14 shows the schematic images of the recorded magnetization and head field

distribution in writing process of isotropic recording system. The orientation of

magnetization becomes like a obliquely oriented media such as Co oxide tapes prepared

by evaporation. Generally, underlayers are not necessary in this system and the

reproduced wave form is close to single pulse, conventional type of recording system,

such as ring type head, signal processing etc would be able to used easily. Therefore, it

is one of solution for attaining high-density recording system to develop this 'isotropic'

recording system.

head pole
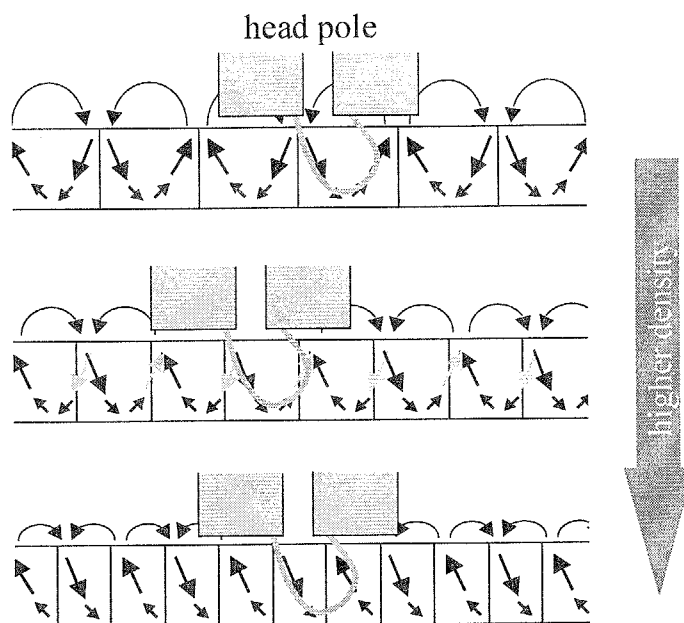


Fig. 2-14   Isotropic recording system using ring type head.

---

[33] I. Tagawa, Y. Shimizu, and Y. Nakamura : J. Magn. Soc. Jpn., 15[S2], pp.827-832 (1991)

However, this system has been investigated and utilized only for tape systems to date and not for rigid disks. Because it was difficult to prepare recording media with sufficient magnetocrystalline anisotropy, which enables to have isotropic orientation of magnetization, due to prevent a circular mode of magnetization.

The recorded magnetization in the evaporated tape media is canted at an angel to film plane. In this media, the anisotropy of evaporated Co and Co-CoO particles are applied and their magnetization are aligned anti parallel each other. High recording density has been achieved in tape media, the restrict control of column structure and grain boundaries should be achieved for higher recording density.

It seems that this system is also applicable in rigid disks. Dr. Morisako et al. reported that MnAlCu($\tau$) films with isotropic magnetization attained relative high recording density of 59 kfrpi even for large thickness of 300 nm[34]. One of representative candidates as isotropic recording layer is Co ferrite film with (111) orientation. Since the easy of Co ferrite is in <100> direction, the magnetization vectors are distributed in circular cone whose mother line is canted at angle of 35.3 from grand plane. Therefore, it has almost same in-plane and perpendicular coercivities. In this thesis, it was clarified that Co ferrite and Co-Zn ferrite film with (111) orientation possessed isotropic magnetization and quite large magnetocrystalline anisotropy, and the read/write characteristics of Co-Zn ferrite rigid disk with isotropic magnetization were investigated. The dependence of linear recording density $D_{50}$ and the noise spectra on anisotropy of the recorded magnetization would be mentioned in the *Chapter 7*.

---

[34]  森迫昭光：東京工業大学学位論文, pp.296-299 (1987) (in Japanese)

## 2-7 Summary

In this chapter, the brief history of magnetic recording system and the simple explanation of magnetic recording media with high density were described. It was clarified that the development of a contact type of recording layer will be necessary as well as the development of signal processing, servo tracking technology, and the appearance of spin valve head with higher sensitivity.

The simple explanation longitudinal magnetic recording system which is commonly used in practical applications and the perpendicular magnetic recording system which seems to be able to attain recording density higher than 20 Gbits/inch$^2$ was also. In addition to them, the brief introduction of 'isotropic recording system,' which was proposed by Lemke and seems to have potential to attain high density, was also described.

Although the development of perpendicular recording system is important for attaining ultra-high density above 20 Gbits/inch$^2$, the isotropic recording system which can utilize the field distribution of ring type head also seems to be applicable as recording layer with high density.

In this thesis, therefore, a spinel type of Co ferrite film and a magnetoplumbite type of Ba ferrite film was investigated for contact type of isotropic and perpendicular recording layers as mentioned in later chapters.

# Chapter 3

# Preparation Method and Measurements of Specimen Films

## 3-1   Introduction

There are several key technologies required for the deposition of ferrite films. They are sputtering system, target material, substrate heater and so on.

Sputtering system is considered to be the most suitable production technique and therefore, it has been intensively investigated. Several types of sputtering system for deposition, such as triode and magnetron, have been proposed to improve the demerits of the diode sputtering system, and some of them are successfully applying for industrial applications. However, they also have several demerits. It is difficult for them to deposit magnetic films at high deposition rate and at low temperature process because of the serious damage of the growing film surface from plasma and the unnecessary confinement of magnetic flux into target material. This unnecessary flux confinement in magnetron sputtering system makes impossible to sustain the discharge of plasma. Especially for the deposition of oxide films such as spinel and magnetoplumbite type of ferrite films, the formation of most closely packed structure of oxygen atom whose atomic weight is as small as 16.0 should be promoted by using "damage-free" deposition process. The facing targets sputtering (FTS) system invented by Prof. Naoe et al.[1] can realize a damage-free deposition. In this study, therefore, all specimen films were prepared by using FTS system. FTS system has several merits compared with the

---

[1] M. Naoe, S. Yamanaka and Y. Hoshi : IEEE Trans. on Magn. MAG-16, pp646 (1980)

other conventional type of sputtering systems.

Crystallographic and magnetic characteristics of the deposited films depend on the composition and impurities of the films. The targets with little impurity are required for this study and therefore, targets used in this study were sintered from starting powders with purity above 99.9 %. Some ferrite plates with different composition were sintered using dry ceramic technique, and the crystallographic and magnetic characteristics of the deposited films were compared for each composition.

A quite high substrate temperature of 600°C and above are necessary for the deposition of oxide films with complex crystallite structure such as magnetoplumbite type of Ba ferrite film. Usually, the conventional types of metallic wire heater and lamp heater are used for heating substrates. However, sometimes these kinds of heater cause unnecessary discharge plasma around its electrode due to high applying voltage and it makes the discharge plasma of FTS system unstable. A heater with low voltage, which does not affect to the discharge plasma and enables to the effective and reproducible deposition of oxide film should be developed.

Therefore, in this chapter, sputtering phenomena and conventional type of sputtering systems were briefly described in the next paragraph 3-2 and the principle and merits of FTS system, especially for the deposition of magnetic oxide films, will be described in 3-3. After that, the sintering process of ferrite targets and the structure of the improved substrate heater used in this study will be described in 3-4 and 3-5, respectively. In addition to them, the measurement method of the deposited films will be described in 3-6.

## 3-2   Sputtering method

A lot of deposition processes have been proposed and improved to present due to the requirement of thin film devices. Such deposition processes can be divided into two major groups, i.e. physical vapor deposition (PVD) process and chemical vapor deposition (CVD) one. Generally, PVD process can achieve the film deposition at lower process temperature than CVD process. Since the depositing films are subjected to special conditions such as material vaporization, rapid quenches and so on, therefore, PVD method makes possible to produce specialized phase of materials and the compounds which are difficult to synthesize in thermal equilibrium condition. On the other hand, in CVD deposition, the compound gas, which include the atom of objective material and whose vapor pressure is quite higher than that of single atom, are introduced into reactive chamber. In this process the films with high quality can be deposited on substrates using thermal decomposition, plasma disassociation, reduction, gas and solid phase reaction. Fig. 3-1 shows the schematic illustration of various PVD and CVD methods.

It is called as 'sputtering' that cathode material atoms are back scattered from target to the space due to momentum transfer. There are atomic excitation caused by the collision with electrons and ions, and their chemical activity is highly promoted. And therefore, it enable the formation of compounds at lower process temperature than that of thermal equilibrium process. Since it also enables the deposition of materials with low melting points as well as those with high melting ones and it also can be applied for the deposition on large-scale substrate, they are applied in many industrial applications. It is recognized as one of basic technologies that sustaining the development of new type

devices, and it is also used for the deposition of magnetic layers in rigid disks and heads for magnetic recording systems.

As is well known, sputtering phenomena occur on a cathode surface in glow discharge. When the ionized particles in glow discharge are accelerated to the cathode surface, they make elastic and inelastic collisions with target molecules and atoms, and it cause various phenomena on target surface as shown in Fig. 3-2.
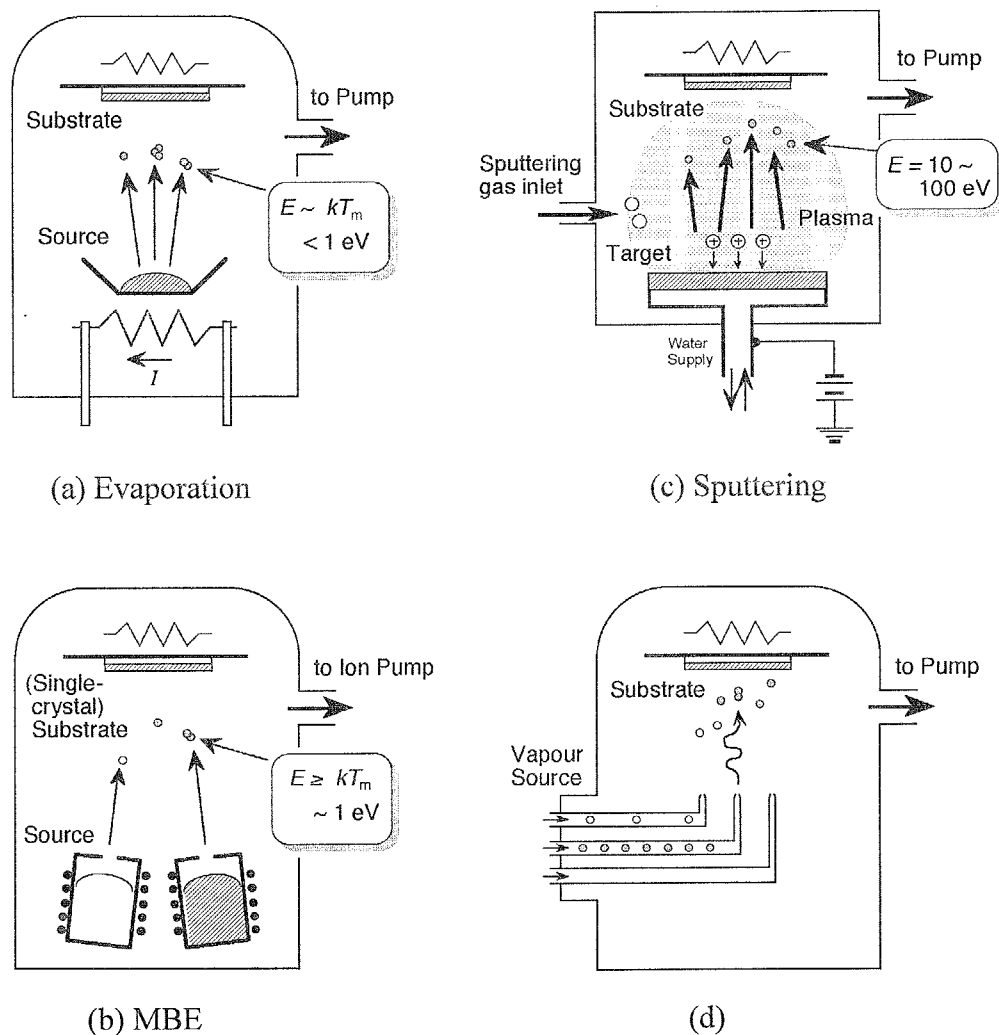


(a) Evaporation

(c) Sputtering

(b) MBE

(d)

Fig. 3-1   Schematic illustration of (a)evaporation, (b)sputtering, (c)Molecular Beam Epitaxy, and (d)Chemical Vapor Deposition.
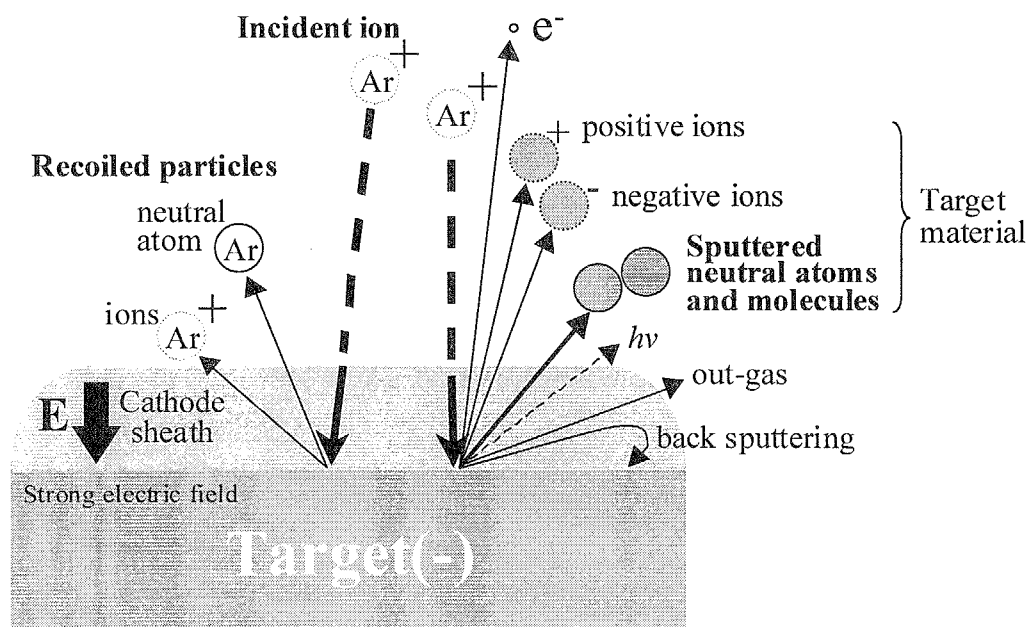
Fig. 3-2   Various phenomena caused by ion collision onto target surface.

The stable glow discharge with high ionization, sustained by applying voltage from 0.1 to 10 kV in low gas pressure from $10^{-1}$ to $10^{-4}$ Torr, are useful for the deposition of thin films. Since the numbers of the many ions and electrons in the plasma are almost the same, the plasma is nearly neutral. The excited neutral atoms coexist with these ions and electrons in the plasma and all of them come into collision, exchange electric charges and combine constantly with each other. High-energy particles, so-called 'hot-particles', such as $\gamma$-electrons, negative ions and recoiled atoms are ejected from the surface of the cathode target by the collision of $Ar^+$ with large momentum as shown in Fig. 3-2. Since there is a strong electric field in the region around the cathode surface, the 'cathode dark space', $Ar^+$ ions in the plasma are strongly accelerated and bombarded surface of the cathode target as a result of which the target material is sputtered as atoms. When the maximum power is applied most efficiently in low gas pressure below $10^{-3}$

Torr, the sputtered particles are ejected to the side rather than to the front of the target plane. On the other hand, 'hot particles' are ejected mainly normal to the target, therefore, if the substrate is placed facing to the target plane, the substrate and the growing film are bombarded by these high energy particles. Such bombardment during deposition causes serious differences in composition, defects of structure and deterioration of various characteristics of the films.

Fig. 3-3 illustrates the problems caused by the bombardment of $\gamma$-electrons. Since $\gamma$-electrons are quite small in size and weight, sputtering on the substrate cannot occur, however, a unnecessary thermal elevation will occur at the substrate surface. Moreover, if a dielectric substrate is used, high negative bias appears around the substrate and since the substrate is exposed to the plasma, many $Ar^+$ are incident upon the substrate. This bombardment by $Ar^+$ ions can also cause the deterioration of the uniformity of structure at substrate and film surface
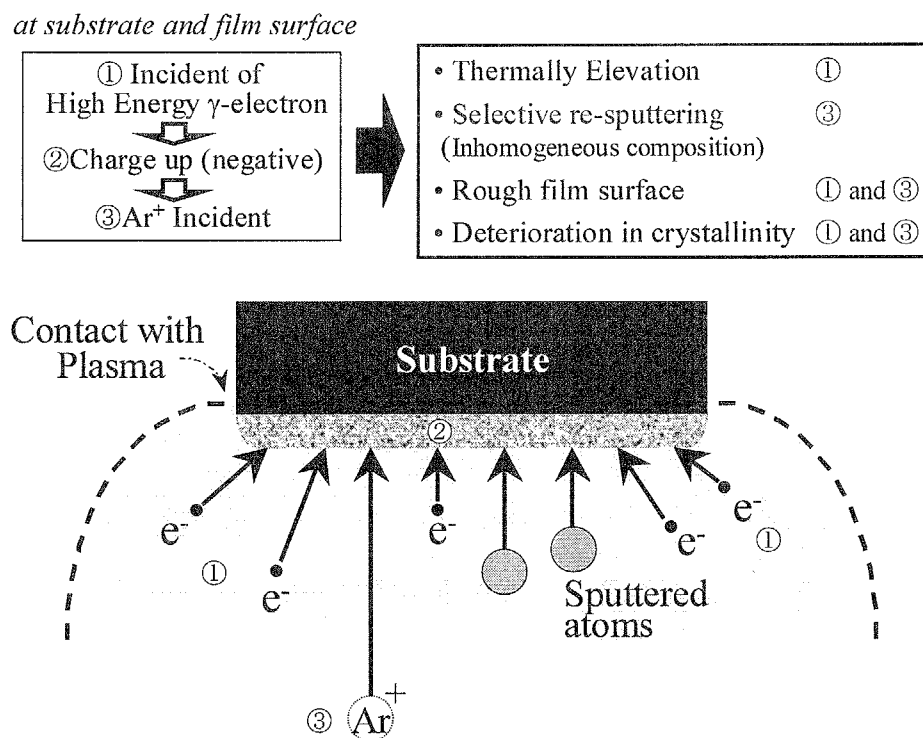


Fig. 3-3   Problems caused by bombardment of $\gamma$-electrons on substrate surface.

and the crystallinity of the films, and since selective re-sputtering also occurs, it can cause significant difference in composition between the film and the target. The elevation of substrate temperature and the bombardment of growing films have to be prevented completely because the magnetic properties of the resulting films are very sensitive to these factors.

The problems caused by the recoiled Ar and negative ions are shown schematically in Fig. 3-4. They are also serious because the recoiled Ar atoms possess very high kinetic energy, even after they bombard the target surface. They tend to destroy the morphological uniformity and to deteriorate the crystallinity. In addition to them, their incorporation into the film would cause large internal stress. Since oxygen atoms are likely to be negative oxygen ions such as $O^-$ and $O^{2-}$, their existence should be carefully considered for the sputter deposition of ferrite films in which the oxide targets and gas



| Recoiled Ar | Negative Ion |
|---|---|
| • Selective re-sputtering<br>• Deconstruction of oxygen plane<br>• Incorporation into film<br>• Origin of internal stress | • Direct bombardment to substrate<br>• Large number<br>• Large kinetic energy and moment<br>• Large destructive power |
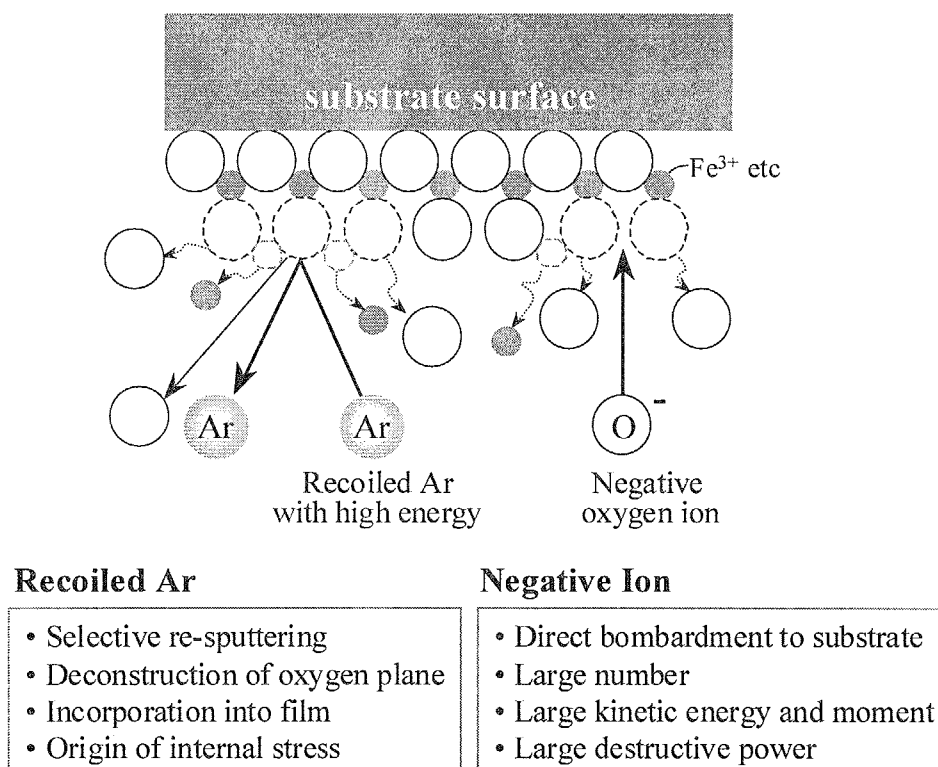
Fig. 3-4 Problems caused by bombardment of recoiled Ar and negative ions.

mixture including oxygen are used. In addition to their high energy on ejection from the target, they are strongly accelerated in the cathode dark space by the large electric field. Therefore, many accelerated negative ions bombard the substrate surface[1]. Since the mass of negative ion is $10^5$ times as large as that of electron, their kinetic energy and moment are very large, they often cause significant differences in film composition.

Although sputtering methods have a lot of superior merits than those of other deposition technologies, there also have several demerits. These are mainly attributed to the bombardment from 'plasma.' The bombardment from high energetic $\gamma$-electrons, $O^-$ and recoiled particles to substrates deteriorate the surface smoothness, fine structure, crystallographic and magnetic characteristics. Sometimes it may be a origin of the inert stress in films. Two of the most important points for the sputtering depositions are how the plasma is confined efficiently and how the damage from plasma is restricted enoughly. These are quite important and therefore, several new types of sputtering process have been proposed, developed and improved. The most representative technique to confine plasma is the applying of magnetic field. The most major and common sputtering system using magnetic field is a magnetron type sputtering system. There are several types of magnetron sputtering system, such as planar type, post type, hollow cathode type and so on, and their configurations of plasma confining field and shapes of targets are different each other. The planar type magnetron sputtering system which is the most simple in configuration is schematically shown in Fig. 3-5. In this system the plasma-confining field applied parallel to target surface so that donuts type plasma is formed on target surface. However, the target usability of this system is not so

---

1 K. Tominaga, S. Iwamura, Y. Shintani, and O. Tada : Jpn. J. Appl. Phys., 21, pp.688 (1982)
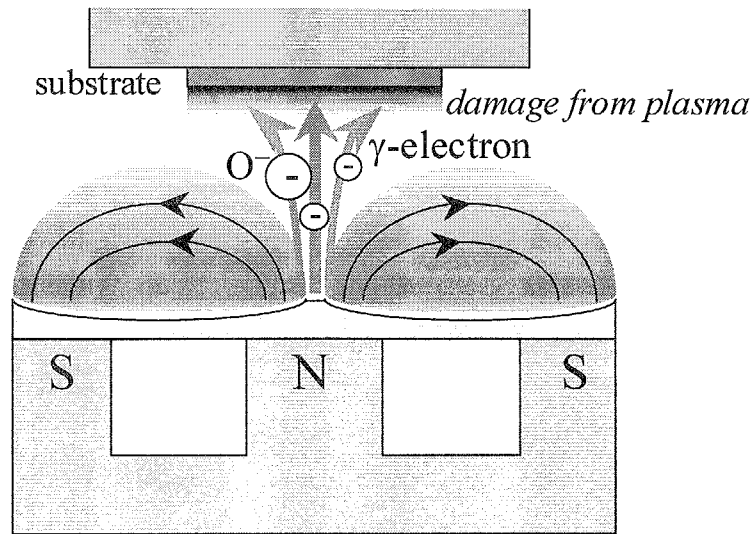
Fig. 3-5   Schematic illustration of magnetron sputtering system, the shape of
plasma and target erosion patterns.

large, and γ-electrons and negative ions ejected along the flux generate from target

center bombarded directly to substrate. It is another problem for this system that the

plasma-confining field at target surface is insufficient when magnetic material is used as

target as will be mentioned in 3-3-2.

Although these problems do not have to be considered for post and hollow cathode

types, shapes of targets are complicated and it makes target cost very high. Commonly

electron reflection panels are equipped at the edge of these types of sputtering

apparatuses, the applied negative bias should be small not to be sputtered the reflection

panel. Therefore the power efficiency used for sustaining plasma is smaller than those of

planar type are. Anyway, it should be considered for magnetron sputtering systems that

the damages from plasma are not perfectly restrained. The facing targets sputtering

system invented by Prof. Naoe et al. is superior system because it achieve 'damage-free'

deposition as described in next paragraph 3-3.

## 3-3   Facing targets sputtering system

### 3-3-1   Principle and merits of facing targets sputtering

All specimen films in this study were prepared by using the facing targets sputtering (FTS) apparatus with and without post-annealing process. The picture of the sputtering apparatus used in this study is shown in Fig. 3-6. Fig. 3-7 shows the schematic illustration of dc-FTS apparatus and Fig. 3-8 shows the picture of the target of the facing targets of FTS-V used in this study.

A pair of targets faced each other are connected and used as cathodes, while the chamber wall and shield rings are used as anodes. The plasma-confining field $H_p$ is applied normal to the target plane using permanent magnets, which are mounted behind the targets. Since $\gamma$-electrons and negative ions are accelerated from the cathode and forced the spiral motion along their flux by Lorentz force so that their path length are extended as shown in Fig. 3-9.
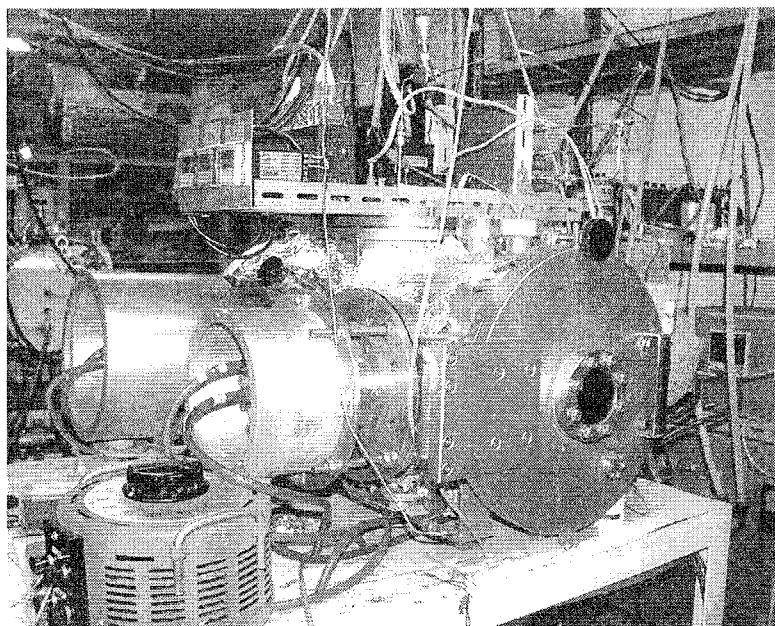


Fig. 3-6 Facing targets sputtering apparatus(FTS-V) used in this study.

Heater

damage-free

substrate

Excited oxygen ⊕   ◎   Sputtered atoms

Ar ion ⊕

Hp

N  S   ⊖

γ-electron

Confined

Plasma

Targets

$V_a$ : 300-1000

DC  Power Supply
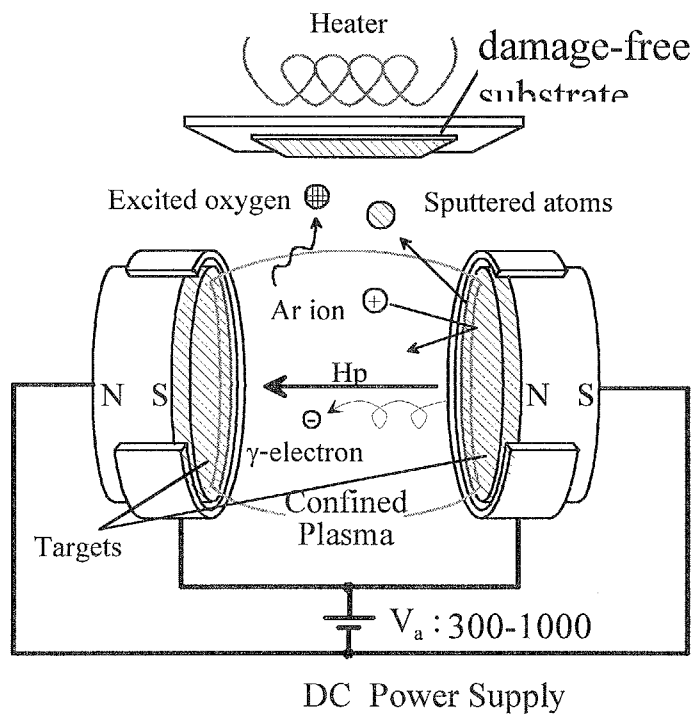
Fig. 3-7   Schematic illustration of facing targets sputtering system.
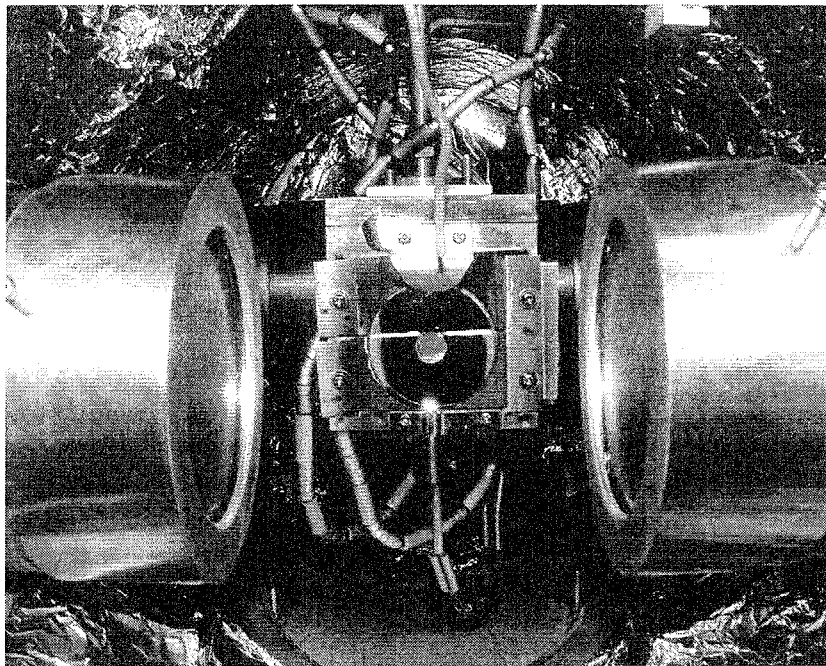
Fig. 3-8   Configuration of the facing targets and substrate holder.
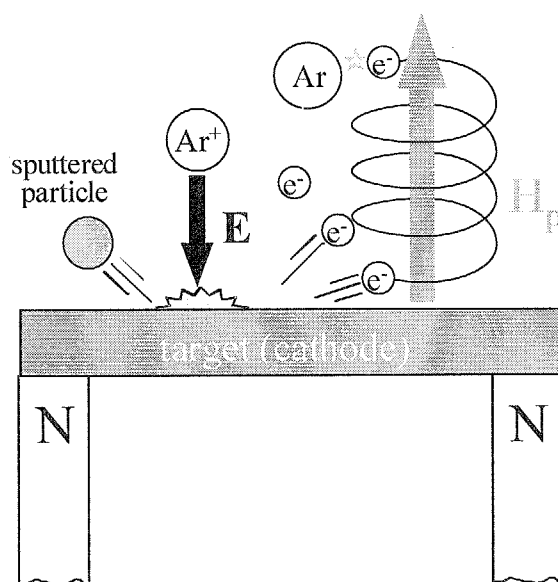
Fig. 3-9   Spiral motion of γ-electrons by magnetic and electric field at target surface of FTS system.

These "trapped" γ-electrons promote the ionization of working gases such as Ar and $O_2$ during back and forth movement between targets, especially near the target surface owing to stronger magnetic field. Since the plasma of this glow discharge is almost perfectly confined in the space between facing targets by cylindrical magnetic wall and the surface of two targets, the stable glow discharge for sputtering can be generated and sustained even at very low gas pressure in the range below $10^{-4}$ Torr. And because of such a low gas pressure, the atoms sputtered from targets can reach at substrate with high kinetic energy enough to promote the crystallization of grains in the films.

In addition to the perfect plasma confinement, since the substrate holder, which is electrically isolated and placed outside of the plasma as shown in Fig. 3-7, substrates and depositing films are not exposed to the bombardment of high-energy particles such as γ-electrons and negative ions. Therefore, the defects and the damages in the growing films caused by charged particles such as γ-electrons and negative ions can be kept at

relatively low level during deposition. Consequently, the films with high crystallization, flat surface and low internal stress can be deposited at high deposition rate by using FTS apparatus. However, the existence of recoiled particles has to be considered when target is composed of atoms with very large atomic weight. Because most of sputtering gas recoiled at target surface do not have electron charge and these neutral atoms can not be trapped in the plasma by Lorents force and these recoiled particles with high kinetic energy bombards at growing film surface. It will be seriously deteriorate the crystallization of ferrite films because the most closely packed structure of oxygen, which is basic structure in ferrite, is likely to be destroyed by this bombardment of recoiled Ar atoms. The precise explanation for this problem will be mentioned in *Chapter 8 'Ba Ferrite/ZnO Double Layered Films.'*

Fig. 3-10 shows the schematic illustration of FTS apparatus for depositing the multilayers films used in this study. The Ar and $O_2$ gases were introduced separately into the chamber as working gases and it was adjustable independently using regulator valves. As it has two facing targets units in the same chamber, the multilayers composed of two different kinds of layers can be deposited without breaking the vacuum. Targets and chamber wall were cooled by water until the glow discharge was started. This cooling of target is very important for the deposition of ferrite films, because the surface of ferrite target with high resistivity, is likely to heated up during deposition. It causes an unintentional heating-up at the substrate surface and some times it seriously deteriorate the characteristics of the deposited films when the films contains the atom with high vapor pressure.
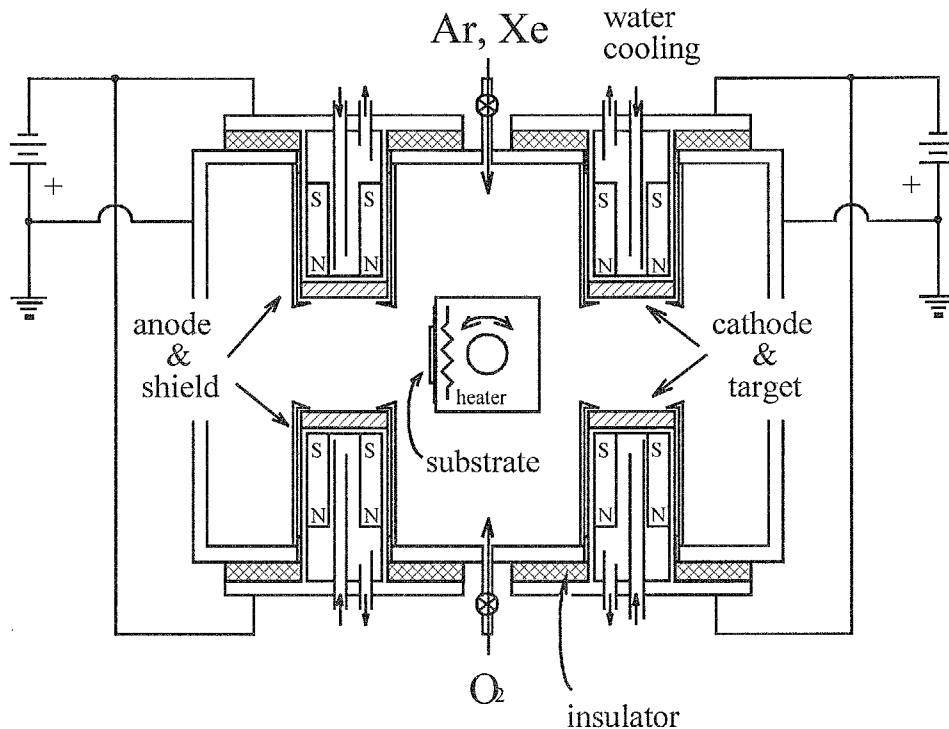
Fig. 3-10   Schematic illustration of FTS apparatus for deposition of the
multilayered films. (Cutting image viewing from top)

### 3-3-2   Deposition of magnetic material

It should be noted that FTS system is very useful for the deposition of magnetic films. In conventional type of magnetron sputtering system, the magnetic flux has to be cross over the target surface, so that one portion of it which is parallel to the target surface works effectively to confine the discharge plasma as shown in Fig. 3-11(a). However, when magnetic material is used as target, almost magnetic flux is confined in the target plane and not cross over the target surface, and there is little leakage of magnetic flux from target surface as shown in Fig. 3-11(b). It makes impossible to occur and to sustain the stable glow discharge. It is one of a serious demerits of magnetron sputtering system for the deposition of the magnetic films and it is more serious for the deposition of

substrate                              substrate

magnetic
flux     E                                  E
                                magnetic
                                flux

| S | N | S |                     | S | N | S |

magnet                                magnet

(a) non magnetic target          (b) magnetic target
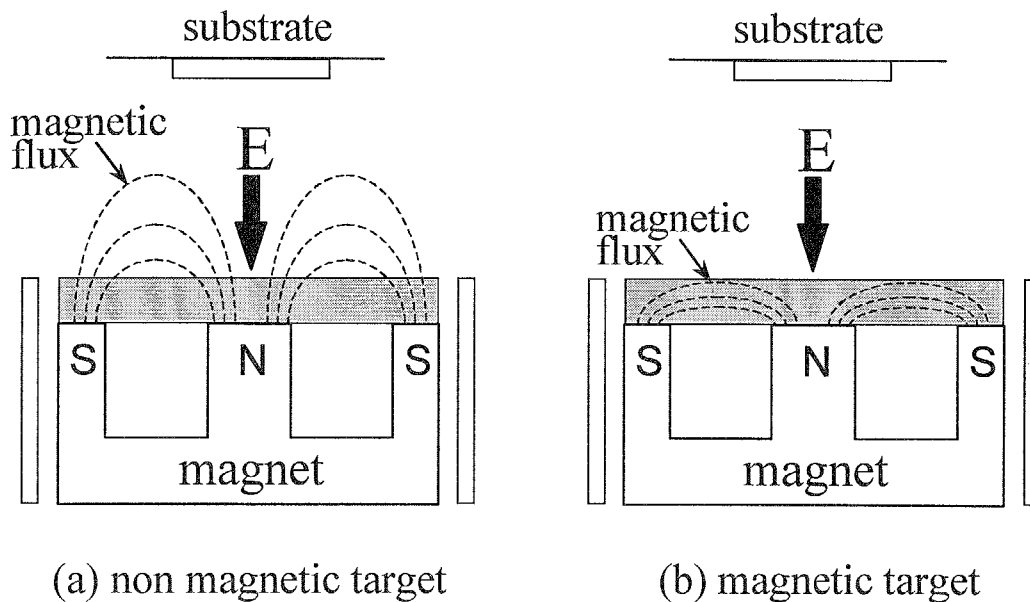
Fig. 3-11  Path of magnetic flux in magnetron sputtering system.
(a)non-magnetic material    (b)magnetic material

magnetic material with very high permeability such as Ni-Fe alloy, Fe-Co alloy, Mn-Zn

ferrite and Ni-Zn ferrite films.

On the other hand, since the magnetic flux of FTS system is applied perpendicular to

the target, there exists strong enough magnetic flux between targets to sustain glow

discharge stable even at relatively low gas pressure as mentioned before. From the

configurations of FTS system, the impedance of the discharge plasma is very low and

oxide material whose resistivity is relative high can be also used as targets even in dc

discharge. Excited and radical oxygen atoms are produced in high density plasma, FTS

system seems to be a very suitable method for depositing the films of magnetic oxide

materials such as spinel and magnetoplumbite type of ferrite.

## 3-4   Sintering process of targets

Fig. 3-12 shows the typical flow diagram of the sintering process of polycrystalline ferrites. This process is an example for sintering of $CoFe_2O_4$ targets. The raw materials, starting powders, were the mixture of $(CoO)_{1.0}$ and $(\alpha\text{-}Fe_2O_3)$. They are weighed to desirable amounts, usually 300 g in total for two targets 90 mm$\phi$ in diameter and $4\sim6$ mm in thickness, in the correct portions and then mixed and stirred with a turbine blade. Then they are placed in a rotating steel-lined drum with steel balls and a medium of isopropyl alcohol(IPA). It is normally called "wet-milling" or "ball-milling." Steel is used for the material because any iron picked up by the mixture due to wear of the lining and balls may be allowed for in the initial composition of the powder. The fluid is mainly for cooling and mixing the purposes. After the wet-milling, this slurry including starting powders are dried in an oven until IPA is perfectly vaporized. These powders were stirred with a turbine blade again and a few drops of water solution of Polyvinyl Alcohol(PVA) was added to it as binder and then it was dry-pressed to have a fugure of target. Next this pressed powders are pre-baked at 300℃ for 3 hours to PVA is fully vaporized and then pre-sintered at 600℃ for 1 hour. After it is crushed and stirred, they are separated to quarter and three quarters, and three-quarter portion undergo the same cycle with changing the wet-milling time and pre-sintering temperature. They are mixed together after that and undergo the third cycle. After the third sintering, these ferrite plates were heated at 800℃ for 2 hours in Ar and $H_2$ atmosphere to decrease the surface resistivity. Although the as-sintered ferrite plates are insulator and their resistivity were too high to occur and sustain stable dc discharge plasma.

```
┌─────────────────────┐
│ Weighing and Mixing │
│ of Raw Materials    │
│ (CoO, a-Fe₂O₃ : 300g)│
└─────────────────────┘
           │
           ▼
    ┌─────────────┐              ┌──────────────────┐
    │ Stirring 1h.│─────────────▶│ Wet Milling 15h. │
    └─────────────┘              └──────────────────┘
                                          │
                                          ▼
  ┌────────────────┐              ┌──────────────┐
  │ Stirring 30min.│◀─────────────│   Drying     │
  └────────────────┘              └──────────────┘
           │
           ▼        ┌──────────────────┐
           ◀────────│ Mixing with PVA  │
           │        └──────────────────┘
           ▼                           ┌──────────────────┐
   ┌──────────────┐                    │ Pre-baking       │
   │ Pressing     │───────────────────▶│ 300°C 30min.     │
   │ 300 kg/cm²   │                    │ Pre-sintering    │
   └──────────────┘                    │ 600°C 1h.        │
                                       └──────────────────┘
                                                │
  1/4                                           ▼
   ┌──────────────┐                    ┌──────────────┐
   │ Stirring 8h. │◀───────────────────│  Crushing    │
   └──────────────┘                    └──────────────┘
           │  3/4
           ▼
  ┌──────────────────┐                 ┌──────────┐
  │ Wet Milling 20h. │────────────────▶│  Drying  │
  └──────────────────┘                 └──────────┘
                                              │
   ┌──────────────┐                    ┌────────────────┐
   │ Pressing     │◀───────────────────│ Stirring 30min.│
   │ 300 kg/cm²   │                    └────────────────┘
   └──────────────┘
           ▲     ┌──────────────────┐
           │─────│ Mixing with PVA  │
           ▼     └──────────────────┘
   ┌──────────────┐                    ┌──────────────┐
   │ Pre-baking   │                    │  Crushing    │
   │ 300°C 30min. │───────────────────▶│              │
   │ Pre-sintering│                    └──────────────┘
   │ 900°C 1h.    │                           │
   └──────────────┘                           ▼
           │                          ┌──────────────┐
           ▼                          │ Stirring 12h.│
   ┌──────────────────┐               └──────────────┘
   │ Wet Milling 24h. │◀──────────────────────┘
   └──────────────────┘
           │
           ▼                          ┌────────────────┐
     ┌──────────┐                     │ Stirring 30min.│
     │  Drying  │────────────────────▶│                │
     └──────────┘                     └────────────────┘
           ▲    ┌──────────────────┐
           │────│ Mixing with PVA  │
           ▼    └──────────────────┘
   ┌──────────────┐                   ┌──────────────┐
   │ Pre-baking   │                   │ Pressing     │
   │ 300°C 30min. │◀──────────────────│ 300 kg/cm²   │
   │ Main Sintering│                  └──────────────┘
   │ 1000°C 1h.   │
   └──────────────┘
           │
           ▼
   ┌──────────────┐                   ┌──────────────────┐
   │ Reducing in He+H₂│──────────────▶│ Grinding of Surface│
   │ 800°C 2h.    │                   └──────────────────┘
   └──────────────┘
```

Fig. 3-12   Typical flow diagram of sintering process of polycrystalline ferrites.

## 3-5   Si heater

Sometimes, quite high substrate temperature of 600°C and above are necessary to deposit oxide films, especially for the films possessed complex crystallite structure such as hexagonal, perovskite and so on. It is necessary for the effective and reproducible deposition of oxide films to develop the substrate heater with characteristics as follows;

1) the maximum temperature higher than 700 °C

2) little amount of out-gas

3) small heat capacitance

4) uniformity of temperature at surface

There are several types of heater which are used in sputtering apparatus, i.e. wire heater, lamp heater, sheet heater and so on. The most conventional one is wire heater using spiral wire of tungsten(W) or tantalum(Ta). The current is applied to the wire and the substrates are heated indirectly by the heat radiation from them. Although such metal wire heaters are available up to 500°C even in evacuated condition, some oxides layer are formed at wire surface when oxygen was mixed in the working gas and they are likely to sublime at temperature lower than the melting point of metallic wire. It make wires thinner with increasing of temperature and partial oxygen pressure. Therefore, tempered Kanthal(Fe-Cr-Al) wire which have stable oxides layer at surface is used for the repeatable deposition of oxide films up to 800°C. However, since the resistivity of these metallic wire is high, high voltage around 60-100 V should be applied to attain substrate temperature higher than 600°C. This high voltage may occur awkward plasma discharge just around the substrate and it makes discharge plasma between targets unstable and sometime it cause an arc discharge. Heater with low resistivity are

necessary to solve these problems.

In this study, Si plate with concentration of donor impurities in the magnitude of $10^{18}$ were used as heater. Substrate was attached onto the surface of it and direct heating were possible as shown in Fig. 3-13. Although Si is semiconductor and possesses high resistivity at lower than 120°C, it is drastically decreased at around 150°C because it transit to an intrinsic region. The impedance of this heater keeps very low and the applied voltage is lower than 15 V and it does not affect to the condition of discharge plasma. In addition to that the amount of out-gas is quite small even when substrate temperature reached to 700°C.

Substrate temperature was measured by contacting thermocouple(Almel-Cromel-) substrate surface.
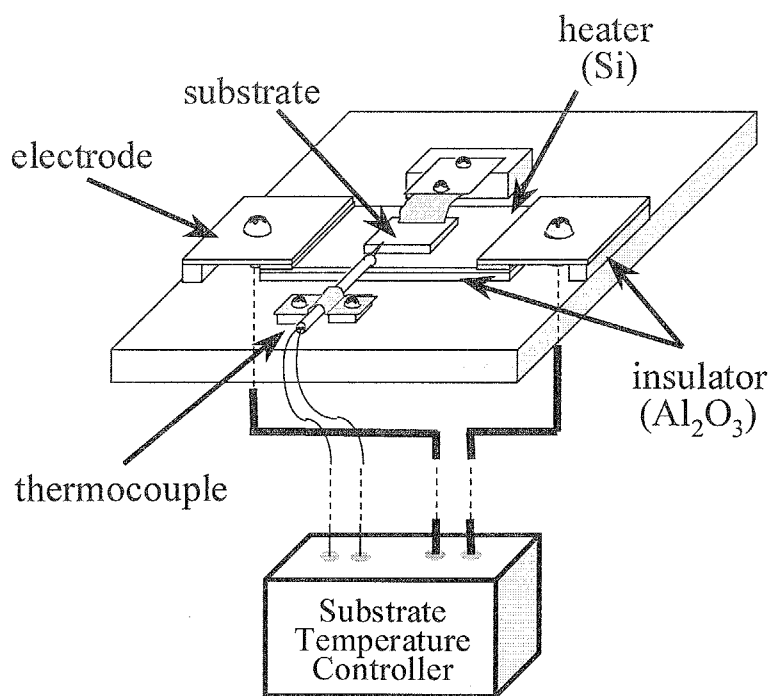


Fig. 3-13   Schematic illustration of substrate holder used in this study.

## 3-6   Measurements

### 3-6-1   Film composition and microstructure

The composition and uniformity of deposited films were investigated by inductively coupled plasma spectrometry(ICPS) and auger depth profile(AES), respectively. The surface texture and cross-sectional morphology were observed by scanning electron microscope(SEM) and surface roughness such as center-line average roughness $R_a$ and the root-mean-square roughness $R_{rms}$, were measured by atomic force microscopy(AFM), respectively.

### 3-6-2   Crystallographic characteristics

Various crystallographic characteristics such as the crystal structures, crystallite orientation, interplaner distance $d$, the full width at half maximum of rocking profiles $\Delta\theta_{50}$ were also calculated and evaluated by peak position of $\theta$-$2\theta$ chart and rocking curves analyzed X-ray diffraction(XRD) diagrams using Cu-K$\alpha$ ($\lambda$ = 1.5418 Å). Crystallite size <D> was calculated using Sherrer equation as shown in (3.1).

$$<D> = \frac{0.9\lambda}{B\cos\theta} \qquad (3.1)$$

where B is the width of the diffraction line, i.e. the full width at half maximum of the $2\theta$ peak(in radian), s is the diffraction angle(in degree).

Deposited Co ferrite films were composed of crystallites with various orientation such as (311), (111), (400) and so on. In this study, the degree of spinel crystallites with (mmm) orientation was defined by the way of Lotgering[1] as follows;

----

[1] F. K. Lotgering, J. Inorganic Nucl. Chem., 9, pp.113 (1959)

$$f_{spinel(mmm)} = \frac{P - P_0}{1 - P_0},\qquad\qquad (3.2)$$

where,

$$P_0 = \frac{\sum I_{0\,s(mmm)}}{\sum I_{0(hkl)}},\quad (\text{from JCPDS card})$$

$$P = \frac{\sum I_{s(mmm)}}{\sum I_{(hkl)}},\quad (\text{from the XRD diagram of deposited film})$$

The $f_{spinel(mmm)}$ of 1.0 shows that the film is composed of crystallites with perfect (111) orientation and the $f_{spinel(mmm)}$ of 0.0 shows that the film is composed of crystallites with other orientation.

The degree of c-axis orientation of Ba ferrite film, $f_{BaM(00l)}$, was also defined as same as above definition.

3-6-3   Magnetic characteristics

The magnetic characteristics such as saturation magnetization $4\pi M_s$, in-plane and perpendicular coercivities $H_{c//}$ and $H_{c\perp}$ and were determined on the hysteresis loops measured by using a vibrating sample magnetometer(VSM) with applying field of 12 kOe.

Torque curves were also measured by torque magnetometer for the calculation of the magnetic anisotropy constant $K_u$ and anisotropy field $H_k$ for Ba ferrite films in *Chapter 8*.

Conversion types of Mössbauer spectra of several Co-Zn ferrite films were also measured to identify the degree of orientation of magnetization in *Chapter 6*.

## 3-7   Summary

The principle and merits of the facing targets sputtering apparatus especially for the deposition of magnetic oxide films were described in the first one third of this chapter. In the second one third, the sintered process of ferrite targets and the design of the improved Si substrate heater used in this study were described. The measurement system and the evaluations were described in the last one third.

FTS system can realize the damage free deposition at high deposition rate and at low temperature process. It also possess some other merits compared with other kind of sputtering systems. Because of well designed configuration such as the direction of plasma confining field, FTS system is applicable for the deposition of magnetic material. It also seems suitable for the deposition of oxides such as spinel and magnetoplumbite type of ferrite.

A piece of Si wafer was used as the substrate heater in this study and it does not have any interruption to the stable discharge of plasma during deposition even for high substrate temperature above 600℃ because it has very low impedance in intrinsic region at 150℃ and above. Substrate temperature up to 600℃ was controllable by using this type of Si heater and it enables the repeatable deposition of ferrite films with good crystallographic and magnetic characteristics.

# Chapter 4

# Co Ferrite Films

## 4-1 Introduction

Particulate media with Co modified fine ferrite particles have been applied for magnetic recording media from 1960's because of their chemical stability, low cost and mass productivity. However, it became difficult to increase linear recording density using these particulate media because of small signal due to their small magnetization and insensitive head in those days. Therefore, the films of Co-based alloys such as Co-Cr[1], Co-Cr/Cr[2] and Co-Ni-Cr have being mainly used as magnetic recording layer in rigid disk media. However, protective layers such as carbon are necessary on them because of their poor chemical stability and low corrosion resistance, and this layer is a neck to decrease actual spacing. In addition to that, the media noise, which increases with the increase of linear recording density, is one of serious problems for these alloy media at ultra-high density. These days, the spacing between a head and disk media are being decreased down to 40 nm to increase the recording density and media for direct contact recording will be required in the near future.

Here, I concentrated a spinel type of Co ferrite ($CoFe_2O_4$) films. Co ferrite are very attractive material because they are expected to be applicable for magneto-optical

---

[1] S. Yamamoto, Y. Nakamura and S. Iwasaki: IEEE Trans. Magn., MAG-23, pp.2070-2072 (1987)

[2] H. Suzuki, N. Goda, S. Nagaike, Y. Shiroishi, N. Shige and N. Tsumita, IEEE Trans. Magn. MAG-27, pp.4718-4720 (1991)

devices[3,4], SAW transducers and so on because of their large Faraday rotation angle and magnetostriction. Since they possess moderate saturation magnetization $4\pi M_s$ and high coercivity $H_c$ they are expected as high density recording media[5,6] In addition to that, since it is a stable oxide at room temperature and possess an excellent chemical stability and corrosion resistance, it seems to be applicable a contact type of recording layer. However, there is key point to prepare Co ferrite films with well magnetic characteristics. Fig. 4-1 shows the lattice structure of a spinel type of Co ferrite. The smallest cell of the spinel lattice that has cubic symmetry contains eight $MeFe_2O_4$. The relatively large oxygen ions form a f.c.c. lattice. In this cubic closely packed structure
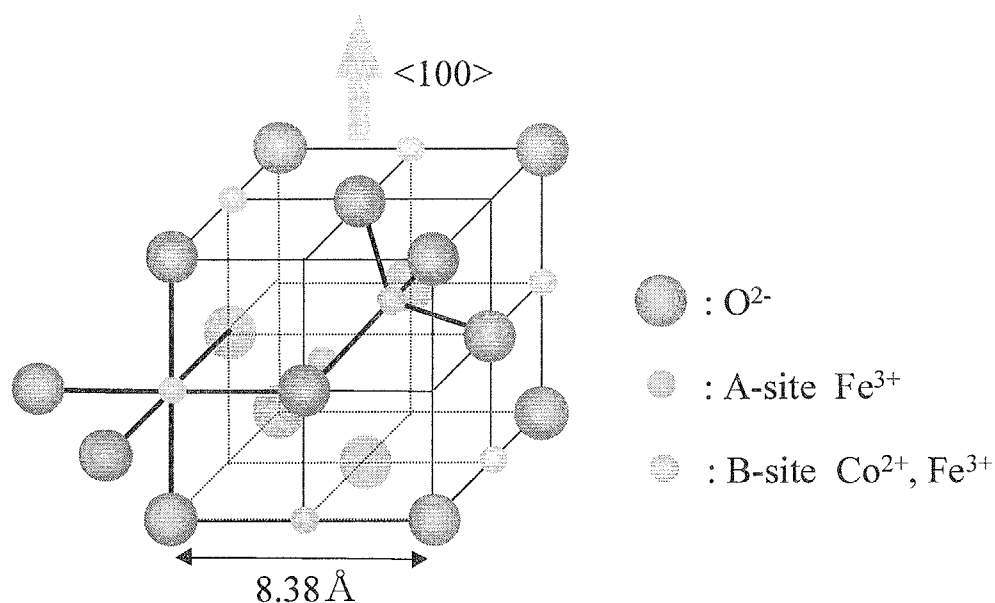


Fig. 4-1 Lattice structure of spinel type of Co ferrite.

[3] J. W. D. Martens : J. Appl. Phys., 59, pp.3820 (1986)
[4] Ostorero, M. Guillot and M. Artinian: IEEE Trans. Magn. MAG-24, p2560(1988)
[5] H. Torii, E. Fujii and M. Hattori : IEEE Trans. J. Magn. Soc. Jpn., JMJ-6, pp.765-767 (1991).
[6] M. Matsuoka, Y. Hoshi, M. Naoe and S. Yamanaka : IEEE Trans. Magn., MAG-18, pp.1119-1121 (1982).

two kinds of interstitial sites occur the tetrahedral and the octahedral sites which are surrounded by 4 and 6 oxygen ions and they are called A and B sites, respectively. The magnetic characteristics of Co ferrite is originated from the ions placed in A and B sites. However, the base structure of spinel is formed by oxygen ions with farily larger ion radius. Therefore, how to form the closely packed structure of oxygen is a key point to prepare Co ferrite film with high crystallinity and excellent magnetic characteristics. However, it has been difficult to prepare ferrimagnetic oxide films with good crystallinity and sufficient magnetic characteristics by conventional sputtering system, such as diode and magnetron, because of serious plasma damage and the low kinetic energy of adatoms.

In this study, therefore, single layer films of spinel type of Co ferrite were deposited directly on substrate by using "damage-free" Facing Targets Sputtering (FTS) apparatus and their crystallographic and magnetic characteristics were investigated by changing the deposition conditions such as partial oxygen gas pressure $P_{O_2}$ and substrate temperature $T_s$.

## 4-2 Deposition conditions of Co ferrite films

All specimen films were prepared by using FTS apparatus as shown in Fig. 4-2 and they were not subjected to post-annealing process.   Table 4-1 shows deposition conditions of Co ferrite film.
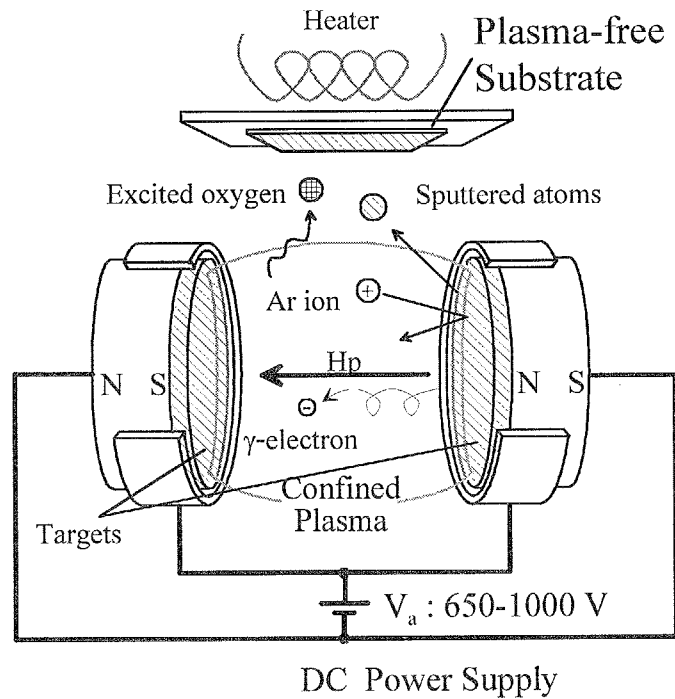
Fig. 4-2　Schematic illustration of the facing targets sputtering apparatus.

Table 4-1　Deposition conditions of Co ferrite films

|  | Co ferrite film |
|---|---|
| Target Composition | $Co_{1.03}Fe_{1.97}O_y$ |
| Substrate material | $SiO_2/Si$ |
| Total gas pressure $P_{total}$ | 2.0 mTorr |
| Partial oxygen gas pressure $P_{O_2}$ | 0.0~2.0 mTorr (0.02mTorr) |
| Substrate temp. $T_s$ | without heating - 600℃ (300 or 500℃) |
| Discharge current $I_d$ | 0.10 A |
| deposition time | 120~180 min. |

Here, sintered Co ferrite($Co_1Fe_2O_4$) disk plates 90 mm$\phi$ in diameter 7 mm in thickness were used as targets. They were prepared by dry ceramic technique process as mentioned in 3-3. They were sintered from starting mixture of $(CoO)_{1.0}$ and $(\gamma\text{-}Fe_2O_3)_{1.0}$ powders with purity higher than 99.9 %. Target composition measured by ICPS was $Co_{1.03}Fe_{1.97}O_y$.

Specimen films were deposited on thermal oxidized Si wafer $SiO_2/Si$ substrates. Since this substrate possess excellent surface smoothness, it seems that the most closely packed plane of crystal structure is likely to be formed parallel to the film plane when the 'damage-free' facing targets sputtering apparatus were used for the deposition. Matsuoka et al. reported that $SiO_2/Si$ substrates were suitable for the deposition of Ba ferrite films with well crystallinity[7], which also have the most closely packed structure of oxygen.

In this study, the substrate temperature $T_s$ and partial oxygen gas pressure $P_{O_2}$ was changed as deposition conditions. For the investigation of $P_{O_2}$ dependence, $T_s$ was set at 300 or 500°C constant and $P_{O_2}$ was changed in the range 0-2.0 mTorr, i.e. partial pressure ratio of 0-100 %. For the investigation of $T_s$ dependence, $P_{O_2}$ was set at 0.02 mTorr constant, i.e. partial pressure ratio of 1.0 %, and $T_s$ was changed in the range from 90(without heating) to 600 °C. Since there is no bombardment of high energy $\gamma$-electrons onto substrate in FTS system, the $T_s$ was increased up to 90°C during deposition even without heating substrate because of heat radiation from plasma. However, this temperature is quite lower than that of other sputtering system, which has plasma-

---

[7] Morito Matsuoka : Ph.D Thesis, p203, Tokyo Institute of Technology (1985) (in Japansese)

damage to the substrate as mentioned in 3.3. In this study, $T_s$ of 90°C corresponds to the substrate temperature measured at substrate surface just after the deposition without heating substrate.

All specimen films were deposited for 2 or 3 hours after pre-sputtering of 1 hour.

## 4-3 Discharge voltage and deposition rate

The reduced targets from stoichiometric composition were used as mentioned in 3-4 to obtain relatively low resistivity, which enable to sustain dc glow discharge. Some times high substrate temperature above 500°C are necessary for the deposition of Co ferrite films, the oxygen content in the deposited film was likely to be insufficient when they were deposited only in Ar gas. Therefore, most films were deposited by reactive sputtering using $O_2$ as well as Ar. The oxygen partial pressure $P_{O_2}$ may influence the degree of oxidation of target surface during deposition and it may change not only the voltage of discharge plasma but also the deposition rate. Therefore, the dependence of the discharge voltage and deposition rate on $P_{O_2}$ were investigated at $P_{O_2}$ from 0 to 2.0 mTorr, in which the ratio of partial oxygen pressure in the total gas pressure was from 0 to 100 %. The direct current power supply was used and the discharge current was set at 0.1 A.

Fig. 4-3 shows the dependence of discharge voltage on $P_{O_2}$, where sintered Co ferrite plates with composition of $Co_{1.03}Fe_{1.97}O_y$ were used as targets and total pressure ($P_{Ar}$ + $P_{O_2}$) were set at 2.0 mTorr. It was about 1000 V at $P_{O_2}$ of 0 mTorr and it drastically decreased with the increase of $P_{O_2}$ up to 0.02 mTorr where discharge voltage was 650 V. Although the reason of the drastic decrease of the discharge voltage at $P_{O_2}$ of 0.02
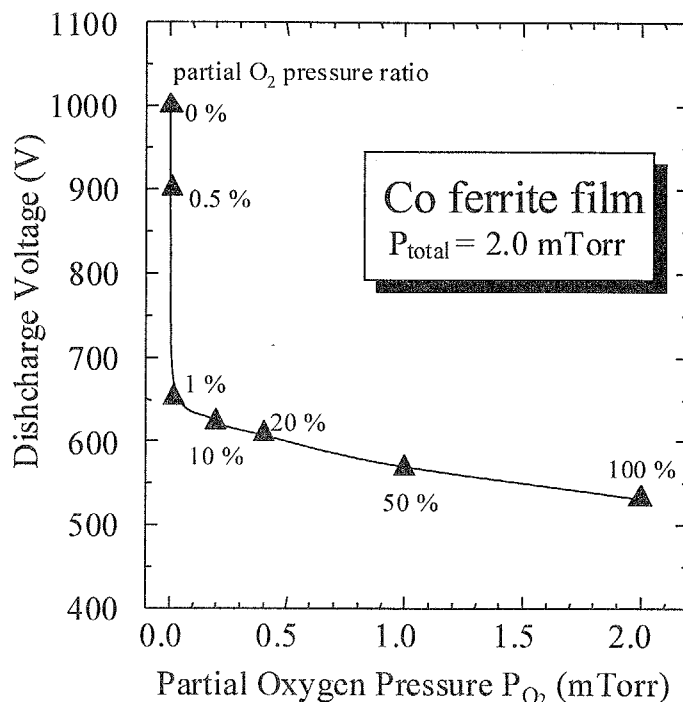
Fig. 4-3   $P_{O_2}$ dependence of discharge voltage. ($Co_{1.03}Fe_{1.97}O_y$ target)

mTorr is not clear, it seemed to be concerned with the oxidation condition of target surface. Discharge voltage slightly decreased at $P_{O_2}$ above 0.02 mTorr. The surface of as-reduced target was composed of metal atoms as well as oxides. Since the electron emission from oxides seems to be easier than that from metals and the ratio of oxides at target surface increased with the increase of $P_{O_2}$, the discharge voltage also decreased.

Fig. 4-4 shows the dependence of the deposition rate of Co ferrite film on $P_{O_2}$. Here, it should be noted that the film deposited without $O_2$ gas was composed of excessive growth crystal grains and its surface was very bumpy and therefore, the film thickness might be over-estimated. There was also drastic decrease at $P_{O_2}$ from 0 to 0.02 mTorr where the discharge voltage deceased. Since the deposition rate was linearly increased with increase of input power $P_{in}$, this decrease seemed to be caused by the decrease of
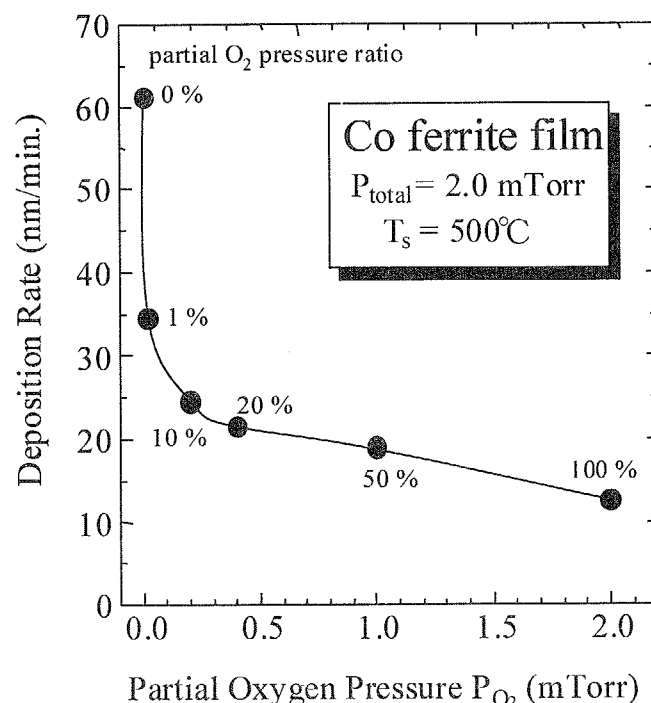
Fig. 4-4   $P_{O_2}$ dependence of deposition rate for Co ferrite film.

the discharge voltage as shown in Fig. 4-3.

To eliminate the effect of the decrease of $P_{in}$, the dependence of normalized deposition rate by input power $P_{in}$ on $P_{O_2}$ was investigated as shown in Fig. 4-5. Here, the drastic decrease was also observed at $P_{O_2}$ up to 0.2 mTorr. It seemed that this decrease of deposition rate was caused not only by the decrease of discharge voltage but also the change of the oxidation condition at target surface and the degree of growth of ferrite crystallites. Since the formation of oxide layer at target surface may progress at higher $P_{O_2}$, the sputtering yield from targets might be decreased and therefore, the deposition rate seemed to be decreased.
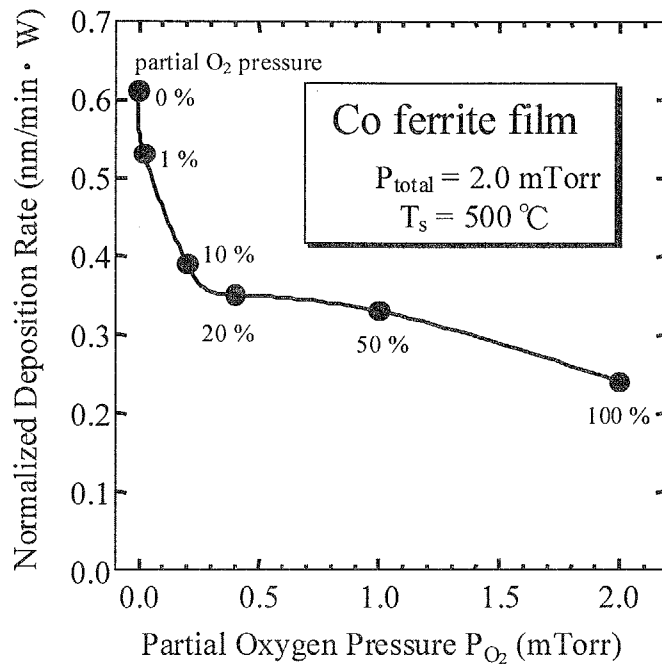
Fig. 4-5   $P_{O_2}$ dependence of normalized deposition rate by
input power.

In consequence, it was clarified that $P_{O_2}$ during deposition depends drastically not only discharge voltage but also the deposition rate. Therefore, it is important to adjust and to modify the $P_{O_2}$. In this study, Co ferrite single layer films were deposited in $P_{O_2}$ of 0.02 mTorr. Discharge current 0.1 A was applied to the target by direct current power supply and then discharge voltage decreased with increase of $P_{O_2}$ and they were 650 V for $P_{O_2}$ of 0.02 mTorr.

## 4-4 Partial oxygen gas pressure dependence

4-4-1 Crystallographic characteristics

As mentioned in 4-3, the deposition rates and discharges voltage depended on $P_{O_2}$ and these changes caused the change of crystallite orientation of the deposited films. Fig. 4-6 shows the change of XRD diagramss for Co ferrite films deposited at various $P_{O_2}$ and $T_s$ of 500°C. The film deposited at $P_{O_2}$ of 0.0 mTorr was composed of $\alpha$-$Fe_2O_3$ crystallites as well as spinel crystallites. Large (311) orientation was observed at $P_{O_2}$ of 0.02 mTorr. This (311) orientation corresponds to the formation of most closely packed structure of metallic ions parallel to the substrate plane. Fig. 4-7(a) shows the A and B site distribution in spinel ferrite crystallite structure with (001) orientation. Although they are not on the same plane exactly, they aligned almost in one plane. A ground plane of (311) plane was shown in Fig. 4-7(b) and we can see that A and B sites are closely packed in this plane. And this (311) peak is the largest one in powder X-ray diffraction diagram of spinel ferrite. Therefore, this peak seems to be observed mainly for polycrystalline spinel ferrite films. The peak intensity of (311) decreased with the increase of $P_{O_2}$ and (111) peak was observed at $P_{O_2}$ higher than 0.2 mTorr. Almost perfect (111) orientation was observed at $P_{O_2}$ of 2.0 mTorr even for the film with relatively small thickness because of lower deposition rate at higher $P_{O_2}$ as shown in Fig. 4-4. This (111) orientation which was observed at $P_{O_2}$ above 0.02 mTorr corresponds to the formation of the most closely packed plane of oxygen. From these results, it seemed that the change of orientation from (311) to (111) was caused by the increase of oxygen atoms at growing film surface.
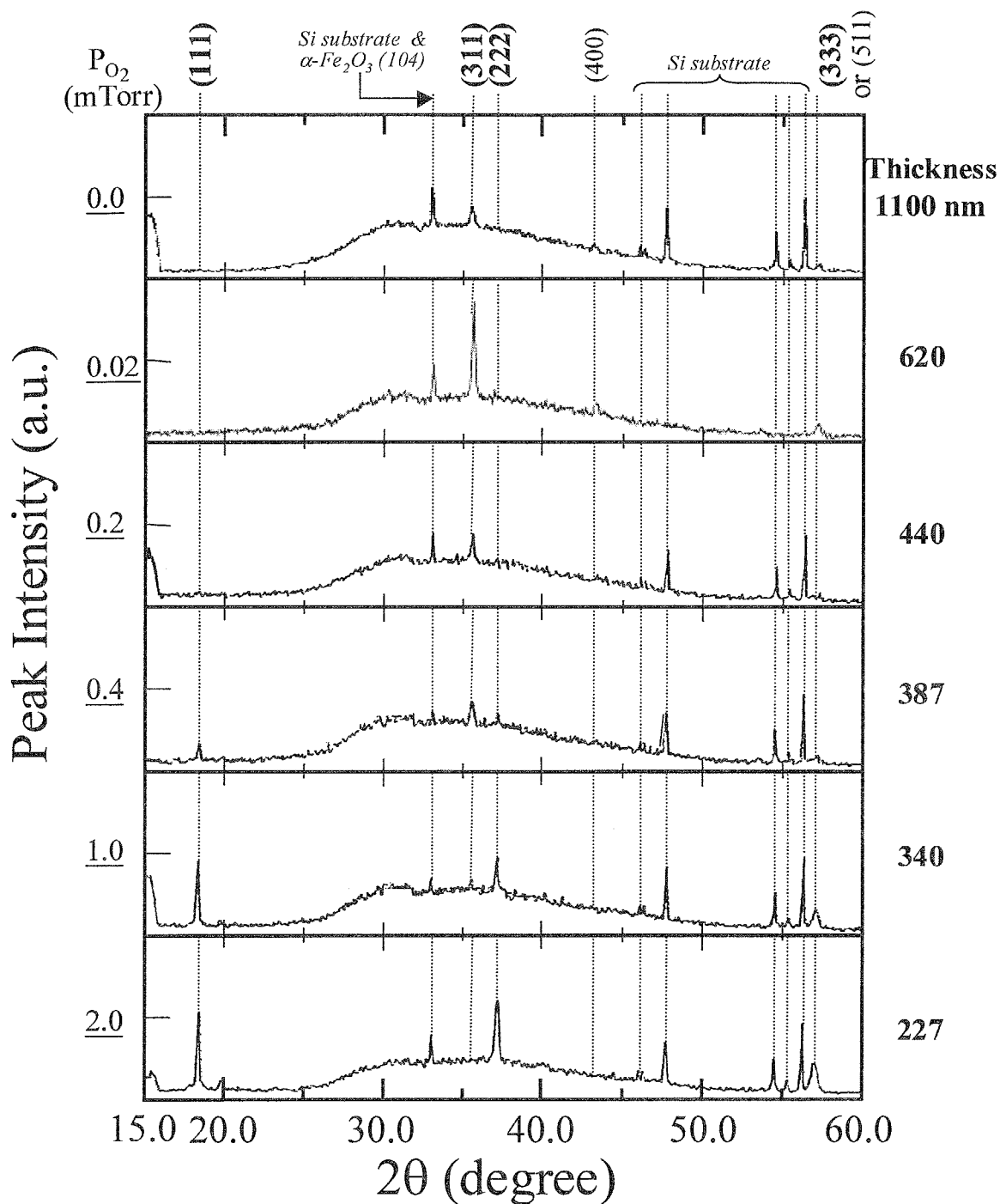
Fig. 4-6    XRD charts for Co ferrite single layer films deposited at
various $P_{O_2}$ and $T_s$ of 500℃.

○ : O2- site
A, B : A site, B site

O2-(311) plane
B-(311) plane
O2-plane

[001]

aspects view

quasi-closely
packed ion
plane
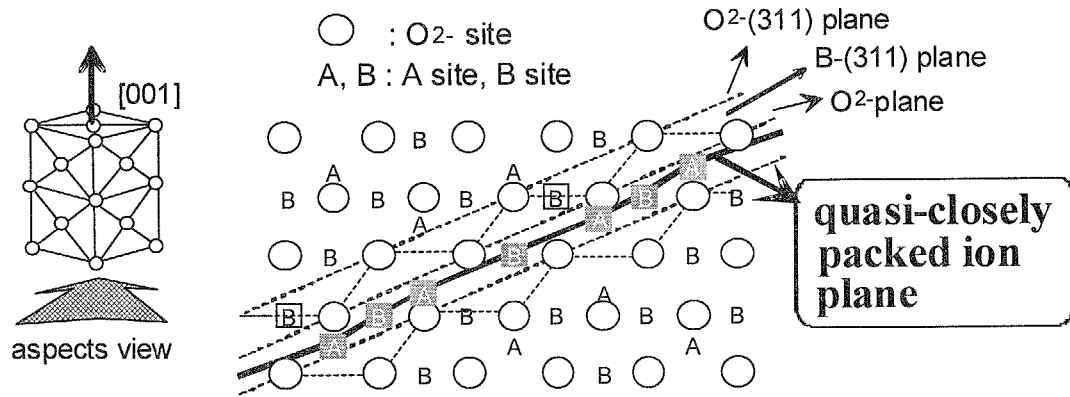
(a) Cross-section view from [1̄10]

[311]

O2-
B
O2-
A B A
B A B A
O2-
B
O2-
A B A
B A B A
O2-

$\frac{\sqrt{22}}{4}a$

(311) plane

$\frac{\sqrt{13}}{4}a$

A-site

B-site

neighbor O 2-

● : B-sites on (311) plane

Ⓜ , Ⓝ : A-sites above/below B-(311) plane
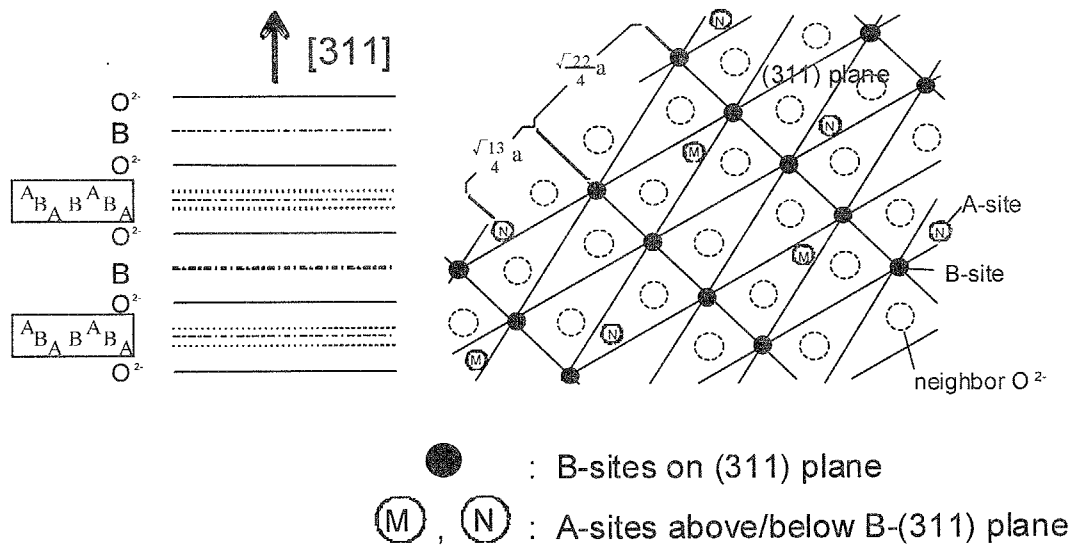
(b) Ground plane view

Fig. 4-7   A  and  B  site  distribution  in  spinel  ferrite  crystallite
structure with (001) orientation of (a) Cross section and (b)
Ground plane.

4-4-2 Magnetic characteristics

Fig. 4-8 shows the dependence of the saturation magnetization $4\pi M_s$ and the in-plane

and perpendicular coercivities $H_{c//}$ and $H_{c\perp}$ on $P_{O_2}$ at $T_s$ of 500°C. Although crystallite

orientation changed from (311) to (111) with the increase of $P_{O_2}$ as shown in Fig. 4-6,

$4\pi M_s$ was about 300 emu/cc constant. Although $H_{c//}$ was larger than $H_{c\perp}$ for whole

range of $P_{O_2}$ from 100 to 600°C, their difference became smaller with the increase of

$P_{O_2}$. This decreased seemed to be attributed to the change of crystallite orientation from

(311) to (111), because Co ferrite film with (111) orientation revealed almost the same

$H_{c//}$ and $H_{c\perp}$ as shown in Fig. 5-12.
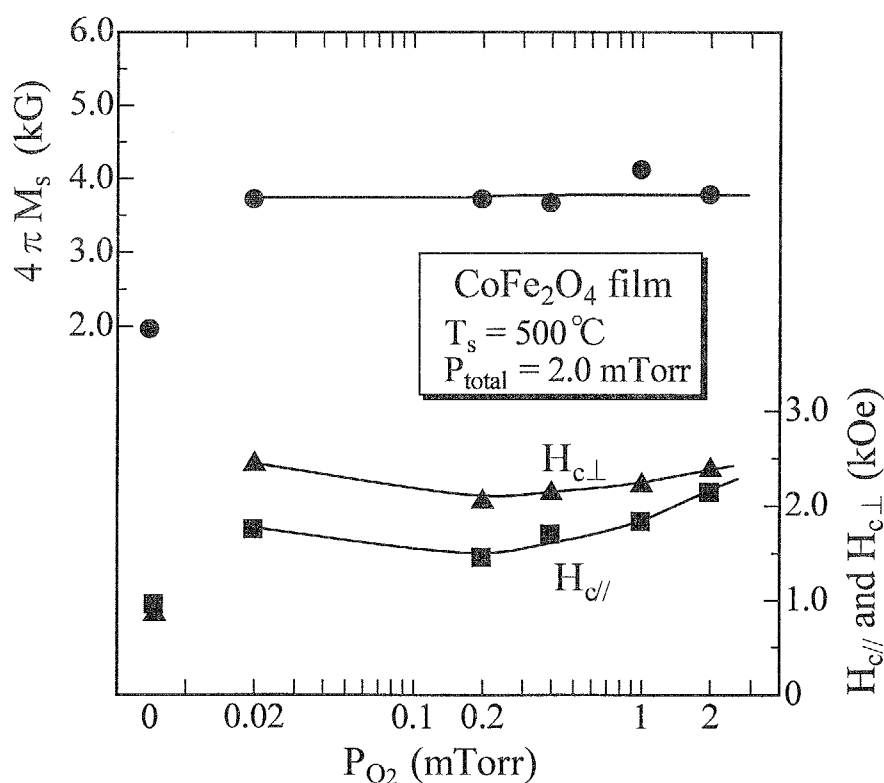


Fig. 4-8   Dependence of $4\pi M_s$ and $H_{c//}$ and $H_{c\perp}$ on $P_{O_2}$ at $T_s$ of 500°C.

## 4-5 Substrate temperature dependence

4-5-1 Crystallographic characteristics

Co ferrite single layer films were deposited in partial oxygen gas pressure $P_{O_2}$ of 0.02 mTorr at various substrate temperature $T_s$. Discharge current 0.1 A was applied to the target by direct current power supply and then discharge voltage was 650 V.

Fig. 4-9 shows the XRD diagram of Co ferrite single layer film deposited at $T_s$ of 500℃ and $P_{O_2}$ of 0.02 mTorr. There was only (311) peak, and this peak could observe at $T_s$ of 200℃ and above. Although its peak intensity increased with the increase of $T_s$ as shown in Fig. 4-10, other peaks were not observed at $T_s$ up to 400℃ and they were quite small even at $T_s$ of 500℃.

Fig. 4-11 shows the dependence of $<D>_{(311)}$ on $T_s$, where $<D>_{(311)}$ was calculated by Scherrer equation using (311) peak. While it was only 16 nm at $T_s$ of 200℃, it gradually increased with the increase of $T_s$ and it was about 35 nm even at high $T_s$ of 500℃.
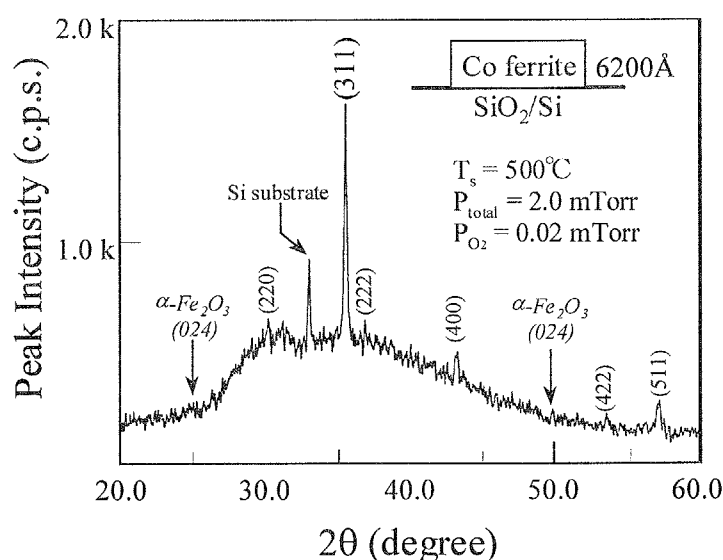


Fig. 4-9　XRD charts for Co ferrite single layer films deposited at $T_s$ of 500℃ and $P_{O_2}$ of 0.02 mTorr.
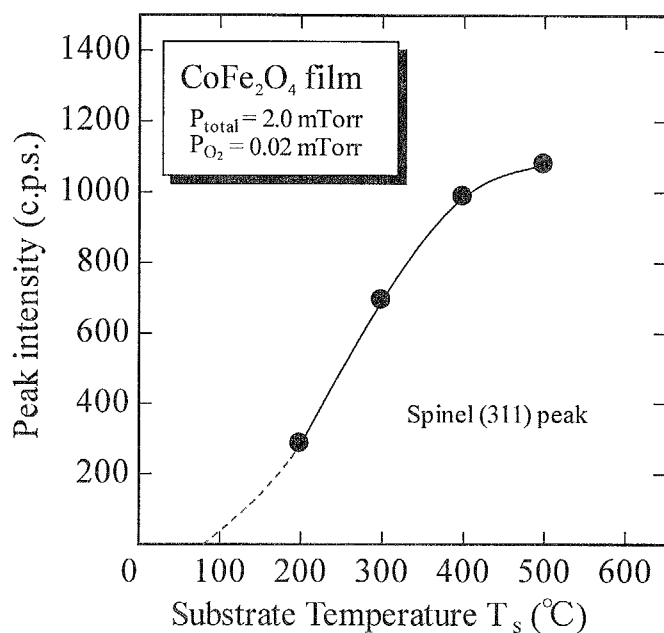
Fig. 4-10 Change of XRD peak intensity for Co ferrite single layer films deposited at various $T_s$ and $P_{O_2}$ of 0.02 mTorr.
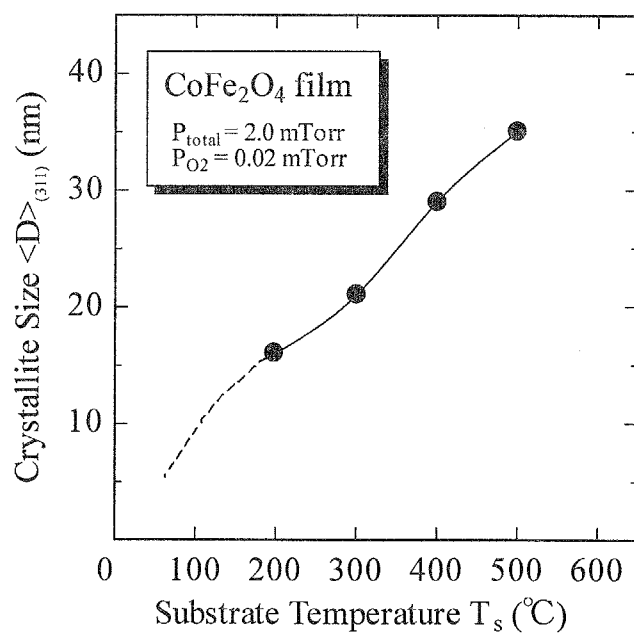


Fig. 4-11  Dependence of $<D>_{(311)}$ on $T_s$ at $P_{O2}$ of 0.02 mTorr.

4-5-2 Magnetic characteristics

Fig. 4-12 shows the change of B-H hysteresis loops measured by applying magnetic field to in-plane and perpendicular direction for Co ferrite films deposited at various $T_s$ and $P_{O_2}$ of 0.02 mTorr. Both of the in-plane and perpendicular B-H loops at $T_s$ of 300°C are not saturated. Although the in-plane orientation of magnetization seemed to be fairly superior than the perpendicular one at low $T_s$ up to 400°C, magnetization measured in perpendicular direction become close to the saturation at $T_s$ higher than 500°C. Co ferrite films seemed to show "isotropic like" magnetization when they were deposited at $T_s$ above 500°C. Anyway they were not perfectly saturated even at high $T_s$ of 600°C.
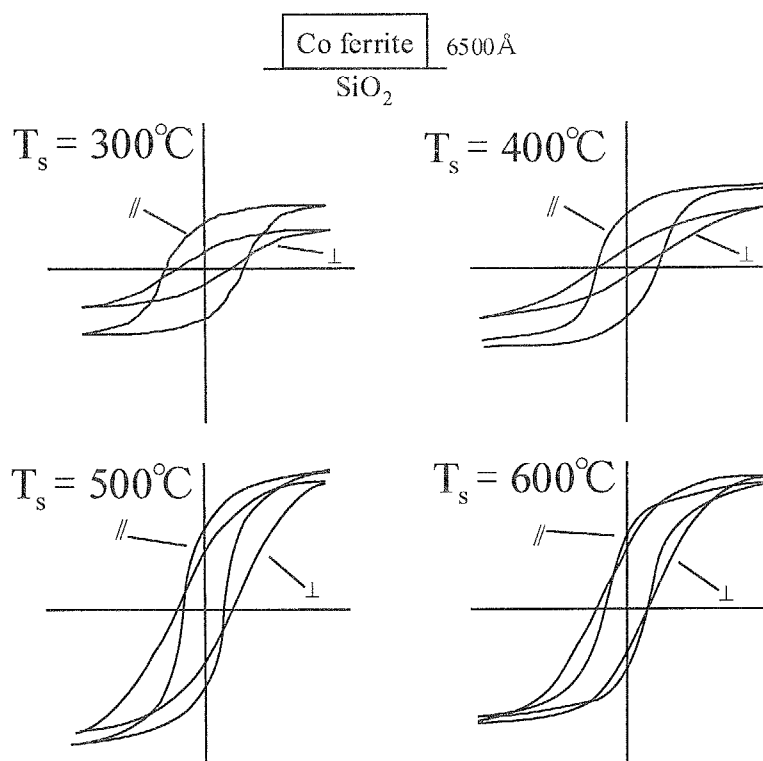


Fig. 4-12   Change of B-H loops of Co ferrite films deposited at various $T_s$ and $P_{O_2}$ of 0.02 mTorr.

Fig. 4-13 shows the dependence of $4\pi M_s$ and $H_{c//}$ and $H_{c\perp}$ on $T_s$ at $P_{O_2}$ of 0.02

mTorr. Although $4\pi M_s$ increased linearly with the increase of $T_s$, in which crystallite

size <311> increased as shown in Fig. 4-11, it was almost saturated at high $T_s$ of 600°C

and took the maximum value of 3.7 kG. It was only about 70 % of bulk Co ferrite. Here,

it should be noted that Co ferrite films deposited in this study, has extremely large

magneto crystalline anisotropy and the applying field as high as 12 kOe was not enough

to make the samples saturated perfectly. It means that $4\pi M_s$ was evaluated smaller than

its intrinsic value. Here, $4\pi M_s$ means the magnetization, which measured by applying

field of 12 kOe. $H_{c//}$ took the maximum value of 3.8 kOe at $T_s$ as high as 300°C and

then decreased to the minimum value of 1.75 kOe at $T_s$ of 500°C. This decrease seemed

to be caused by the growth of crystallites as shown in Fig. 4-11. On the other hand, $H_{c\perp}$

were gradually decreased and it became larger than $H_{c//}$ at $T_s$ above 500°C.
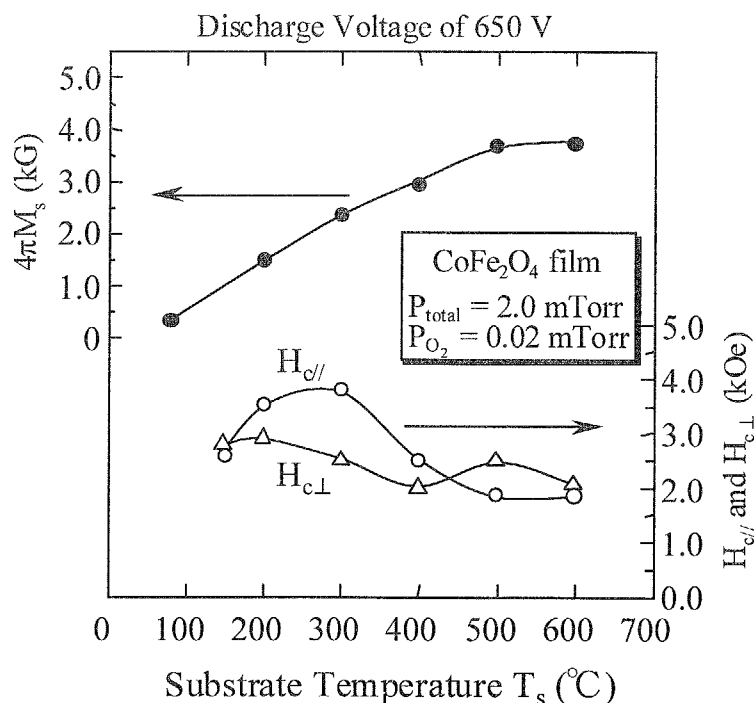


Fig. 4-13  Dependence of $4\pi M_s$ and $H_{c//}$ and $H_{c\perp}$ on $T_s$ at $P_{O_2}$ of 0.02 mTorr.

## 4-6 Summary

In this study, Co ferrite single layer films were deposited by the facing targets sputtering apparatus in the mixture of Ar and $O_2$ and the following results were obtained:

1) Both of the discharge voltage and the deposition rate decreased drastically with mixing of very small amount of oxygen and those at $P_{O_2}$ of 0.02 mTorr ($Ar:O_2 = 99:1$) was about 65 % of those at $P_{O_2}$ of 0.0 mTorr. The normalized deposition rate by input power was also decreased with the increase of $P_{O_2}$ and that at $P_{O_2}$ of 2.00 mTorr ($Ar:O_2 = 100:0$) was about 37 % of those at $P_{O_2}$ of 0.0 mTorr.

2) Crystallite orientation of the deposited films changed from (311) to (111) with the increase of $P_{O_2}$ from 0.02 to 2.0 mTorr at substrate temperature $T_s$ of 500°C.

3) The deposited films were composed of crystallites with (311) orientation. The maximum $4\pi M_s$ was about 3.7 kG(about 70 % of bulk value) at $T_s$ of 600°C. Both of the in-plane and perpendicular coercivities, $H_{c//}$ and $H_{c\perp}$, decreased from 3.8 to 1.8 kOe and 2.8 to 2.1 kOe, respectively, with the increase of $T_s$ from 300 to 600°C.

Although moderately high coercivity above 3.0 kOe was easily obtained at relatively low $T_s$ below 400°C, $4\pi M_s$ was not sufficient even at high $T_s$ above 500°C. It corresponds to insufficient crystallite growth. In conventional type of rigid disks glass slide disk are mainly used as substrates and its heat resistant temperature is at most 350°C. Therefore, it is necessary to crystallize Co ferrite film at $T_s$ lower than 300°C for the application as recording layer of rigid disks.

In the next chapter ZnO(00n) layer is used for the epitaxial growth of Co ferrite layer and their crystallographic and magnetic characteristics would be investigated precisely.

# Chapter 5

# Co ferrite/ZnO Double Layered Films

## 5-1 Introduction

A spinel type of cobalt ferrite with the composition of $CoFe_2O_4$ is well known to possess excellent chemical stability and high corrosion resistivity. The Co ferrite thin films are very attractive because they exhibit high coercivity due to their large magnetocrystalline anisotropy, large Faraday rotation angle, and magnetostriction for new devices such as magnetic recording media with ultra-high density, magneto-optical wave guides[1], magnetic static wave devices[2] and surface acoustic wave transducers. Although they have a lot of possibilities applying to the above mentioned devices, it has been difficult to prepare Co ferrite films with sufficient crystallinity at low substrate temperature and without post-annealing. And high substrate temperature above 500℃ was necessary to possess well magnetic characteristics which are suitable for recording layers in rigid disks, such as large saturation magnetization $4\pi M_s$ above 3.5 kG and moderately high coercicity $H_c$ abobe 2.0 kOe.

Thin film of ZnO is very famous as oxide electrode with transparency and are tried to apply for window electrode in solar cell device. It has been reported that the layers of a spinel type of Mn-Zn ferrites and a magnetoplumbite type of Ba ferrites(Ba-M) with excellent crystallite orientation were deposited on ZnO underlayer with (00n) orientation

[1] J.W.D.Martens: J.Appl.Phys.59, pp.3820(1986)

[2] A.D.Fisher: Circuits System & Signal Process, 4, pp.265

owing to the epitaxial effect [3,4].

In this study, the bilayered films composed of Co ferrite and ZnO layers were deposited on the plasma-free substrates by using a facing targets sputtering(FTS) apparatus and their structure and magnetic characteristics were investigated for application in magnetic recording media with ultra-high density.

## 5-2 Deposition conditions of ZnO and Co ferrite layers

All doublelayered films were prepared by using FTS apparatus for multilayered films as shown in Fig. 5-1. As it has two pairs of facing targets in the same chamber, the multilayered films can be prepared without breaking the vacuum. All specimen films were started after pre-sputtering of 1 hour. The Ar and $O_2$ gases were introduced individually into the chamber as working gases.

Table 5-1 shows deposition conditions for both ZnO and Co ferrite layers. At first, the ZnO layer was deposited from a pair of pure Zn(99.99%) targets on Si wafer substrates with thermal oxidized surface layer $15 \times 15$ mm$^2$ in area by reactive sputtering using Ar and $O_2$ as sputtering gases for 30 minutes. ZnO films were deposited by Matsuoka et al. in only oxygen atmosphere at $P_{O_2}$ of 2.0 mTorr. Although excellent c-axis orientation, $\Delta\theta_{50} < 1.9$degree, was attained for this condition, the formation of oxides at target surface was superior than the sputter etching of it. Therefore, discharge characteristics and deposition conditions were changed in each deposition even at the same conditions. While pre-sputtering by only Ar gas was effective to remove oxides at

[3] M.Matsuoka, Y.Hoshi and M.Naoe: IEEE Trans. on Mag., 18[6], pp.1119-1121(1982)

[4] M.Naoe, S.Yamanaka and Y.Hoshi: IEEE Trans. on Mag., 16, p646(1980)

targets, hysteresis phenomena of oxidation at target surface should be considered. Moreover, sputtered Zn by only Ar is likely to be condensed and adheres on chamber wall, so that it made background pressure worse seriously. Therefore, in my study, gas mixture of Ar and $O_2$ was used as sputtering gas. After the deposition of ZnO underlayer, deposition conditions were changed for those for Co ferrite layer. Subsequently, Co ferrite layer was deposited on the ZnO one at various substrate temperature $T_s$ for 3 hours.

A pair of Co ferrite($Co_2Fe_3O_4$) disk plates 90 mm$\phi$ in diameter 7 mm in thickness prepared by dry ceramic technique process were used as targets for the deposition of Co ferrite layers. The deposition conditions of Co ferrite layers were almost same as that of Co single layer film as mentioned in Chapter 4.

For the investigation of $T_s$ dependence, $P_{O_2}$ was set at 0.02 mTorr constant, i.e. partial pressure ratio of 1.0 %, and $T_s$ was changed in the range from 90(without heating) to 600 °C.

Film composition were evaluated by ICPS. Crystallite sizes <D> of Co ferrite and ZnO layers were calculated by X-ray diffraction peak profiles corresponding to (111) orientation of Co ferrite and (001) orientation of ZnO layers. Magnetic characteristics such as $4\pi M_s$ and $H_c$ were measured by using a vibrating sample magnetometer.
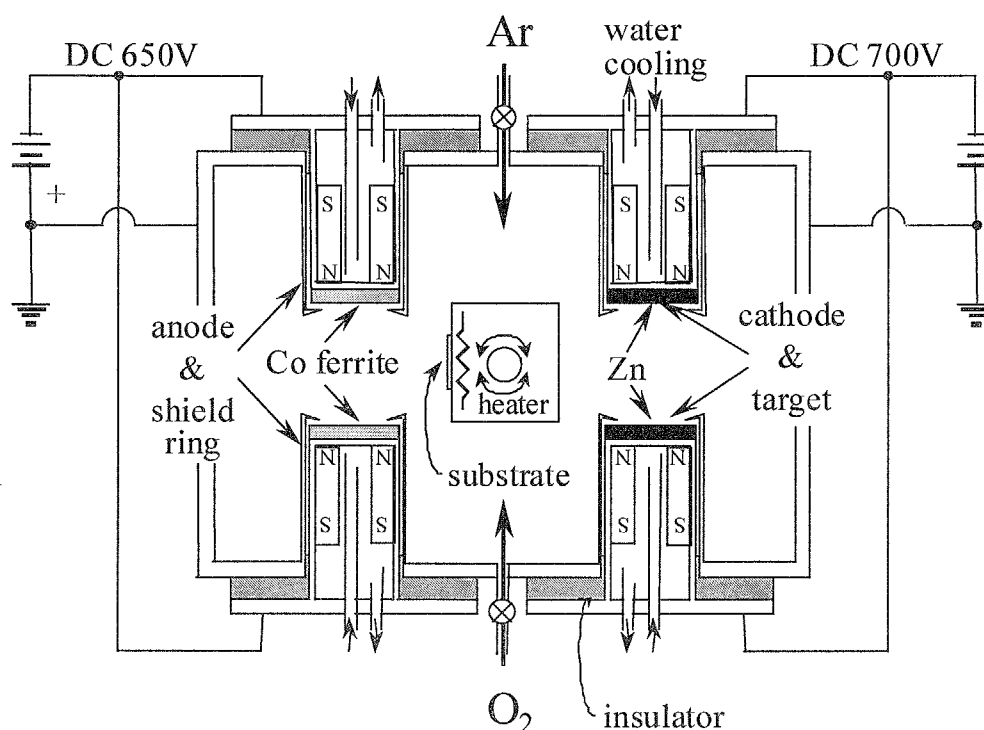
Fig. 5-1   Schematic illustration of the facing targets sputtering apparatus for multi-layered films.

Table 5-1    Deposition conditions of ZnO and Co ferrite layers.

|  | ZnO layer | Co ferrite layer |
|---|---|---|
| Target composition | Pure Zn (99.99%) | $Co_{1.03}Fe_{1.97}O_y$ |
| Substrate material | $SiO_2/Si$ | $ZnO/SiO_2/Si$ |
| Total gas pressure $P_{total}$ | 2.0 mTorr | 2.0 mTorr |
| Partial oxygen gas pressure $P_{O_2}$ | 1.0 mTorr | 0.02mTorr |
| Substrate temp. $T_s$ | 300℃ | without heating – 600℃ |
| Discharge current $I_d$ | 0.10 A | 0.10 A |
| Deposition time | 30～60 min. | 120～180 min. |

## 5-3 Crystallite orientation of ZnO film

ZnO is non-magnetic material and has high photoconductivity, and the electron conductivity changes from insulator to semiconductor with the amount of the lack of oxygen. It has würtzite structure whose lattice constant a and c were 3.243 and 5.195 Å, respectively as shown in Fig. 5-2. There is the most closely packed structure of $O^{2-}$ ions on c plane, i.e. (001) plane, and $Zn^{2+}$ ions are sited in tetrahedral sites. The distance between the closest atoms in most closely packed plane of oxygen in (00n) plane, 3.243 Å, is close to that in (111) plane of Co ferrite, 2.963 Å as shown in Fig. 5-3. Since the misfit between them is only 9 % and is within the maximum limit enable to epitaxial growth (<15 %), the epitaxial growth of Co ferrite layer with (111) orientation was respected by using ZnO(00n) underlayer.

Although ZnO layer changes from insulator to semiconductor with the amount of lack of oxygen, ZnO layer deposited in the condition as shown in Table 5-1 was almost perfect insulator and it revealed perfect c-axis orientation as shown in Fig. 5-4.
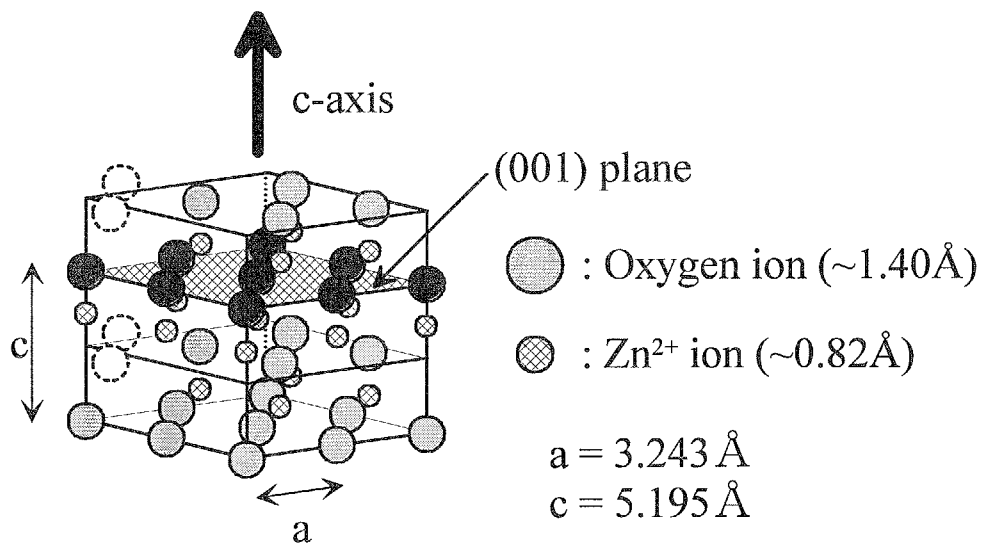


Fig. 5-2  Crystallite structure of ZnO.

Co ferrite
Spinel (fcc)

2.463 Å

ZnO
Würtzite (hcp)

a = 3.242 Å
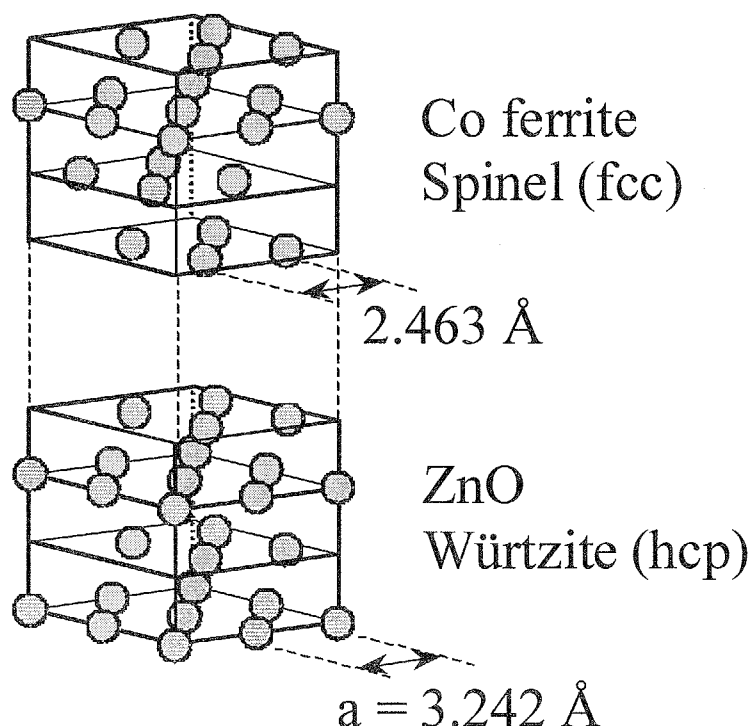
Fig. 5-3    Schematic illustration of epitaxial growth of ZnO
and Co ferrite layers.

This c-axis orientation was observed even at very small layer thickness of 100 Å.

Crystallite size $<D>_{ZnO(002)}$ calculated by Scherrer equation was about 35 nm and the full

width of half maximum rocking profiles $\Delta\theta_{50\_ZnO(002)}$ was about 2.5-3.0 degree for

simple ZnO films 300 nm thick.

## 5-4 SEM images of Co ferrite layer

Fig. 5-5(a) and (b) show the scanning electron micrographs (SEM) of the films

deposited at $T_s$ of 300 and 500°C, respectively. The surface appearance was a little

rough even at relatively low $T_s$ of 300°C. In (b), very rough surface was observed

resulting from excessive growth of crystallites.
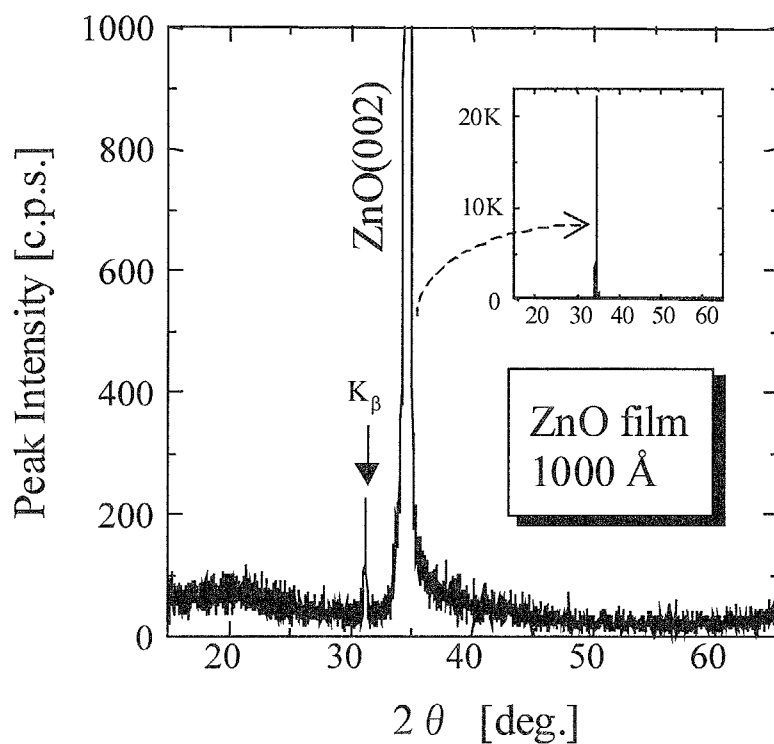
Fig. 5-4 XRD diagram of ZnO film deposited on SiO₂/Si substrate. ($T_s$ = 300°C, $P_{total}$ = 2.0 mTorr, $P_{O_2}$ = 1.0 mTorr)
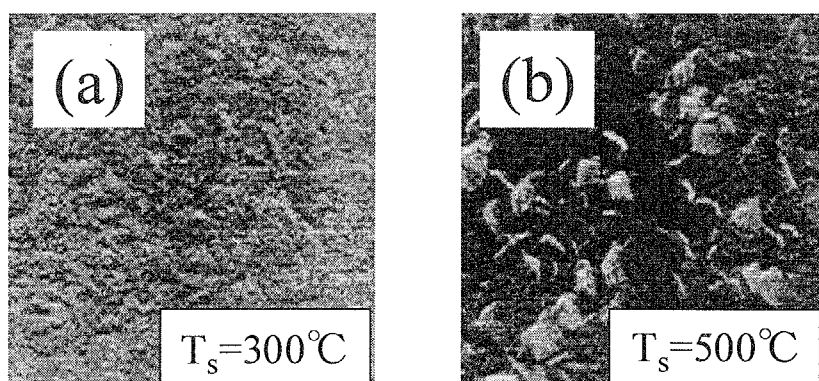


Fig. 5-5 SEM images of Co ferrite layer deposited at $T_s$ of (a)300°C and (b)500°C, respectively.

## 5-5 Crystallographic characteristics of Co ferrite/ZnO films

### 5-5-1 Co ferrite layer

The Co ferrite layers deposited on highly crystallized ZnO(001) underlayers were composed of crystallite with almost perfect orientation of the spinel (111) plane, and (111) orientation was observed even in films prepared at $T_s$ as low as 80℃ as shown in Fig. 5-6(a). On the other hand, Co ferrite layers deposited directly on $SiO_2$/Si substrates were composed of the crystallites with random or a weak orientation of the spinel (311) plane. These orientations of Co ferrite layer were observed even at $T_s$ as high as 500℃ as shown in Fig. 5-6(b). This indicates that the ZnO underlayer is very suitable for extremely good epitaxial growth and orientation of Co ferrite crystallites with (111) orientation.

All films deposited at various $T_s$ from 90 to 600℃ with and without ZnO underlayer by FTS apparatus had almost the same stoichiometric coefficient of $CoO \cdot Fe_2O_3$. It indicated that FTS system could achieve excellent sputtering deposition without a composition difference between targets and films.
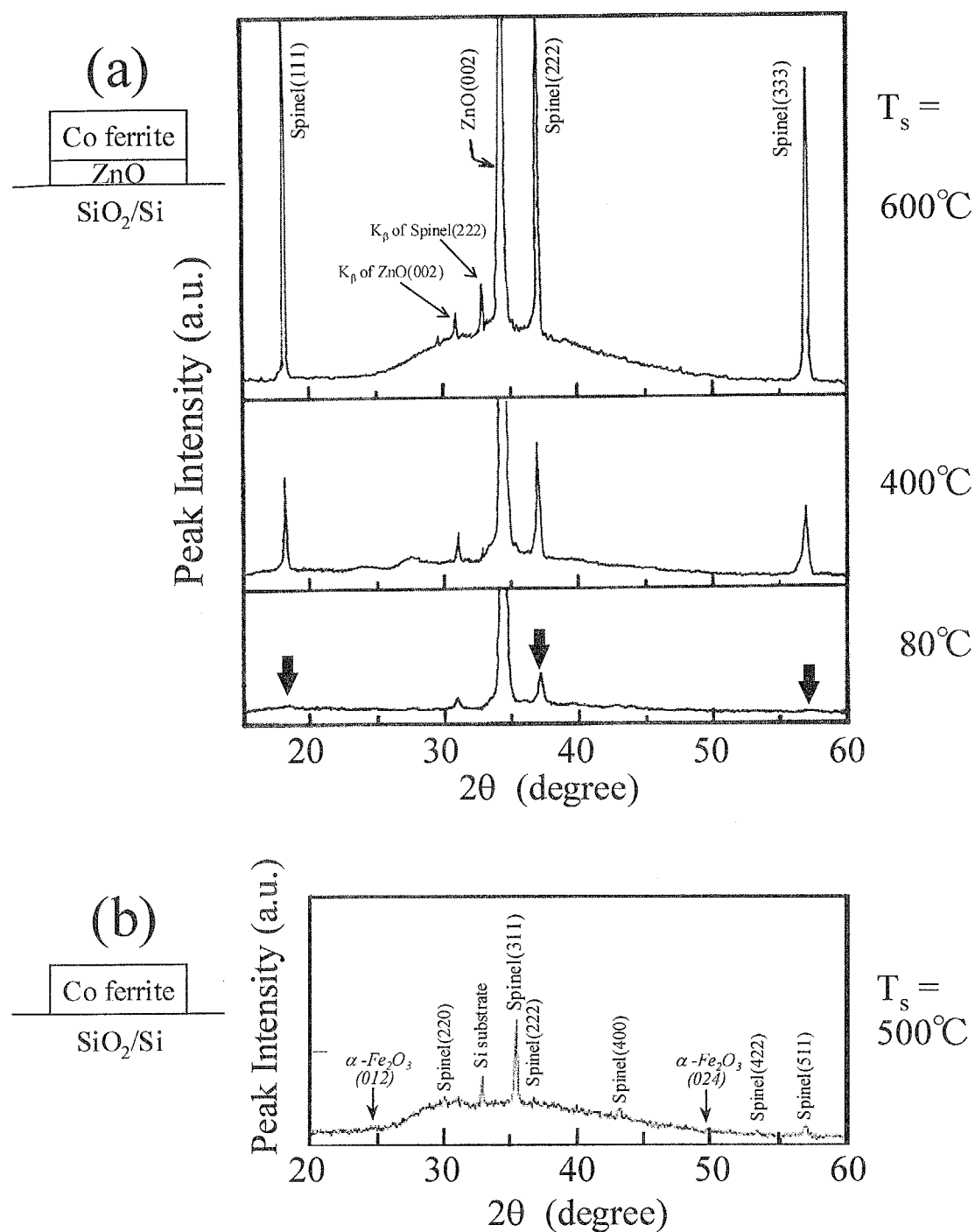
Fig. 5-6    X-ray diffraction diagrams of (a) Co ferrite/ ZnO films deposited at various $T_s$ and (b)Co ferrite single layer film deposited directly on $SiO_2/Si$ substrate at $T_s$ of 500°C.

Fig. 5-7 shows the $T_s$ dependence of the (222) inter-planar spacing $d_{spinel(222)}$ of Co ferrite layer. The $d_{spinel(222)}$ increased with increase of $T_s$ up to $400\,^\circ C$ and then drastically decreased. As the thermal expansion coefficient of Co ferrite layer is larger than that of ZnO layer and the films deposited at $T_s$ above $400\,^\circ C$ had small cracks on their surface and, it seemed that the Co ferrite layers underwent the increasing compressive stress in the in-plane with increase of $T_s$ up to $400\,^\circ C$.
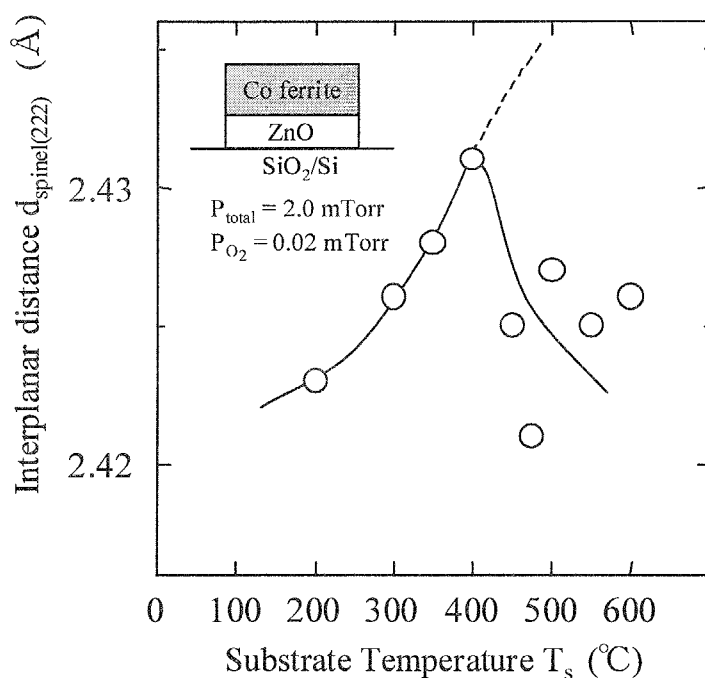


Fig. 5-7    $T_s$ dependence of (222) interplanar spacing d(222) of Co ferrite crystallites.

Fig. 5-8 shows the $T_s$ dependence of the crystallite size $<D>_{spinel(222)}$ which was calculated by Scherrer's equation and the full width of half maximum of rocking profiles of (222) plane $\Delta\theta_{50\_spinel(222)}$ of Co ferrite layers. $<D>_{spinel(222)}$ decreased gradually with increase of $T_s$ up to 450℃ and then increased steeply at $T_s$ of 500℃. On the other hand, $\Delta\theta_{50\_spinel(222)}$ increased at $T_s$ up to 450℃ and then took the maximum value of 4.4° at $T_s$ of 475℃ and decreased and exhibited the minimum value of 1.4° at $T_s$ of 600℃. Since the Co ferrite layer seemed underwent the compressive stress at $T_s$ up to 450℃ as mentioned above, $<D>_{spinel(222)}$ decreased and $\Delta\theta_{50\_spinel(222)}$ increased with increase of $T_s$ up to 450℃.
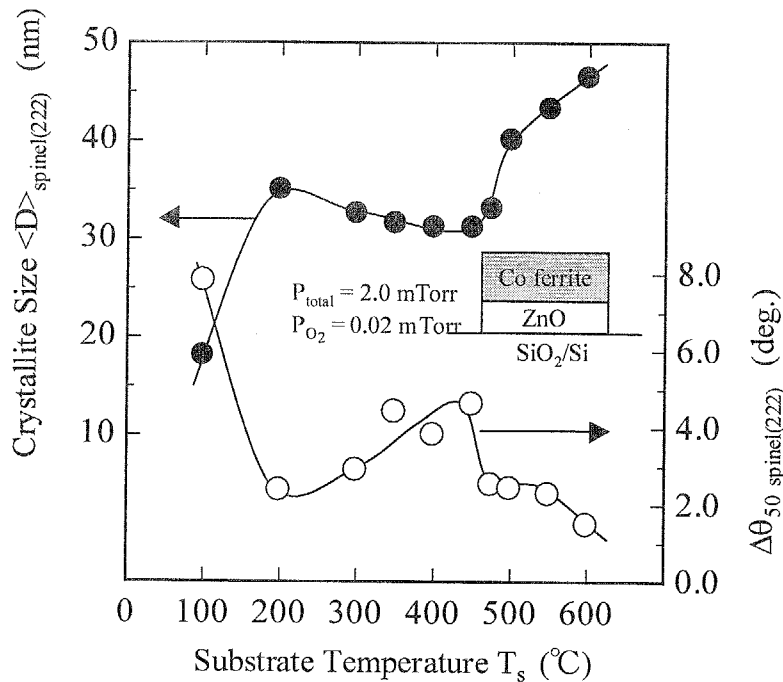


Fig. 5-8    $T_s$ dependence of grain size $<D>_{spinel(222)}$ and the full width at half maximum of rocking profiles $\Delta\theta_{50\_spinel(222)}$ of Co ferrite layers.

## 5-5-2 ZnO underlayer

$<D>_{ZnO(002)}$ and $\Delta\theta_{50\_ZnO(002)}$ of ZnO underlayer were calculated for ZnO(002) peak which was observed in the X-ray diffraction diagrams of Co ferrite/ZnO films, as seen in Fig. 5-9. Although $<D>_{ZnO(002)}$ was almost constant for $T_s$ below 550°C and increased at $T_s$ of 600°C, $\Delta\theta_{50\_ZnO(002)}$ steeply increased with increase of $T_s$ in the range from 400 to 500°C. It seemed that the interdiffusion between Co ferrite and ZnO layers occurred at $T_s$ above 400°C and therefore, $\Delta\theta_{50\_ZnO(002)}$ once decreased at $T_s$ of 300°C and then steeply increased at $T_s$ from 400 to 500°C. Such steep changes of crystallographic characteristics were also observed for Co ferrite layer at almost the same range of $T_s$. It seemed that although the growth of spinel crystallites were restrained by the crystallite size of ZnO layer, it was able to be grown up without the restraint of crystallite size of ZnO layer at $T_s$ above 500°C.
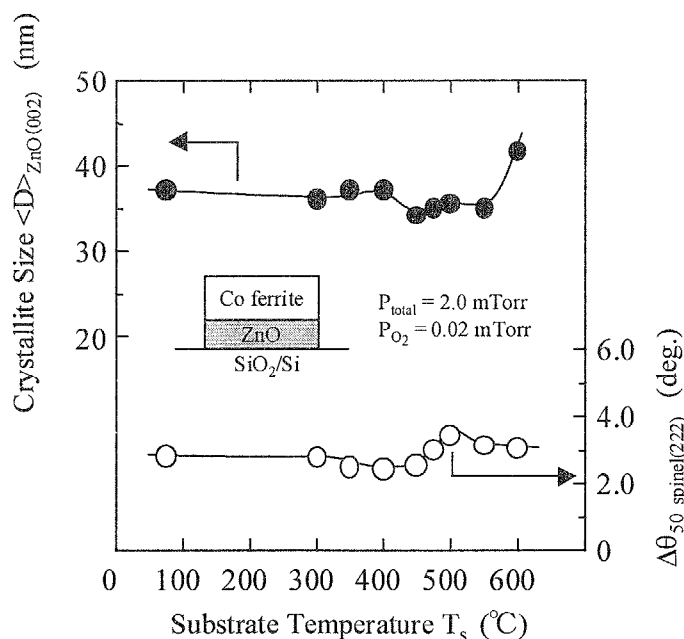


Fig. 5-9 $T_s$ dependence of grain size $<D>_{ZnO(002)}$ and the full width of half maximum of rocking profiles $\Delta\theta_{50}$ of ZnO Layers.

## 5-6 Magnetic characteristics

Fig. 5-10 shows the B-H hysteresis loops of Co ferrite/ZnO films deposited at $T_s$ from 300 to 600°C. Both of $H_{c//}$ and $H_{c\perp}$ decreased with the increase of $T_s$ and they took almost the same value for all $T_s$. However, the films prepared at high $T_s$ above 400°C had their easy axis in the in-plane directions because their B-H loop in in-plane direction were saturated and those in perpendicular direction were not fully saturated.

Fig. 5-11 shows the $T_s$ dependence of $4\pi M_s$ of Co ferrite/ZnO films. Although $4\pi M_s$ increased with increase of $T_s$ in the whole range of $T_s$, the steep increase was observed in the narrow range from 450 to 500°C and took the maximum value of 4.6 kG at $T_s$ of 600°C. Since such a steep increase was also observed in the $T_s$ dependence of $<D>_{spinel(222)}$ as shown in Fig. 5-8, it seemed that this steep increase of $4\pi M_s$ seemed to be attributed to the increase of the volume fraction of ferrimagnetic crystallites in the Co ferrite layer. It also seemed that the substitutions of $Zn^{2+}$ ions on to the tetrahedral sites of Co ferrite layer due to the diffusion from ZnO underlayer also contributed to the increase of $4\pi M_s$ at $T_s$ above 500°C. Since the B-H hysteresis loops of the films which were deposited at $T_s$ below 450°C were not fully saturated even when the maximum field of 12 kOe was applied to the specimen films as shown in Fig. 5-10, $4\pi M_s$ of these films seemed to be estimated lower than its real saturated value.
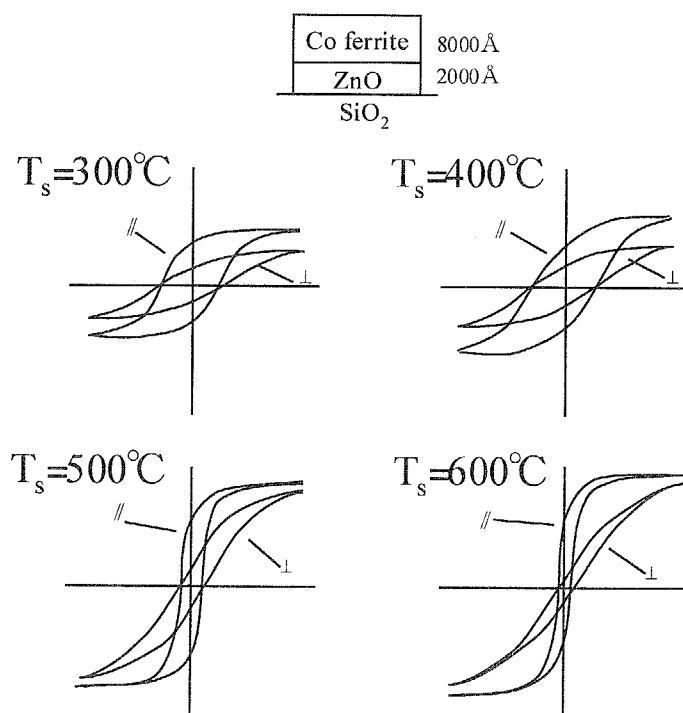
Fig. 5-10  B-H hysteresis loops of Co ferrite/ZnO films
deposited at various $T_s$.
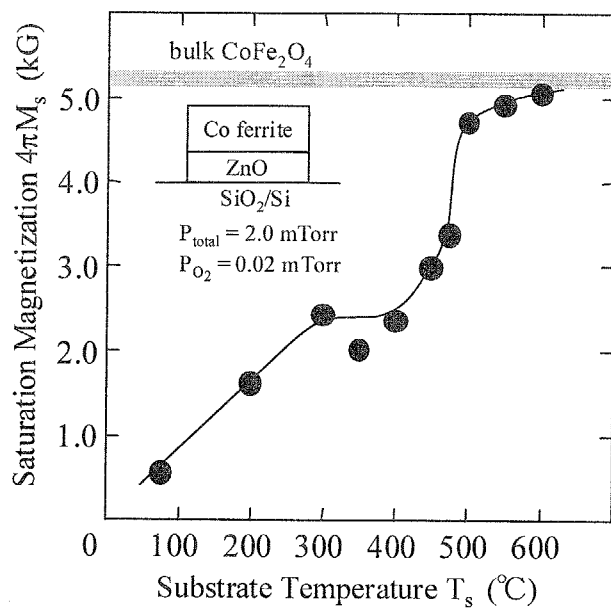


Fig. 5-11  $T_s$ dependence of $4\pi M_s$ of Co ferrite/ZnO films
and Co ferrite films.

Fig. 5-12 shows the $T_s$ dependence of the in-plane and perpendicular coercivities $H_{c//}$ and $H_{c\perp}$ of Co ferrite/ZnO films. $H_{c//}$ and $H_{c\perp}$ took almost the same value at various $T_s$ and their figures were very similar each other. As <100> and <111> axes of spinel type of Co ferrite are easy and hard axes, respectively, as shown in Fig. 5-13, these films seem to have both of easy and hard axes in in-plane and perpendicular to the substrate, respectively. They took the same maximum values of 3300 Oe at $T_s$ of 300℃. Both $H_{c//}$ and $H_{c\perp}$ decreased with increase of $T_s$ in the range above 300℃ and exhibited minimum values of 480 and 500 Oe, respectively, at $T_s$ of 600℃.
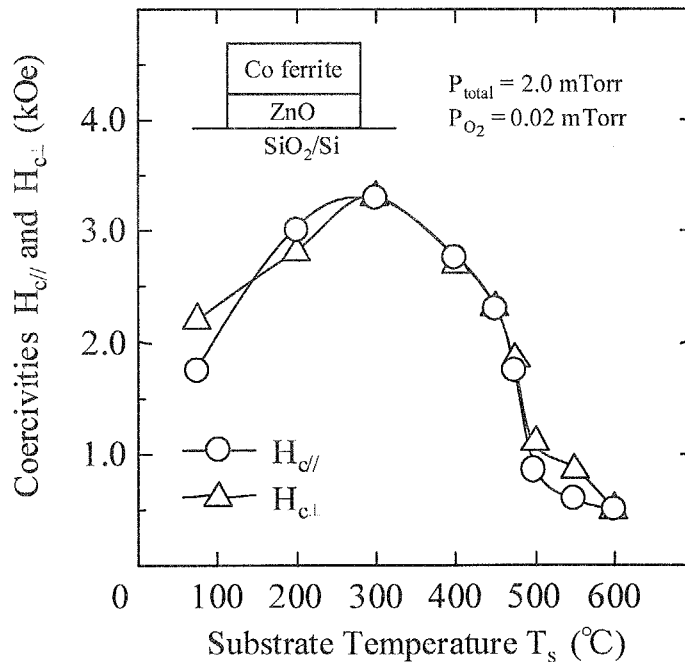
Fig. 5-12    $T_s$ dependence of $H_{c//}$ and $H_{c\perp}$ of Co ferrite/ZnO films.

easy axis <100>            hard axis<111>
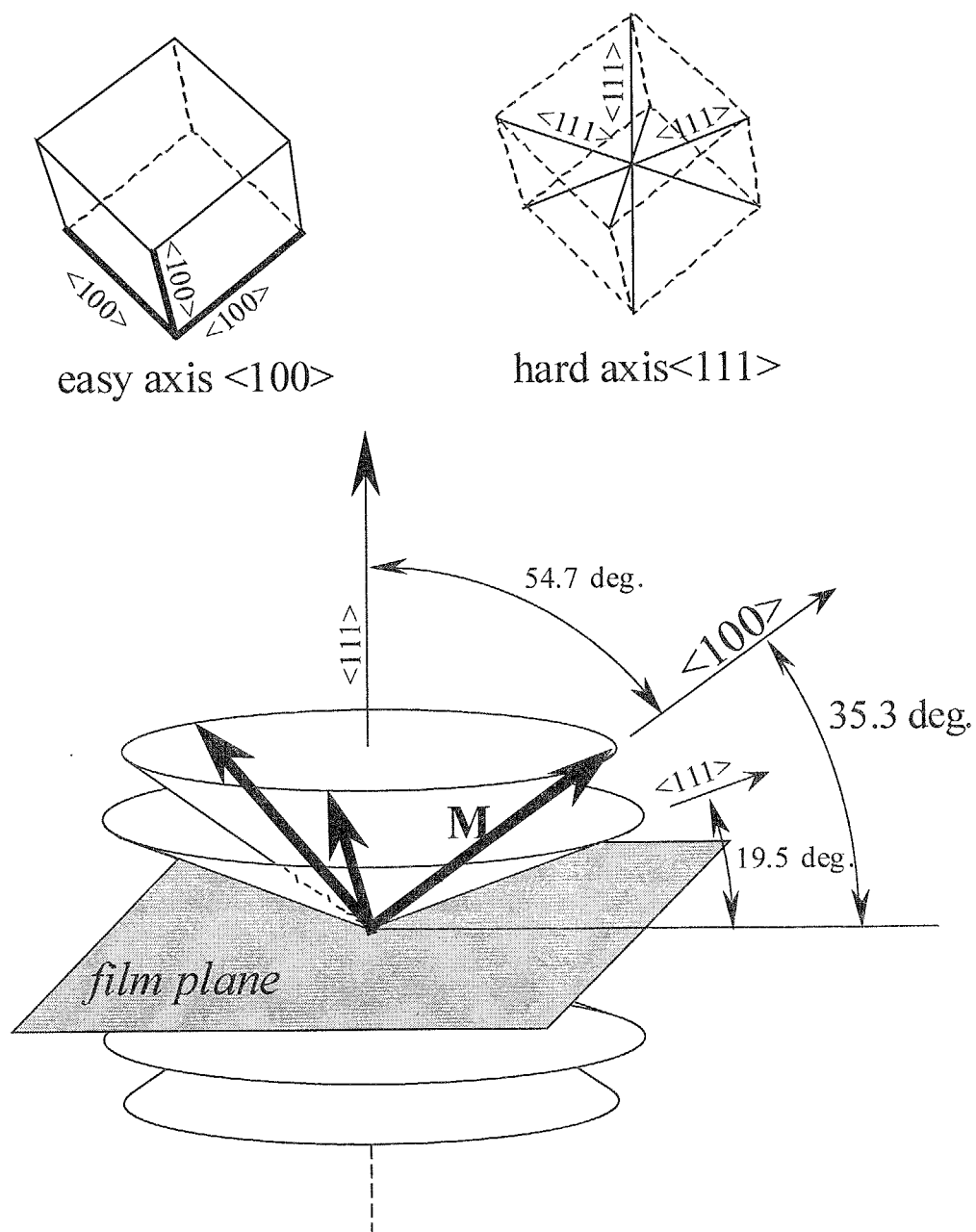
Fig. 5-13    Sketch of easy and hard axes, <100> and <111>, of Co
ferrite crystallites with (111) orientation.

$4\pi M_s$ and $H_c$ drastically increased and decreased, respectively, with increase of $T_s$ from 450 to 500°C. Such a steep change seemed to be attributed to the increase of the volume fraction of ferrimagnetic crystallites in the whole Co ferrite layer as well as the increase of $<D>_{spinel(222)}$ in the same range of $T_s$, as shown in Fig. 5-8. On the other hand, the decrease of both $H_{c//}$ and $H_{c\perp}$ seemed to be attributed to the decrease of distance and the enhancement of magnetic coupling among the isolating ferrimagnetic crystallites in the Co ferrite ferrite layer. In addition, the decrease may be caused by the change of the magnetocrystalline anisotropy due to the change in distribution of metallic ions among the sites in ferrite lattice and the substitution of $Zn^{2+}$ ions on to tetrahedral sites.

Squareness ratios were about 0.65 at $T_s$ below 450°C. They decreased for $T_s$ above 450°C and were about 0.5 at $T_s$ of 600°C.


## 5-7 Summary

The doublelayered films composed of Co ferrite and ZnO layers have been deposited using the facing targets sputtering(FTS) apparatus and their $T_s$ dependence of crystallographic and  magnetic characteristics have been investigated. The results obtained in this study were as follows;


1)   SEM images revealed that the film surface was not smooth at relatively low $T_s$ of 300°C  and the film was composed of large grain with diameter of several 100 nm at $T_s$ of 500°C.

2)   Apparent orientation of spinel (222) was observed even at very low substrate

temperature $T_s$ of 90℃, i.e. without intentional heating.

3)    The steep increase of $<D>_{spinel(222)}$ of Co ferrite layer at $T_s$ of 500℃  cause the steep increase of the saturation magnetization $4\pi M_s$ and the decrease of coercivity $H_c$.

4)    Although large $4\pi M_s$ of 4.6 kG was obtained at $T_s$ of 500℃, $H_c$ was smaller than 1.0 kOe and too small to be used as recording layer of rigid disks.

5)    Since $H_{c//}$ and $H_{c\perp}$ took almost the same value at various $T_s$ from 90 to 600℃, this films have a possibility to be applied as isotropic magnetic recording layer.


Consequently, the usage of ZnO underlayer for Co ferrite layer was effective to decrease the crystallization temperature of ferrite layer and for eptaxial growth of crystallites with (111) orientation. Although the isotropic magnetic orientation was obtained, ZnO underlayer was not effective to exhibit suitable $4\pi M_s$ and suitable $H_c$ for recording layer in rigid disks with high density at low $T_s$.

# Chapter 6

# Co-Zn Ferrite Films

## 6-1 Introduction

Since the films of a spinel type of Co ferrite have become attractive for recording media because of their capability of forming the smallest magnetic domains among all kinds of ferrites. However, it has been difficult to deposit these films with sufficient magnetic characteristics due to their poor crystallinity as mentioned in *Chapter 4*. Therefore, $CoFe_2O_4$ layers were deposited on ZnO underlayers in *Chapter 5*. Although $CoFe_2O_4$/ZnO doublelayered films revealed <111> orientation even without heating substrate, high $T_s$ above 400°C was necessary to obtain sufficiently large $4\pi M_s > 3.0$ kG and then $H_{c//}$ and $H_{c\perp}$ of about 0.8-0.9 kOe were too low to be applied for recording layers in rigid disks. To make matters worse surface smoothness was also insufficient for that kind of application. Low temperature deposition process of ferrite films lower than the softening temperature of glass disks which are commonly used as rigid disk substrates should be achieved. There are several conditions required for recording layer in rigid disks with high density. Of course, although they depends on their conditions such as read/write conditions, S/N characteristics and so on. The typical conditions required for hard ferrite media are as follows;

    1) moderately large $4\pi M_s > 3.0$ kG,

    2) moderately high $H_c > 2.0$ kOe,

    3) low process temperature < 300°C   (for usage of glass substrate)

Generally, magnetic materials with large magneto-crystalline anisotropy and that is composed of single domain possessed high coercivity. Co ferrite has large positive magneto-crystalline anisotropy constant $K_u = +2.9 \times 10^5$ [J/m$^3$] and this is much larger than the other spinel ferrites[1]. This is the reason why Co ferrite single layer films in *Chapter 4* and Co ferrite/ZnO double layered films in *Chapter 5* possessed too high $H_c$ to be applied for recording layer in rigid disks even for the films deposited at relatively low substrate temperature $T_s$. Since $K_1$ is an inherent value for each ferrites, the variety of composition, especially the substitution of $Co^{2+}$ ions for non magnetic ions, seems to be one of promising method to decrease the magneto-crystalline anisotropy and so that to attain moderately high $H_c$. It is also well known that the substitution of magnetic ions in a ferrimagnetic substance by non-magnetic ions, such as $Zn^{2+}$, $Cd^{2+}$, $Ga^{3+}$ and $In^{3+}$, can lead to an change in the saturation magnetization. Among these ions, $Zn^{2+}$ has a strong preference for tetragonal site(A site) in spinel crystallite and therefore total magnetization in unit volume would be increased.

Therefore, Zn substituted Co ferrite targets with various Zn compositions were prepared for increasing the $4\pi M_s^2$ and decreasing the $H_c$ of the deposited films. And their dependences of the crystallographic and magnetic characteristics as well as surface texture and cross-section morphology on various deposition conditions were precisely investigated in this chapter.

---

[1] J. Smit and H.P.J.Wijn, "FERRITES", Philips' Technical Library(Tokyo Electrical Engineering College Press), pp.163 (1965)

## 6-2 Deposition conditions of Co-Zn ferrite films

All specimen films were deposited by using FTS apparatus as shown in Fig. 6-1 without post-annealing process. Table 6-1 shows the deposition conditions of Co-Zn ferrite films. A pair of $Co_{0.51}Zn_{0.45}Fe_{2.04}O_{3-y}$ disk plates 90 mm in diameter and 7 mm(or 5mm) in thickness were used as targets for the investigation of the substrate temperature $T_s$ dependence, the film thickness t dependence and the input power $P_{in}$ dependence. The targets with this composition were sintered from the starting mixture of $(CoO)_{0.5}$, $(ZnO)_{0.5}$ and $(\alpha\text{-}Fe_2O_3)_{1.0}$ powder at 1200$^\circ$C in air by a conventional dry ceramic technique process as shown in '3-4 *Sintering process of targets*.' Another 3 pairs of targets with different compositions were also used for investigating the target composition dependence as mesntioned in later section. Since Co-Zn ferrite targets sintered by these process had too high a resistivity to sustain stable dc glow discharge of plasma, they were reduced in hydrogen atmosphere at 600-800$^\circ$C for 1 hour to decrease their resistivity. Nearly all films were deposited on thermal oxidized Si wafer $SiO_2/Si$ substrates($15 \times 15$ mm$^2$) and the others were deposited on quartz substrate. Since $SiO_2/Si$ and quartz substrates possess excellent surface smoothness, the most closely packed plane of spinel structure, (111) plane, is likely to be constructed parallel to the film plane when the 'damage-free' facing targets sputtering apparatus were used for the deposition. Ar and $O_2$ gases were introduced individually into the chamber as working gases. The total gas pressure $P_{total}$ and the partial oxygen gas pressure $P_{O_2}$ were mainly set at 2.0 and 0.02 mTorr, respectively. The substrate temperature $T_s$ was varied in the

---

[2] G.A.Petitt and D.W.Forester, Phys. Rev. B, 4[11], 3912-3923 (1971)

range from 90-100°C(without intentional substrate heating) to 600°C(with intentional substrate heating) in the investigation of $T_s$ dependence. The substrate temperature increased up to 90°C during deposition even without heating substrate because of heat radiation from plasma. However, this temperature is quite lower than the case of other sputtering system which has plasma-damage to the substrate as mentioned in *Chapter 3*. In this study, $T_s$ of the films deposited without heating substrate meant the temperature measured just after the deposition. The direct discharge current was set at 0.1 A, while it was changed in the range from 0.035 to 0.125A for the investigation of the input power dependence. The deposition time T was set at 120 min and it was also changed from 20 to 180 min. for the investigation of the film thickness t dependence. As a result, t was changed in the range from 80 to 700 nm. All specimen films were deposited after pre-sputtering of 1 hour. The direct current power supply was used for sustaining the discharge plasma and the film deposition.

Fig. 6-2 shows the relationship between the discharge current $I_d$ and voltage $V_d$. $V_d$ increased monotonically with the increase of $I_d$. Large $I_d$ made targets temperature higher during deposition and it finally seemed to cause cracks of targets. In addition to that, small deposition rate seemed necessary to make crystallite grow enough, the discharge current was mainly set at relatively low value of 0.1 A.
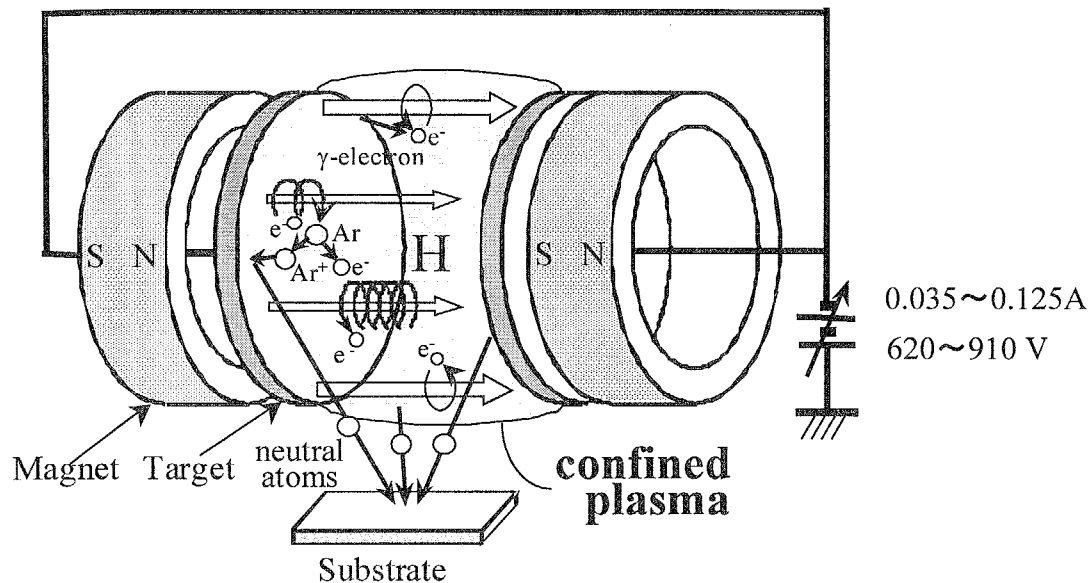
Fig. 6-1　Schematic illustration of facing targets sputtering apparatus.
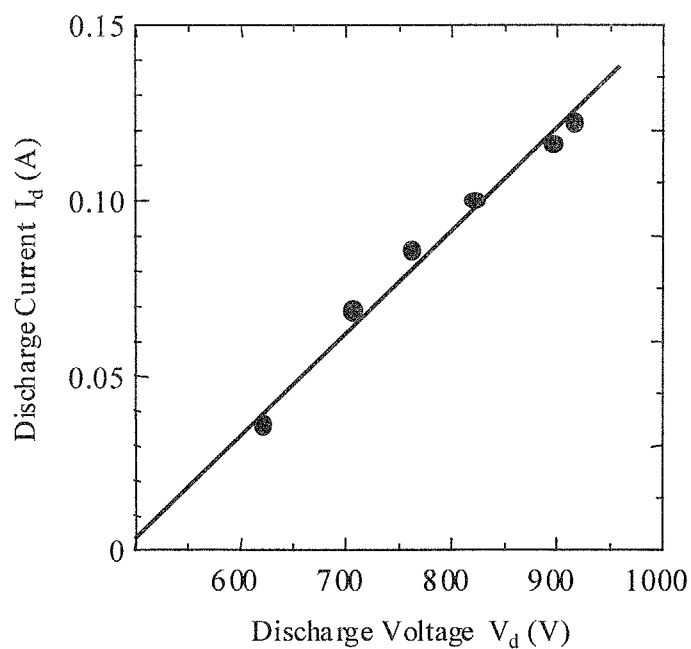


Fig. 6-2　Relationship between discharge current $I_d$ and voltage $V_d$.

Table 6-1    Deposition conditions of Co-Zn ferrite films for substrate temperature $T_s$, film thickness t and input power $P_{in}$ dependence.

| | Co-Zn ferrite film |
|---|---|
| Target Composition | $Co_{0.51}Zn_{0.45}Fe_{2.04}O_{4-y}$ |
| Substrate material | $SiO_2/Si$ |
| Total gas pressure $P_{total}$ | 2.0 mTorr |
| Partial oxygen gas pressure $P_{O_2}$ | 0.02mTorr |
| Substrate temp. $T_s$ | Without heating – 600°C |
| Discharge current $I_d$ | 0.10 A |
| Deposition time | 20~180 min. |

## 6-3 Substrate temperature dependence

6-3-1 Chemical compositions of targets and deposited films

The compositions were determined by inductive coupled plasma analysis(ICPA) and Auger depth profiles.

Fig. 6-3 shows the compositions of the target used in this study and those of films deposited at various $T_s$, where the content of metallic ion is normalized for $C_{Co} + C_{Zn} + C_{Fe} = 3.0$. The substrate temperature without intentional heating was elevated up to 90°C by the radiation from the plasma. While $C_{Co}$ were almost constant in the target and all films, $C_{Zn}$ of the films deposited at 90°C was smaller than that of target and

decreased gradually with increasing of $T_s$ up to 400°C and was almost zero at $T_s$ of

400°C. On the other hand, $C_{Fe}$ increased with increasing of $T_s$ instead of decrease of $C_{Zn}$.

The amount of substituted Zn ions in the films became small with increasing of $T_s$. It

seemed that the distribution of Zn and Fe ions had a close relationship to the

crystallographic and magnetic characteristics and as discussed later.

Fig. 6-4 shows the Auger depth profile of the films deposited at $T_s$ of 90 and 400°C

($P_{O_2}$ of 0.02 mTorr), respectively. Although the resolution of Auger depth profile in

metallic content was not so high, it suggested that the ratio in metallic content of Co-Zn

ferrite film in depth direction was almost constant.
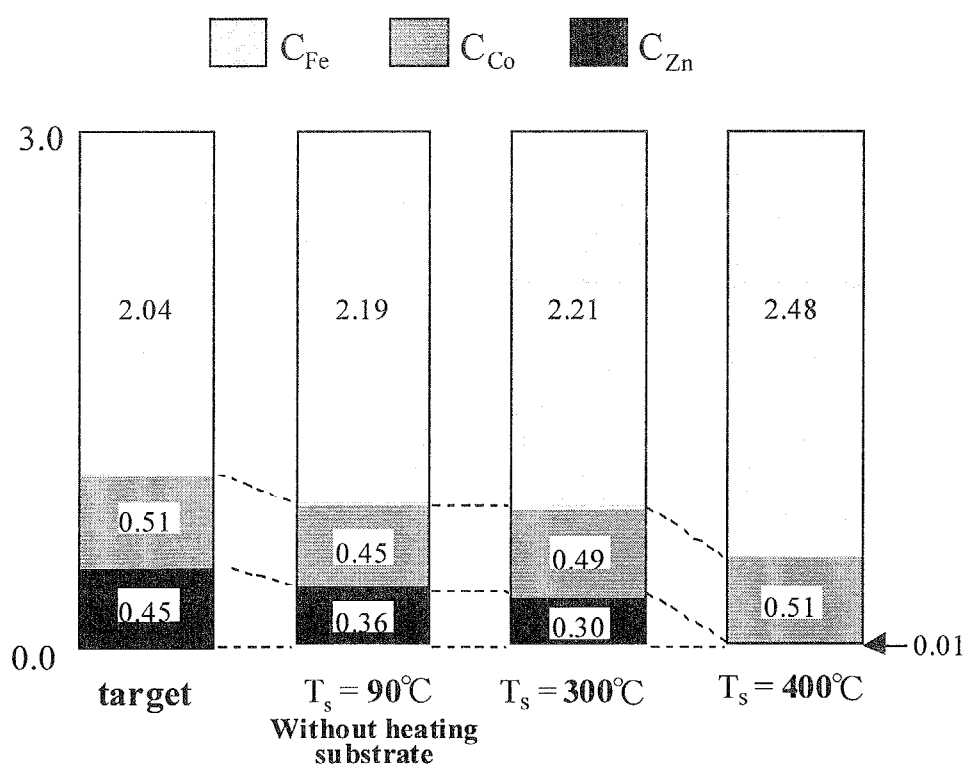


Fig. 6-3    Metallic contents of target and films deposited at
various $T_s$.
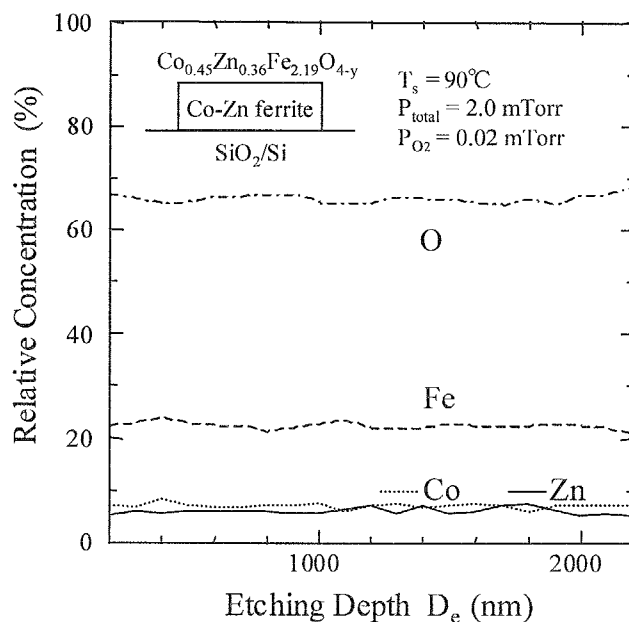
Fig. 6-4    Auger depth profiles of Co-Zn ferrite films deposited at $T_s$ of 90°C and $P_{O_2}$ of 0.02 mTorr.

## 6-3-2 Surface and cross-sectional SEM images

The surface texture and cross-section morphology was observed by scanning electron microscope(SEM). The films deposited at $T_s$ of 90 and 400°C revealed completely different surface textures and cross-section morphologies as seen in Fig. 6-5(a) and (b), respectively. The film was composed of very fine column and uniform morphology and very flat surface were seen in (a). The film deposited at $T_s$ of 200°C also revealed relatively smooth surface. However film surface became very rough at $T_s$ higher than 300°C as same as (b). It seemed to be caused by the excessive growth of crystalline grains. Their grain size was about several hundreds nm. The center line average roughness $R_a$ and the root mean square roughness $R_{rms}$ for them were measured by using the atomic force micropcopy(AFM). $R_a$ and $R_{rms}$ of (a) were 1.42 and 1.73 nm, and

110

those of (b) were 9.4.9 and 116.8 nm, respectively.

Several reasons for very rough surface texture at $T_s > 400°C$ are listed as follows;

1) Damage from discharge plasma($\gamma$-electrons, negative oxygen ions and so on).

2) Duplex structure.

3) Heat radiation from target surface.

Since "damage-free" FTS apparatus was used in this study, 1) can not be a reason. Although substrate temperature $T_s$ increased up to 90°C even without heating substrate, it was quite lower than those of other other RF-diode and magnetron sputtering apparatuses and very smooth surface was observed as shown in (a). It is well known that the duplex structures are often observed in the sintered ferrites. However, this duplex structure should be composed of small and large grains. In (b), only large grains were observed. This is not duplex structure but the excessive growth of crystallites.

It was confirmed that the insufficient cooling of targets caused the heat up of target surface and shield rings and therefore, the unstable discharge plasma deteriorate the crystallite growth. Therefore the films were deposited by using targets with small thickness.

Fig. 6-6 shows AFM images of the deposited films at $T_s$ of 90 and 400°C with sufficient targets cooling, respectively. The sufficient target cooling condition was achieved by using thinner targets, 4–5 mm, and by pouring much amount of water behind the targets during deposition. In Fig. 6-6(b), the centerline average roughness was quite smooth and $R_a$ was smaller than 5.0 nm even at $T_s$ of 400°C. From these results, it was clarified that sufficient target cooling is one of important conditions to deposit the films with excellent smoothness.

## (a) $T_s = 90°C$ (without heating substrate)



1 μm
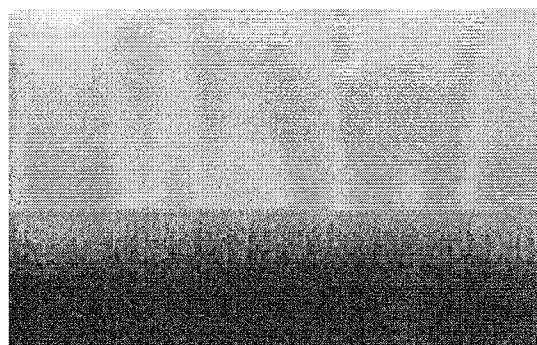
× 20,000

from AFM $\begin{cases} R_a & = 1.42 \text{ nm} \\ R_{rms} & = 1.73 \text{ nm} \end{cases}$

## (b) $T_s = 400°C$



1 μm

× 20,000

from AFM $\begin{cases} R_a & = \ \ 94.9 \text{ nm} \\ R_{rms} & = 116.8 \text{ nm} \end{cases}$

Fig. 6-5    SEM images of Co-Zn ferrite films deposited at $T_s$
of   (a)90°C  and (b)400°C.

(a) $T_s = 90°C$ (without heating substrate)
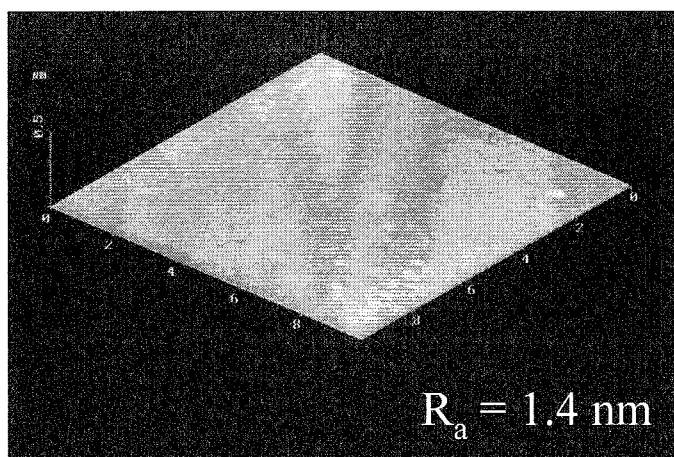


(b) $T_s = 400°C$
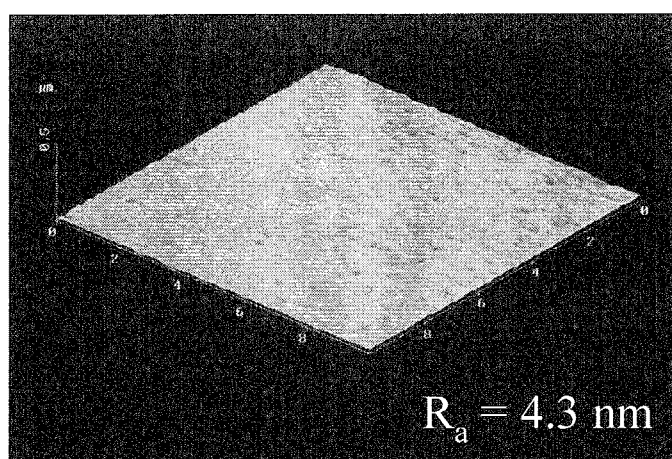


Fig. 6-6　AFM images of deposited films at $T_s$ of 90 and 400 °C with insufficient targets cooling and sufficient targets cooling.

6-3-3 Crystallographic characteristics

The crystallographic characteristics such as crystallite orientation, crystallite size $<D>$ and the full width at half maximum of rocking profiles $\Delta\theta_{50}$ were estimated from X-ray diffraction diagrams.

Fig. 6-7 shows the X-ray diffraction diagrams of the films deposited at various $T_s$. The film deposited at 90°C was only composed of crystallites with well (111) orientation. For the film deposited at $T_s$ of 250°C, although the X-ray diffraction intensity $I_{X.D.}$ corresponding to (111) fairly increased, (311) peak was also visible. $I_{X.D.}$ of (311) increased with increasing of $T_s$ and the films deposited at $T_s$ above 400°C were composed of only crystallites with (311) orientation, where metallic Zn content was almost zero as shown in Fig. 6-3. In addition to this result, the Co ferrite($CoFe_2O_4$) films deposited under the same sputtering conditions : $P_{total}$ of 2.0 mTorr, $P_{O_2}$ of 0.02 mTorr and $T_s$ up to 600°C were mainly composed of crystallites with (311) orientation as shown in Fig.4.7. Therefore, the difference of the crystal structure between Co-Zn ferrite and Co ferrite films deposited at lower $T_s$ below 300°C seemed to be closely related to the substitution of Zn ions in tetrahedral A site of spinel structure. This (111) orientation of spinel ferrite shows that the most closely packed plane of oxygen oriented parallel to the film plane as shown in Fig. 6-8. On the other hand, (311) peak is commonly visible and exhibits the largest intensity in powder X-ray diffraction diagram of spinel type of ferrite. This orientation is correspond to the formation of the most closely packed structure of metallic ions parallel to substrate as shown in Fig. 6-9.

It is known that the most closely packed plane of the film are likely to be formed in

the films deposited by sputtering. In addition to that since Zn ions work as an adhesive

agent for the formation of most closely packed plane of oxygen as shown in Fig. 6-10,

(111) orientation was observed even without heating substrate. However, since metallic

ions can obtain enough mobility to form the most packed plane of them and the number

of adhesive agents, Zn ions, decreased, (311) orientation was mainly formed at high $T_s$

above 300°C.
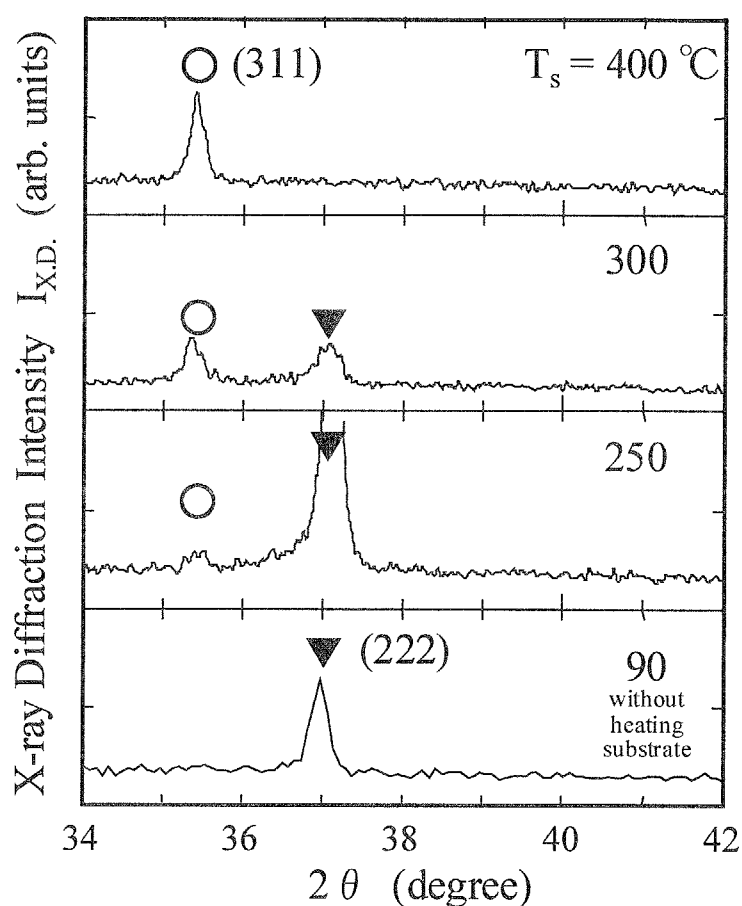


Fig. 6-7    Change of X-ray diffraction diagrams of Co-
Zn ferrite single layer films deposited at
various $T_s$ and $P_{O_2}$ of 0.02 mTorr.

# (111) orientation

## most closely packed plane of oxygen ions



○ : $O^{2-}$ site      A, B : A site, B site

[001]

Stereogram
from
[110] view

$O^{2-}$ (111)
plane

B(111)
plane

$O_{2-}$
B
$O_{2-}$
AB$_A$
$O_{2-}$
B
$O_{2-}$
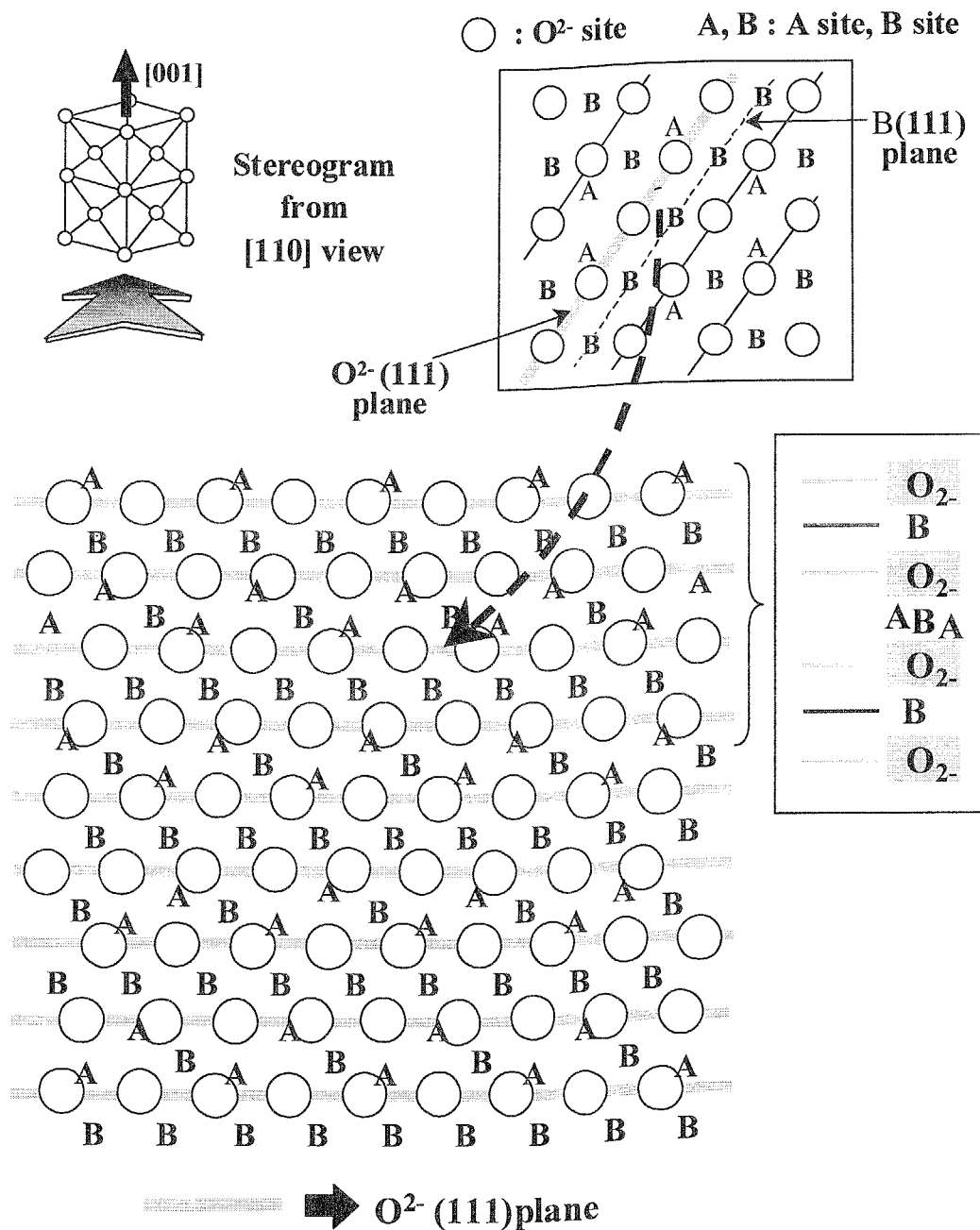
$O^{2-}$ (111)plane

Fig. 6-8      Stereogram of most closely packed (111) plane of
oxygen.

116

# (311) orientation

*quasi-closely packed plane of metallic ions*

○ : $O^{2-}$ site    A, B : A site, B site

Stereogram
from
[110] view

[001]

$O^{2-}$
(311)plane

A,B(311)
plane

── $O_{2-}$
**ABAB**
── $O_{2-}$
**B**
── $O_{2-}$
**ABAB**
── $O_{2-}$
**B**
── $O_{2-}$
**ABAB**
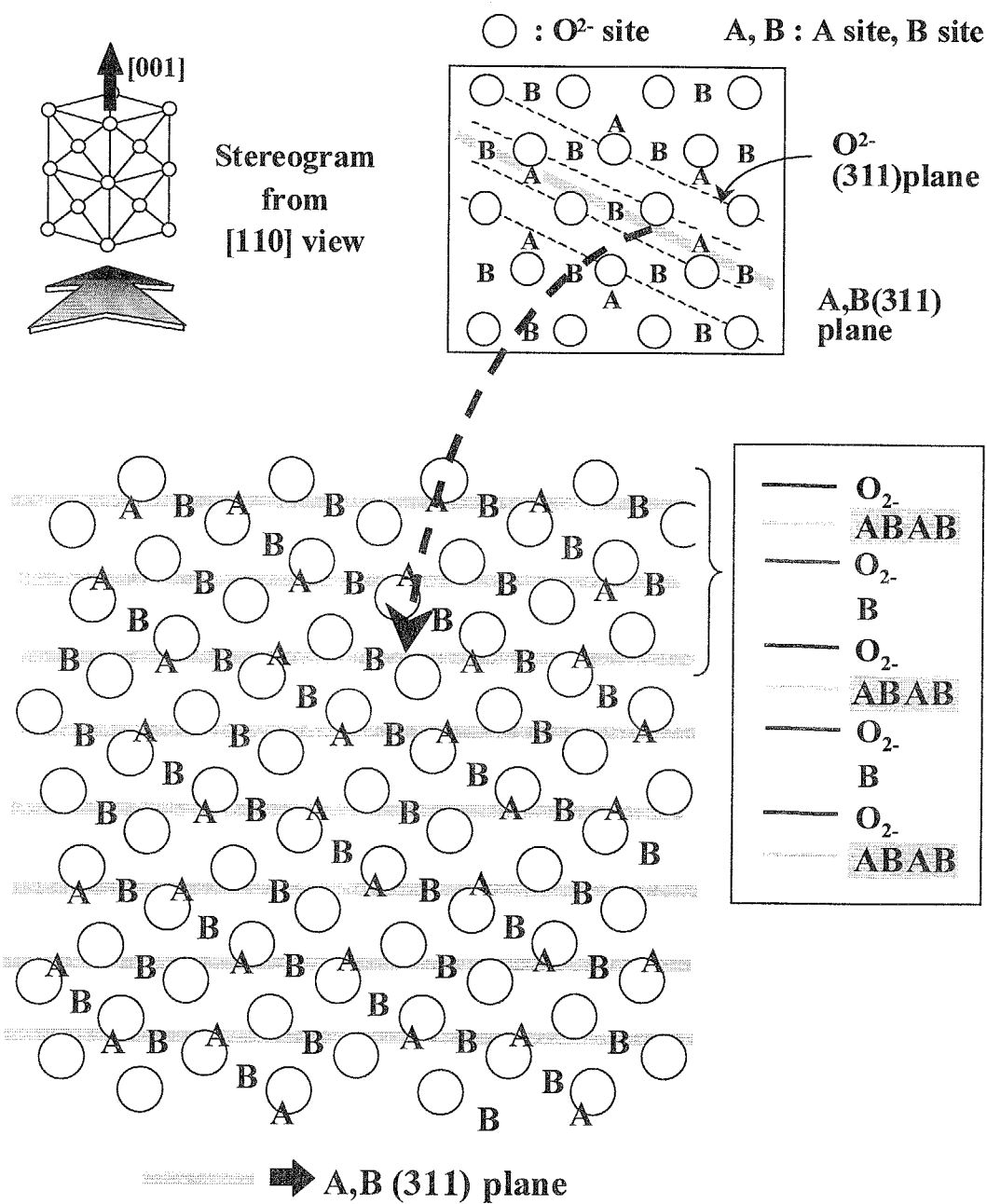
➡ A,B (311) plane

Fig. 6-9    Stereogram of quasi closely packed (311) plane of metallic cations.
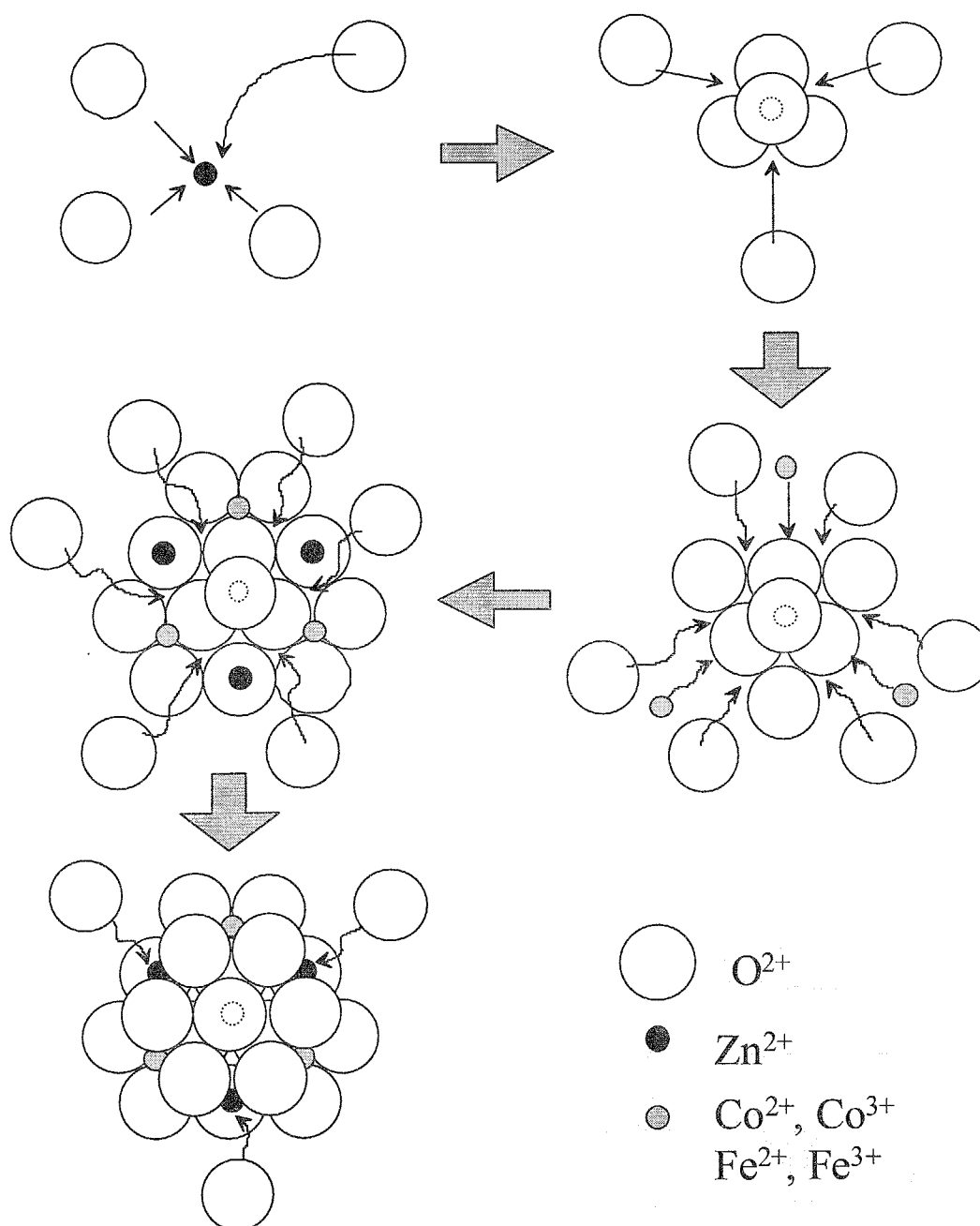
Fig. 6-10    Schematic illustration of formation of most closely packed structure of oxygen.

118

Fig. 6-11 shows the dependence of crystallite sizes, $<D>_{spinel(222)}$ and $<D>_{spinel(311)}$, which were calculated by Sherrer's equations on (222) and (311) peaks in XRD diagram, respectively and the full width at half maximum rocking profiles $\Delta\theta_{50\_spinel(222)}$ on substrate temperature $T_s$. Although the peak intensity of (311) was smaller than that of (222), $<D>_{spinel(311)}$ became larger than $<D>_{spinel(222)}$ at $T_s>250°C$ as shown in Fig. 6-11. $<D>_{spinel(222)}$ was as large as 32 nm even at relatively low $T_s$ of 90°C. This value was much larger than that of Co single layer films deposited at $T_s$ of 90°C. It seemed that Zn substitution promoted the crystallite growth especially at relatively low $T_s$.

The $\Delta\theta_{50(222)}$ took the minimum value of 2.5 degree at $T_s$ of 250°C and it was as small as about 5 degree even at low $T_s$ of 90°C. As simple Co ferrite films deposited at lower $T_s$ were mainly composed of small crystallites with (311) orientation and had large $\Delta\theta_{50(311)}$ in 'Chapter 4,' this small $\Delta\theta_{50(222)}$ suggested that the formation of the most closely packed plane was promoted by the Zn substitution especially at low $T_s$.
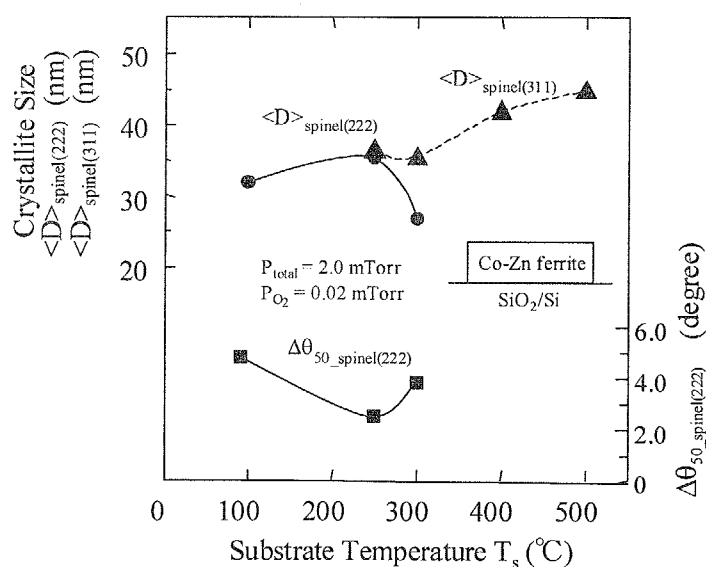


Fig. 6-11    $T_s$ dependence of crystallite size $<D>_{spinel(222)}$, $<D>_{spinel(311)}$ and
the full width at half maximum of rocking profiles $\Delta\theta_{50\_spinel(222)}$
of Co-Zn ferrite films.

6-3-4 Magnetic characteristics

The magnetic characteristics such as $4\pi M_s$ and $H_c$ were determined from the B-H hysteresis loops measured by a vibrating sample magnetometer(VSM).

Fig. 6-12 shows the change of B-H hysteresis loops measured by applying magnetic field to in-plane and perpendicular direction of Co-Zn ferrite films deposited at $T_s$ of (a)90℃ and (b)400℃, respectively. They were composed of crystallites with (111) and (311) orientation, respectively, as shown in Fig. 6-7. In (a), both B-H loops possessed almost same figure and it was suggested that the films with (111) orientation possessed isotropic orientation of magnetization. On the other hand, although there was vertical magnetization component as well as in-plane one, the in-plane loops was preferential to the in-plane one for the film with (311) orientation as shown in (b).

The conversion type of Mössbauer spectra of Co-Zn ferrite films with (111) and (311) orientation are shown in Fig. 6-13(a) and (b), respectively. Six peaks were observed for both spectra due to the existence of $Fe^{57}$. The peak intensity ratio is 3:0:1 and 3:4:1 for the films in which the spins orientated perpendicularly and parallel to the film plane, respectively, and it is 3:2:1 for the film which reveals random spin orientation. The intensity ratio was 3:1.8:2.2 in Fig. 6-13(a) and it suggested that the film with (111) orientation possessed a certain extent of perpendicular magnetization component. On the other hand, Fig. 6-13(b) showed that the spin orientation of the film with (311) orientation was close to the in-plane orientation compared with perpendicular one. This difference in magnetization orientation seemed to be attributed to the magnetocrystalline anisotropy as shown in Fig. 6-12.

typical in-plane media
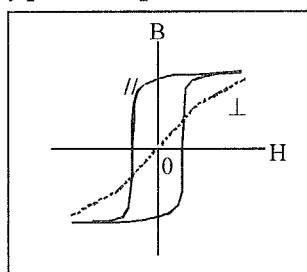
typical perpendicular media
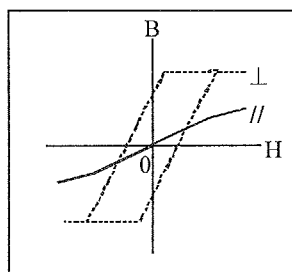
*(a) (111) orientation*

$T_s = 90°C$
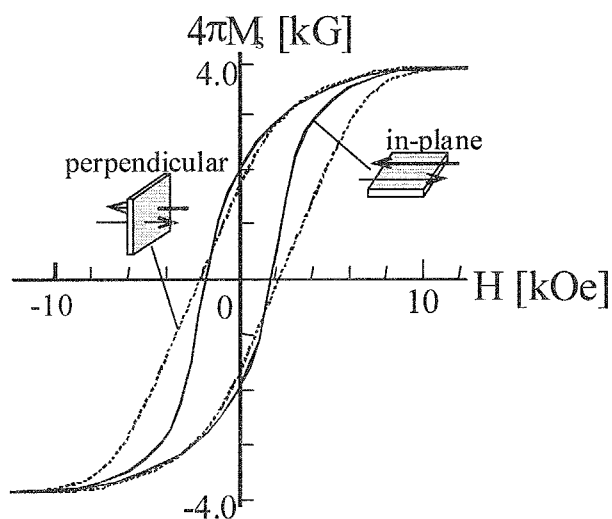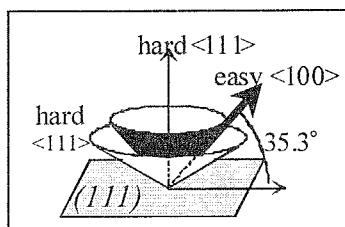
*(b) (311) orientation*

$T_s = 400°C$
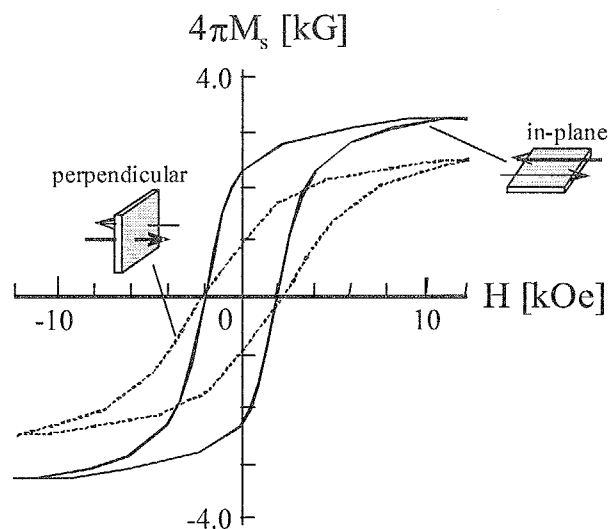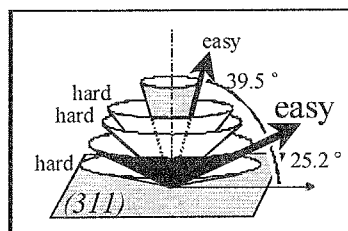
Fig. 6-12    Typical B-H loops of in-plane and perpendicular recording media and change of B-H loops of Co ferrite films deposited at $P_{O_2}$ of 0.02 mTorr and $T_s$ of (a)90°C and (b)400°C.

121

perpendicular                    In-plane

3 : 0 : 1   1 : 0 : 3            3 : 4 : 1   1 : 4 : 3

(a) (111) orientation

3.0 : 1.8 : 2.2

(b) (311) orientation

3.0 : 3.0 : 2.4

Count [arb.unit]

-10              0              10

Velocity [mm/s]
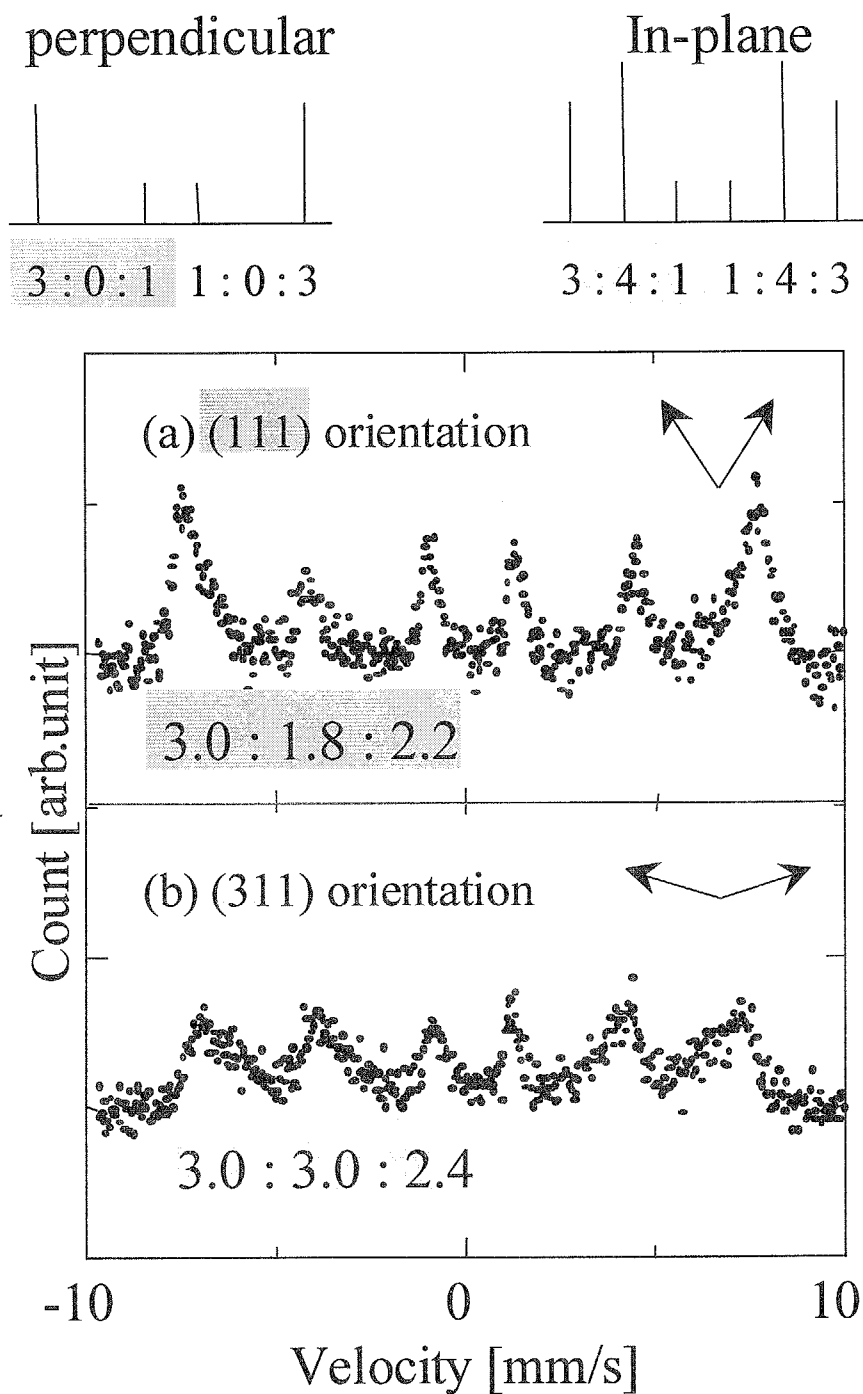
Fig. 6-13   Mössbauer spectra of Co-Zn ferrite films with
(111) and (311) orientation.

The canting angle from film plane estimated from the peak fitting of Mössbauer spectra was 58.19 and 35.96 degree for Co-Zn ferrite films with (111) and (311) orientations, respectively. This angel is larger than that of easy axis <100> of of 35.3 and 25.2 degree as shown in Fig. 6-12. From these results, it was suggested that this larger perpendicular component of the deposited Co-Zn ferrite films were attributed to the inverse magneto-striction.

Fig. 6-14 and Fig. 6-15 show the $T_s$ dependence of $4\pi M_s$, and the in-plane and perpendicular coercivity, $H_{c//}$ and $H_{c\perp}$, of Co-Zn ferrite and Co ferrite films, respectively. It was confirmed that $4\pi M_s$ was increased by the substitution of Zn ions onto tetrahedral A site of spinel structure at $T_s$ up to 250°C. It took the maximum value of 4.8 kG at $T_s$ of 250°C and then decreased with increasing of $T_s$ above 250°C. This decrease seemed
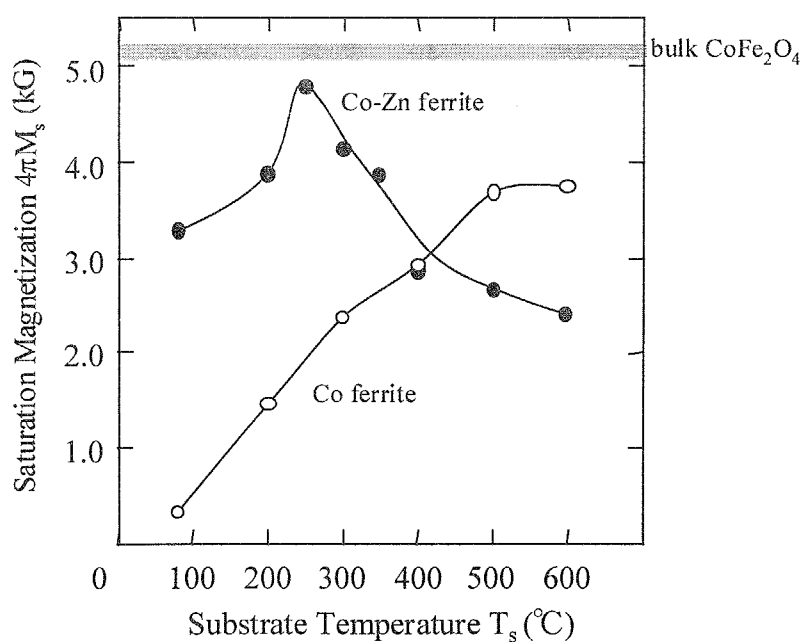


Fig. 6-14    Dependence of $4\pi M_s$ on $T_s$ at $P_{O_2}$ of 0.02 mTorr.
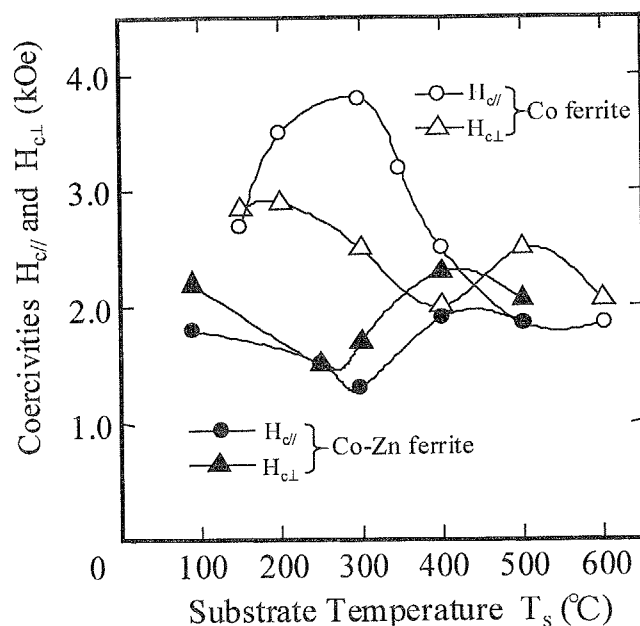
Fig. 6-15    Dependence of $H_{c//}$ and $H_{c\perp}$ on $T_s$ at $P_{O_2}$ of 0.02 mTorr.

to be attributed to the increase of the number of $Fe^{3+}$ occupying A site with decreasing the number of $Zn^{2+}$ at $T_s$ above 250°C, as mentioned above and shown inFig. 6-3. The over-estimation of the volume of the deposited film due to a porous structure might be one reason for this decrease.

Anyway, it should be noted that $4\pi M_s$ of Co-Zn ferrite film was as large as 3.3 kG even at $T_s$ of about 90 °C(without intentional heating substrate), while those of Co ferrite single layer film was almost 0.3 kG. Co-Zn ferrite films could be deposited with good magnetic characteristics even on substrates with weak heat resistance such as flexible disks and tapes.

Co-Zn ferrite films possessed moderate in-plane and perpendicular coercivities $H_{c//}$ and $H_{c\perp}$ of about 1.5-2.0 kOe which are suitable for the magnetic recording media in

124

the whole range of $T_s$, from 90 to 500°C, while Co ferrite films exhibited too high $H_{c//}$ up to 3.8 kOe. Since the easy and hard axes of Co ferrite are <100> and <111>, respectively, and <100> axes are distributed in circular cone whose generation line canted at an angle of 35.3 degree to film plane when films had (111) orientation as seen in Fig. 6-12. $H_{c//}$ and $H_{c\perp}$ were not so different each other. Therefore, these films may be applicable for isotropic media with ultra-high density. From these magnetic characteristics, the substitution of Fe ions by Zn ones in tetrahedral A sites seemed to be useful not for increasing $4\pi M_s$ and decreasing $H_c$. It also seemed effective to promote the formation of the most closely packed plane of oxygen ions and to decrease the crystallization temperature of the deposited film.

## 6-4 Target composition dependence

The Zn content of Co-Zn ferrite films affected to crystallographic characteristics and film structure as well as magnetic characteristics as seen in 6.3, 6.4, 6.5 and 6.6. In this section, the films were deposited mainly from Co-Zn ferrite targets with four different Zn composition, i.e. $Co_{0.51}Zn_{0.45}Fe_{2.04}O_{4-y}$, $Co_{0.68}Zn_{0.45}Fe_{1.87}O_{3-y}$, $Co_{0.54}Zn_{0.72}Fe_{1.74}O_{3-y}$, $Co_{0.20}Zn_{0.90}Fe_{1.90}O_{3-y}$ and their crystallographic and magnetic characteristics were compared each other.

6-4-1 Deposition conditions of specimen films

There were two ways of sputtering deposition, which enable to control the Zn content of the deposited films. One of them is to use targets with modified compositions and the other one is to use composite target composed of Co ferrite(or Co-Zn ferrite) target and

125

several pieces of metallic Zn chips.

The discharge plasma of composite targets seemed unstable because the plasma density on metal and oxide surface are quite different each other and oxidation of Zn chip surface is likely to be changed at each time of the deposition. Therefore, the reproducibility of the deposited films does not have confidence.

In this study, therefore, the films were deposited from four kinds of sintered targets with different Zn compositions($Co_{0.51}Zn_{0.45}Fe_{2.04}O_{4-y}$, $Co_{0.68}Zn_{0.45}Fe_{1.87}O_{3-y}$, $Co_{0.54}Zn_{0.72}Fe_{1.74}O_{3-y}$, $Co_{0.20}Zn_{0.90}Fe_{1.90}O_{3-y}$). Their deposition conditions are listed in Table 6-2.

6-4-2 Chemical compositions of targets and deposited films

The metallic content ratio of Fe, Co and Zn ions of sintered targets with three different Zn content $C_{Zn}$ were almost perfectly controlled to the expected values as shown in Fig. 6-16(a), (b) and (c). However that of the deposited films were slightly fluctuated for various $T_s$. In (a), although $C_{Zn}$ was almost constant at $T_s$ up to 500℃ except for those of the films deposited at $T_s$ of 100℃, they decreased definitely at $T_s$ of 500℃. Because, such high $T_s$ promoted the evaporation of Zn atoms from substrate surface and it made difficult the incorporation of ones as a film component. $C_{Zn}$ at $T_s$ lower than 500℃ in (a) was almost constant and same as that of target. On the other hand, $C_{Zn}$ was smaller than that of target value in (b) and (c) even at $T_s$ lower than 500℃ and there were remarkable decrease at $T_s$ of 100℃. It suggested that the heating substrate at $T_s$ higher than 100℃ was necessary for incorporating Zn ions to films at $C_{Zn}$ higher than 0.5.

Table 6-2    Deposition conditions of Co-Zn ferrite films
for target composition dependence.

|  | Co-Zn ferrite film |
|---|---|
| Target Composition | $Co_{0.51}Zn_{0.45}Fe_{2.04}O_{4-y}$ $Co_{0.68}Zn_{0.45}Fe_{1.87}O_{4-y}$ $Co_{0.54}Zn_{0.72}Fe_{1.74}O_{4-y}$ $Co_{0.20}Zn_{0.90}Fe_{1.90}O_{4-y}$ |
| Substrate material | $SiO_2/Si$ |
| Total gas pressure $P_{total}$ | 1.5 mTorr |
| Partial oxygen gas pressure $P_{O_2}$ | 0.0075 mTorr |
| Substrate temp. $T_s$ | Without heating – 600℃ |
| Discharge current $I_d$ | 0.10 A |
| Deposition time | 90 min. |
| Film thickness | 400～500 nm. |
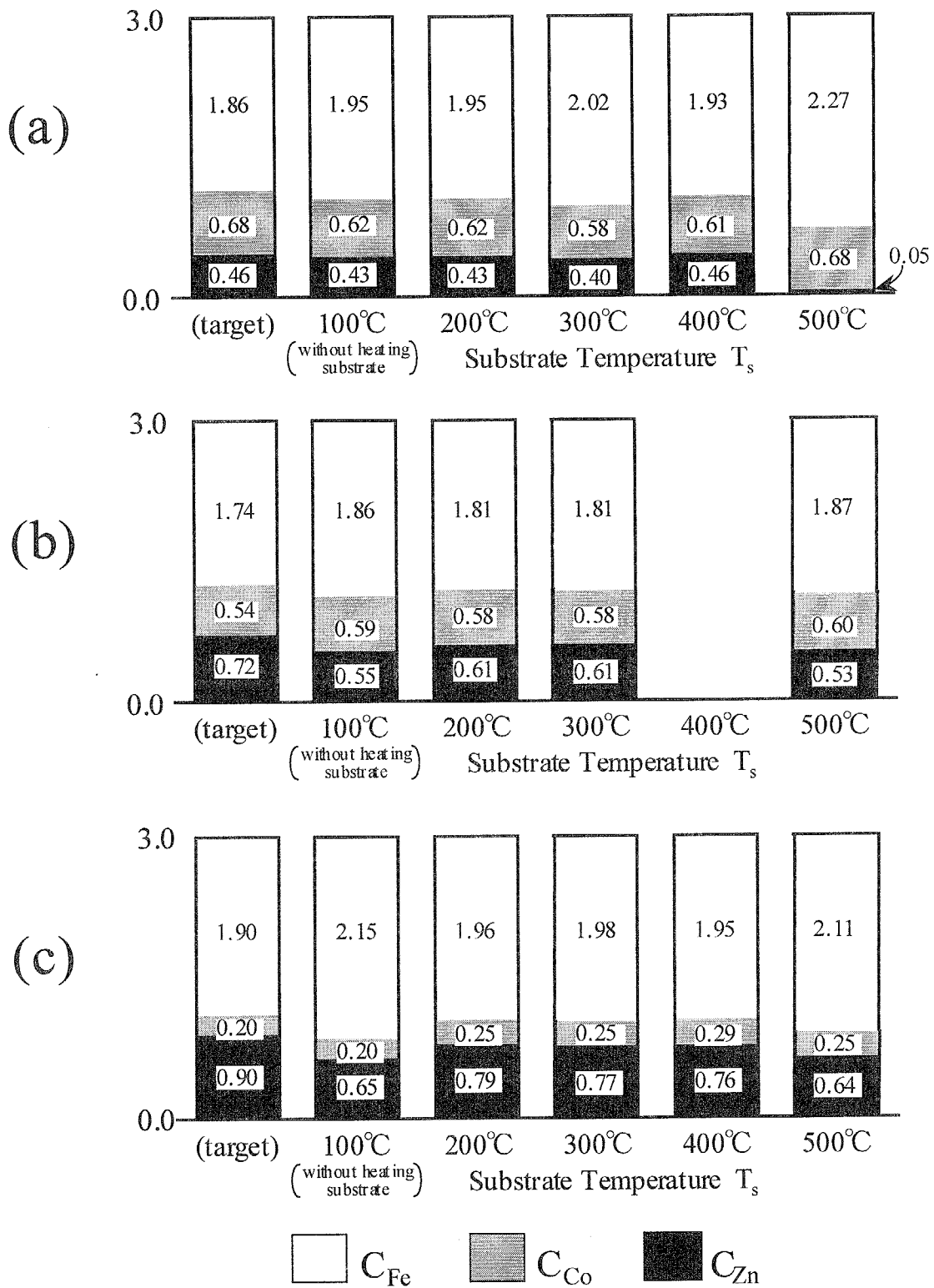
Fig. 6-16   Metallic contents of sintered targets with different amount of Zn substitution and those of films deposited from them.

6-4-3 Crystallographic and magnetic characteristics

Fig. 6-17 shows the $T_s$ dependence of ratio in intensity peak of spinel(111) to all ones, $f_{s(111)}$. The value of $f_{s(111)}$ was calculated after Lotgering, see equation (3.2) , and the same equation is shown again in Fig. 6-17. The $f_{s(111)}$ was almost 1.0 and almost perfect (111) orientation was obtained at $T_s$ of 100℃ for the films deposited from targets with $C_{Zn}$ of 0.45(targets with the composition of $Co_{0.51}Zn_{0.45}Fe_{2.04}O_{3-y}$ and $Co_{0.68}Zn_{0.45}Fe_{1.87}O_{3-y}$). That value is fairly larger than that of Co ferrite films. At $T_s$ of 100℃, while the value of $f_{s(111)}$ of the film deposited from targets with larger $C_{Zn}$ were larger than that of Co ferrite film, they were smaller than those of the films deposited from targets with $C_{Zn}$ of 0.45. The $f_{s(111)}$ of all Co-Zn ferrite films decreased with the increase of $T_s$, especially at $T_s$ higher than 200℃. This tendency was more remarkable for films deposited from larger $C_{Zn}$ targets and their $f_{s(111)}$ became almost zero at higher $T_s$. The preferential orientation at $T_s$ in the range from 100-200℃ and above 300℃ was (111) and (311), respectively, and this tendency was accordance with that of the films deposited from target with almost same $C_{Zn}$ as seen in Fig. 6-11.

Fig. 6-18 shows the substrate temperature $T_s$ dependence of crystallite sizes, $<D>_{spinel(311)}$ and $<D>_{spinel(222)}$, and the full width at half maximum of rocking profiles, $\Delta\theta_{50\_spinel(311)}$ and $\Delta\theta_{50\_spinel(222)}$, of the films deposited from (a)$Co_{0.68}Zn_{0.45}Fe_{1.87}O_{3-y}$, (b)$Co_{0.54}Zn_{0.72}Fe_{1.74}O_{3-y}$ and (c)$Co_{0.20}Zn_{0.90}Fe_{1.90}O_{3-y}$ targets. Crystallite size $<D>_{(111)}$ at $T_s$ of 100℃ became larger for the films deposited from targets with larger $C_{Zn}$. They increased 37nm $\rightarrow$ 40nm $\rightarrow$ 41nm as $C_{Zn}$ of targets increased 0.45 $\rightarrow$ 0.72 $\rightarrow$ 0.90. On the other hand, their $\Delta\theta_{50\_spinel(111)}$ at $T_s$ of 100℃ increased slightly as $C_{Zn}$ of targets

increased. From these results, it was suggested that Zn substitution of $C_{Zn}$ up to 0.5 is effective for the crystallite growth with (111) orientation at relatively low $T_s$ (<300°C), whereas too high $T_s$ and too high $C_{Zn}$ deteriorate simple (111) orientation and promote the random one. Here, the $\Delta\theta_{50\_spinel(111)}$ and $\Delta\theta_{50\_spinel(311)}$ were above 6° and these values were larger than those seen in Fig. 6-11. It might be attributed to the small film thickness and small amount of Fe ions. These films revealed very smooth surface even for the films deposited at high $T_s$ above 400°C, because the target was sufficiently cooled due to its small thickness.
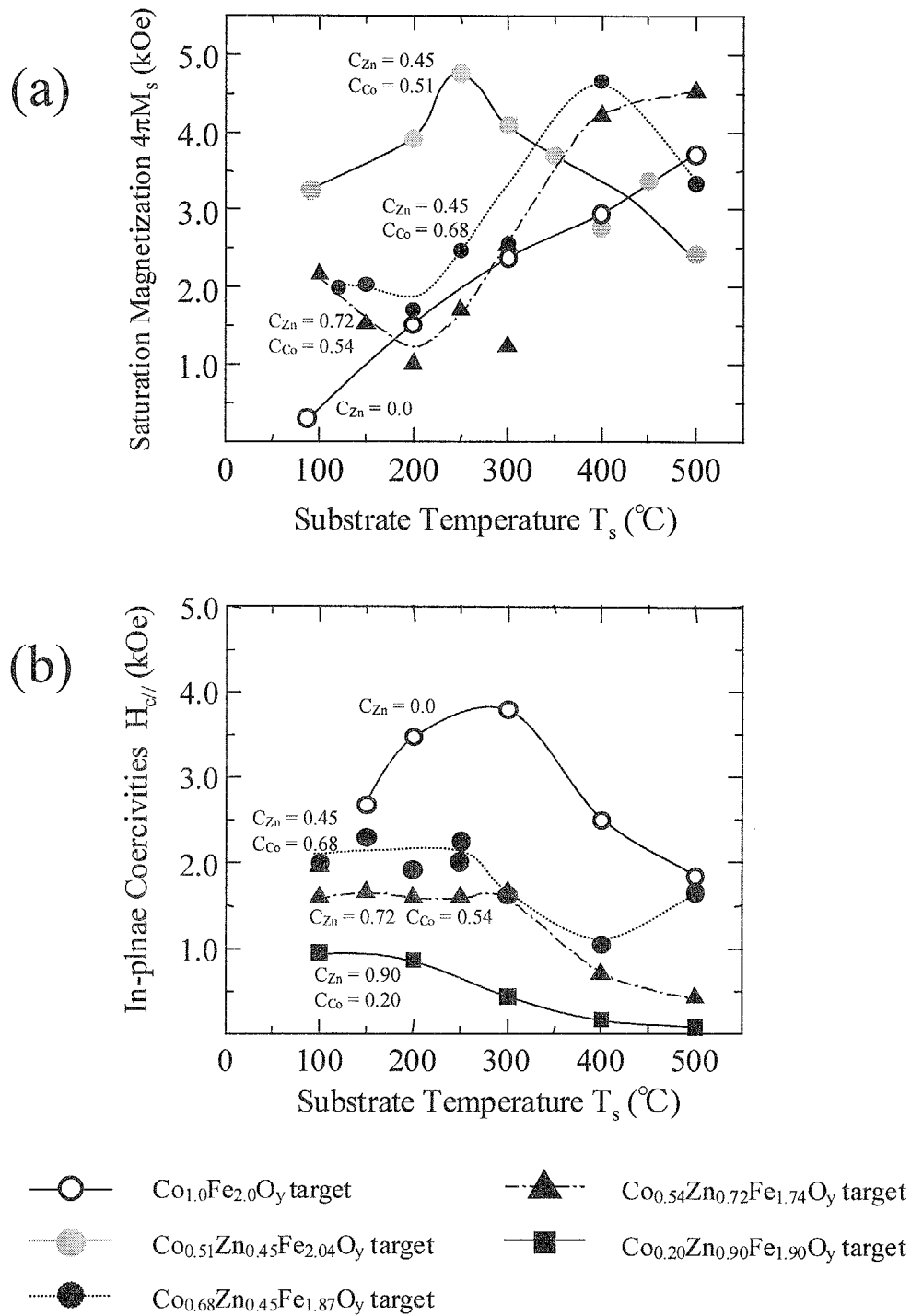
Fig. 6-19 shows the $T_s$ dependence of (a)saturation magnetization $4\pi M_s$ and (b)in-plane coercivity $H_{c//}$ of films deposited from Co-Zn ferrite targets with different Zn content. In (a), while the films deposited from the targets with composition of $Co_{0.68}Zn_{0.45}Fe_{1.87}O_{3-y}$ and $Co_{0.54}Zn_{0.72}Fe_{1.74}O_{3-y}$ exhibited larger $4\pi M_s$ than that of simple Co ferrite film at $T_s$ of 100°C and below, they were fairly smaller than that of the films deposited from targets with composition of $Co_{0.51}Zn_{0.45}Fe_{2.04}O_{3-y}$. Although the maximum $4\pi M_s$ was as almost same as 4.5 kG for the films deposited from targets with different compositions, higher substrate temperature was necessary to attain the maximum $4\pi M_s$ for the films deposited from targets with larger $C_{Zn}$.

At $T_s$ of 100°C, $H_{c//}$ took smaller value for the films deposited from targets with larger $C_{Zn}$ as seen in Fig. 6-19, because magnetocrystalline anisotropy were decreased by the increase of Zn substitution. The decrease of $H_{c//}$ with the increase of $T_s$ were attributed to the growth of crystallites with (311) orientation whose magnetic easy axes are oriented to quasi in-plane as shown in Fig. 6-12.
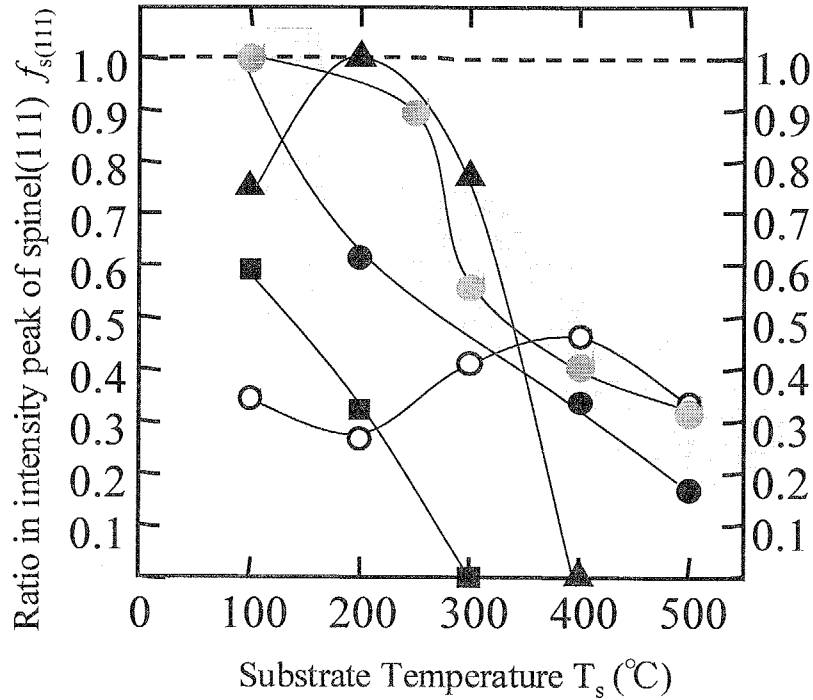
$$f_{s(111)} = \frac{P - P_0}{1 - P_0}$$

$$P = \frac{\sum I_{s(mmm)}}{\sum I_{(hkl)}} \quad \text{( from XRD diagram of the deposited film)}$$

$$P_0 = \frac{\sum I_{0s(mmm)}}{\sum I_{0(hkl)}} \quad \text{( from JCPDS card)}$$

—O—  $Co_{1.0}Fe_{2.0}O_y$ target

——  $Co_{0.51}Zn_{0.45}Fe_{2.04}O_y$ target

—●—  $Co_{0.68}Zn_{0.45}Fe_{1.87}O_y$ target

—▲—  $Co_{0.54}Zn_{0.72}Fe_{1.74}O_y$ target

—■—  $Co_{0.20}Zn_{0.90}Fe_{1.90}O_y$ target

Fig. 6-17   $T_s$ dependence of ratio in intensity peak of spinel(111) peaks to all ones.
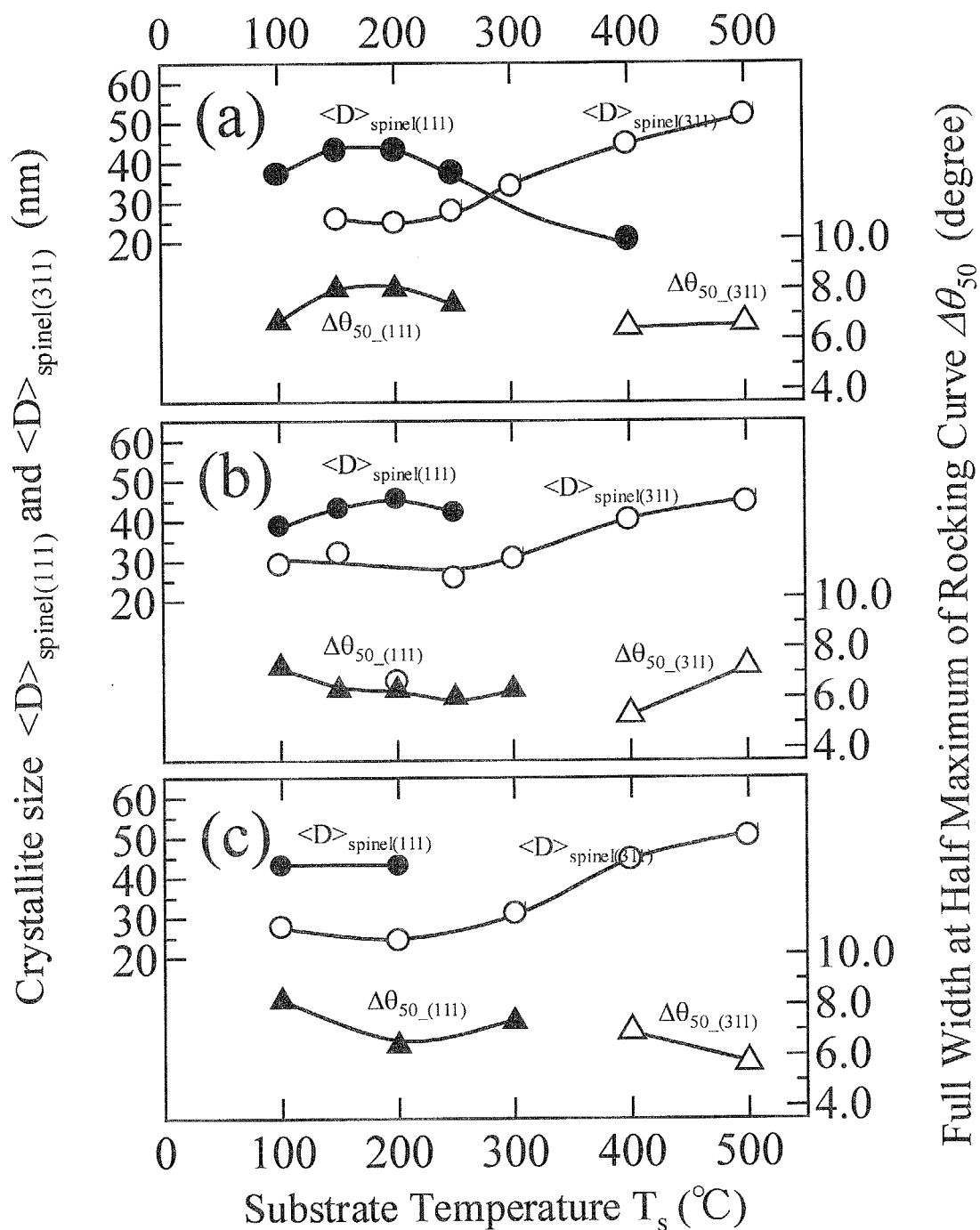
Fig. 6-18 $T_s$ dependence of crystallite sizes, $<D>_{(311)}$ and $<D>_{(222)}$, and the full width at half maximum of rocking profiles, $\Delta\theta_{50}$ of the films deposited from (a)$Co_{0.68}Zn_{0.46}Fe_{1.86}O_{3-y}$, (b)$Co_{0.54}Zn_{0.72}Fe_{1.74}O_{3-y}$, (c)$Co_{0.20}Zn_{0.90}Fe_{1.90}O_{3-y}$ targets.

Fig. 6-19    $T_s$ dependence of (a)saturation magnetization $4\pi M_s$ and (b)in-plane coercivity $H_{c//}$ of films deposited from Co-Zn ferrite targets with different Zn content.

## 6-5 Film thickness dependence

Thickness of magnetic films as magnetic recording media should be thinner than 100 nm for both in-plane and perpendicular recording media. Their purposes are to decrease demagnetizing field, to decrease thickness loss, to control grain size smaller, to make recording media lighter and thinner, to make tape media flexible, and so on. In addition to them, large film thickness makes magnetic field distribution wider and recording efficiency worse in perpendicular magnetic recording system. However, there are problems for making film thickness smaller. There is possibility that crystallographic characteristics are changed and as a result, magnetic characteristics would be deteriorated due to the existence of initial growth layer. Therefore, in this section, film thickness dependence of crystallite orientation and magnetic characteristics such as saturation magnetization $4\pi M_s$ and in-plane and perpendicular coercivity, $H_{c//}$ and $H_{c\perp}$, were investigated.

Fig. 6-20 shows the change of XRD diagrams of Co-Zn ferrite films deposited at $T_s$
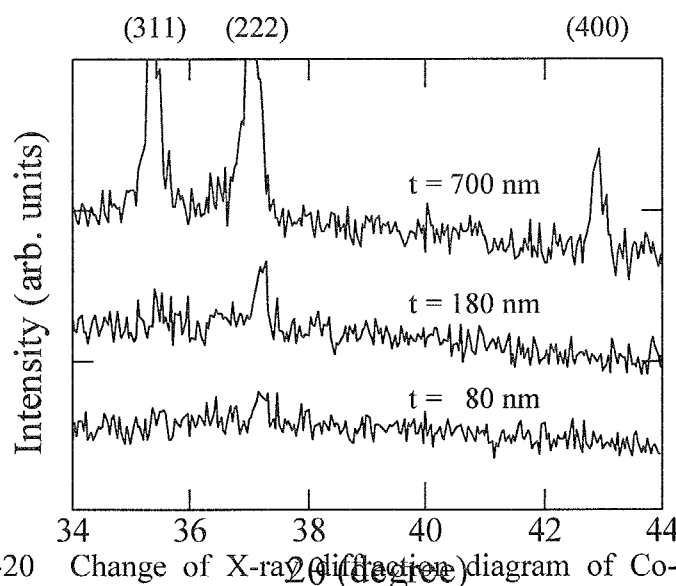


Fig. 6-20   Change of X-ray diffraction diagram of Co-Zn ferrite films on film thickness t.

of 300°C and $P_{O_2}$ of 0.02 mTorr for the films with various film thickness t. While (311)

and (400) peaks as well as (222) one was observed in XRD diagram for the film 700 nm

thick, only (222) peak was observed for film 180 nm thick. (222) was clearly observed

even for small thickness of 80 nm. From these charts, it was cleared that spinel

crystallites with the most closely packed plane of oxygen ions were formed at initial

growth of crystallite and then crystallites with other orientations were formed on them.

Fig. 6-21 shows the dependence of magnetic characteristics of those films on film

thickness t. Although the value of $4\pi M_s$ of about 4.2 kG was almost constant for the

change of thickness t, $H_{c//}$ increased from 1.0 to 1.6 kOe and $H_{c\perp}$ decreased from 1.7 to

1.0 kOe with the decrease of $T_s$ from 700 to 80 nm. This increase of $H_{c//}$ and decrease of

$H_{c\perp}$ was caused by the change of shape anisotropy.

It is noted that the films exhibited large $4\pi M_s$ and moderately high $H_{c//}$ and $H_{c\perp}$ even

at small thickness of 80 nm.
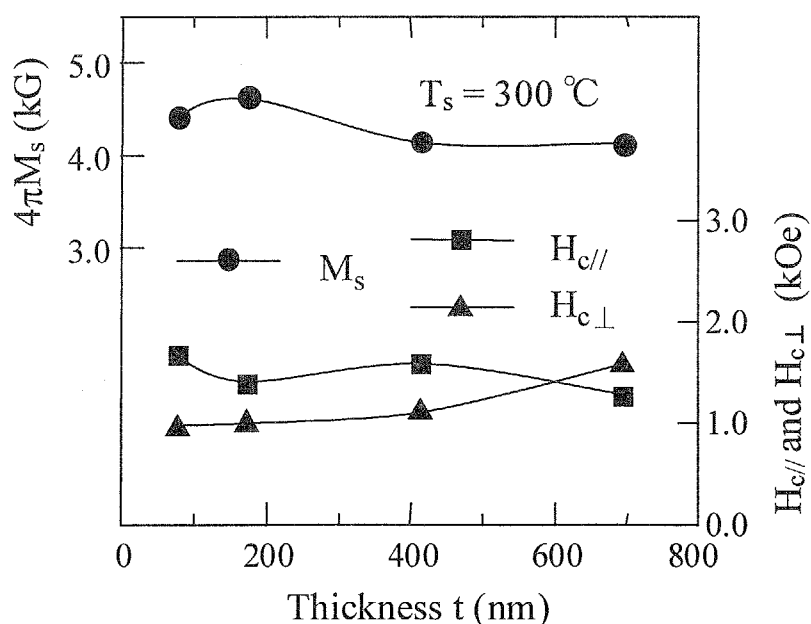


Fig. 6-21    Dependence of magnetic characteristics of Co-Zn ferrite films
deposited at $T_s$ of 300°C on film thickness t.

## 6-6 Input power dependence

Since the input power changes the energy of sputtered particles as well as the deposition rate, it seemed to affect the crystallite growth, especially at lower $T_s$. In this section, therefore, the in-put power, $P_{in}$, were changed by changing the discharge current and the dependence of crystallite orientation and magnetic characteristics on $P_{in}$ were investigated. The specimen films were deposited at $P_{in}$ in the range from 20 to 90 W(dc). The substrate temperature $T_s$, was set at 100°C, and the total and partial oxygen gas pressure $P_{total}$ and $P_{O_2}$ was set at 2.00 and 0.01 mTorr constant, respectively.

The Zn content $C_{Zn}$ was constant for the change of $P_{in}$ and was almost same as those of target($C_{Co}$ = 0.51, $C_{Zn}$ = 0.45, $C_{Fe}$ = 2.04).

Although the films deposited at smaller $P_{in}$ had random orientation and only slight (311) peak was observed in XRD diagram, small but clear (111) peak was observed for the films deposited at $P_{in}$ larger than 70 W.    (111) and (311) orientation corresponds to the formation of the most closely packed plane of oxygen and metallic ions, respectively, as shown in Fig. 6-8 and Fig. 6-9. Fig. 6-22 shows the dependence of the crystallite size, $<D>_{spinel(311)}$ and $<D>_{spinel(111)}$, on $P_{in}$. The films deposited at $P_{in}$ larger than 70 W had $<D>_{spinel(111)}$ of above 30 nm, while $<D>_{spinel(311)}$ was as small as about 25 nm at $P_{in}$ smaller than 50 W. The most stable structure in case of spinel ferrite is f.c.c and the stable structure appears at the lowest surface energy[3]. However, the films deposited at $P_{in}$ smaller than 50 W had random orientation while the most intense peak was (311). It was cleared that $P_{in}$ above 50 W was necessary for obtaining (111) orientation.

---

[3] K. R. Dixit: Phylosophycal Mag. and J. of Sci., pp. 1049 (1933)
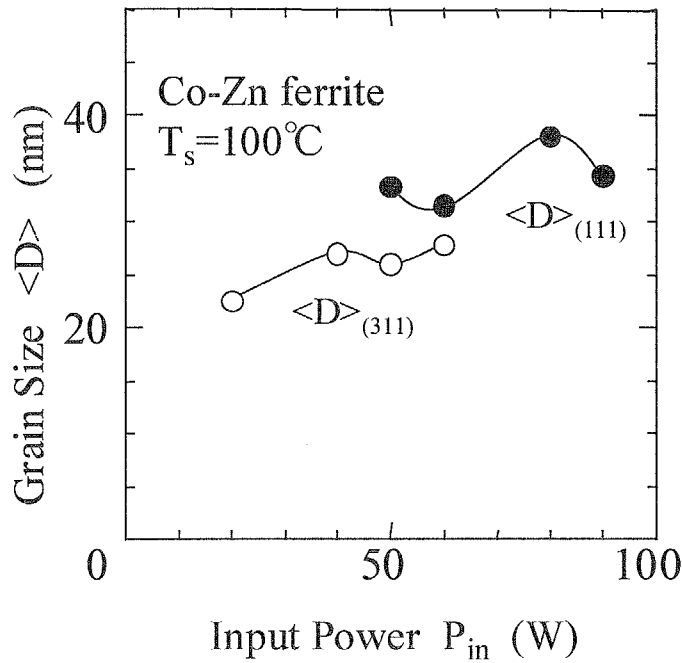
Fig. 6-22   Dependence of crystallite size, $<D>_{spinel(311)}$
and $<D>_{spinel(111)}$, on input power $P_{in}$.

Although $4\pi M_s$ of 3.5 kG was almost constant for the variety of $P_{in}$, $H_{c//}$ and $H_{c\perp}$

increased slightly with the increase of $P_{in}$ as shown in Fig. 6-23. This increase of $H_c$

corresponds to the gradual crystallite growth as seen in Fig. 6-22. Since the crystallite

grew larger, they could possess their intrinsic large magnetocrystalline anisotropy.

Although the reason was not clear, $H_{c\perp}$ drastically increased at $P_{in}$ of 50 W and took

moderate value for magnetic recording media, where crystallite orientation was changed

from (311) to (111). It was suggested that the input power also changes the crystallite

orientation and the film with (111) orientation exhibited higher coercivity than those

with (311) orientation.

137
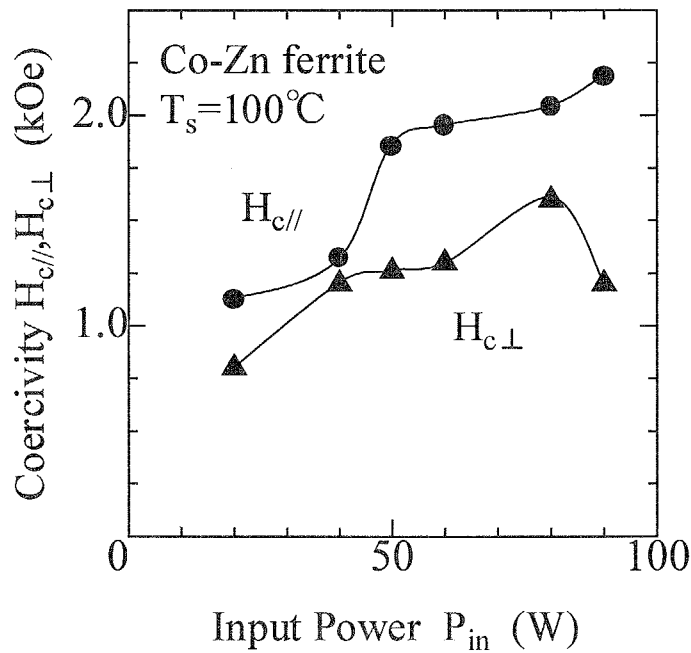
Fig. 6-23    Dependence of in-plane and perpendicular coercivity, $H_{c//}$ and $H_{c\perp}$, on input power $P_{in}$.

## 6-7 Summary

In this chapter, Co-Zn ferrite single layer films with various composition were deposited by the facing targets sputtering apparatus without subsequent annealing process. The dependence of surface observation, crystallographic and magnetic characteristics on the substrate temperature $T_s$ dependence, target composition one, the film thickness one and the input power $P_{in}$ one were investigated, respectively. The following results were obtained:

$T_s$ dependence(with sufficient target cooling):

1) Surface and cross-sectional texture of the deposited films were excellent smoothness and the center-line roughness $R_a$ were 1.4 and 4.3 nm at $T_s$ of 90 and 400°C, respectively.

138

2) The films deposited at $T_s$ of 90 and 400°C had (111) and (311) orientation and they correspond to the formation of the most closely packed structure of oxygen and metallic ions, respectively.

3) The films deposited at $T_s$ of 90°C with (111) orientation showed isotropic orientation of magnetization. It possessed the moderate saturation magnetization $4\pi M_s$ of 3.3 kG and high in-plane and perpendicular coercivity $H_{c//}$ and $H_{c\perp}$ of 1.8 and 2.2 kOe, respectively.

4) The films deposited at $T_s$ of 400°C with (311) orientation showed quasi in-plane orientation of magnetization. It exhibited $4\pi M_s$ of 3.7 kG and high in-plane and perpendicular coercivity $H_{c//}$ and $H_{c\perp}$ of 2.0 and 2.3 kOe, respectively.

Target composition dependence:

1) Zn atoms were likely evaporated from the film especially at higher substrate temperature.

2) All Co-Zn ferrite films had larger $f_{s(111)}$ than Co ferrite and the largest $f_{s(111)}$ of about 1.0 was obtained for film deposited from target with $C_{Zn=0.45}$. The value of $f_{s(111)}$ decreased with the increase of $T_s$.

3) Higher $T_s$ was necessary to attain maximum $4\pi M_s$ of about 4.5 kG for films deposited from larger $C_{Zn}$ targets.

4) It was confirmed that the film deposited from larger $C_{Zn}$ target at same $T_s$ exhibited lower $H_c$, and $H_c$ decreased with the increase of $T_s$.

Film thickness dependence:

1) Spinel crystallites with the most closely packed plane of oxygen were formed from initial growth of crystallites.

2) $4\pi M_s$ of about 4.2 kG was constant and $H_{c//}$ increased (1.0-1.6 kOe) and $H_{c\perp}$ decreased(1.7-1.0 kOe) for the change of thickness t from 700 to 80 nm.

In-put power $P_{in}$ dependence(with sufficient target cooling):

1) The Zn content $C_{Zn}$ was constant for the change of $P_{in}$ and was almost same as those of target.

3) A clear (111) peak was observed for the films deposited at $P_{in}$ larger than 50 W and crystallite size increased with the increase of $P_{in}$.

4) $4\pi M_s$ of 3.5 kG was constant and $H_{c//}$ and $H_{c\perp}$ increased slightly with the increase of $P_{in}$.

For the application as a recording layer of rigid disk with ultra high density, the centerline of surface roughness $R_a$ smaller than 4 nm is required due to low flying height. $R_a$ was small enough for Co-Zn ferrite films and they seemed applicable as contact type of recording layer. Since a very low temperature process has been achieved in this study, Co-Zn ferrite films seemed to be applicable for flexible disk and tape with high recording density even when low heat resistance sheets such as PC disks and PET tapes are used as substrates.

Since the films deposited at $T_s$ of 200 and 400℃ exhibited different crystallite orientation and anisotropies, isotropic and quasi in-plane, their read/write characteristics were investigated in *Chapter 7*.

# Chapter 7

# Read/Write Characteristics of Co-Zn Ferrite Disks

## 7-1 Introduction

The spacing between head and rigid disk have been fairly decreased with increase of recording density and the contact recording media will be required in the near future. Although the films of Co-based alloy such as Co-Cr-Ta and Co-Pt-Cr are commonly used as a recording layer, the protective and lubricant layers are required on them because of their low corrosion resistance and poor durability.   Moreover, the media noise of Co-Cr based alloy disks become a serious trouble at ultra-high density[1].

On the other hand, ferrite media are taking much interest again as contact and semi-contact recording media because of their good tribology and low media noise even at high densities as well as excellent chemical stability and corrosion resistance. Although the ferrite possesses smaller magnetization than the Co-based alloy, the use of MR head with high sensitivity will solve that problem. Co-Zn ferrite films seemed to be one of superior candidates as recording layer for contact recording media, because it possessed excellent surface smoothness and highly dense cross-sectional morphology as well as moderate magnetic characteristics as mentioned in *Chapter 6*. Since Co-Zn ferrite films deposited at $T_s$ up to 250°C and at $T_s$ of 400°C were composed of crystallites with (111) and (311) orientations, respectively.

The films with (111) orientations possessed isotropic magnetic properties, while

---

[1] S. Tsuboi, T. Korenai, N. Ishiwata, K. Yamada and K. Tagami, "Noise Characteristics for Co-Cr-Ta Media and Ferrite Media," *J. Mag. Soc. Japan*, vol. 18, No. S1, pp. 95-98, 1994.

there was vertical magnetization as well as in-plane one, the in-plane orientation is preferential to the vertical one in (311) orientation. Therefore, Co-Zn ferrite films with (111) and (311) orientation seems to be applicable as isotropic and in-plane recording layers, respectively, as shown in Fig. 7-1

In this study, therefore, Co-Zn ferrite films with two different magneto-crystalline anisotropy were deposited on rigid disks without a post annealing process. Their read/write characteristics without protective overcoatings, i.e. quasi contact mode, were examined, respectively, by using the metal in gap(MIG) type head and the merged magneto resistance(MR) type head.

ring head    ring head

Isotropic recording    In-plane recording

(a)    (b)
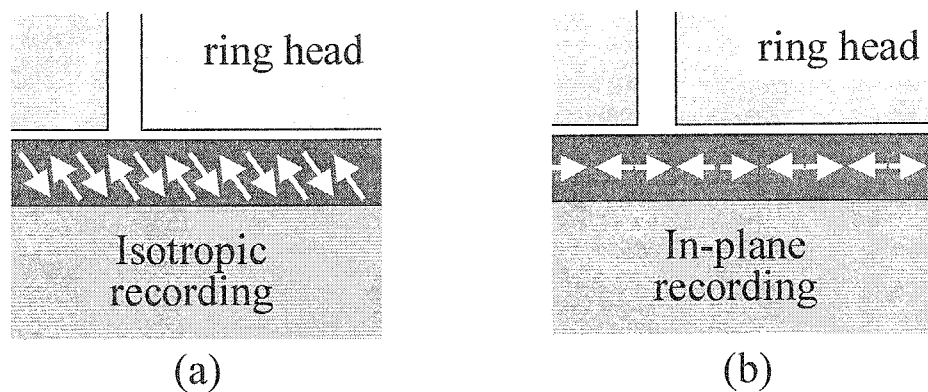
Fig. 7-1    Schematic illustration of ring type head and (a)isotropic
recording layer and (b)in-plane recording layer.

**7-2 Preparation Conditions of Co-Zn ferrite disks**

All specimen disks were prepared by using FTS apparatus without post-annealing process. Table 7-1 shows the deposition conditions of Co-Zn ferrite disks. A pair of $Co_{0.51}Zn_{0.45}Fe_{2.04}O_x$ plates were used as targets and these targets were the same one used in *Chapter 6*. Ar and $O_2$ were used as working gases and the total gas pressure and the partial oxygen gas pressure were 2.0 and 0.02 mTorr, respectively. Specimen films was deposited on 2-inch$\phi$ disks of thermally-oxidized silicon wafer($SiO_2$/Si) and 1.89-inch$\phi$ disks of glass ceramics(OHARA corp.). The substrate temperature $T_s$ was set at relatively low, i.e. lower than 250℃ and at relatively high, i.e. higher than 350℃, to control the magnetocrystalline anisotropy. The $T_s$ of the films deposited without intentional heating substrate increased up to about 90℃ just after the deposition.

Table 7-1　Deposition conditions of Co-Zn ferrite disks

| | Co-Zn ferrite film |
|---|---|
| Target Composition | $Co_{0.51}Zn_{0.45}Fe_{2.04}O_{3-y}$ |
| Substrate material | $SiO_2$/Si disks(2 inch$\phi$)<br>Glass Ceramics(1.89 inch$\phi$) |
| Total gas pressure $P_{total}$ | 2.0 mTorr |
| Partial oxygen<br>gas pressure $P_{O_2}$ | 0.02 mTorr |
| Substrate temp. $T_s$ | 90℃, 200℃, 300℃, 400℃ |
| Discharge current $I_d$ | 0.10 A |
| Film Thickness | 30-280 nm |

All disk specimens were deposited after pre-sputtering of 1 hour. The direct current power supply was used for sustaining the discharge plasma and the film deposition and the discharge current was set at 0.1 A.

Although the crystallite orientation were analyzed for disk samples using XRD diagrams, their surface texture, cross-section morphology, the surface roughness as well as magnetic characteristics were evaluated from the results obtained in *Chapter 6* using by scanning electron microscopy(SEM), atomic force microscopy(AFM), and vibrating sample magnetometer (VSM), respectively.

## 7-3 Surface smoothness

Fig. 7-2 shows the AFM images of deposited films at $T_s$ of (a)90, (b)200 and (c)400°C with sufficient targets cooling. The films deposited at $T_s$ of 90, 200 and 400°C revealed relatively smooth surface as mentioned in *6-3-2* and the center-line average roughness $R_a$ evaluated by using the atomic force micropcopy(AFM) were of 1.0, 1.2 and 4.0 nm, respectively. The surface smoothness was almost same for the films deposited on both $SiO_2/Si$ disks and glass ceramics disks.

## 7-4 Crystallographic and Magnetic characteristics

Fig. 7-3 shows the X-ray diffraction diagrams of disk specimens deposited on $SiO_2/Si$ disks at $T_s$ of (a)200°C and (b)400°C. The films deposited at $T_s$ of 90°C was only composed of crystallites with excellent (111) orientation.
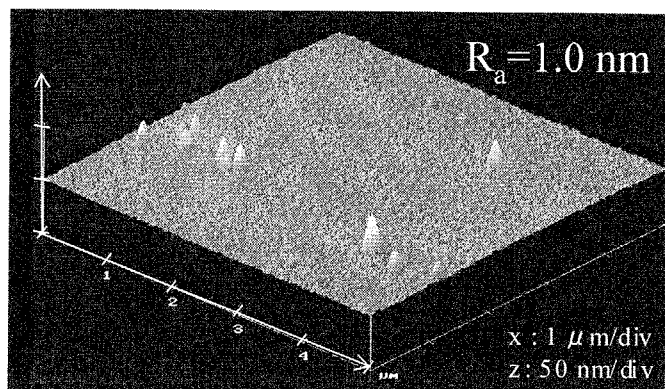
(a)without heating
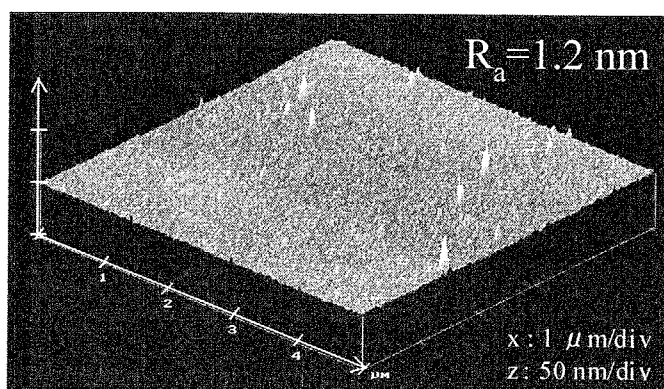


(b)$T_s$=200℃



(c)$T_s$=400℃
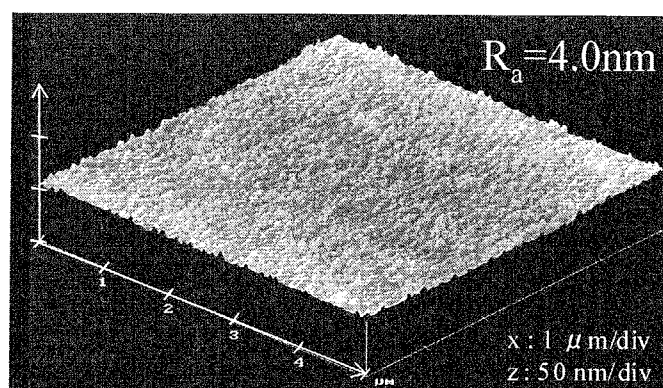
Fig. 7-2    AFM images of the films deposited at $T_s$ of (a)90, (b)200 and (c)400℃  with insufficient targets cooling and sufficient targets cooling.

145
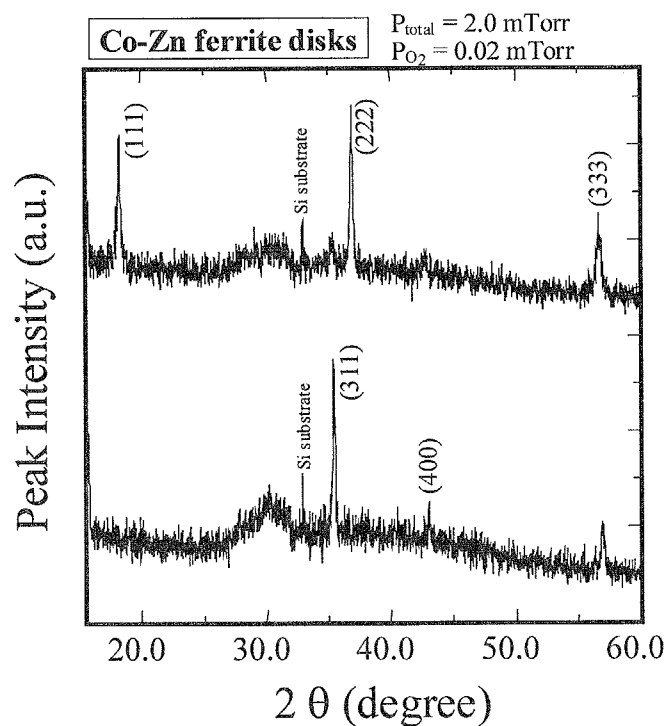
Fig. 7-3 X-ray diffraction diagrams of Co-Zn ferrite films deposited on $SiO_2$/Si susbstrate at $T_s$ of 200 and 400°C.
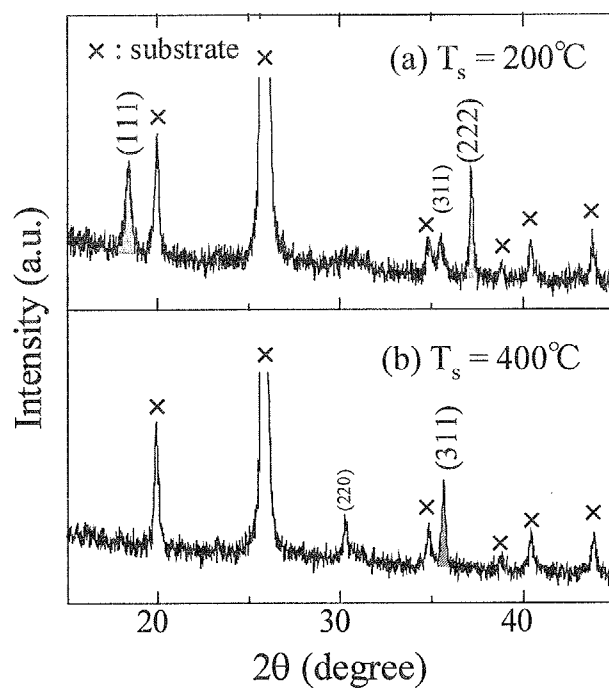


Fig. 7-4 X-ray diffraction diagrams of Co-Zn ferrite films deposited on glass ceramics substrate at $T_s$ of (a)200 and (b)400°C.

146

Since the (111) plane in crystallites of a spinel type of Co-Zn ferrite is the most closely packed plane of oxygen ions as shown in Fig.6-8, it seemed that the films with this orientation should reveal smooth surface and possess excellent pass-wear durability. On the other hand, the films deposited at $T_s$ of 400℃ were composed of only crystallites with (311) orientation. As mentioned in *Chapter 6*, this (311) orientations of spinel ferrite correspond to the formation of most closely packed planes of metallic ones. The specimen films deposited on the disks of transparent glass ceramic TS-CZ(OHARA INCORPORATED) 1.89 inch in diameter exhibited almost same tendency on $T_s$. as shown in Fig. 7-4.

## 7-5 Read/Write Characteristics

Since Co-Zn ferrite films with (111) and (311) orientation revealed flat surface and strong adhesion to substrate disk as well as hardness, the read/write characteristics of the specimen magnetic disks were evaluated without protective layers.

Schematic illustration and picture of spin stand, head and disk configurations are shown in Fig. 7-5 and Fig. 7-6. Although lubricant layer was deposited on disk specimens for the measurement using MR type head to protect the damage from head crush, it was not deposited for the measurement using MIG type head.
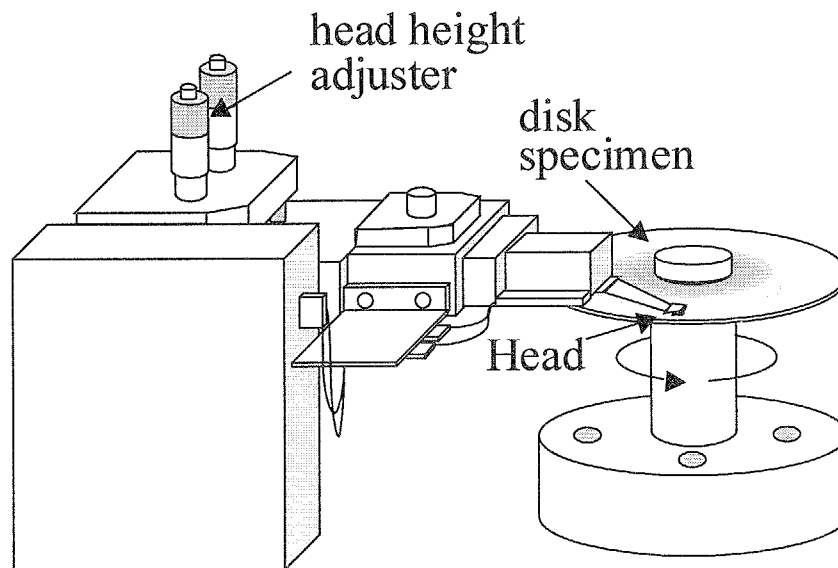
Fig. 7-5    Schematic illustration of spin stand, head and disk specimens.
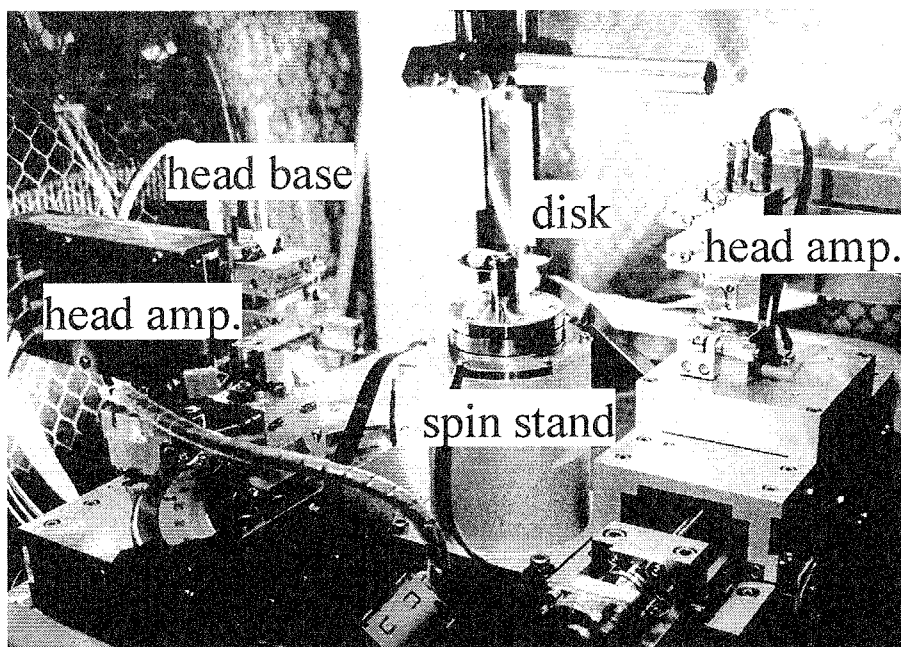


Fig. 7-6    Picture of spin stand and disk used in R/W characteristics.

7-5-1 Measurements using MIG type head

Table 7-2 and Table 7-3 list the characteristics of Co-Zn ferrite disk with (111) and (311) orientations, Disk(111) and Disk(311), and that of MIG type head, respectively.

MIG type heads with gap length of 0.35 μm was used for evaluating read/write characteristics. The coil turn number and relative velocity were 34 and 2.3 m/s, respectively.

Table 7-2  Crystallite orientation and magnetic characteristics of specimen disks

|  | Disk(111) | Disk(311) |
|---|---|---|
| Substrate Temperature $T_s$ | 200℃ | 400℃ |
| Crystallite orientation | (111) | (311) |
| Saturation magnetization $4\pi M_s$ | 3.9 kG | 4.5 kG |
| Squareness S | 0.55 | 0.70 |
| $4\pi M_r \cdot \delta$ | 493.4 G·μm | 882.0 G·μm |
| In-plane coercivity $H_{c//}$ | 1.8 kOe | 2.0 kOe |
| Perpendicular coercivity $H_{c\perp}$ | 2.7 kOe | 2.0 kOe |

Table 7-3  Specifications of MIG type head

| Head type | Co-Zr-Nb layer laminated MIG |
|---|---|
| Pole 1    width/thickness | 9.0 μm / 5.5 μm |
| Pole 2    width/thickness | 7.1 μm / 3.5 μm |
| Gap length   g | 0.35 μm |
| Coil turn number    T | 34 |
| Coil resistance    R | 37 Ω |
| Inductance    L | 1000 nH |
| Relative head speed | 2.3 m/s(at 1,200 r.p.m.) |
| Flying height | 70-100 nm or 50 nm |

Although the deposited films revealed relative high coercivity, 1.8 to 2.7 kOe, it was confirmed that they were fully saturated at the head current higher than 50 mA$_{p-p}$.

Fig. 7-7 shows the dependence of normalized output on writing head current measured at linear recording density of 0.35 kfrpi. Although Disk(111) which had higher coercivity needed higher saturation heading current $I_h$, all of them saturated at $I_h$ >50 mA and they indicated almost constant output at $I_h$ up to 140 mA. Therefore, in the measurement of the dependence of linear recording density, the rectangular wave function of 62 mA$_{p-p}$ was used as recording head current.

Fig. 7-8 shows comparison of roll-off curves for disks with different crystallite orientation.
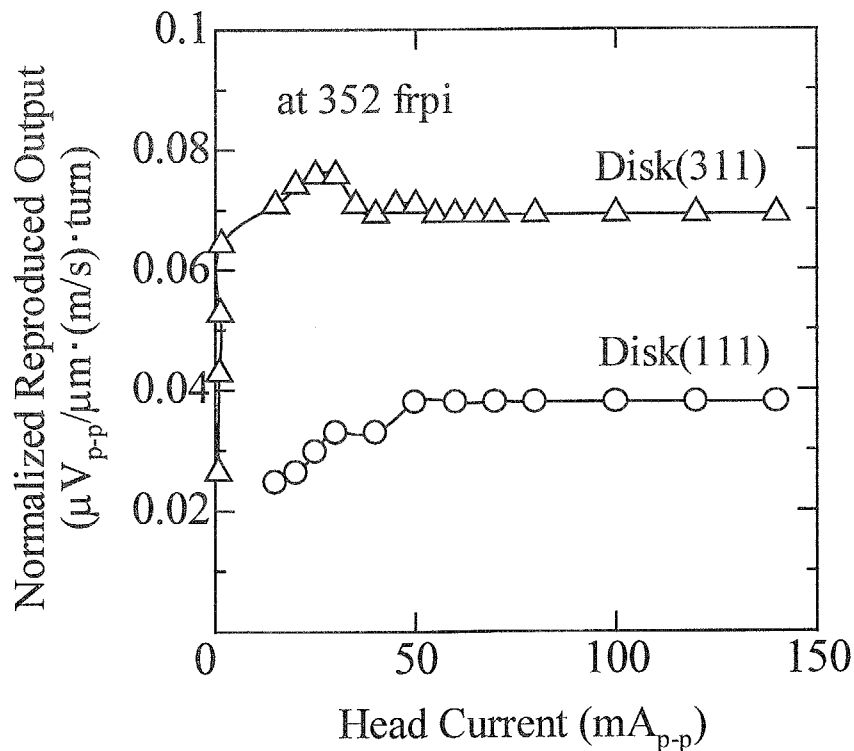


Fig. 7-7　Dependence of output voltage on writing head current.
(at 352 frpi)
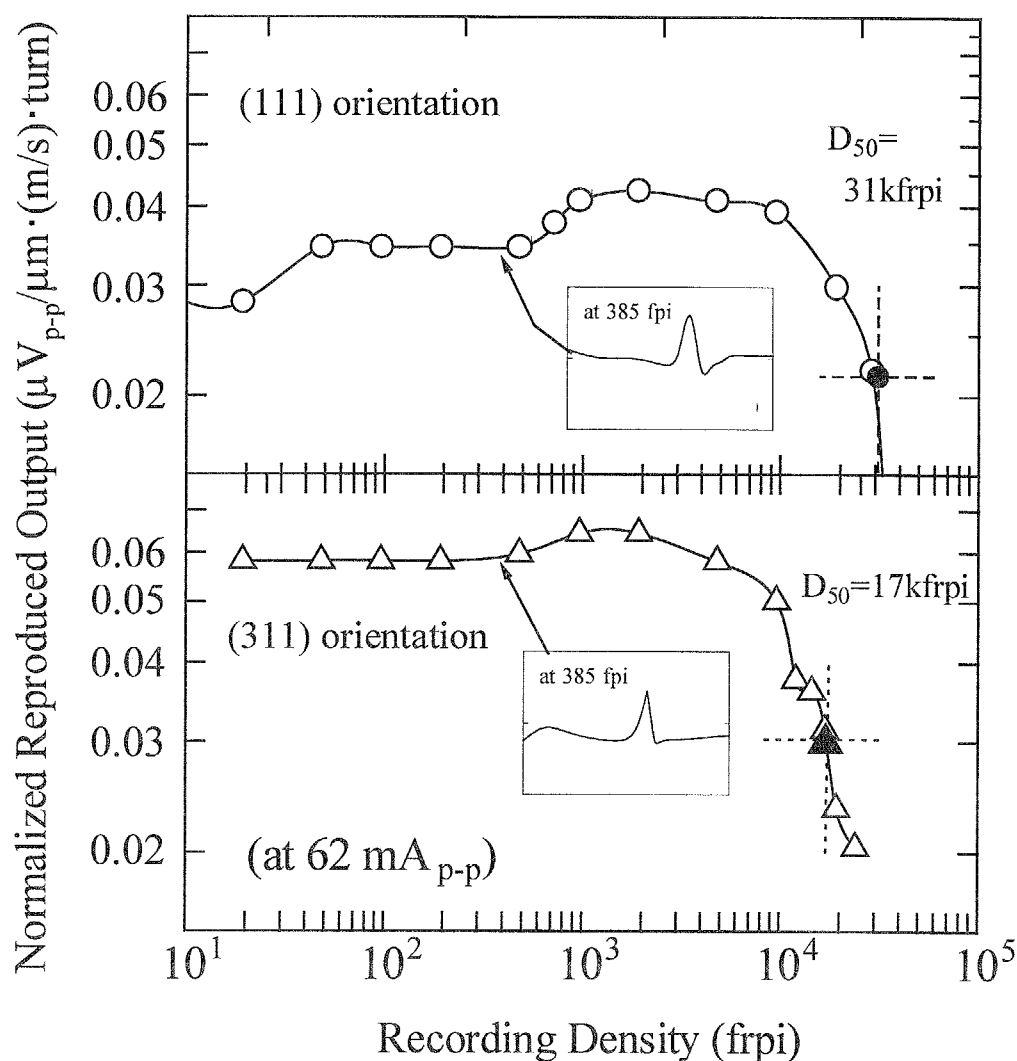
Fig. 7-8   Comparison of roll-off curves for disks with different crystallite orientation.

For Disk(111), the normalized output has a 'shoulder' at linear density from 0.4 to

10 kFRPI and linear recording density $D_{50}$ of 31 kFRPI was attained. Since the narrow

'shoulder' was generally observed for the measurement of perpendicular recording layer

using ring type head, it was confirmed that the magnetization of Co-Zn ferrite disk with

(111) orientation has perpendicular component.

On the other hand, a slight shoulder was observed for Disk(311), which has quasi in-plane anisotropy due to (311) orientation, it was not so clear as that shown in Disk(111) and $D_{50}$ was about 17 kfrpi.

Disk(111) which attained isotropic orientation of magnetization has higher linear recording density $D_{50}$ than Disk(311) which has quasi in-plane anisotropy. Since various magnetic characteristics such as saturation magnetization $4\pi M_s$ and in-plane and perpendicular coercivities were different each other, it is difficult to clarify the reason of higher $D_{50}$ for isotropic recording media. The larger $4\pi Mr \cdot \delta$ as shown in Table 7-2 seemed to be one of reasons for lower $D_{50}$ in Disk(311). However, it also seemed that magnetization component which oriented perpendicularly to film plane contributes somewhat to increase the linear recording density when ring type head was used as writing and reading ones.

Roll-off curve for Disk(111) with smaller $4\pi M_r \cdot \delta$ of about 150 G·μm was also measured by using head with narrower gap. Fig. 7-9 shows the normalized output voltage on linear recording density of Disk(111) measured by head with narrower gap length of 0.27 μm. The normalized output in this case also had a 'shoulder' at linear density from 5 to 20 kFRPI and very high recording density $D_{50}$ of 105 kFRPI was attained. The reason much higher recording density was attained for the measurement using MIG type head with gap of 0.27 μm was not only attributed to narrower gap but also large amplitude of reproduced signal due to smaller flying height even for smaller $4\pi M_r \cdot \delta$. Since much larger signal could be detected for the measurement using narrower gap of 0.27 μm, smaller signal at higher recording density was able to be detected.

Although $D_{50}$ of Co-Zn ferrite disk to date was not still so high as conventional Co-Cr/Cr media, there is possibility that it is fairly increased by the optimization of the magnetic properties of Co-Zn ferrite films and by using MR head for reading, because the media noise level of ferrite disks was low and almost constant even at high recording density[2].

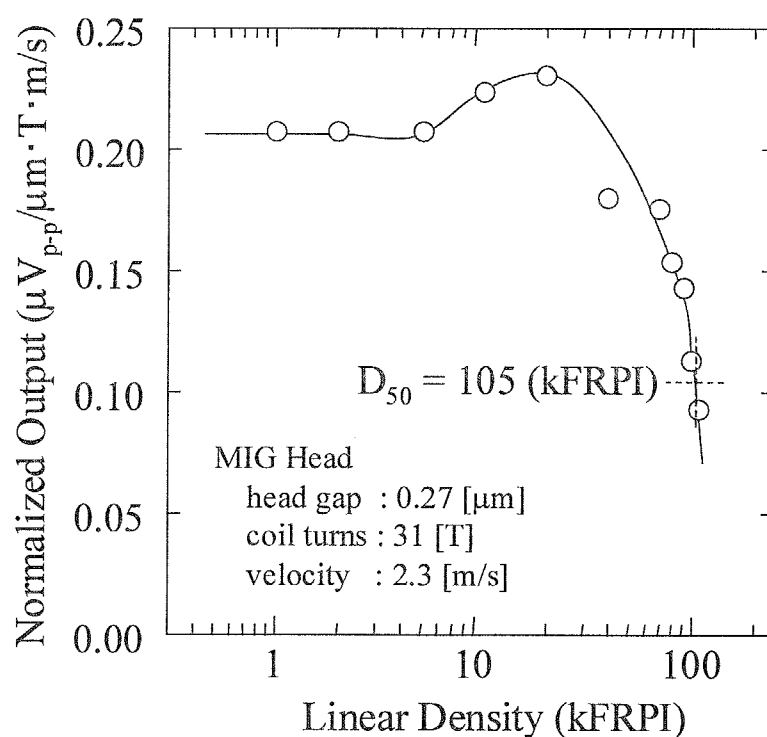Therefore, read/write characteristics were also investigated by using MR type head as mentioned in next section.



Fig. 7-9   Roll-off curve for disk with (111) orientation measured by using MIG type head with narrower gap of 0.27 μm.

---

[2] S. Tsuboi, T. Korenai, N. Ishiwata, K. Yamada and K. Tagami, *J. Mag. Soc. Japan*, vol.18, pp95- 98, 1994.

7-5-2 Measurements using merged type MR head

In this study, the films were deposited on transparent glass ceramics disk substrates of 1.89 inch in diameter. The read/write characteristics of specimen disk with (111) and (311) orientation, Disk(111) and Disk(311), were examined in semi-contact mode without over coating protective layer. The lubricant layer was spin-coated on the as-deposited film.

Table 7-4 lists crystallite orientation and magnetic characteristics of Disk(111) 75 nm thick and Disk(311) 65 nm thick, which were deposited at substrate temperature $T_s$ of 200 and 400°C, respectively.

Fig. 7-10 shows their in-plane and perpendicular B-H. The saturation and remanent magnetization $M_{s//}$ and $M_{r//}$ were determined on in-plane M-H loops. Both of in-plane and perpendicular coercivity $H_{c//}$ and $H_{c\perp}$ were higher for Disk(111). This tendency was observed for another disks with different thickness. It seemed to be attributed to larger crystallite size and $4\pi M_s$ due to higher substrate temperature. It should be noted that $H_{c\perp}$ was higher than $H_{c//}$ for both disk specimens.

Table 7-4 Crystallite orientation and magnetic characteristics of specimen disks

|  | Disk(111) | Disk(311) |
|---|---|---|
| Substrate temperature $T_s$ | 200°C | 400°C |
| Crystallite orientation | (111) | (311) |
| Saturation magnetization $4\pi M_s$ | 2.7 kG | 4.5 kG |
| Squareness S | 0.432 | 0.45 |
| Layer thickness | 75 nm | 65 nm |
| $4\pi M_r \cdot \delta$ | 90 G·µm | 132 G·µm |
| In-plane coercivity $H_{c//}$ | 1.86 kOe | 1.26 kOe |
| Perpendicular coercivity $H_{c\perp}$ | 2.62 kOe | 1.52 kOe |
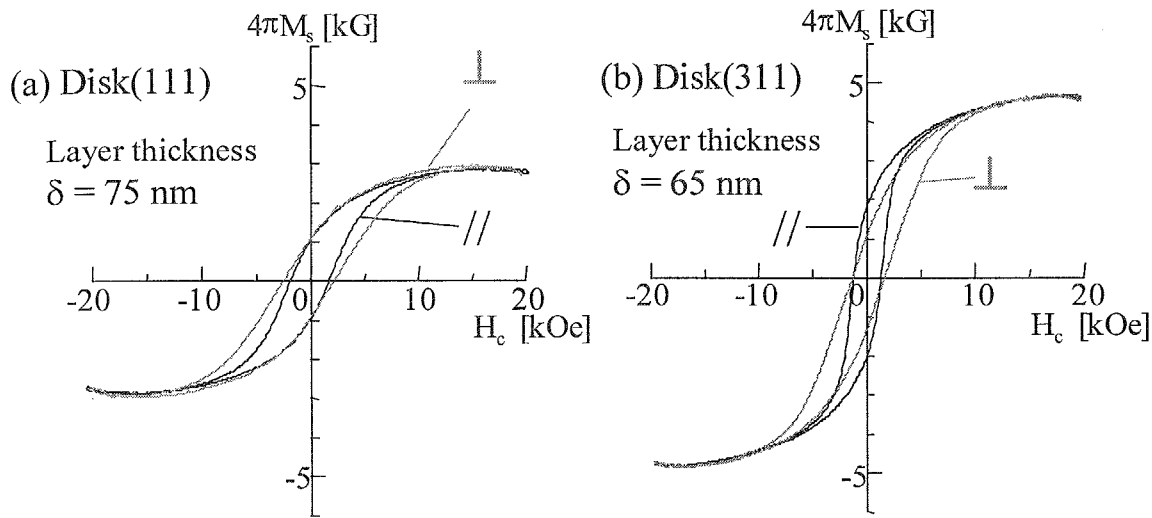
Fig. 7-10    In-plane and perpendicular B-H loops of (a)Disk(111) 75 nm thick
and (b)Disk(311) 65 nm thick.

It suggested that Co-Zn disk, especially Disk(111), have large perpendicular
component as mentioned in *Chapter 6*. The value of $4\pi M_r \cdot \delta$ of disks with smaller
thickness were calculated by assuming that films thickness is proportion to the
deposition time and its squareness was constant even for the decrease of film thickness

Table 7-5 lists the specifications of merged type MR head used in this study. The gap
length and shield gap width were 0.35 and 0.27 μm, respectively. The flying height was
estimated to be about 65 nm at head speed of 8.0 m/s. The write head current and MR
bias current were set at the optimized value of 40 and 10 mA, respectively.

Fig. 7-11 shows the typical isolated waveform of longitudinal and perpendicular rigid disks.
On the other hand, di-pulse waveform is observed at transition region and the
reproduced signal is not zero even at the bit center, where is the most further than
transition, for perpendicular rigid disks. This di-pulse waveform is one of proofs that the
bit is magnetized perpendicular direction.

Table 7-5  Specifications of merged MR type head

| Head type | Merged type MR head |
|---|---|
| Write Pole    width/length | 3.2μm/3.5 μm |
| Gap length    g | 0.35 μm |
| First shield length | 1.0 μm |
| Second shield length | 2.5 μm |
| Shield gap length | 0.27 μm |
| Read track width | 2.7 μm |
| Surface velocity | 7.0 m/s(at 4,200 r.p.m.) |
| Flying height | 65 nm |

Fig. 7-12 shows the isolated wave forms at low linear recording density of about 3.3 kfrpi for Disk(111) 50 nm thick and Disk(311) 35 nm thick, respectively. Since $4\pi M_r \cdot \delta$ of Disk(111) is smaller than that of Disk(311), the amplitude of recorded signal was low compared with that of Disk(311). It is a distinctive point for Disk(111) to have a shoulder as shown in Fig. 7-12(a), while it was not clearly observed in Fig. 7-12(b). This shoulder suggested that the existence of perpendicular component at transition regions is relatively large for Disk(111). Since $H_{c\perp}$ of Disk(111) was much higher than $H_{c//}$, the recorded bit at transition seemed to have large perpendicular component for Disk(111).

Fig. 7-13 shows the envelopes of a)Co-Cr-Ta/Cr longditudinal disks, b)Disk(111) and c)Disk(311), respectively. Although the envelope of a) had constant width and suggested that the bits was recorded constantly through the track, it is not constant in (b) and (c), and suggested that the magnetic characteristics were not uniform through the track. This seemed to be attributed to the inuniformity of substrate temperature and no disk rotation during deposition. They should be improved for obtaining the reproducibility of the measured data.

156
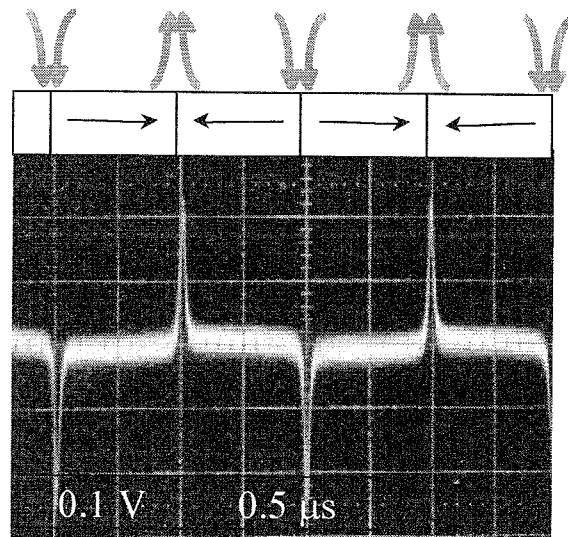
(a) Longitudinal Disk
(Co-Cr-Ta/Cr film)
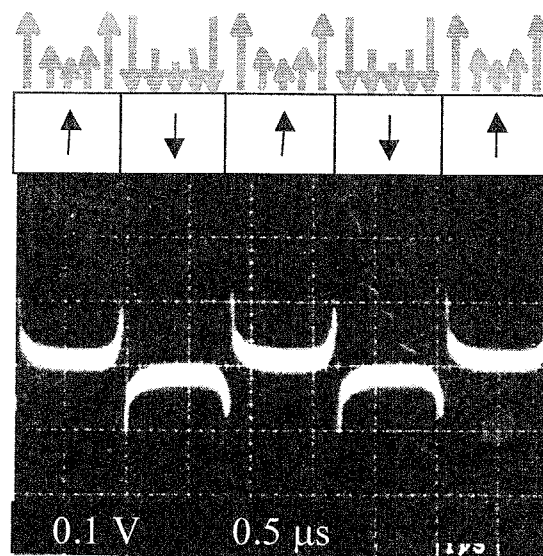


(b) Perpendicular Disk
(Co-Cr-Ta film)

Fig. 7-11    Typical isolated wave form of (a)longitudinal(Co-Cr-Ta/Cr)
and (b)perpendicualr(Co-Cr-Ta) recording layers.

157

(a) Disk(111)    δ = 50 nm

40mV

1μs

Large perpendicular component

Shoulder



(b) Disk(311)    δ = 37 nm
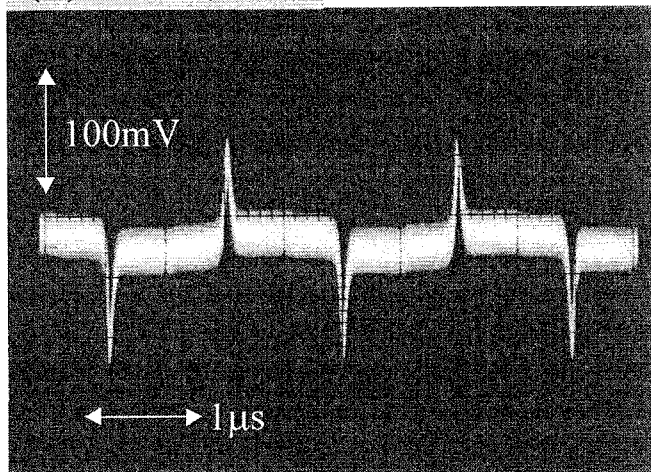
100mV

1μs

Small perpendicular component

No shoulder
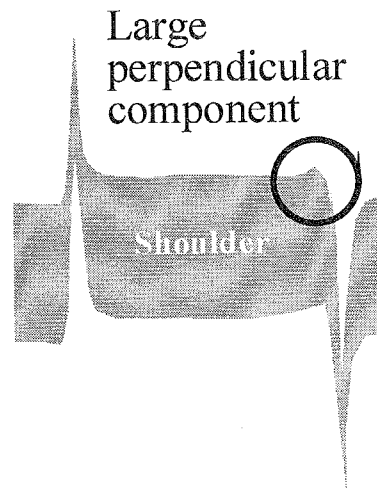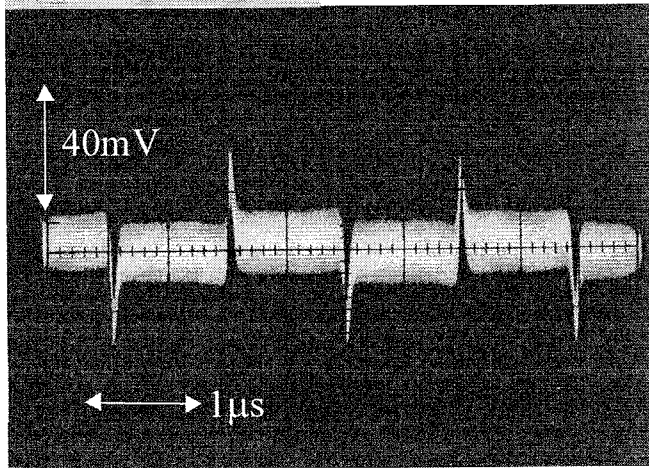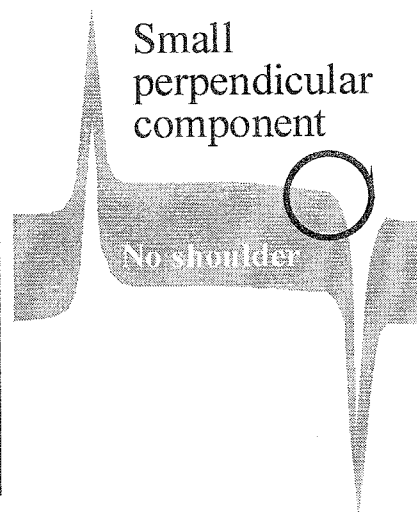
Fig. 7-12    Isolated waveforms of (a)Disk(111) 50 nm thick and (b)Disk(311) 35 nm thick at linear recording density of about 3.3 kfrpi.
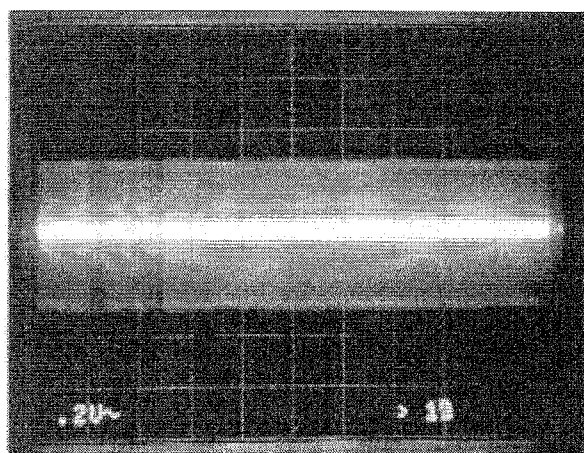
Co-Cr-Ta/Cr longitudinal recording layer $H_c$=1800Oe
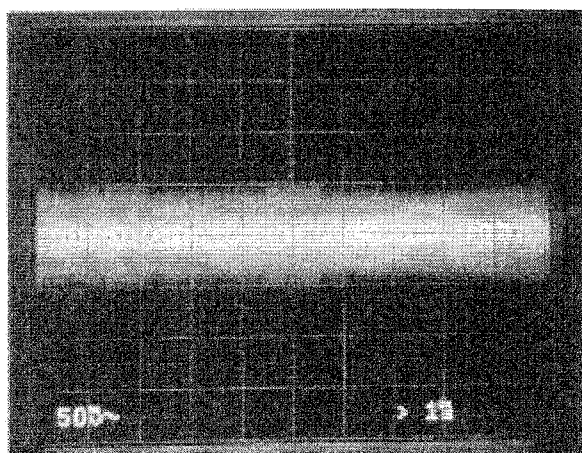
Co-Zn ferrite Disk(111)
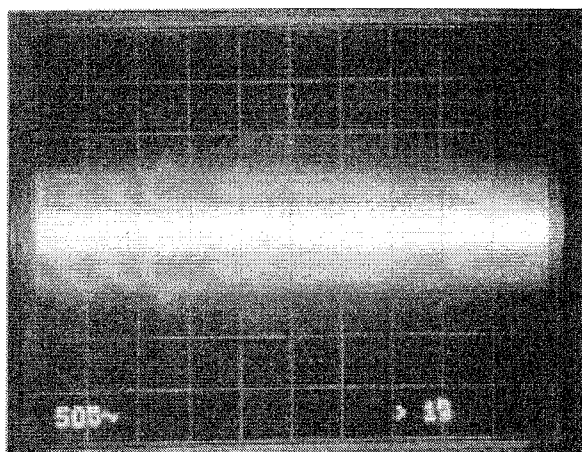
Co-Zn ferrite Disk(311)

Fig. 7-13    Envelopes of a)Co-Cr-Ta/Cr longditudinal disks, b)Disk(111) and c)Disk(311), respectively.

The linear recording density, where the amplitude of the output signal falls down to 50 % of that of the isolated signal, increased with the decrease of layer thickness $\delta$ as shown in Fig. 7-14. It seems to be attributed to smaller transition width $a_W$. In longitudinal recording layer, transition width $a_W$ is proportional to the product of $4\pi M_r \cdot \delta/H_c$. This relation was also applicable for Co-Zn ferrite disk with isotropic orientation of magnetization. The highest $D_{50}$ was 136 kfrpi for Disk(111) 50 nm thick and that of 86 kfrpi for Disk(311) 35 nm thick, respectively.

Fig. 7-15 shows the roll-off curve of Disk(111) and Disk(311) which attained highest $D_{50}$, respectively. The reason why higher recording density was attained for the Disk(111) seemed to be attributed to smaller $4\pi M_r \cdot \delta$ and higher $H_{c//}$ and $H_{c\perp}$. $D_{50}$ of 136 kfrpi was almost same as that of the commercialized Co-Cr-Ta/Cr rigid disks and it might be improved by increasing $H_c$, decreasing the head gap length and flying height and so on.
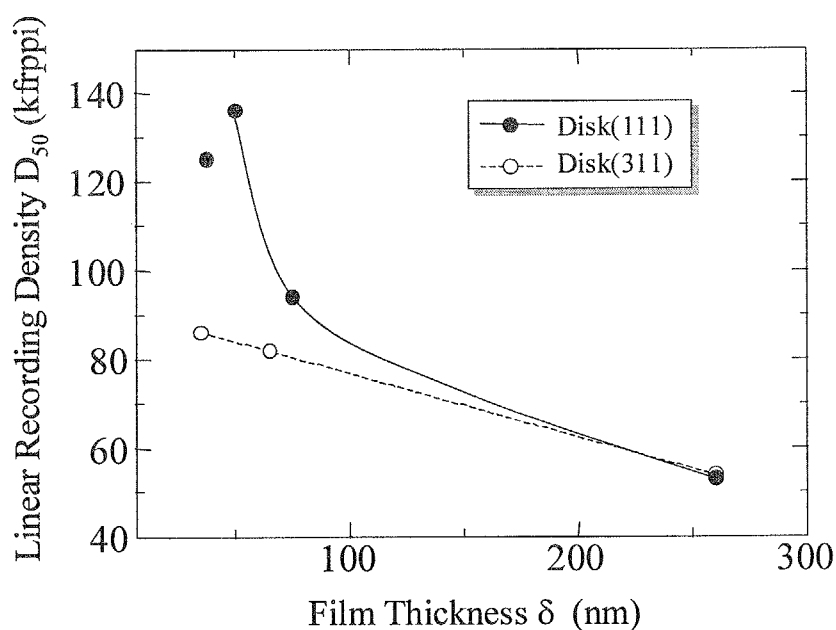


Fig. 7-14    Dependence of linear recording density $D_{50}$ of Disk(111) and Disk(311) on film thickness $\delta$.
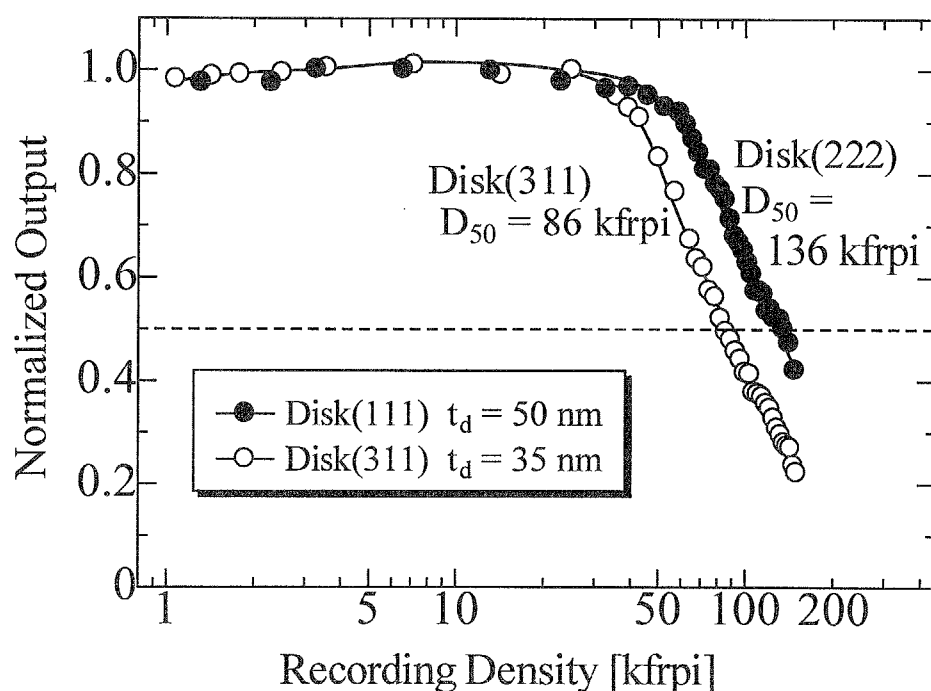
Fig. 7-15   Roll-off curves of Disk(111) and Disk(311) which attained highest linear recording density $D_{50}$.

Fig. 7-16 show noise spectra of Co-Cr-Ta/Cr disks with $H_{c//}$ of (a)1.8 kOe and (b)2.4 kOe, respectively. They were measured at relatively low and high linear recording density of 21 and 102 kfrpi. In these figures, the transition noise was characterized the between area of total and DC erase noise, as shown in Fig. 7-17(a). These transition noise, which is originated from transitions as shown in Fig. 7-17(b), is a seriously large for Co-Cr-Ta/Cr longitudinal recording media with $H_{c//}$ of 1.8 kOe even at relatively low recording density of about 21 kfrpi as shown in (a). For disk specimens with higher $H_{c//}$ of 2.4 kOe, although, the transition noise was smaller at low density of 21kfrpi, it was fairly large at high density of 102 kfrpi as shown in (b).
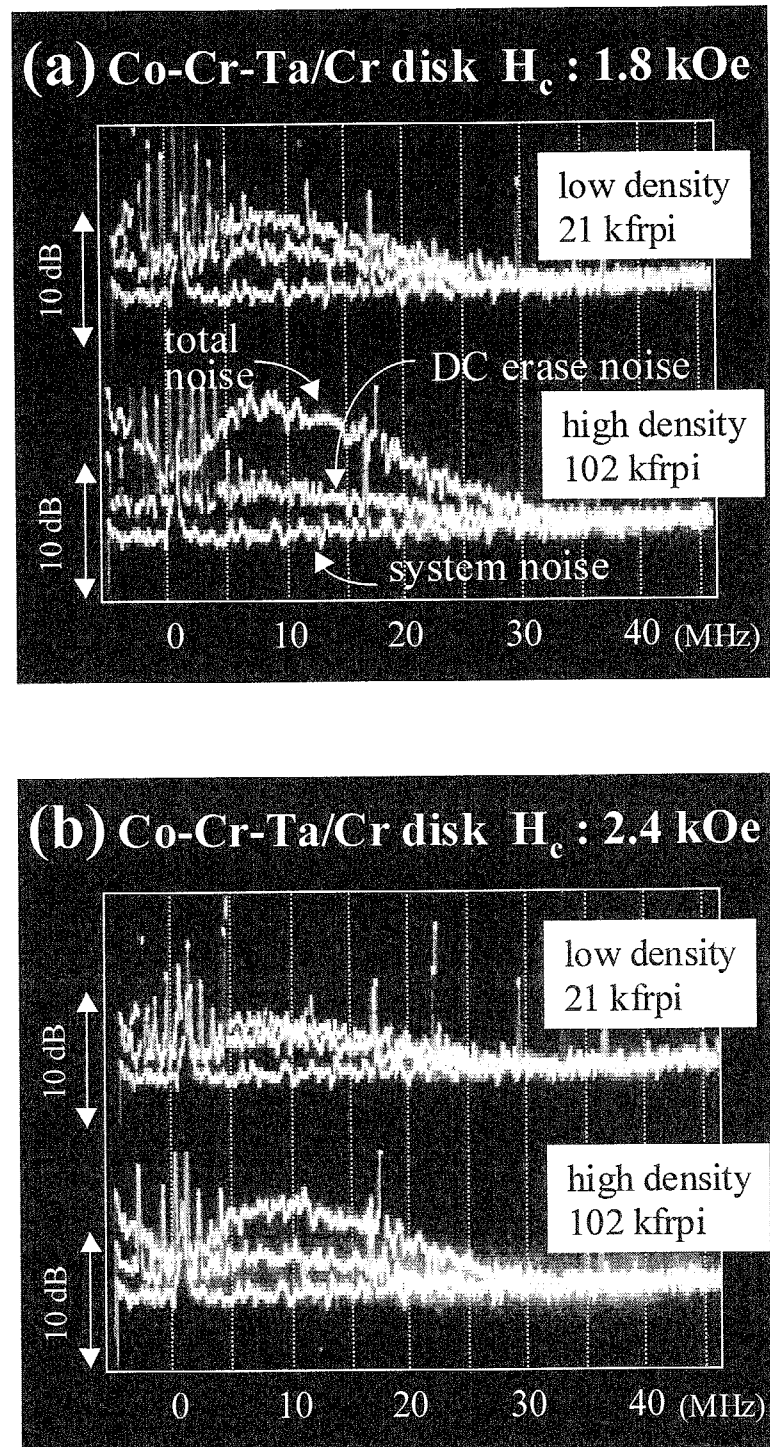
Fig. 7-16  Noise spectra of Co-Cr-Ta/Cr disks with $H_{c//}$ of (a)1.8 kOe
and (b)2.4 kOe, respectively, measured at linear recording
density of 21 and 102 kfrpi.

transition noise

total noise spectra

DC erase noise spectra

(a)

frequency    (MHz)

system noise spectra

source of transition noise

(b)
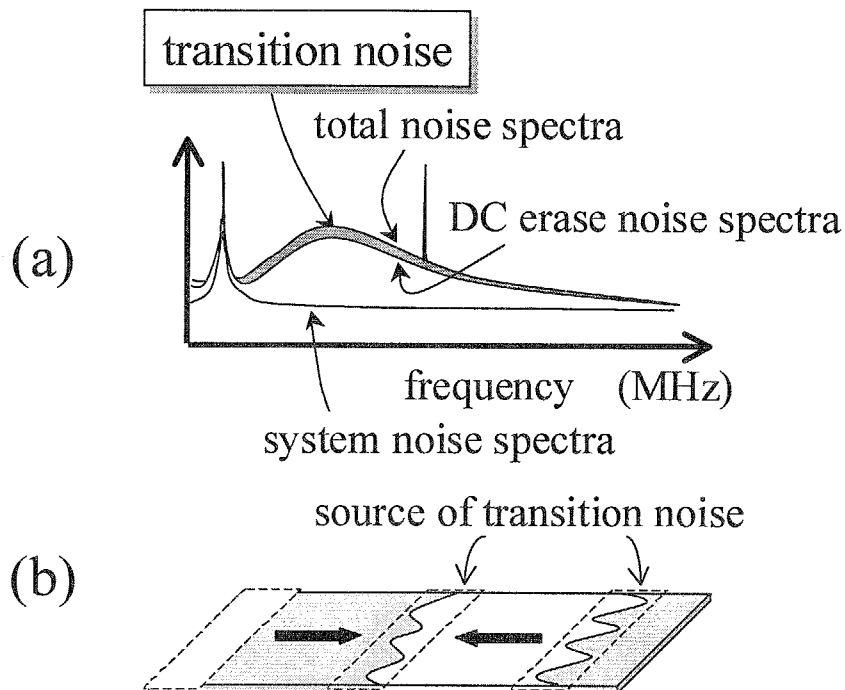
Fig. 7-17  Schematic illustraion of (a)representative total noise,
DC erase noise and system noise spectra and (b)source
of transition noise.

Fig. 7-18 shows noise spectra of (a)Disk(111) and (b)Disk(311) measured at linear

recording density of 24 and 104 kfrpi, respectively. Although DC erase noise was not so

small, its transition noise was very small and total noise of Disk(111) at 104 kfrpi seemed

to be almost same as or smaller than that at 24 krpi. On the other hand, the media noise of

Disk(311) slightly increased at higher recording density of 104 kfrpi. This result, i.e. the

media noise increases with increase of linear recording density, was same as conventional

longitudinal recording layer, such as Co-Cr-Ta/Cr. However, it is relatively small

compared with Co-Cr-Ta/Cr longitudinal recording layers with higher coercivity of 1.8

and 2.4 kOe as seen in Fig. 7-16.
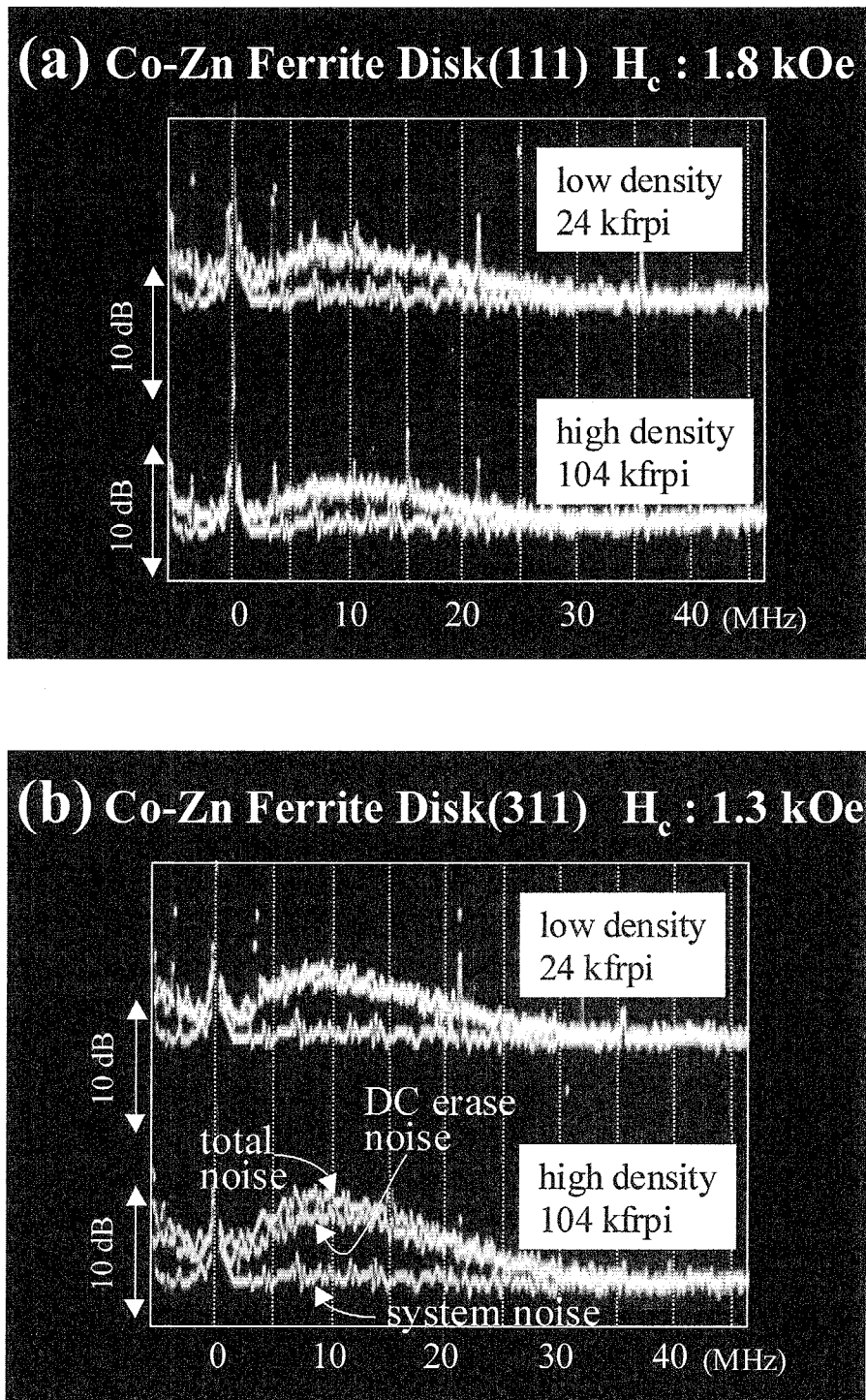
Fig. 7-18    Noise spectra of (a)Disk(111) and (b)Disk(311) measured at linear recording density of 24 and 104 kfrpi.

Fig. 7-19 shows the dependence of noise level for Co-Cr-Ta/Cr longitudinal disks(both of $H_{c//}$ of 1.8 and 2.4 kOe), Disk(111) with $H_{c//}$ of 1.74 kOe and Disk(311) with $H_{c//}$ of 1.26 kOe, respectively. While the noise level of Co-Cr-Ta/Cr disks increased with the increase of recording density, that of Disk(111) was almost zero and that of Disk(311) was also negligible. Since the transition noise for perpendicular recording layer was almost zero even at high linear recording density 200 kfrpi and above, the almost zero transition noise for Disk(111) and quite small one for Disk(311) might be caused by the existence of perpendicular component of magnetization as shown in Fig.6-12 and Fig.6-13. These quite small transition noise characteristics seems very suitable for a recording layer with ultra-high density.

Fig. 7-20 shows the dependence of signal to niose ratio for Co-Cr-Ta/Cr longitudinal disks, Disk(111) and Disk(311), respectively. Since the $4\pi M_r \cdot \delta$ of Disk(111) and Disk(311) were smaller than that of Co-Cr-Ta/Cr disks, the detected signal was small. Therefore, S/N of Disk(111) and Disk(311) was much smaller than those of Co-Cr-Ta/Cr disks at lower recording density. However, they were almost same as that of Co-Cr-Ta/Cr disk with $H_{c//}$ of 1.8 kOe at high recording density of 200 kfrpi, while that of Co-Cr-Ta/Cr disk with $H_{c//}$ of 2.4 kOe was larger due to high $H_{c//}$. In addition, it should be noted that the decrease ratio of Disk(111) at higher recording density was smaller than that of Co-Cr-Ta/Cr disks and Disk(311). These S/N ratio for Co-Zn ferrite disks seems to be fairly improved by increasing coercivity.
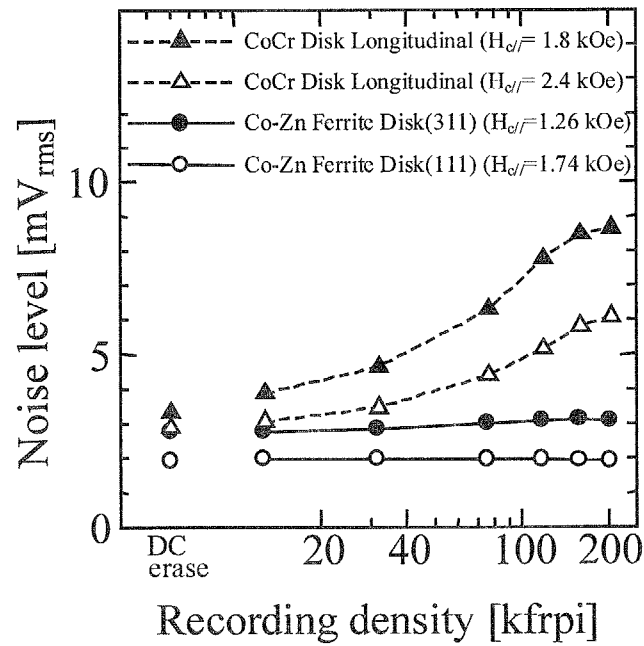
Fig. 7-19  Dependence of noise level for various disk specimens on linear recording density.
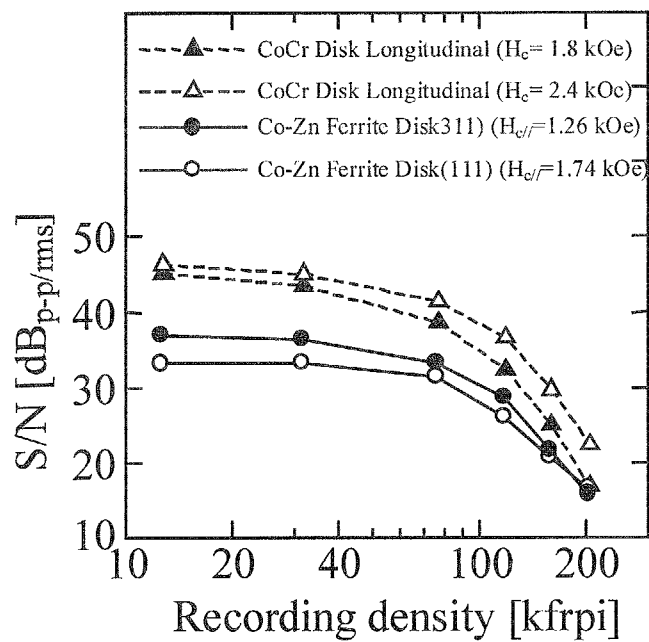
Fig. 7-20  Dependence of signal to noise ratio for various disk specimens on linear recording density.

## 7-6 Summary

In this chapter, Co-Zn ferrite films were deposited on $SiO_2$/Si and glass cramics disk substrates by the facing targets sputtering apparatus without subsequent annealing process. And their crystallite orientation and read/write characteristics using MIG type head and merged type MR head were investigated.   The results obtained in this study were as follows;

1) The films deposited at $T_s$ of 90, 200 and 400°C exhibited the center-line average roughness $R_a$ of 1.0, 1.2 and 4.0 nm, respectively.

2) The disk specimens deposited at $T_s$ of 200 and 400°C were composed of crystallites with excellent (111) orientation and (311) orientation. These tendency was common for both $SiO_2$/Si disk subrtrates and glass ceramics disk substrates.

Measurement using MIG type head

3) Disk(111) with isotropic orientation of magnetization due to the crystallite orientation of (111) revealed higher linear recording density $D_{50}$ of 31 kfrpi than that of Disk(311) with quasi in-plane orientation of magnetization of 17 kprpi when MIG type head with gap length of 0.35 μm was used.

4) A linear density $D_{50}$ of 105 kFRPI was attained for Disk(111) with smaller $4\pi M_r \cdot \delta$ by using a MIG type head with a narrow gap length of 0.27 μm.

Measurement using merged MR type head

5) Isolated waveform of both Disk(111) and Disk(311) with relative large thickness of 260 nm looked like to that of perpendicular recording media such as Co-Cr.

6) Highest $D_{50}$ of Disk(111) and Disk(311) were 136 and 86 kfrpi and their thickness was 50 and 35 nm, respectively.

7) Transition noise of Disk(111) did not increas with the increase of linear recording density and that of Disk(311) was relatively small compared with that of Co-Cr-Ta/Cr longitudinal recording disks.

8) Although S/N ratio of Disk(111) at low recording density up to 200 kfrpi was smaller than that of longitudinal Co-Cr disks, its decrease ratio at high recording density was smaller.

In consequence, Co-Zn ferrite disk with (111) orientation is applicable as contact type of recording layer at ultra-high density because of their surface smoothness and low characteristics noise at high density.

Although surface smoothness should be improved and higher coercivity is necessary, Co ferrite disk with (311) orientation seems also applicable as contact type of in-plane recording layer.

# Chapter 8

# Ba ferrite/ZnO Doublelayered Films

## 8-1  Introduction

A magnetoplumbite type of Ba ferrite (BaM:BaFe$_{12}$O$_{19}$) are usually produced using dry ceramic techniques and since their magnetic characteristics as bulk are very sensitive to its microstructure, they have been engaged in improving the sintering process and controlling the amount of included impurities. The sintered magnets, which have large remanent magnetization and high coercivity, were mass-produced and are applied for many applications as permanent magnets. On the other hand, the film of Ba ferrite has been intensively investigated as magnetic recording media[1,2,3,4,5,6,7]. It seems to be applicable as perpendicular magnetic recording media as well as microwave filters and other devices[8,9,10,11,12,13,14], because it exhibits moderate saturation magnetization $4\pi M_s$ and a large perpendicular magneto-crystalline anisotropy constant $K_{u_\perp}$ as well as

---

[1] T. Fujiwara : IEEE Trans. on Magn, 21[5], pp.1480 (1985)

[2] E. Lacroix, P. Gerard, G. Marest and M. Dupuy : J. Appl. Phys., 69[8], pp.4770-4772 (1991)

[3] K. Yamamori, T. Tanaka and T. Jitosho : IEEE Trans. Mag., 27[6], pp.4960-4962 (1992)

[4] M. Naoe, S. Hasunuma, Y. Hoshi and S. Yamanaka : IEEE Trans. Mag., 17[6], pp.3184-3186 (1981)

[5] I. Zaquine, H. Benazizi and J. C. Mage : J. Appl. Phys., 64[10], pp.5822-5824 (1988)

[6] M. Matsuoka and M. Naoe : J. Appl. Phys. 57[1], pp.4040-4042 (1985)

[7] M. Matsuoka, Y. Hoshi, M. Naoe and S. Yamanaka : IEEE Trans. Magn., 18[6], pp.1119-1121 (1982).

[8] H. Dotsch et al. : Mater. Res. Bull., 18, pp.1209 (1983)

[9] S. Rinaldi and F. Licci : IEEE Trans. Magn., 24, pp.2799 (1988)

[10] I. Zaquine, H. Benazizi and J. C. Mage : J. Appl. Phys. 64, pp.5822 (1988)

[11] D. C. Webb : IEEE Trans. Magn., 24, pp.2799 (1988).

[12] M. S. Yuan et al. : Appl. Phys. Lett., 53, pp.340 (1988)

[13] J. D. Adam et al. : J. Magn. Magn. Mater., 83, pp.419 (1990)

excellent chemical stability, corrosion resistance and hardness. Nowadays, the spacing between head and medium have being decreased with increasing a recording density and the contact recording media without protective layers will be required for achieving an ultra-high recording density. If Ba ferrite films could be successfully deposited with its inherent magnetic characteristics and excellent smooth surface, it would be one of promising candidates as a contact type of perpendicular recording layer in rigid disk with ultra high density.

Several researchers, therefore, had attempted the deposition of Ba ferrite films[15,16]. However, it was not so easy for them to deposit single phase Ba ferrite film with sufficient c-axis orientation and magnetic characteristics such as large $4\pi M_s > 4.0$ kG and anisotropy constant $K_u > 2.0 \times 10^{-5}$ J/m$^3$. Since crystallite structure of Ba ferrite is very complicated, high substrate temperature above 650°C[17] and/or quite high annealing temperature above 750°C were necessary to form Ba ferrite crystallites. These Ba ferrite films were commonly deposited in mixture of Ar and O$_2$ gases by using the diode and magnetron sputtering apparatus[5,18]. The reasons why this Ba ferrite films had poor crystallinity and insufficient magnetic characteristics were not only attributed to the complexity of crystal structure of Ba ferrite. It was also attributed to the serious demerits of these conventional types of sputtering apparatuses such as significant bombardment of high-energy $\gamma$-electrons and negative ions to film surface due to its insufficient

---

[14] D. C. Webb : IEEE Trans. Magn., 24, pp.2799 (1988).

[15] Sui. XY, M. H. Kryder : Appl. Phys. Lett., 63[11], pp.1582-1584 (1993)

[16] T. L. Hylton, M. A. Parker, J. K. Howard : Appl. Phys. Lett., 61[7], pp.867-869 (1992)

[17] A. Morisako et al. : J. Magn. Mat. 57, pp.1657-1658 (1986)

[18] T. L. Hylton, M. A. Parker, K. R. Coffey and J. K. Howard : J. Appl. Phys., 73[10], pp.6257-6259 (1993)

plasma confinement, and inclusion of recoiled Ar atoms into deposited films.

Hoshi and Matsuoka precisely reported in their Ph.D thesis that single phase Ba ferrite films with c-axis oriented perpendicularly to film plane and large $4\pi M_s$ of 4.7 kG were successfully deposited at relatively low substrate temperature of 550℃ without annealing process on a Si wafer substrate with thermally oxidized surface layer($SiO_2$/Si). They used the "damage-free" facing targets sputtering (FTS) apparatus[19] and ZnO underlayer, which has most closely packed structure of oxygen and was very suitable for the epitaxial growth of BaM crystallites[20]. They succeeded to solve the problem of high-energy charged particles such as γ-electrons and negative oxygen ions. However, substrate temperature $T_s$ of 550℃ is not low enough and further decrease of $T_s$ is required for the application and mass production of Ba ferrite film as recording layer in rigid disk. In this study, I engaged in the decreasing of $T_s$ for the formation of Ba ferrite films with excellent c-axis orientation and magnetic characteristics suitable for recording layer.

I paid attention to the existence of Ba atoms in the complicated structure of Ba ferrite crystallite. Since Ba atom is very large and heavy than sputtering gases, i.e. Ar and $O_2$, there are a lot of recoiled particles. Moreover, Ba ions should be sited in regular site to generate large anisotropy field along c-axis, a sufficient momentum transfer from sputtering gas atoms to Ba ones are necessary and Ba atoms should arrive at substrate with high energy. Therefore, the mixing Xe with larger atomic weight into sputtering gas was attempted in this study. Ba ferrite films were deposited on ZnO underlayer in

---

[19] Yoichi Hoshi : Ph.D. thesis, Tokyo Institute of Technology (1984)
[20] Morito Matsuoka : Ph.D. thesis, Tokyo Institute of Technology (1985)

mixture gas of Xe, Ar and $O_2$ for obtaining excellent c-axis orientation and magnetic characteristics. Two kinds of targets with Ba contents higher and lower than stoichiometric ones, i.e. $BaFe_{11.0}Fe_{19-y}$ and $BaFe_{11.0}Fe_{19-y}$, were used for the film depositions. The dependence of their magnetic characteristics such as $4\pi M_s$, $H_{c\perp}$ and perpendicular anisotropy constant $K_\perp$ on $P_{Xe}$ and $T_s$ were investigated, respectively, as well as the evaluation of surface smoothness using SEM and AFM images.

As first stage, the Ba ferrite layers were deposited at relatively high $T_s$ of 600℃ and then the optimization of the partial Xe pressure $P_{Xe}$ on surface smoothness, crystallographic and magnetic characteristics were carried out considering the result of plasma diagnosis. As second stage, the Ba ferrite films were deposited at optimized $P_{Xe}$ changing substrate temperature $T_s$, and the substrate temperature $T_s$ dependence of crystallographic and magnetic characteristics were investigated, respectively.

## 8-2    Difficulty in deposition of Ba ferrite film

In the sputtering deposition of Ba ferrite films, Ba and O atoms are likely to be reduced from the growing film surface by bombardment of high-energy particles[21]. Therefore, Ba ferrite target with Ba content higher than stoichiometric composition of $BaO \cdot 6Fe_2O_3$ has to be used to obtain a stoichiometric Ba ferrite film. The optimized target composition were differ for each apparatus, and it was $BaO \cdot 3.5Fe_2O_3$(or $BaO \cdot 4.0Fe_2O_3$) for the RF diode sputtering (or DC magnetron[22]) apparatus and $BaO \cdot 5.5Fe_2O_3$ for the facing target sputtering apparatus. The scheme of decrease of Ba

---

[21] L. R. Gilbert et al., J. Vac. Sci. Technol., 17[1], pp. 389-391 (0980)
[22] M. Naoe et al. : IEEE Trans. Magn., 17[6], pp.3184-3186 (1981)

content in the film seems to be as follows;

1) Scattering of sputtered Ba during transportation from target to substrate and back scattering to target surface.

2) Selective re-sputtering of sputtered atoms attributed to the difference in adsorption constant at film surface.

Decreasing the distance from target to substrate and increasing the mean free length by making gas pressure low would solve the problem 1). On the other hand, the problem 2) is not easy to solve because it is also concerned with their inherent chemical reaction. In sputtering deposition, the absorption and removal scheme and absorption site of particles arrived at substrate have to be considered carefully. Especially, since oxygen species are included in the sputter deposition of Ba ferrite film, it has to be considered that the absorption condition and chemical reaction with Ba and Fe atoms. From the simulations, the kinetic energy of incident particle is maintained after perfect elastic collision between incident ion and target atom. Then incident atoms become recoiled particles and some of them might direct toward the substrate direction with large kinetic energy. Actually, although there are a lot of recoiled particles with high energy through perfect elastic collision, the confinement of them by magnetic field is impossible because they do not have electric charge. Generally, in the deposition using 'damage-free sputtering' of FTS apparatus, Ba atoms were likely to be incorporated to the deposited films and composition ratio of Ba in the optimized target $n(BaO \cdot n(Fe_2O_3))$ was closer to the target value of 6.0 than that of RF diode sputtering[23]. However, the confinement of recoiled particles is difficult even for FTS system as mentioned in *Chapter 3*. It was reported that their angle distribution to target plane is concentrated

mainly in the range 30-45 degree. Unfortunately this angle is almost accordance with the angle from target surface to substrate one in the configuration of FTS system. Therefore, the recoiled Ar particle has to be fully considered for FTS system. Thornton et al. reported that the number of incorporated Ar was increased with the increase of the number of recoiled Ar atoms[24]. The occurrences of recoiled atoms are much remarkable when the atomic weight of target atoms are much larger than that of incident ions. For the deposition of Ba ferrite film, Ar is commonly used as sputtering gas and in this case, the recoiled Ar by Ba atom seems to cause serious damage to the growing film. Winters et al suggested that the occurrence of the recoiled particles were effectively restrained when the atomic weight of sputtering gas was closer to that of target atoms[25]. Therefore Xe whose atomic weight of 134 is almost same as that of Ba was mixed in the sputtering gases in this study.

## 8-3    Mixing Xe into sputtering gas

In R blocks of BaM crystal lattice, larger $Ba^{2+}$ ions with radius of 1.43 Å should occupy the sites of smaller $O^{2-}$ ones with radius of 1.32 Å as seen in Fig. 8-1. Therefore, it is effective for the formation of Ba ferrite crystallites that the sputtered Ba atoms possess high moment for sufficiently long random walk on substrate surface. However, since the atomic weight of Ba(137.3) is much heavier than that of Ar(40.0) as seen in Fig. 8-2, the momentum transfer from Ba to Ar atoms at the target surface seems to be insufficient.

---

[23] M Matsuoka et al.: IEEE Trans. Magn., 20[5], pp.800-802 (1984).
[24] J. A. Thornton and D. W. Hoffman : J. Vac. Sci. Technol., A3[3] (1985)
[25] H. F. Winters et al. : J. Vac. Sci. Technol., A11[3], pp.657-663 (1993)
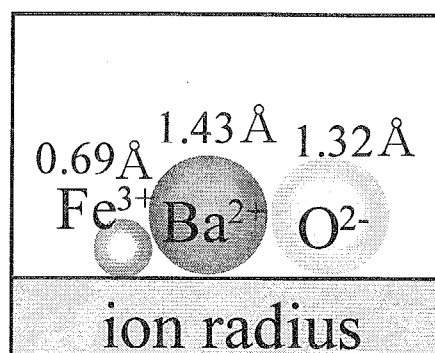
M type ($BaFe_{12}O_{19}$)

$d = 23.2$ Å      $4\pi M_s = 4.8$ kG
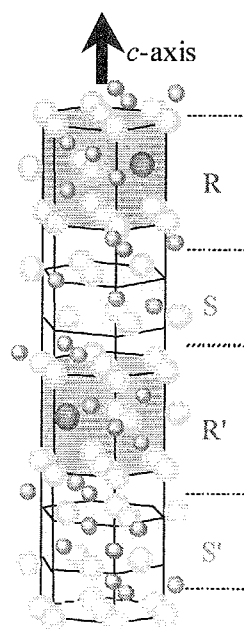


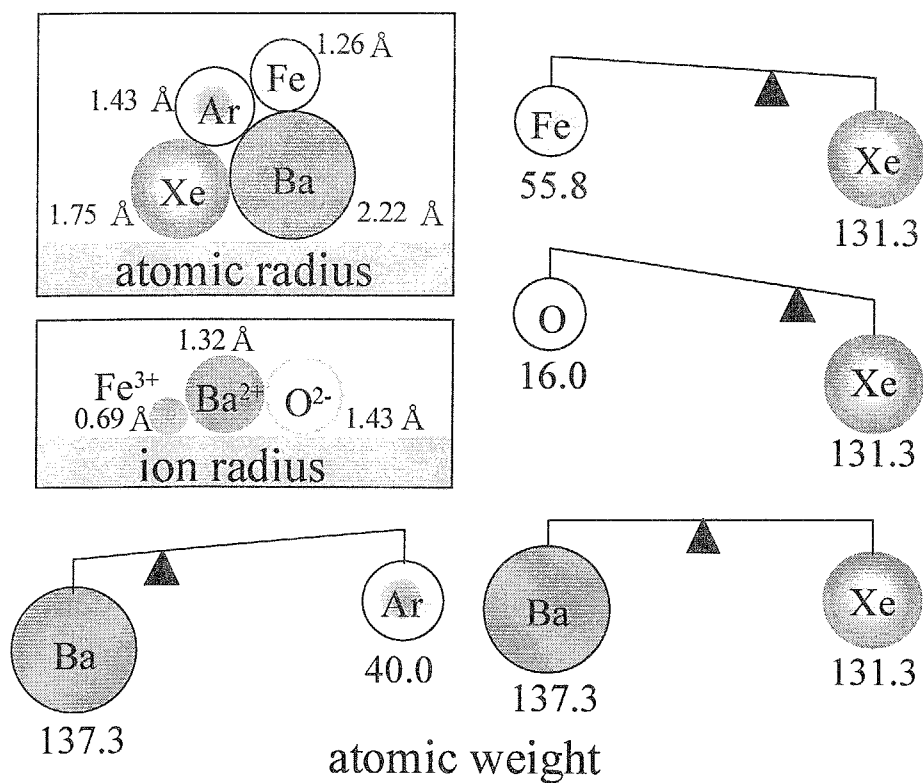Fig. 8-1    Ion radius of $O^{2-}$, $Ba^{2+}$ and $Fe^{3+}$ and crystallite structure of BaM.



Fig. 8-2    Comparison of atomic weight of Ar, Xe, O, Ba and Fe.

Moreover, Ar atom recoiled by heavier Ba atom at target surface bombard to the growing film with high kinetic energy during deposition and they may incorporate into films as impurities and easily destroy the most closely packed structure of oxygen ions whose atomic weight is as small as 16.0.

In this study, Xe atoms, which has heavier atomic weight is mixed into sputtering gases. The atomic weight of Xe(131.3) is much heavier than those of O(16.0) and Fe(55.8), and is not so different from that of Ba. Since the momentum transfer between atoms with almost the same atomic weight is very effective and the sputtered particle by heavier incident ion have larger kinetic energy[26] and moment[27], Ba atoms sputtered by Xe ions seemed to arrive at the substrate with larger moment than those atoms sputtered by Ar ions.

Therefore, the energy and angle of recoiled particles were calculated as shown in Fig. 8-3 using equation (8-1) and (8-2), respectively.
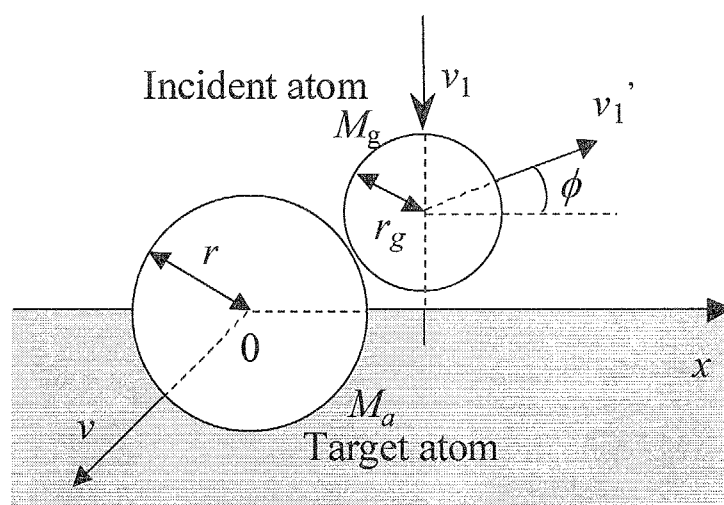


Fig. 8-3  Schematic illustration of recoiled atoms for calculation of their angle and energy.

---

[26] R. V. Stuart and G. K. Wehner : "Energy distribution of sputtered Cu adatoms," J. Appl. Phys., 35, pp.1819 (1964).

$$v_1' = v_1 \frac{|M_g - eM_a|}{M_g + M_a} \sqrt{1 + \left\{ \left( \frac{M_g + eM_a}{M_g - eM_a} \right)^2 - 1 \right\} \frac{x^2}{(r_g - r_a)}} \qquad (8.1)$$

$$\phi = a\tan\left( \frac{M_g + M_a}{M_g - eM_a} \cdot \frac{x}{\sqrt{(r_g + r_a)^2 + x^2}} \right) - a\sin\left( \frac{x}{r_g + r_a} \right) - \frac{\pi}{2} \qquad (8.2)$$

where $M_a$ and $r_a$ are atomic mass and radius of target atom(Ba), and $M_g$ and $r_g$ are

mass and radius of incident ions(Ar or Xe). Here, incident ion energy and collision

coefficient $e$ was defined as follows;

$$E_0 = M_g v_1^2 / 2 = 500 \text{ eV} \qquad (8.3)$$

$$e = 1.0 \qquad (8.4)$$

Fig. 8-4 and Fig. 8-5 show kinetic energy and angle distribution of recoiled $Ar^+$ and

$Xe^+$ at target surface, in which target was assumed as though it was only composed of

Ba atoms. It was clarified for the incident of $Ar^+$ that there were a lot of recoiled Ar with

kinetic energy up to 200 eV. There is a substrate in this direction in the configuration of

FTS system. On the other hand, for $Xe^+$ incident, there was almost zero recoiled particle

and there was no bombardment to substrate surface as shown in Fig. 8-5. Actually, the

possibility of occurrence of perfect elastic collisions are very small and most of

collisions are inelastic collision, and there is no recoiled Xe directed to substrate surface.

In this study, therefore, Xe was mixed as portion of sputtering gases and their effects to

crystallographic and magnetic characteristics were investigated.

---

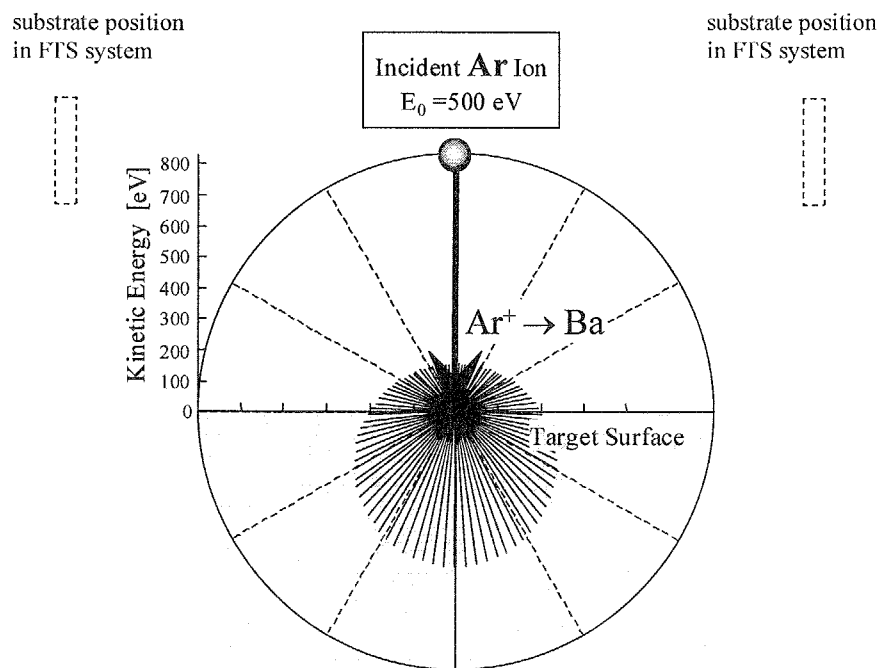[27] H. F. Winters et al. : J. Vac. Sci. Technol., A11[3], pp.657-663 (1993)

substrate position
in FTS system

Incident **Ar** Ion
$E_0 = 500$ eV

Kinetic Energy [eV]

800
700
600
500
400
300
200
100
0

$Ar^+ \to Ba$

Target Surface

substrate position
in FTS system

Fig. 8-4    Kinetic energy and angle distribution of recoiled $Ar^+$ at Ba
target surface.

substrate position
in FTS system

Incident **Xe** Ion
$E_0 = 500$ eV

Kinetic Energy [eV]

800
700
600
500
400
300
200
100
0

$Xe^+ \to Ba$

Target Surface

substrate position
in FTS system
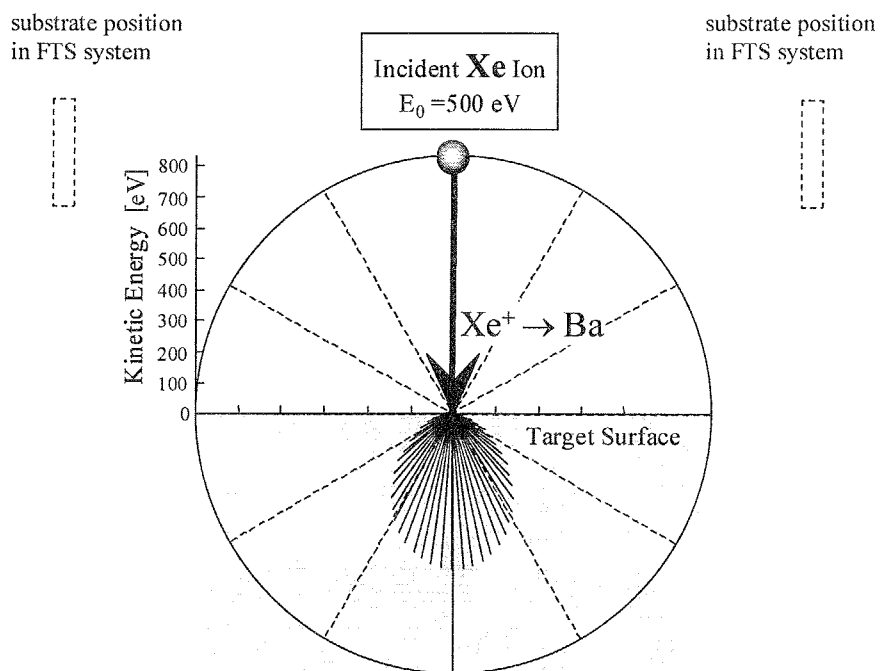
Fig. 8-5    Kinetic energy and angle distribution of recoiled $Xe^+$ at Ba
target surface.

## 8-4    Deposition Conditions of Ba ferrite and ZnO layers

Since Ba ferrite film deposited directly on Si wafer substrates with thermal oxidized surface layer($SiO_2$/Si) revealed random or no orientation in XRD diagram, ZnO(001) underlayer was used for epitaxial growth of Ba ferrite layer with c-axis orientation. It has been found that ZnO(001) underlayers are useful for the epitaxial growth of BaM layers with c-axis orientation as well as spinel ferrite layers with (111) orientation[6,28]. All of Ba ferrite and ZnO(001) layers were prepared by using FTS apparatus for multilayered films as shown in Fig. 8-6. As it has two pairs of facing targets in the same chamber, the multi-layered films can be prepared without breaking the vacuum. All specimen films were not subjected to be post-annealing process at all.

Table 8-1 shows deposition conditions for ZnO layers. ZnO layer was deposited from a pair of pure Zn(99.99%) targets on $SiO_2$/Si substrates $15 \times 15$ mm$^2$ in area by reactive sputtering using gas mixture of Ar and $O_2$ as sputtering gases. Here, partial oxygen gas pressure $P_{O_2}$ was set at 0.6 mTorr(25%) and this value was smaller than that used in *chapter 5* 'Co ferrite/ZnO Double Layered Film.' Since the consecutive depositions of ZnO films at $P_{O_2}$ of 1.0 mTorr(50%) caused a lot of oxide projections on Zn target surface, $P_{O_2}$ was decreased down to 0.5 mTorr to avoid the formation of such oxides. However, the color of ZnO films deposited in these conditions was yellow with transparency and it seemed that oxidation of films were insufficient. Therefore, another oxygen gas at $P_{O_2}$ of 0.1 mTorr(5%) was flow directly onto substrate surface as shown in Fig. 8-6. The substrate temperature $T_s$ was kept at 300°C constant during deposition. Discharge current was 0.1 A and then the discharge voltage was about 550 V.

Crystallographic characteristics of single ZnO films were different from those of ZnO

underlayer, on which Ba ferrite layer was subsequently deposited. Their results would

be mentioned in later sections.

Although the deposition conditions were different from those for ZnO layers

deposited in *chapter 5* 'Co ferrite/ZnO Double Layered Film,' their crystallite
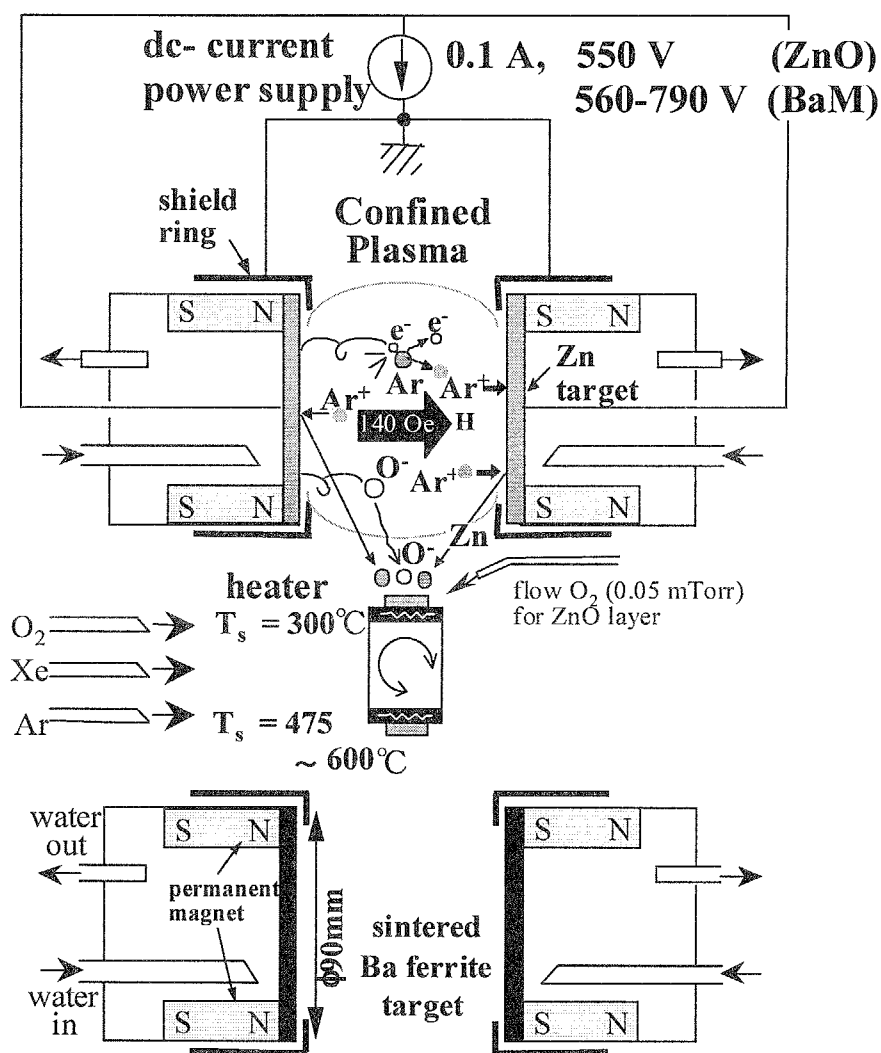


Fig. 8-6   Schematic representation of Facing Targets Sputtering
apparatus for multi-layered films.

[28] M. Naoe, S. Yamanaka and Y. Hoshi; IEEE Tran. Magn., 16, pp.646-648 (1980)

characteristics were almost same as those.

After the deposition of ZnO underlayer for 30 min., the deposition conditions were changed to those for Ba ferrite layer and Ba ferrite layer was subsequently deposited on ZnO one.

Table 8-2 shows deposition conditions for Ba ferrite layers. Two targets with different Ba contents were sintered from the starting mixture of $(BaCO_3)_{1.0}$ and $(\alpha\text{-}Fe_2O_3)_{5.5}$ powder at 1200°C in air by a conventional dry ceramic process following the sequences shown in Fig.3-12.

Table 8-1  Deposition conditions of ZnO layers.

| | ZnO underlayer |
|---|---|
| Target composition | Pure Zn (99.99%) |
| Substrate material | $SiO_2/Si$ (15×15 mm) |
| Total gas pressure $P_{total}$(mTorr) | 2.0 |
| Partial Ar gas pressure $P_{Ar}$   (mTorr) | 1.4 |
| Partial Xe gas Pressure $P_{Xe}$   (mTorr) | —————— |
| Partial $O_2$ gas pressure $P_{O2}$   (mTorr) | 0.6 |
| Substrate temperature $T_s$   (°C) | 300 |
| Discharge current $I_d$   (A) | 0.10 |
| Deposition time t   (min.) | 30 |
| Deposition rate $R_d$   (nm/min.) | 8 – 12 |

Table 8-2  Deposition conditions of Ba ferrite layers.

| | Ba excessive<br>Ba ferrite layer | Fe excessive<br>Ba ferrite layer |
|---|---|---|
| Target composition | $n = 5.5$    $(Ba_{1.00}Fe_{11.0}O_y)$ | $n = 6.5$    $(Ba_{1.00}Fe_{13.0}O_y)$ |
| Substrate material | $ZnO/SiO_2/Si$ | $ZnO/SiO_2/Si$ |
| Total gas pressure<br>$P_{total}$(mTorr) | 1.5 | 1.5 |
| Partial Ar gas pressure<br>$P_{Ar}$    (mTorr) | $1.43 - 0.0$ | $1.35 - 0.0$ |
| Partial Xe gas Pressure<br>$P_{Xe}$    (mTorr) | $0.0 - 1.43$ | $0.0 - 1.35$ |
| Partial $O_2$ gas pressure<br>$P_{O_2}$    (mTorr) | 0.07 | 0.15 |
| Substrate temperature<br>$T_s$    (°C) | 600 ($P_{Xe}$ dependence)<br>500~600 (low $T_s$ deposition) | 600 ($P_{Xe}$ dependence)<br>450~600 ($T_s$ dependence) |
| Discharge current<br>$I_d$    (A) | 0.10 | 0.10 |
| Deposition time<br>t    (min.) | ~120 min. | ~120 min. |
| Deposition rate<br>$R_d$    (nm/min.) | $2 - 4$ | $2 - 4$ |

Ba rich target with composition of $BaO \cdot 5.5(Fe_2O_3)$ was used for the deposition in Ar

+ $O_2$ gas mixture(without Xe) and then Ba content $C_{Ba}$ of the deposited film was almost

1.0. Since $C_{Ba}$ tended to increase with increase of mixing ratio of Xe, Fe rich target with

composition of $BaO \cdot 6.5(Fe_2O_3)$ was also used to adjust $C_{Ba}$ to 1.0 for the deposition in

gas mixture of Ar, Xe and $O_2$. Since the as-sintered Ba ferrite targets were insulator,

they were reduced in hydrogen atmosphere at 1000°C for 1hour to sustain dc glow discharge plasma. The resistance of targets at room temperature was about 500 kΩ after reduction process.

The partial Ar and Xe pressures $P_{Ar}$ and $P_{Xe}$, were varied in the ranges from 0.00 to 1.43 mTorr and 1.43 and 0.00 mTorr, respectively, and the partial $O_2$ pressure, $P_{O2}$, was fixed at 0.07 mTorr for the deposition from Ba excessive targets as shown in Fig. 8-7. On the other hand, $P_{Ar}$ and $P_{Xe}$, were varied in the ranges from 0.00 to 1.35 mTorr and from 1.35 to 0.00 mTorr, respectively, and the partial $O_2$ pressure, $P_{O2}$, was fixed at 0.15 mTorr for the deposition from Fe excessive targets. The total gas pressure $P_{total}$ was constant at 1.5 mTorr.

The substrate temperature $T_s$ was kept constant at 600°C for the partial Xe pressure dependence. In $T_s$ dependence investigation, $T_s$ was decreased in the range from 600 to 450°C to confirm the lowest critical substrate temperature $T_s$.
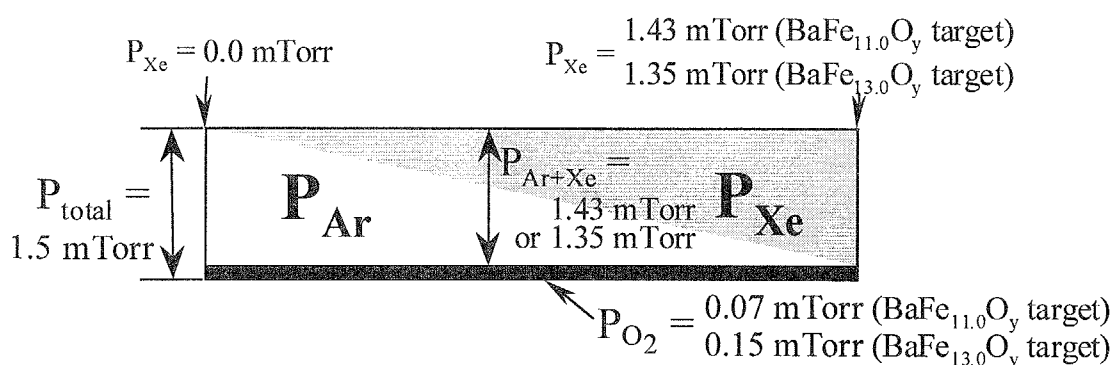


Fig. 8-7    Relationships each partial pressures of Ar, Xe and $O_2$ and the total gas pressure.

The discharge current $I_d$ was set at 0.1 A and then the discharge voltage $V_d$ increased with the increase of $P_{Xe}$ for both of two targets with different Ba content as shown in Fig. 8-8 and Fig. 8-9. Here, $V_d$ means a voltage of power source and it does not mean a potential at target surface. To evaluate exact sheath potential, several origins of power loss should be deducted, i.e. the voltage drop at transition region $2kT_e/2e$, resistive loss inside and surface of the target as well as contact area with backing plate, leak current to insulator and cooling water and power loss originated from incomplete ground potential. However, these loss factors were negligible and this discharge voltage $V_d$ was assumed to be almost same as that of sheath potential at target surface.

Both $V_d$ in Fig. 8-8 and Fig. 8-9 increased gradually with the increase of $P_{Xe}$. Although absolute values of $V_d$ in Fig. 8-8 was about 100 V lower than that in Fig. 8-9, this difference in $V_d$ seemed only to be attributed to the degree of reduction at target surface. The increase of $V_d$ with the increase of $P_{Xe}$, which are inherent phenomena for both targets, will be clarified by using Langmuir probe method in *8.6*.

Since deposition rate $R_d$ of ZnO was likely to be changed at each deposition conditions, it was difficult to determine thickness of Ba ferrite layer using probe contact type measurement(DEKTAK) and the calculation from the products of deposition rate and time. Therefore, Ba ferrite layer thickness was determined from ratio of layer thickness of ZnO and Ba ferrite ones, which were observed in SEM images, respectively. The $P_{Xe}$ dependence of $R_d$ in Fig. 8-8 and Fig. 8-9 were different each other. The reason $R_d$ took the largest value at $P_{Xe}$ of 0.75 mTorr in Fig. 8-8 seemed to be attributed to abnormal growth of Ba ferrite crystallites caused by the incorporation of excessive Ba atoms into films as will be mentioned in 8-5-1-1.
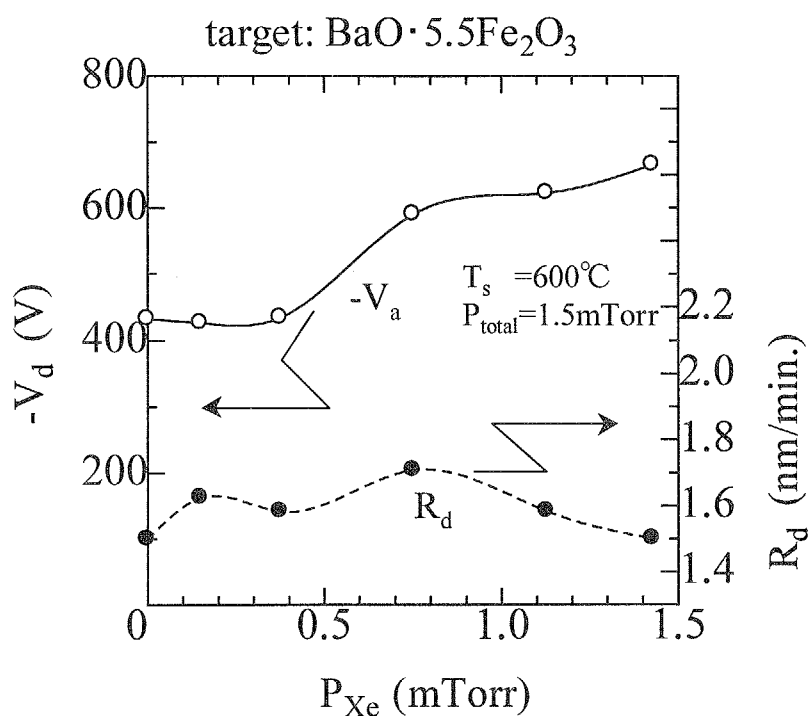
target: $BaO \cdot 5.5Fe_2O_3$



Fig. 8-8    $P_{Xe}$ dependence of discharge voltage $V_d$ and deposition rate $R_d$ of films deposited from $BaO \cdot 5.5(Fe_2O_3)$ targets.
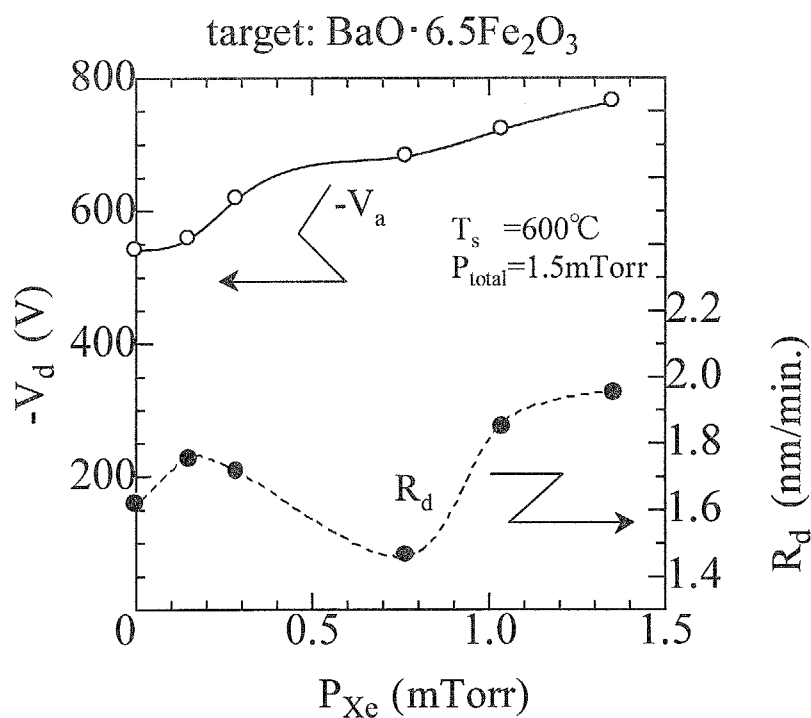
target: $BaO \cdot 6.5Fe_2O_3$



Fig. 8-9    $P_{Xe}$ dependence of discharge voltage $V_d$ and deposition rate $R_d$ of films deposited from $BaO \cdot 6.5(Fe_2O_3)$ targets.

## 8-5　Deposition from Ba excessive targets($Ba_{1.0}Fe_{11.0}O_{19.0-y}$)

### 8-5-1　Partial Xe pressure dependence

#### 8-5-1-1 *Ba content*

The Ba and Fe ion contents $C_{Ba}$ and $C_{Fe}$, were determined by using the inductive coupled plasma spectrometry(ICPS). The dependence of the normalized Ba content x on the partial Xe pressure $P_{Xe}$ was shown in Fig. 8-10, where x is calculated for $C_{Ba}:C_{Fe} = x : 12$, so that x of stoichiometric BaM would be 1.0. Although x was smaller than 1.0 if BaM films were deposited by using conventional diode and magnetron sputtering apparatus in mixture of Ar and $O_2$[1], x was almost equal to 1.0 or larger in the whole range of $P_{Xe}$. It took the maximum value of 1.3 at $P_{Xe}$ of 0.75 mTorr and then it was larger than x of targets used in this study(x = 1.1). The x decreased with the increase of $P_{Xe}$ higher than 0.75 mTorr and was almost stoichiometry at $P_{Xe}$ of 1.5 mTorr. The change of Ba content x on $P_{Xe}$ can be divided into 3 three regions as follows;

　(a)0.0 mTorr < $P_{Xe}$ < 0.38 mTorr : Re-sputtering of Ba atoms,

　(b)$P_{Xe}$ = 0.75 mTorr : Increase of Ba atoms which could arrive at substrate and
　　increase of sticking coefficient of Ba atoms,

　(c)0.75 mTorr < $P_{Xe}$ < 1.5 mTorr : Scattering of Ba atoms during transportation.

In (a), there existed a lot of Ar atoms in the atmosphere gases, the re-sputtering of Ba atoms were easily occurred from severe bombardment of recoiled particles with high energy. In (b), since the collision cross section of Xe, $\sigma_{Xe}$, is much larger than that of Ar, $\sigma_{Ar}$, Ba atoms were likely to be collide with Xe atoms and therefore, the number of Ba atoms arrived at substrate decreased and they lost their kinetic energy. Anyway, it

---

[1] K. Yamamori, T. Tanaka and T. Jitosho : IEEE Trans. Magn., 27[6], pp.4960-4962 (1991).

seemed that Ba atoms were likely to be incorporated in the films by mixing Xe in sputtering gas up to certain value of $P_{Xe}$.

The Ba content x increased and decreased as the deposition rate $R_d$ did as shown in Fig. 8-10 and Fig.8-8, and the highest $R_d$ and largest x was obtained at the same $P_{Xe.}$ This highest $R_d$ seemed to be attributed to abnormal growth of Ba ferrite crystallites caused by the incorporation of excessive Ba atoms into films. On the other hand, X. J. Chen et al. reported that Ba ferrite films with Ba content higher than stoichiometry had high nucleation rates but lower growth rates during the post-deposition crystallization process[2]. This result is completely different from ours. The reason is not clear, it supposed to be that the effect of excessive Ba atoms and their reaction manners with other atoms in crystallite growth during deposition and during annealing process might be completely different.
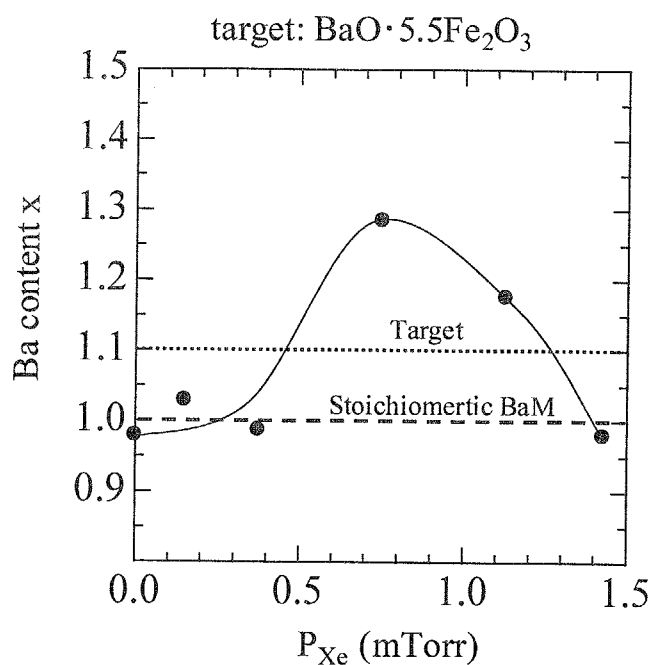


Fig. 8-10    $P_{Xe}$ dependence of Ba content x of films deposited from $BaO \cdot 5.5(Fe_2O_3)$ targets.    $(C_{Ba} : C_{Fe} = x : 12)$

[2] Y. J. Chen and M. H. Kryder : J. Appl. Phys., 81, pp.319-322 (1994)
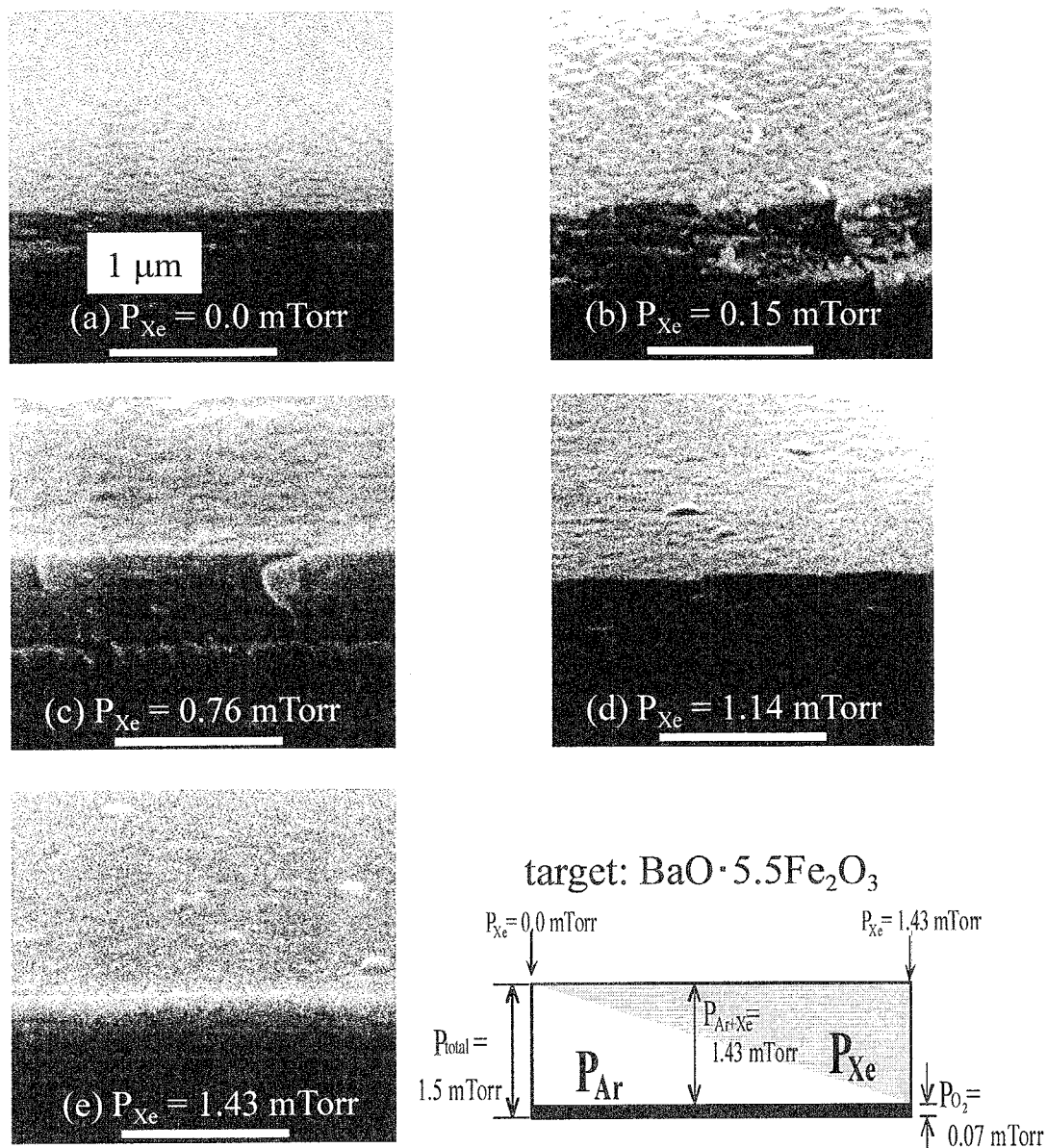
*8-5-1-2 Surface and cross-sectional SEM images*

Fig. 8-11 shows the surface and cross-sectional SEM images of films deposited from

$BaO \cdot 5.5(Fe_2O_3)$ targets at various $P_{Xe}$. Microstructure, which was composed of small

grains, was observed for the films deposited at relatively low $P_{Xe}$ of (a)0.0 mTorr and

(b)0.15 mTorr. On the other hand, larger grains with a hexagonal plate shape were

observed at $P_{Xe}$ of (c)0.75 mTorr, and they looked like to be grown up from the bottom

layer to the top one continuously without making grain boundaries. The deposition rate

$R_d$ as seen in Fig. 8-8 seemed to be directly affected to the difference in the grain

growth. However, grain size evaluated by SEM images do not have any relationship to

the crystallite size $<D>_{BaM(008)}$ as will be shown in Fig. 8-14. At $P_{Xe}$ of (c)1.14 mTorr and

(d)1.43 mTorr, clear grain boundaries were not observed and films revealed flatter

surfaces and denser cross-sectional morphologies than (a), (b) and (c). It seemed that a

lot of island structure existed at initial growth layer of the films, while ideal layered

structure existed for that in which very flat and dense morphology were observed in

SEM images. In this case, the decrease of recoiled particles with the increase of $P_{Xe}$

improved the smoothness and morphology of the deposited films and restrained the

excessive grain growth.

Fig. 8-11 Surface and cross-sectional SEM images of films deposited from BaO·5.5(Fe$_2$O$_3$) targets at various P$_{Xe}$.

*8-5-1-3 Crystallographic characteristics*

Fig. 8-12 shows the X-ray diffraction diagrams of films deposited from BaO·

$5.5(Fe_2O_3)$ targets at various $P_{Xe}$. BaM(00n) peaks were observed for all films as well as

ZnO(002) peak. Spinel(mmm) peaks were also observed(see magnification). On the

other hand, the peak intensity of BaM(00n) was small and BaM(0010), which

corresponded to the plane of $Fe^{3+}$ ions in S blocks, was not observed at $2\theta$ of 38.4

degree at $P_{Xe}$ of 0.75 mTorr. From the results of large x seen in Fig. 8-10 and there was

the increase of inter-planar distance $d_{BaM(008)}$ in Fig. 8-13, it was supposed that the site

of oxygen ion in S block was partially substituted by $Ba^{2+}$ ion.

While $d_{BaM(008)}$ took constant value of about 2.903 Å and they were closer to that of

bulk value of BaM(2.900 Å) at $P_{Xe}$ from 0 to 0.38 mTorr, it drastically increased and

took the maximum value of 2.910 Å at $P_{Xe}$ of 0.75 mTorr. Although it gradually

decreased with further increase of $P_{Xe}$, their values remained at relatively high value and

were larger than those at lower $P_{Xe}$ from 0 to 0.38 mTorr even at $P_{Xe}$ of 1.43 mTorr,

where $C_{Ba}$ was about 1.0. This change of $d_{BaM(008)}$ seemed to be related to the change of x

as seen in Fig. 8-10. The largest $d_{BaM(008)}$ at $P_{Xe}$ of 0.75 mTorr was attributed to the

insertion of excessive Ba ions with larger atomic radius to the site of O ions in

crystallite structure. On the other hand, the $P_{Xe}$ dependence of the normalized X-ray

diffraction peak intensity of spinel(mmm) $f_{spinel(mmm)}$ were inversely changed to that of Ba

content. Here, $f_{spinel(mmm)}$ was defined after Lotgering as mentioned in 3-6. The existence

of enough amounts of Ba atoms arrived at substrate surface seemed to restrain the

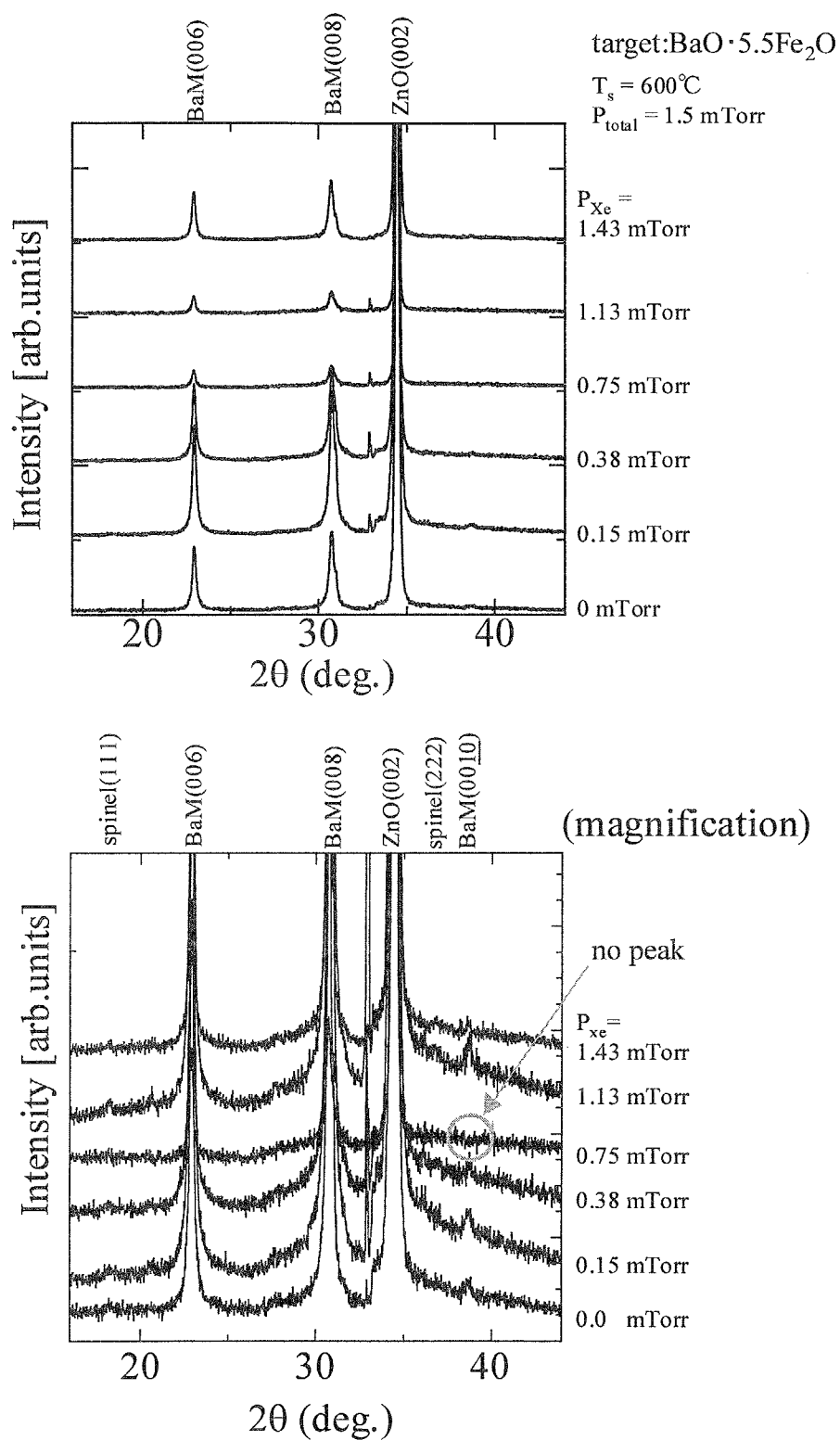formation of spinel crystallites in films.

Fig. 8-12    X-ray diffraction diagrams of films deposited from BaO·
5.5($Fe_2O_3$) targets at various $P_{Xe}$.

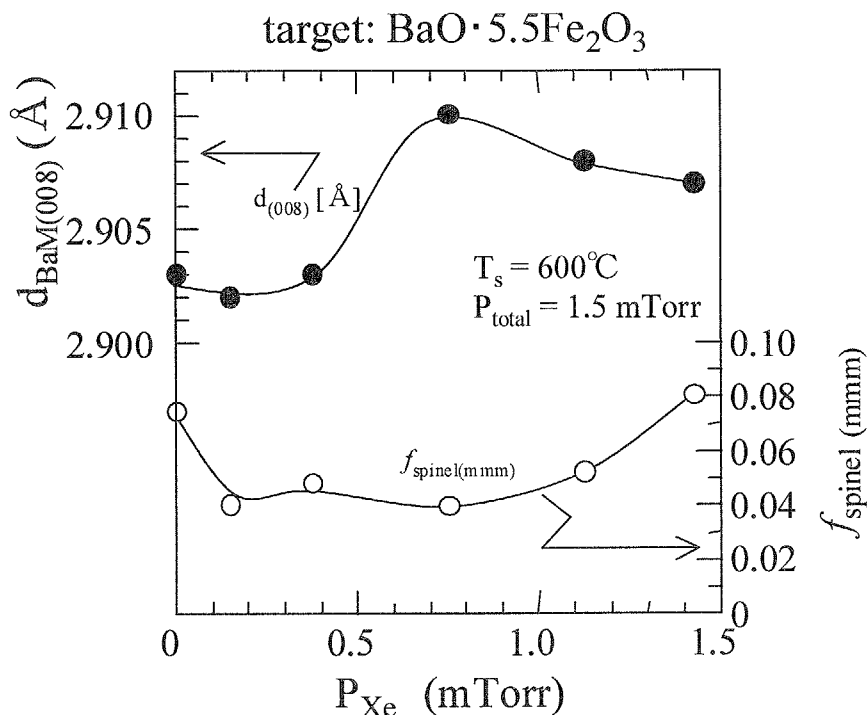Fig. 8-13    $P_{Xe}$ dependences of inter-planar distance $d_{BaM(008)}$ and normalized X-ray diffraction intensity of spinel (mmm) peaks $f_{spinel(mmm)}$ of films deposited from $BaO \cdot 5.5(Fe_2O_3)$ targets.
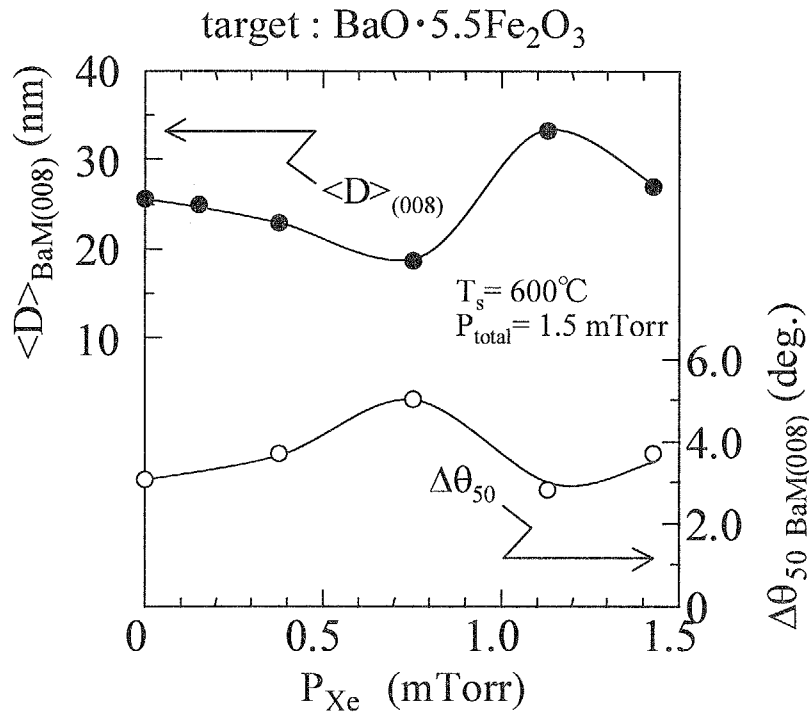
Fig. 8-14 shows the $P_{Xe}$ dependence of crystallite size $<D>_{BaM(008)}$ and full width at half maximum of rocking curve $\Delta\theta_{50\_BaM(008)}$ of films deposited from $BaO \cdot 5.5(Fe_2O_3)$ targets. The $<D>_{BaM(008)}$ and $\Delta\theta_{50\_BaM(008)}$ were calculated and evaluated by the diffraction peak profile and rocking curve one of BaM(008) peaks in X-ray diffraction diagrams(XRD).

The $P_{Xe}$ dependence of $<D>_{BaM(008)}$ and $\Delta\theta_{50\_BaM(008)}$ were just the opposite one each other. $<D>_{BaM(008)}$ gradually decreased with increase of $P_{Xe}$ and took the minimum value of 19 nm at $P_{Xe}$ of 0.75 mTorr. On the other hand, $\Delta\theta_{50\_BaM(008)}$ took the maximum value of 5.0° at $P_{Xe}$ of 0.75 mTorr. The deterioration of crystallinity especially at $P_{Xe}$ of 0.75 mTorr seemed to be attributed to the incorporation of excessive Ba atoms in films as mentioned before.

Fig. 8-14    $P_{Xe}$ dependences of crystallite size $<D>_{BaM(008)}$ and full width at half maximum of rocking curve $\Delta\theta_{50\_BaM(008)}$ of films deposited from $BaO \cdot 5.5(Fe_2O_3)$ targets.

Fig. 8-15 and Fig. 8-16 show the $P_{Xe}$ dependence of inter-planar distance, $d_{ZnO(002)}$, and crystallite size, $<D>_{ZnO(002)}$, and full width at half maximum of rocking curve, $\Delta\theta_{50\_ZnO(002)}$, of ZnO underlayer, on which Ba ferrite layer was deposited from $BaO \cdot 5.5(Fe_2O_3)$ targets, respectively. They were calculated and evaluated by the diffraction peak profiles and rocking ones of ZnO(002) peak in X-ray diffraction diagrams(XRD).
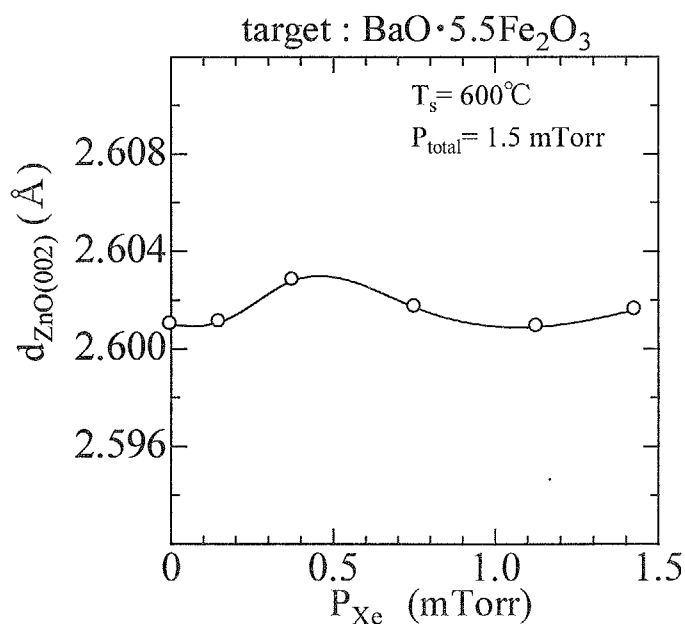
Fig. 8-15    $P_{Xe}$ dependences of inter-planar distance $d_{ZnO(002)}$ of ZnO underlayer deposited under Ba ferrite layers deposited from BaO $\cdot$ 5.5($Fe_2O_3$) targets.
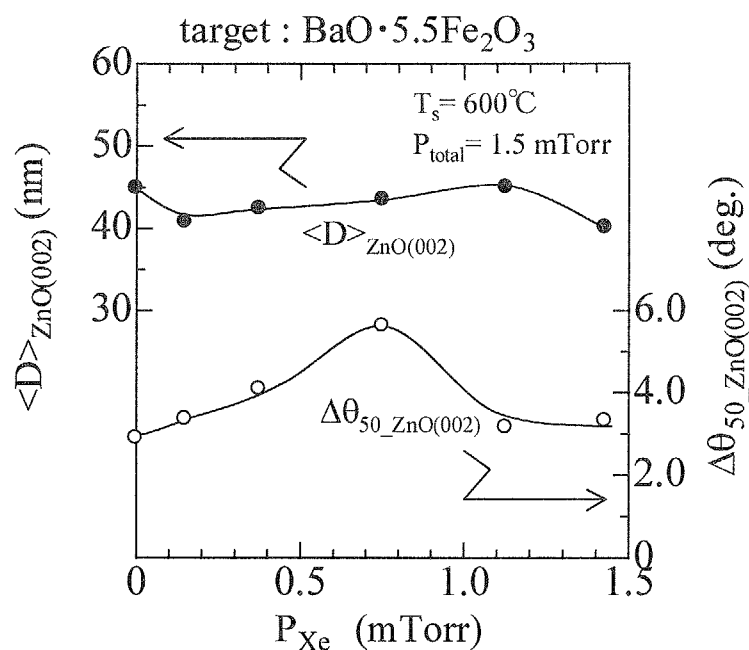


Fig. 8-16    $P_{Xe}$ dependences of crystallite size $<D>_{ZnO(002)}$ and full width at half maximum of rocking curve $\Delta\theta_{50\_ZnO(002)}$ of ZnO underlayer deposited under Ba ferrite layer deposited from BaO $\cdot$ 5.5($Fe_2O_3$) targets.

Although $d_{ZnO(002)}$ and $<D>_{ZnO(002)}$ were almost constant with the increase of $P_{Xe}$, $\Delta\theta_{50\_ZnO(002)}$ increased with the increase of $P_{Xe}$ up to 0.75 mTorr and took the maximum value of 5.5 degree at $P_{Xe}$ of 0.75 mTorr, where Ba ferrite layer also took the maximum $\Delta\theta_{50\_BaM(008)}$. There was a possibility that this worse $\Delta\theta_{50\_ZnO(002)}$ of ZnO underlayer deteriorated the c-axis orientation of Ba ferrite layer. $<D>_{ZnO(002)}$ of simple ZnO films deposited at same conditions was small when $\Delta\theta_{50\_ZnO(002)}$ became large. In this case, $\Delta\theta_{50\_ZnO(002)}$ became large, while $<D>_{ZnO(002)}$ were almost constant. Therefore, it was supposed that this largest $\Delta\theta_{50\_ZnO(002)}$ at $P_{Xe}$ of 0.75 mTorr was attributed to the internal stress which was caused by depositing Ba ferrite layer on them. My co-worker Dr. Noma explained that the difference in temperature dependence of thermal expansion in percentage of a-axis in Ba ferrite and ZnO crystallites cause internal stress for both layers, and as a result, micro cracks creased in BaM layer[3]. However, the relationship between internal stress and the crystallographic characteristics of Ba ferrite layer and ZnO underlayer was not clear and it should be investigated in further experiments.

### 8-5-1-4 *Magnetic Characteristics*

Magnetic characteristics such as saturation magnetization $4\pi M_s$, in-plane and perpendicular coercivities $H_{c//}$ and $H_{c\perp}$ were measured by using a vibrating sample magnetometer(VSM) and torque magnetometer, respectively.

The $P_{Xe}$ dependence of saturation magnetization $4\pi M_s$ and perpendicular and in-plane coercivity $H_{c//}$ and $H_{c\perp}$ of films deposited from $BaO\cdot5.5(Fe_2O_3)$ targets are shown in Fig. 8-17. The minimum value of $4\pi M_s$ was 2.3 kG at $P_{Xe}$ of 0.15 mTorr and it

---

[3] K. Noma et al. : IEEE Transactions Magn., 32[5], pp.3822-3824 (1996)

increased with increase of $P_{Xe}$ and took the maximum value of 4.9 kG, which was larger than that of bulk BaM ferrite of 4.8 kG. Normally, although $4\pi M_s$ of Ba ferrite film is closely related to crystallite size, such relation was not seen in Fig. 8-18 and Fig. 8-14. Usually, $4\pi M_s$ of sputtered thin films are likely to be smaller than that of bulk value because of defects in crystallite structure and amorphous portion in films and therefore, this value of $4\pi M_s$ is quite large for that of sputter-deposited BaM film. As a reason of this increase of $4\pi M_s$, it was suggested that berthollide crystallites with larger $4\pi M_s$, like magnetite $Fe_{3-\delta}O_4$, were formed in films. However, from the results of stoichiometric composition of this film shown in Fig. 8-10, the increase of $f_{spinel(mmm)}$ and increase of $d_{BaM(008)}$ shown in Fig. 8-13, it seemed to be attributed to the change of layered structure of BaM film. For example, the insertion of spinel blocks to magnetoplumbite type of structure. Although the peak was not identify in X-ray diffraction diagram as shown in Fig. 8-12, there is possibility that small $Fe_2W$ crystallites with large $4\pi M_s$ of 5.1 kG was formed in films. The unit structure of M and W types of Ba ferrite are illustrated in Fig. 8-18: (a)M type (BaM) and (b)W type ($Fe_2W$), respectively. $Fe_2W$ unit is constructed by the insertion of S and S* blocks to M type unit and $Fe_2W$ crystallites had larger $4\pi M_s$ than that of BaM crystallites.
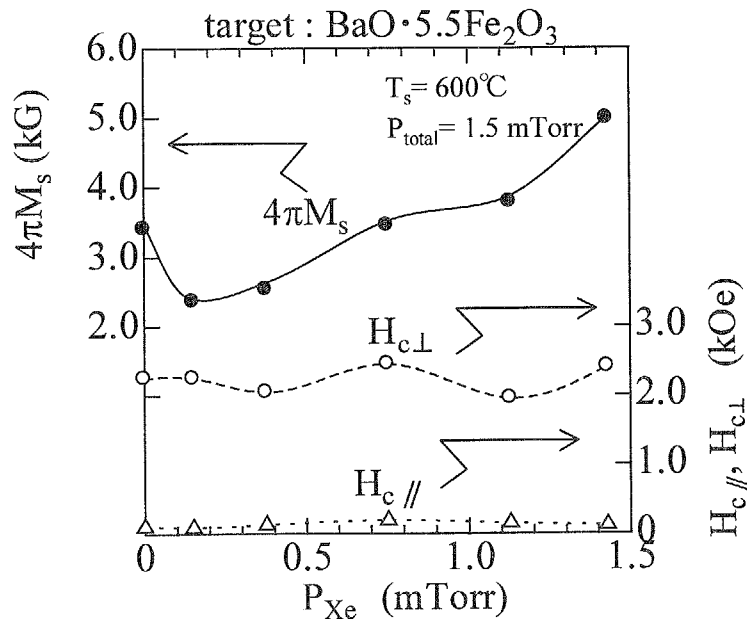
Fig. 8-17    $P_{Xe}$ dependence of saturation magnetization $4\pi M_s$ and perpendicular and in-plane coercivity $H_{c//}$ and $H_{c\perp}$ of films deposited from $BaO \cdot 5.5(Fe_2O_3)$ targets.
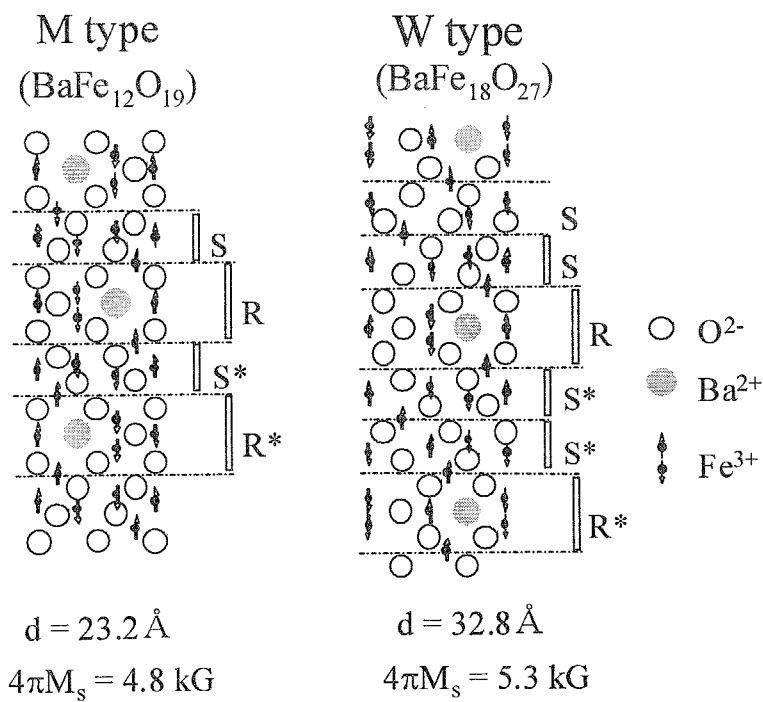


Fig. 8-18    Structure of unit cell of (a)M and (b)W type Ba ferrite..

All specimen films exhibited large perpendicular anisotropy energy and the perpendicular coercivity $H_{c\perp}$ was higher than 2.0 kOe and the in-plane coercivity $H_{c//}$ was lower than 0.28 kOe. $H_{c\perp}$ increased and decreased following the changes of $\Delta\theta_{50}$ as shown in Fig. 8-14. It took the maximum value 2.3 kOe at $P_{Xe}$ of 0.75 and 1.43 mTorr. High $H_{c\perp}$ at $P_{Xe}$ of 0.75 mTorr was attributed to the longer c-axis of crystallite as shown in Fig. 8-13 and was also attributed to the magnetic de-coupling between grains due to incorporation of excessive Ba atoms. The reason of latter increase of $H_{c\perp}$ seemed to be caused by the increase of tension due to decrease of defect in crystallite structure and reverse magnetic torsion. $H_{c//}$ took the maximum value of 0.19 kOe at $P_{Xe}$ of 0.75 mTorr due to deterioration of c-axis orientation as shown in Fig. 8-14.

Fig. 8-19 shows $P_{Xe}$ dependence of perpendicular anisotropy constant $K_{\perp}^{*}$ and effective anisotropy field $H_{keff}^{*}$ of films deposited from $BaO \cdot 5.5(Fe_2O_3)$ targets. They were evaluated using in-plane M-H loops measured by VSM. $K_{\perp}^{*}$ took the maximum value at $P_{Xe}$ of 1.14 and 1.43 mTorr and this result was accordance with those of $4\pi M_s$ and $H_{c//}$. $H_{keff}^{*}$ was in the range from 4.0 to 5.3 kOe and $H_{keff}^{*}$ took smaller value at $P_{Xe}$ of 0.75 mTorr, where $H_{c\perp}$ took the maximum value. Anyway, these $K_{\perp}^{*}$ and $H_{keff}^{*}$ were much smaller than those of bulk Ba ferrite.

Relationships among Ba content x, inter-planer distance $d_{\_BaM(008)}$, saturation magnetization $4\pi M_s$ and schematical blocks structure of films deposited from $BaO \cdot 5.5(Fe_2O_3)$ targets at various $P_{Xe}$ were shown in Fig. 8-20. At lower $P_{Xe}$, in the range from 0 to 0.38 mTorr, $d_{\_BaM(008)}$ and x were almost same as those of bulk BaM. It was suggested that the film was composed of BaM crystallites, while $4\pi M_s$ was smaller than that of bulk BaM due to serious damage from a lot of recoiled Ar atoms. On the other

hand, at relatively higher $P_{Xe}$, in the range from 0.75 to 1.13 mTorr, Ba content x

increased up to 1.3 and $d_{BaM(008)}$ also increased with increase of x. The degree of c-axis

orientation $\Delta\theta_{50\_BaM(008)}$ became large with the increase of x and took the maximum value

of 5.0 where x took the maximum value and then in-plane coercivity $H_{c//}$ increased with

the increase of $\Delta\theta_{50\_BaM(008)}$. Several conditions seemed to cause the deterioration of the

c-axis orientation. The most important one is incorporation of excessive Ba atoms into

film. Since $4\pi M_s$ was not so small at $P_{Xe}$ of 0.75 mTorr and there was no peaks in XRD

diagram, the possibility of formation of BaO crystallites was very small. Here,

substitution of $O^{2-}$ ions to $Ba^{2+}$ ones was suggested. The combination in ion structure is

very strong and the change of it affects in relatively long distance. The substitution of

Ba ions to oxygen ions weaken the strength of combination among ions and therefore

super exchange coupling was weakened and the anisotropy field decreased due to the

change of $Fe^{3+} \rightarrow Fe^{2+}$. On the other hand, at $P_{Xe}$ of 1.43 mTorr, $d_{BaM(008)}$ was about

0.15 % longer than the film deposited at $P_{Xe}$ of 0.0 mTorr, $4\pi M_s$ increased, and spinel

phase was observed in XRD diagram, it was suggested that the number of S-bloks in

crystallite structure was increased while x was stoichiometric one. This speculation

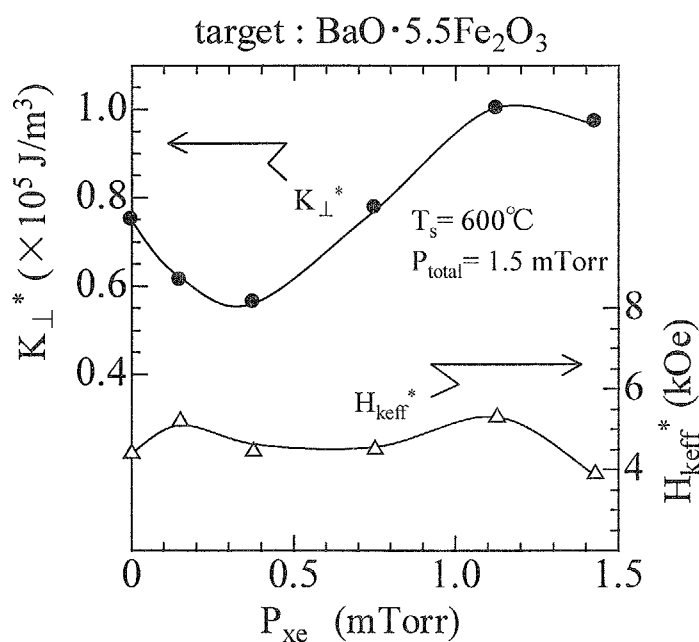would be considered in later section precisely, where Fe excessive targets were used.

target : $BaO \cdot 5.5Fe_2O_3$



Fig. 8-19　$P_{Xe}$ dependences of effective anisotropy field $H_{keff}^*$ and perpendicular anisotropy constant $K_\perp^*$ of films deposited from $BaO \cdot 5.5(Fe_2O_3)$ targets.



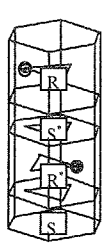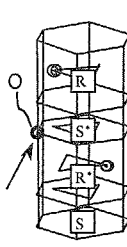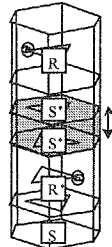| Partial Xe Pressure $P_{Xe}$ | 0.0-0.38 mTorr | 0.75-1.13 mTorr | 1.43 mTorr |
|---|---|---|---|
| Inter-planer distance $d_{(008)}$ | 2.903Å | ~2.910Å | ~2.907Å |
| Ba content $C_{Ba}$ | 0.8~1.0 | 1.2~1.3 | ~1.0 |
| $4\pi M_s$ | <3.4kG | ~3.4kG | ~4.9kG |
| Blocks Structure | Normal Strucure? | Excessive Ba & Lattice Defects | Insertion of S blocks ? |

Fig. 8-20　Relationships among Ba content x, inter-planer distance $d_{BaM(008)}$, saturation magnetization $4\pi M_s$ and crystallite structure of films deposited from $BaO \cdot 5.5(Fe_2O_3)$ targets.at various $P_{Xe}$.

8-5-2    Substrate temperature dependence

From above results, the maximum $4\pi M_s$ of 4.9 kG was attained at substrate temperature of 600℃ and $P_{Xe}$ of 1.43 mTorr, where only Xe and $O_2$ were mixed as sputtering gas. Here, the films were deposited at lower $T_s$ at optimized $P_{Xe}$ of 1.43 mTorr and the critical $T_s$ for c-axis orientation was confirmed as shown in Fig. 8-21.

The peak intensity of BaM(001) peaks decreased with the decrease of $T_s$. Although c-axis orientation was observed clearly at $T_s$ of 575℃ and small peak was observed even at $T_s$ of 550℃, there was no peak and only hallo was observed due to amorphous structure. Matsuoka et al. succeeded to deposit Ba ferrite film with well c-axis orientation even without ZnO under layer low $T_s$ of 500℃, however initial 'spinel' layer existed between BaM ferrite layer and $SiO_2$/Si substrate. For their results of Ba ferrite layer deposited on ZnO layer, critical $T_s$ for c-axis orientation was 550℃ and was same as our result. From these results, it was suggested that although ZnO layer is effective for the deposition of c-axis oriented Ba ferrite without initial layer, it was not effective for decrease the critical $T_s$ for c-axis orientation.

Anyway, it was cleared that the lowest critical $T_s$ of c-axis orientation was not decreased by using Xe mixture gas. That was because, while $P_{Xe}$ of 1.43 mTorr was optimized condition in which the maximum $4\pi M_s$ was obtained, the largest $<D>_{BaM(008)}$ and the smallest $\Delta\theta_{50\_BaM(008)}$ was not attained. There might be no damage from recoiled particles at $P_{Xe}$ of 1.43 mTorr. However, from the results of Ba content x smaller than stoichiometric one and large $\Delta\theta_{50\_BaM(008)}$, there seemed to be some other reasons to deteriorate crystallite growth at $P_{Xe}$ of 1.43 mTorr. Since plasma became wider with increase of $P_{Xe}$, there was a possibility that a extended plasma very close to substrate

deteriorated the formation of most closely packed structure oxygen and decreased the stacking coefficient of Ba atoms. To confirm this speculation, plasma conditions should be investigated. Such as plasma diagnosis would be done later section, while target composition was different in this case.
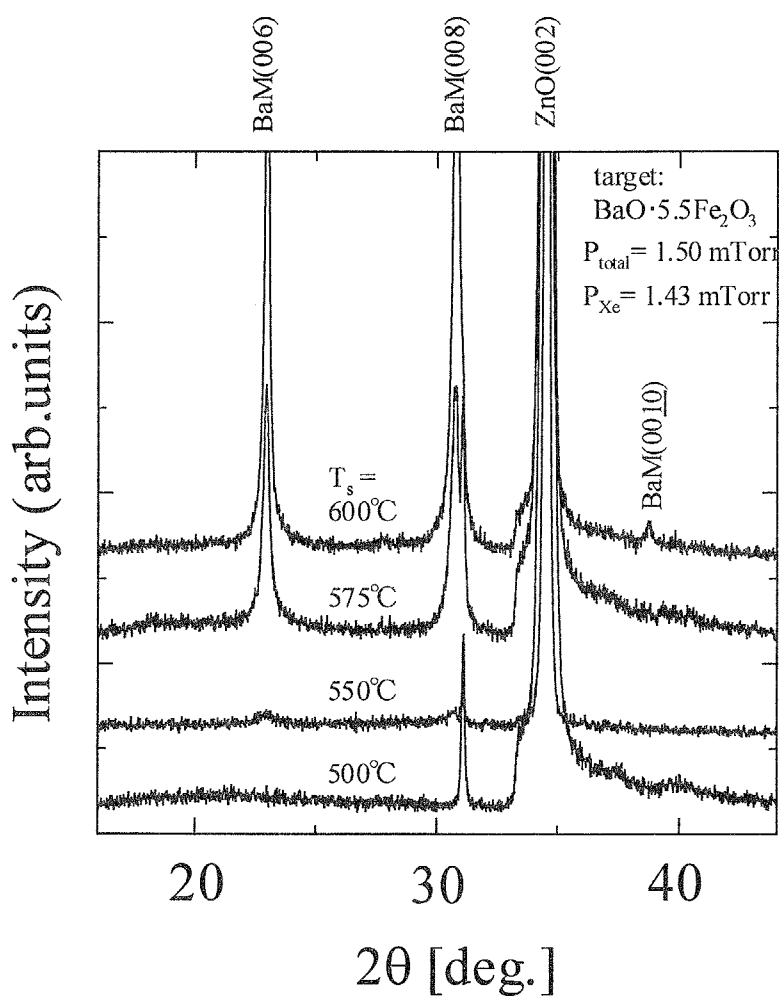


Fig. 8-21　X-ray diffraction diagram of film deposited from BaO ·
5.5(Fe$_2$O$_3$) targets at various T$_s$. (P$_{Xe}$ of 1.43 mTorr)

## 8-6  Deposition from Fe excessive targets($Ba_{1.0}Fe_{13.0}O_{19.0-y}$)

In the before section, the films deposited at $P_{total}$ of 1.5 mTorr and $P_{Xe}$ of 1.43 mTorr exhibited the maximum $4\pi M_s$ of 4.9 kG and it was larger than that of bulk value. However, critical $T_s$ for c-axis orientation could not be decreased lower than 550°C, which Matsuoka et al. achieved. BaM film deposited directly on $SiO_2$/Si substrate had c-axis orientation even at low $T_s$ of 500°C, while there was initial 'spinel' layer. In this section, therefore, Fe excessive Ba ferrite targets were used to promote the formation of spinel ferrite crystallites. Target composition was $BaO \cdot 6.5(Fe_2O_3)$, and therefore $C_{Ba} = 0.923$. Although other deposition conditions were almost same as those used in 8-5, oxygen pressure was set at 0.15 mTorr constant as shown in Table 8-2. Prior to the deposition of Ba ferrite layer, the diagnosis of plasma at various $P_{Xe}$ was investigated. Their results would be shown in next section.

8-6-1   Plasma diagnosis

The diagnosis of the plasma in mixture gas of Ar, Xe and $O_2$ was performed by using a single type of Langmuir's probe.

Fig. 8-22 shows (a)Langmuir's probe used in this study and (b)typical relationship between prove current $I_{pr}$ and voltage characteristics $V_{pr}$. In this figure, positive $I_{pr}$ meant the current came out from the probe. Plasma potential $V_p$ was about 2.9 V and was almost constant at various $P_{Xe}$.
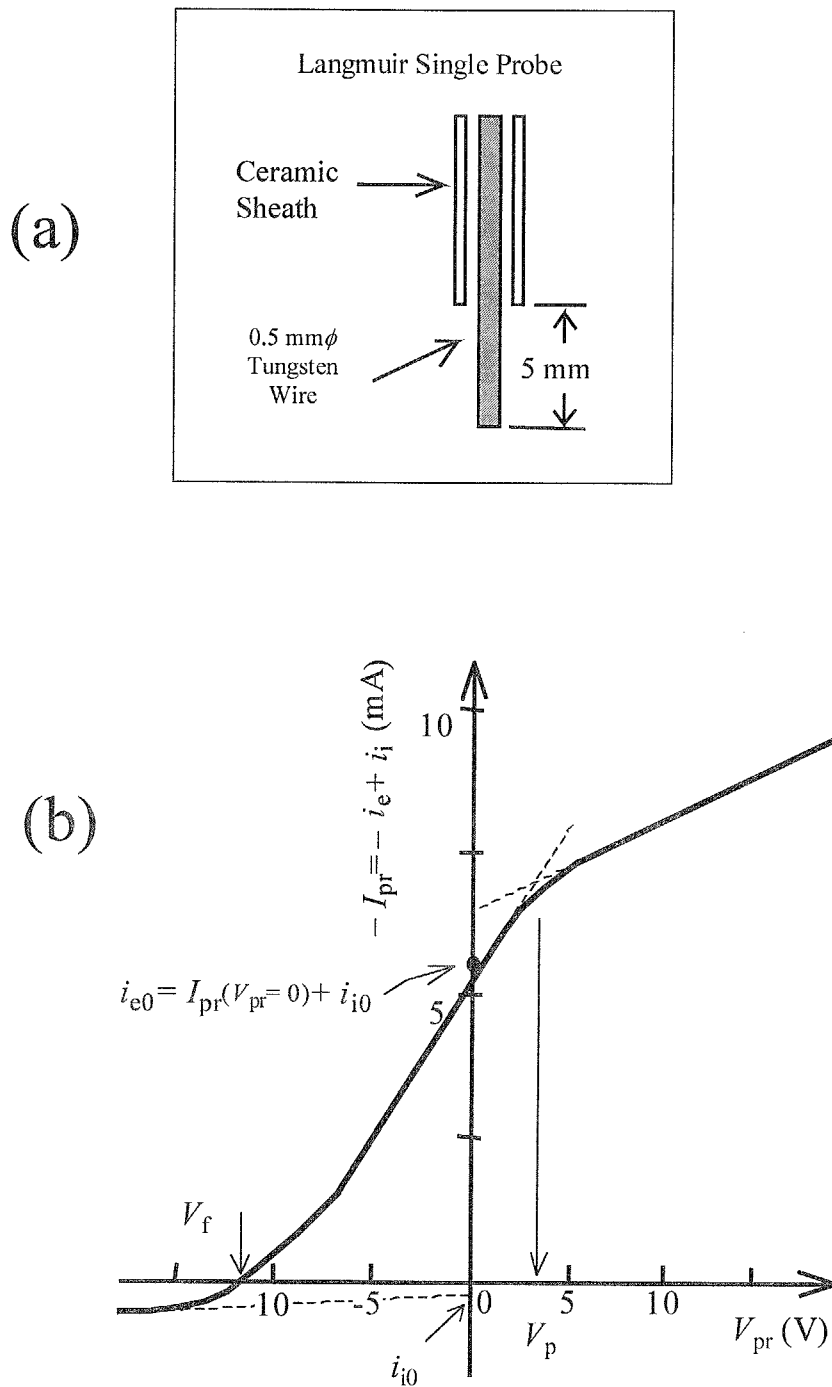
Fig. 8-22 Schematic illustration of (a)structure of edge of Langmuir prove and (b)typical $I_{pr}$-$V_{pr}$ characteristic.

The electron density $N_e$ and the electron temperature $T_e$ were evaluated at the center of the plasma and at the neighborhood of the anode ring. Fig. 8-23 shows the electron density $N_e$ and the electron temperature $T_e$ which were measured at the center of the plasma. $T_e$ decreased and $N_e$ increased with the increase of $P_{Xe}$. This increase of $N_e$ seemed to be attributed to larger collision cross section of Xe than that of Ar. Since $T_e$ decreased with the increase of $P_{Xe}$, the mixing of Xe seemed to decrease the plasma temperature in sputtering system.

Fig. 8-24 shows the dependence of discharge voltage $V_d$ and floating potential $V_f$ measured at the plasma center on $P_{Xe}$. $V_d$ increased linearly with the increase of $P_{Xe}$. This increase of $V_d$ seemed to be caused by the larger plasma loss. The number of ions ionized by one secondary electron is given by

$$N_{IP} = \frac{eV_d}{E_i} \cdot \varepsilon_i \cdot \varepsilon_e \qquad (8.5)$$

where $V_d$ is the discharge voltage, $E_i$ is average energy which is necessary for ionization, $\varepsilon_i$ ($>0$) is electron confinement, $\varepsilon_e$ ($< 1$) is the possibility that electron loses its energy before arriving at anode, respectively.

The discharge can be maintained when the number of ionized ions($I_i$) are larger than that of the incident ions to target ($\gamma \cdot I_i \cdot N_{IP}$), discharge voltage is given by

$$V_d > \frac{E_i}{e \cdot \varepsilon_i \cdot \varepsilon_e \cdot \gamma} \qquad (8.6)$$

where $\gamma$ is secondary electron emission coefficient. Although $E_i$ which corresponds to the primary ionization potential $V_{i1}$ of Xe (12.1 V) is smaller than that for Ar(15.8 V), $\varepsilon_i$ is smaller for Xe due to the extension of plasma. Since the mean free path of electron is very long in total gas pressure of 1.5 mTorr, $\varepsilon_e$ can be assumed as almost 1.0 for both Ar and Xe.
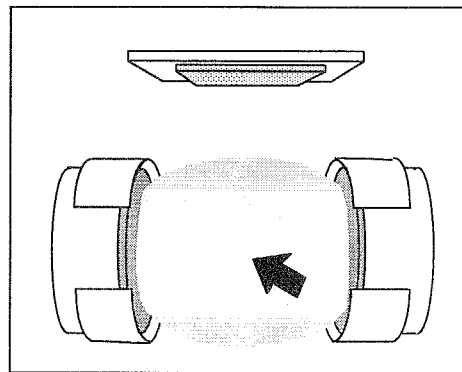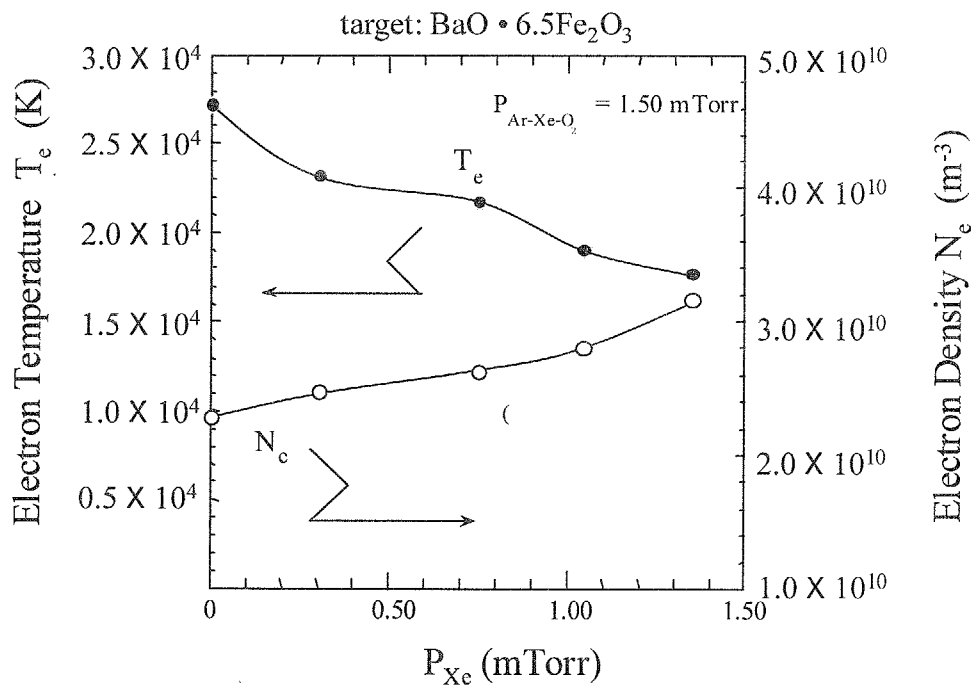
(at center of plasma)



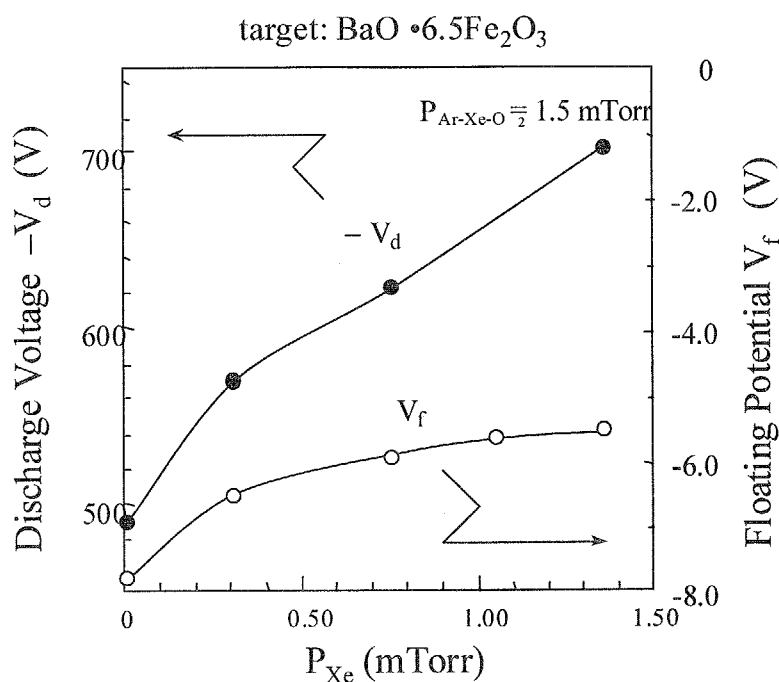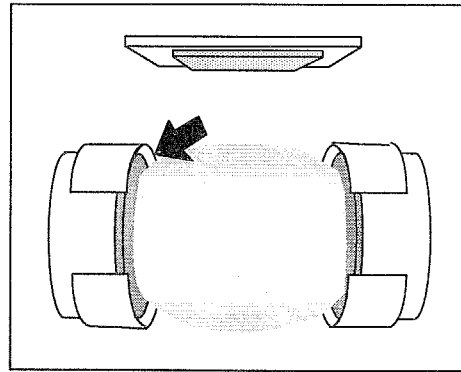Fig. 8-23   $P_{Xe}$ dependence of electron density $N_e$ and electron temperature $T_e$ measured at center of plasma.

target: BaO •6.5Fe$_2$O$_3$



Fig. 8-24    P$_{Xe}$ dependence of discharge voltage V$_d$ and floating potential
V$_f$ measured at plasma center in Ar mixture.

Therefore, it was clarified that the decrease of $\varepsilon_i$ due to the plasma extension was main reason for the increase of V$_d$. V$_f$ became closer to 0 with the increase of P$_{Xe}$ due to the decrease of T$_e$ as shown in Fig. 8-24.

Fig. 8-25 shows the P$_{Xe}$ dependence of N$_e$ and T$_e$ which were measured at the neighborhood of the anode ring. Although T$_e$ was almost constant over the whole range of P$_{Xe}$, N$_e$ slightly decreased and took a minimum value at P$_{Xe}$ of 0.75 mTorr and increased at P$_{Xe}$>0.75 mTorr. There seemed to be a lot of recoiled Ar and it ionized atmosphere gases in the region outside of the plasma at P$_{Xe}$ from 0.0 to 0.3 mTorr. It seemed that since the Larmor radius r$_c$, i.e. equal to m$_i$v$_i$/eB, of Xe ion was larger than that of Ar ion, the diameter of discharge plasma was extended to the direction perpendicular to the applied field with increase of P$_{Xe}$ at higher than 0.75 mTorr.
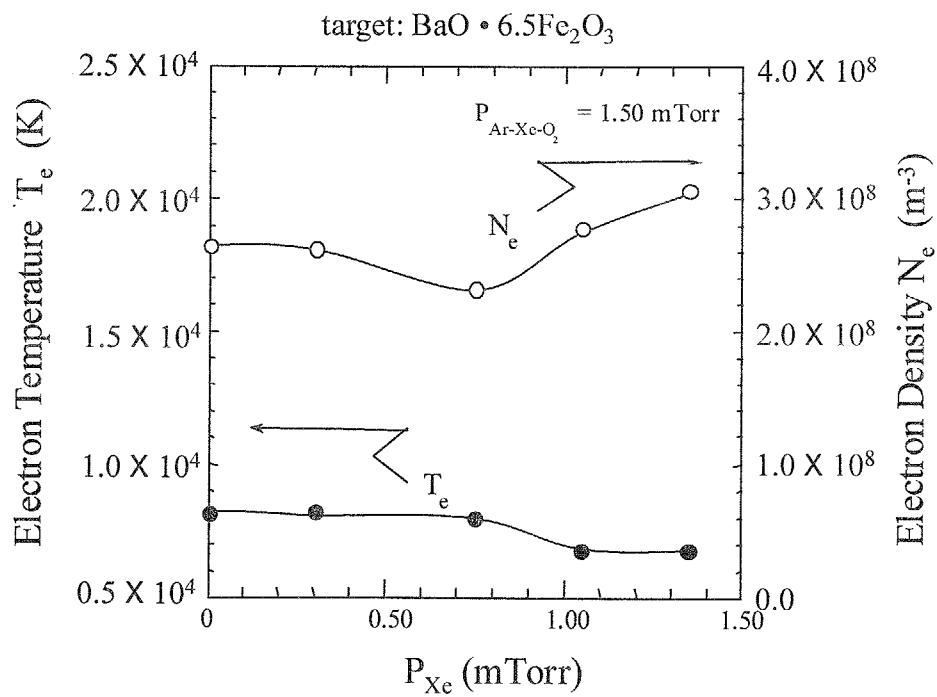
(at neighborhood of anode ring)



Fig. 8-25  $P_{Xe}$  dependence  of  electron  density  $N_e$  and  electron temperature $T_e$ measured at neighborhood of anode ring.

The schematic illustration of plasma exposure to substrate at various $P_{Xe}$ were shown in Fig. 8-26. Since the substrate surface free from plasma damage and free from recoiled particles were realized, it was expected that surface smoothness, crystallographic and magnetic characteristics of deposited films would be improved at $P_{Xe}$ of 0.75 mTorr.
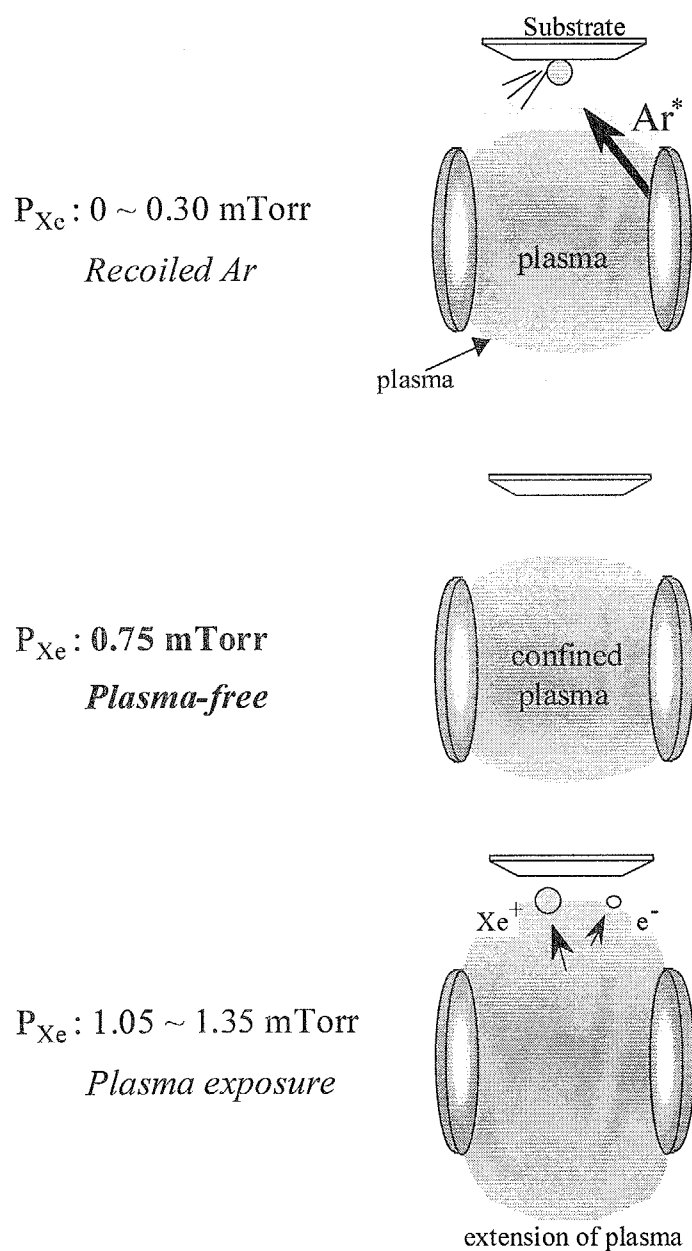
$P_{Xe}$: 0 ~ 0.30 mTorr

*Recoiled Ar*

$P_{Xe}$: 0.75 mTorr

*Plasma-free*

$P_{Xe}$: 1.05 ~ 1.35 mTorr

*Plasma exposure*

Fig. 8-26   Schematic illustration of plasma exposure to substrate at various $P_{Xe}$.

8-6-2      Partial Xe pressure dependence

8-6-2-1 *Chemical compositions*

Fig. 8-27 shows $P_{Xe}$ dependence of Ba content x of films deposited from BaO ·

6.5($Fe_2O_3$) targets, where $C_{Ba} : C_{Fe} = x : 12$. While x at $P_{Xe}$ of 0.0 mTorr of 0.95 was

very close to stoichiometric value, x was much smaller than not only stoichiometric but

also target at $P_{Xe}$ of 0.15-0.3 mTorr. It took the maximum value of about 1.0 at $P_{Xe}$ of

0.75 mTorr and was almost constant or gradually decreased at higher $P_{Xe}$. The increase

and decrease of x with the increase of $P_{Xe}$ was almost same as that of Fig. 8-10, in which

targets with highr Ba content than stoichiometric were used. From these results, it was

clarified that the composition of deposited films are affected by $P_{Xe}$ and Ba atoms are

effectively incorporated film at $P_{Xe}$ of 0.75 mTorr. The decrease of x at $P_{Xe}$<0.75 mTorr

and at $P_{Xe} > 0.75$ mTorr seemed to be attributed to the bombardment of recoiled

particles and to the scattering of Ba atoms during transportation from target to atoms[1],

respectively. It should be noted that although the incorporation Ba in films had been

thought difficult by many researchers, much amount of Ba was easily incorporated and

x was larger than that of target value at $P_{Xe}$ of 0.75 mTorr, where "damage-free"

deposition was achieved. It was confirmed that Ba atoms are likely to be incorporated in

the films due to their chemical activity and serious bombardment of charged particles

and recoiled ones in their sputtering system caused the lack of Ba contents.

---

[1] Kenji Noma : Ph.D. thesis, Tokyo Institute of Technology (1997) (in Japanese)
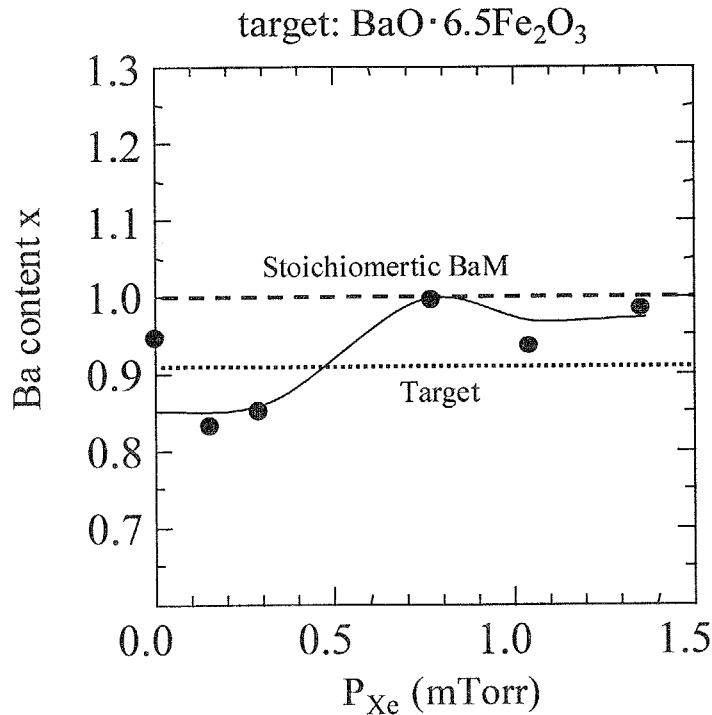
target: $BaO \cdot 6.5Fe_2O_3$



Fig. 8-27    $P_{Xe}$ dependence of Ba content x of films deposited from
$BaO \cdot 6.5(Fe_2O_3)$ targets.    ($C_{Ba} : C_{Fe} = x : 12$)

8-6-2-2 *Surface and cross-section al SEM images*

Fig. 8-28 shows the SEM images and centerline average roughness $R_a$ of films

deposited from $BaO \cdot 6.5(Fe_2O_3)$ targets at various $P_{Xe}$. Although the film deposited

without Xe gas revealed relatively smooth surface as seen in (a), the grain growth and

rough surface was observed at $P_{Xe}$ of 0.15 and 0.30 mTorr as seen in (b) and (c).

The reason was attributed to the bombardment of recoiled Ar. On the other hand,

very smooth surface was observed at $P_{Xe}$ of 0.75 mTorr in (d), where the damage during

deposition seemed to be most effectively restrained as seen in Fig. 8-25 and Fig. 8-26.

The rough surface at $P_{Xe}$ of 0.75 mTorr and higher in (e), might be caused the lack of Ba

atom in the film due to the scattering atoms during transportation from target to
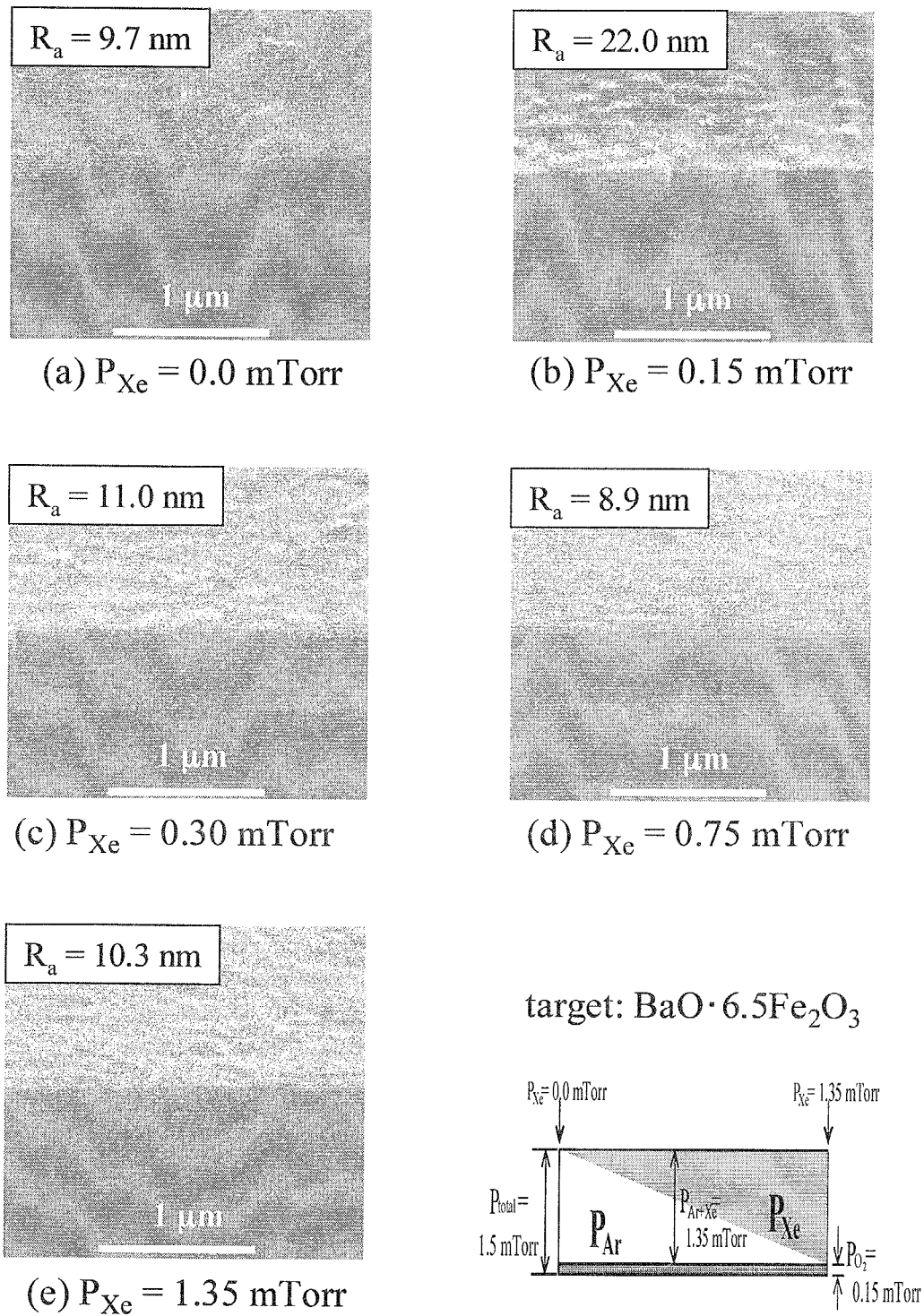
substrate.

211

$R_a$ = 9.7 nm

1 μm

(a) $P_{Xe}$ = 0.0 mTorr

$R_a$ = 22.0 nm

1 μm

(b) $P_{Xe}$ = 0.15 mTorr

$R_a$ = 11.0 nm

1 μm

(c) $P_{Xe}$ = 0.30 mTorr

$R_a$ = 8.9 nm

1 μm

(d) $P_{Xe}$ = 0.75 mTorr

$R_a$ = 10.3 nm

1 μm

(e) $P_{Xe}$ = 1.35 mTorr

target: BaO·6.5Fe$_2$O$_3$

$P_{Xe}$= 0.0 mTorr       $P_{Xe}$= 1.35 mTorr

$P_{total}$= 1.5 mTorr    $P_{Ar}$    $P_{Ar+Xe}$= 1.35 mTorr    $P_{Xe}$    $P_{O_2}$= 0.15 mTorr

Fig. 8-28    Surface and cross-sectional SEM images of films deposited from BaO·6.5(Fe$_2$O$_3$) targets at various $P_{Xe}$.

212

## 8-6-2-3 *Crystallographic characteristics*

Fig. 8-29 shows the X-ray diffraction diagrams of films deposited from $BaO \cdot 6.5(Fe_2O_3)$ targets at various $P_{Xe}$. Small but clear spinel(mmm) peaks were observed in magnification as well as clear BaM(00l) peaks for all diagrams. Since the spinel peaks was easily formed in the films compared with the deposition using Ba excessive target, the peak intensity of spinel(mmm) was larger than that. The peak intensity of BaM(00l) was large at $P_{Xe}$ of 0.75-1.35 mTorr and the improvement of crystallinity was suggested.

The inter-planar distance $d_{BaM(008)}$ and normalized X-ray diffraction intensity of spinel (mmm) peaks $f_{spinel(mmm)}$ of films were calculated from these diagrams as shown in Fig. 8-30. $d_{BaM(008)}$ took the maximum value at $P_{Xe}$ of 2.904Å at $P_{Xe}$ of 0.75 mTorr, where x took the maximum value. The shape of this figure is almost same that of Fig. 8-13. However, it was clear that this increase of $d_{BaM(008)}$ was not attributed to the incorporation of Ba atoms into irregular site, because the film composition was same as that of stoichiometric one. From this viewpoint, these results were common with that of the films deposited from target with Ba content higher than stoichiometric one at $P_{Xe}$ of 1.43 mTorr, which exhibited $4\pi M_s$ of 4.9 kG. Since larger spinel peaks were observed in XRD diagrams, $f_{spinel(mmm)}$ took larger value than those in Fig. 8-12. The minimum value of 0.08 was obtained at $P_{Xe}$ of 0.75 mTorr.

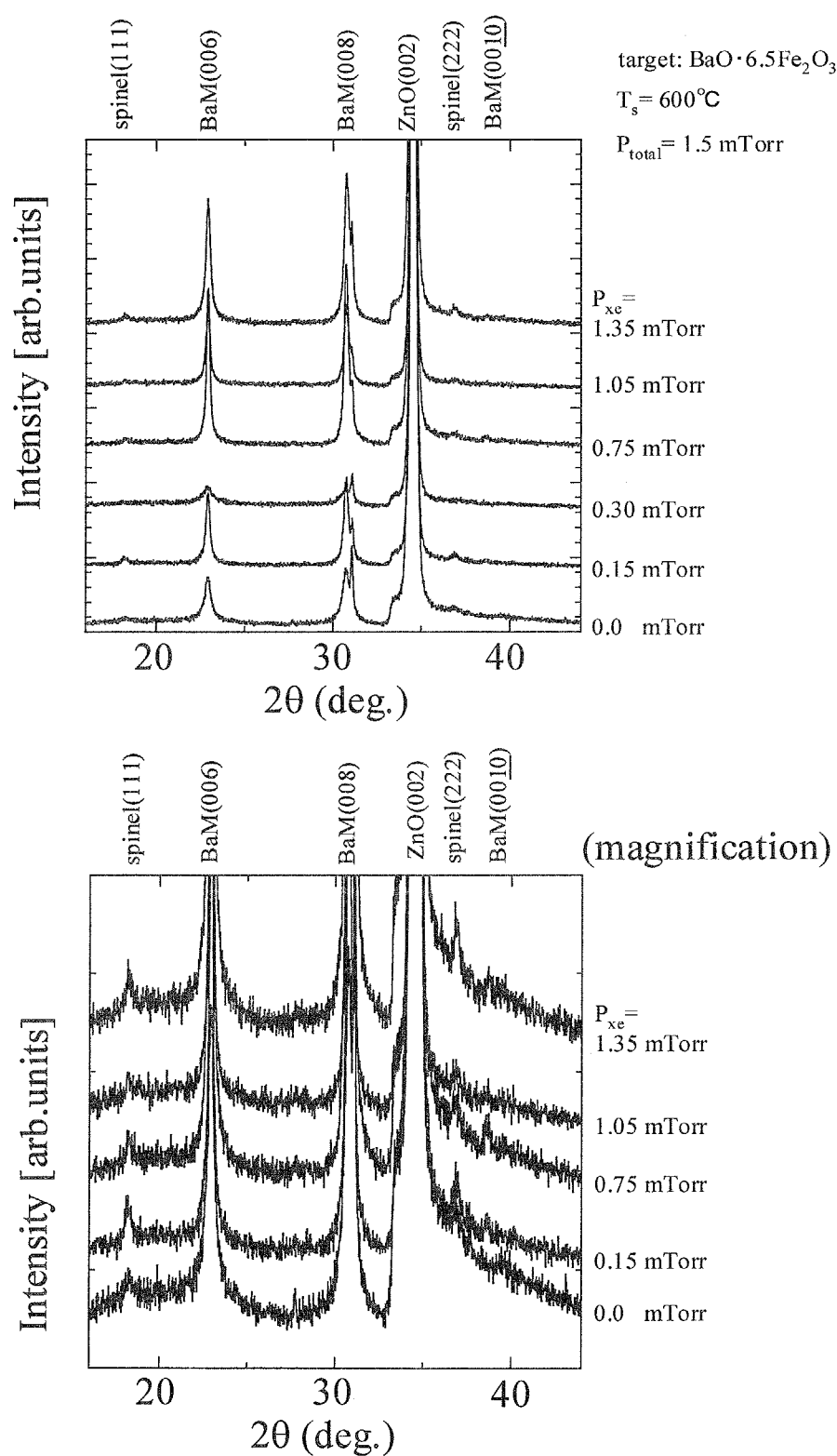Fig. 8-29　X-ray diffraction diagrams of films deposited from BaO·
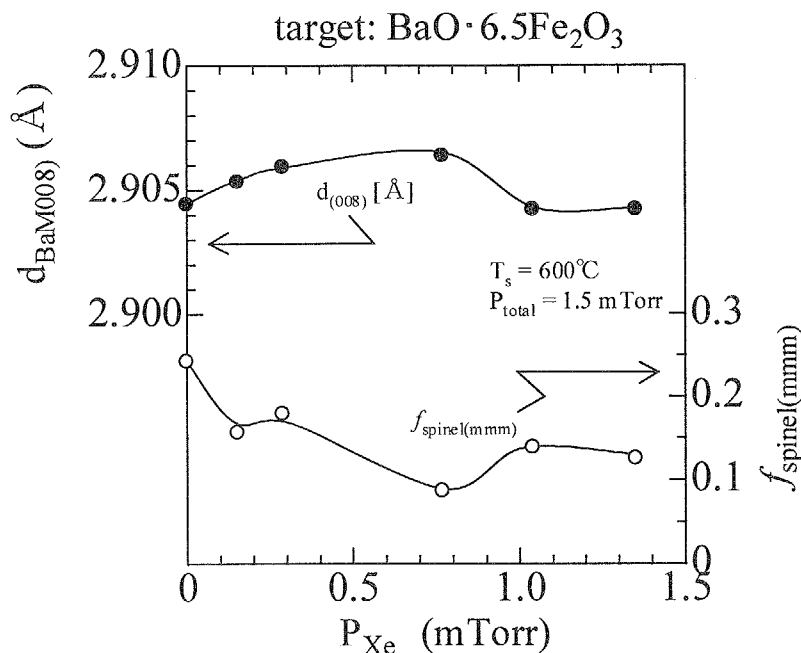6.5(Fe$_2$O$_3$) targets at various P$_{Xe}$.

Fig. 8-30   $P_{Xe}$   dependence   of   inter-planar   distance   $d_{BaM(008)}$   and normalized X-ray diffraction intensity of spinel (mmm) peaks $f_{spinel(mmm)}$ of films deposited from $BaO \cdot 6.5(Fe_2O_3)$ targets.

Fig. 8-31 shows $P_{Xe}$ dependence of crystallite size $<D>_{BaM(008)}$ and full width at half maximum of rocking curve $\Delta\theta_{50\_BaM(008)}$ of films deposited from $BaO \cdot 6.5(Fe_2O_3)$ targets. Although the increase and decrease of $<D>_{BaM(008)}$ was smaller than those in Fig. 8-13, largest $<D>_{BaM(008)}$ and smallest $\Delta\theta_{50\_BaM(008)}$ was obtained at $P_{Xe}$ of 0.75 mTorr, where most efficiently plasma damage was restricted as seen in Fig. 8-26. It was confirmed that the reason of deterioration of $\Delta\theta_{50\_BaM(008)}$ in Fig. 8-13 was attributed to the excessive incorporation of Ba atoms.

Fig. 8-32 and Fig. 8-33 show the $P_{Xe}$ dependence of inter-planar distance, $d_{ZnO(002)}$, and crystallite size, $<D>_{ZnO(002)}$, and full width at half maximum of rocking curve, $\Delta\theta_{50\_ZnO(002)}$, of ZnO underlayer, on which Ba ferrite layer was deposited from $BaO \cdot 6.5(Fe_2O_3)$ targets, respectively.
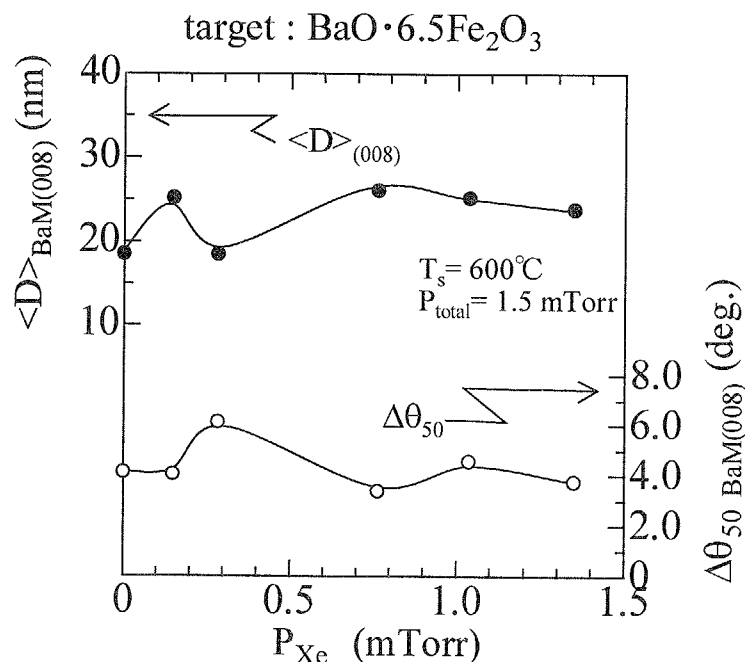
target : $BaO \cdot 6.5Fe_2O_3$

Fig. 8-31    $P_{Xe}$ dependence of crystallite size $<D>_{BaM(008)}$ and full width at half maximum of rocking curve $\Delta\theta_{50\_BaM(008)}$ of films deposited from $BaO \cdot 6.5(Fe_2O_3)$ targets.

They were calculated and evaluated by the diffraction peak profiles and rocking profiles in X-ray diffraction(XRD) diagrams corresponding to (002) orientation of ZnO underlayer. Although $d_{ZnO(002)}$ was almost constant with the increase of $P_{Xe}$, the increase and decrease of $<D>_{ZnO(002)}$ and $\Delta\theta_{50\_ZnO(002)}$ were very similar to those of Fig. 8-31. The same similarity was observed in Fig. 8-14 and Fig. 8-16, and there was possibility that the insufficient reproducibility of ZnO underlayer directly affected to crystallinity of Ba ferrite layer. However, since any relationship between the $P_{Xe}$ dependence of $<D>_{ZnO(002)}$ and $\Delta\theta_{50\_ZnO(002)}$ were not observed, it seemed that this change of ZnO crystallinity was caused by the deposition of Ba ferrite layer on it. It was suggested that inter-diffusion between ZnO and Ba ferrite layers during deposition of Ba ferrite layer might affect to the ZnO crystallinity.
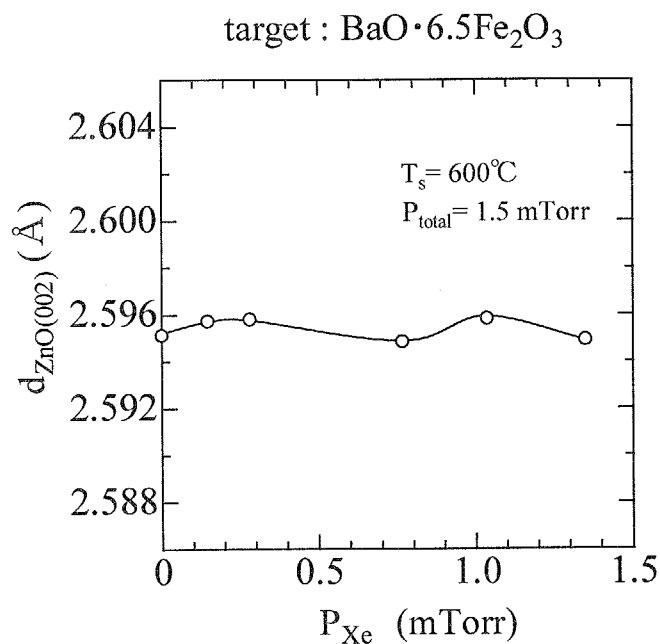
target : $BaO \cdot 6.5Fe_2O_3$



Fig. 8-32    $P_{Xe}$ dependence of inter-planar distance $d_{ZnO(002)}$ of ZnO underlayer, on which Ba ferrite layers were deposited from $BaO \cdot 6.5(Fe_2O_3)$ targets.

target : $BaO \cdot 6.5Fe_2O_3$
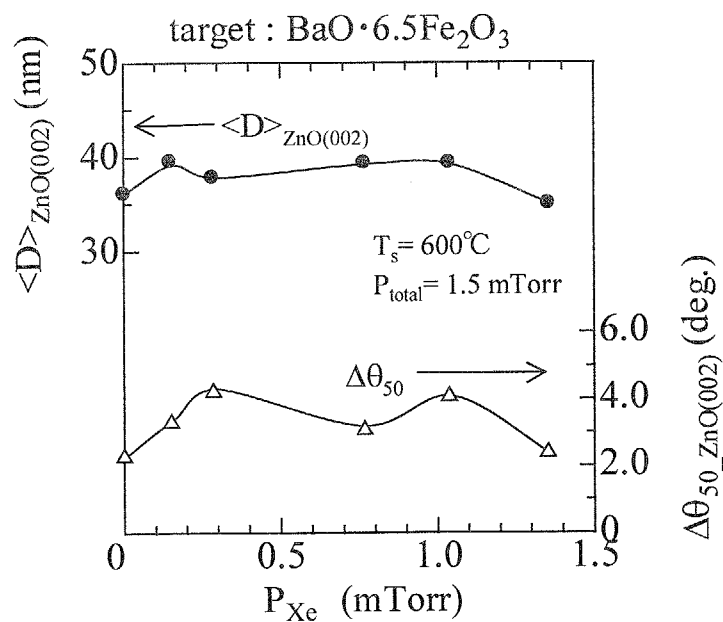


Fig. 8-33    $P_{Xe}$ dependences of crystallite size $<D>_{ZnO(002)}$ and full width at half maximum of rocking curve $\Delta\theta_{50\_ZnO(002)}$ of ZnO underlayer, on which Ba ferrite layers were deposited from Ba ferrite layer deposited from $BaO \cdot 6.5(Fe_2O_3)$ targets.

8-6-2-4 *Magnetic Characteristics*

Fig. 8-34 shows $P_{Xe}$ dependence of saturation magnetization $4\pi M_s$ and perpendicular and in-plane coercivity, $H_{c//}$ and $H_{c\perp}$, of films deposited from $BaO \cdot 6.5(Fe_2O_3)$ targets. The films deposited at $P_{Xe}$ of 0.0 mTorr possessed very small $4\pi M_s$ of 2.1 kG and it was smaller than that of Ba ferrite film deposited from $BaFe_{11.0}O_{19.0-y}$ targets at same deposition conditions due to insufficient Ba content. The value of $4\pi M_s$ increased with increase of $P_{Xe}$ up to 0.75 mTorr and reached at the maximum value of 5.1 kG, which was larger than that of bulk BaM of 4.8 kG. A larger $4\pi M_s$ than bulk value was also observed in the films deposited from Ba excessive targets at $P_{Xe}$ of 1.43 mTorr. There was a possibility that $Fe_2W$ crystallites with larger $4\pi M_s$ of 5.3 kG were incorporated in the films. The crystallite structures of BaM and $Fe_2W$ ferrite were illustrated in Fig. 8-35. The W-type unit ($SSRS^*S^*R^*$) is constructed by insertion of the S and $S^*$ blocks into the M-type unit ($SRS^*R^*$). It has longer c-axis length and larger $4\pi M_s$ than BaM ferrite due to the increase in the number of S blocks. Moreover, it was reported that the spinel intergrown Ba ferrite crystallite which is formed by inserting another $S^*$ block into BaM crystal structure exhibited larger $4\pi M_s$ than BaM crystallites[2].

---

[2] H. Yokoyama, T. Maeda, T. Nomura, O. Kubo and T. Ido, Proceedings of The Sixth International Conference on Ferrites (ICF-6), pp 1418-1421 (1992).

target : BaO·6.5Fe$_2$O$_3$

$T_s$= 600℃
$P_{total}$= 1.5 mTorr

$4\pi M_s$

$H_{c\perp}$

$H_{c//}$

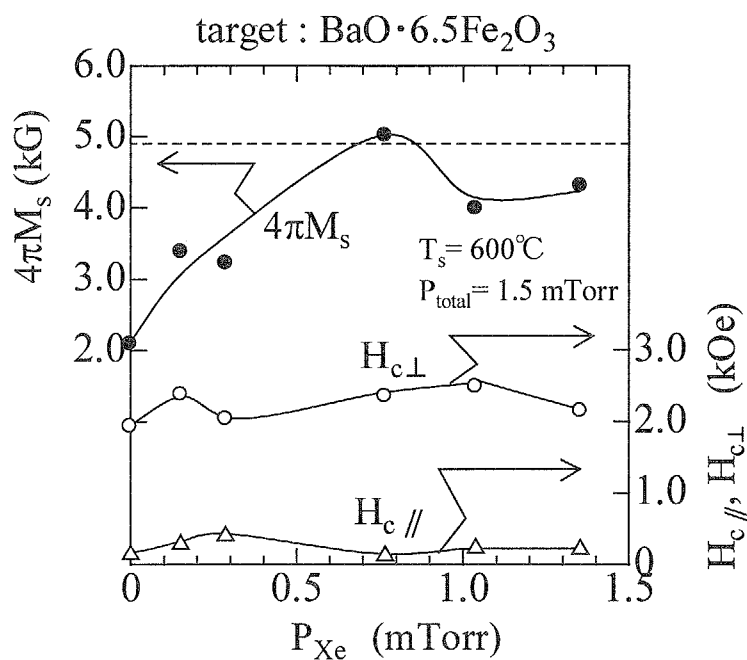Fig. 8-34  $P_{Xe}$ dependence of saturation magnetization $4\pi M_s$ and perpendicular and in-plane coercivity $H_{c//}$ and $H_{c\perp}$ of films deposited from BaO·6.5(Fe$_2$O$_3$) targets.

M type
(BaFe$_{12}$O$_{19}$)

W type
(BaFe$_{18}$O$_{27}$)

O  O$^{2-}$
Ba$^{2+}$
Fe$^{3+}$

d = 23.2 Å
$4\pi M_s$ = 4.8 kG

d = 32.8 Å
$4\pi M_s$ = 5.3 kG

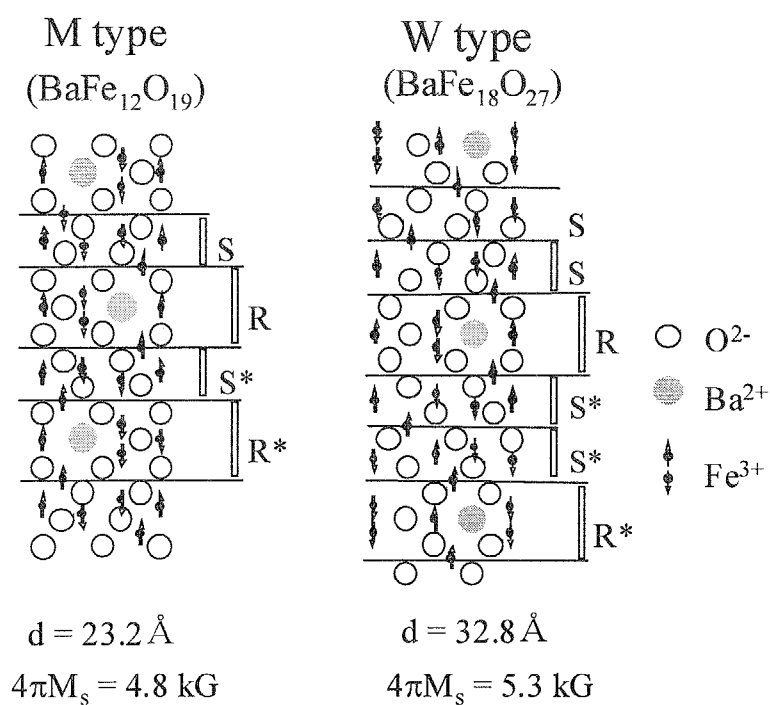Fig. 8-35  Structure of unit cell of (a)M and (b)W type Ba ferrite.

Since $d_{BaM(008)}$ also reached at the maximum value at $P_{Xe}$ of 0.75 mTorr, this extremely large $4\pi M_s$ of 5.1 kG seemed to be attributable to the formation of Ba ferrite crystallites which inserted the spinel blocks as well as to the formation of berthollide spinel crystallites($Fe_{3-\delta}O_4$). $H_{c\perp}$ was above 1.8 kOe for the whole range of $P_{Xe}$ and the ratio of $H_{c\perp}/H_{c//}$ reached the maximum value of about 19 at $P_{Xe}$ of 0.75 mTorr, where largest $4\pi M_s$ was attained.

The dependence of perpendicular anisotropy constant $K_\perp$ and anisotropy field $H_k$ of films deposited from $BaO\cdot6.5(Fe_2O_3)$ targets on $P_{Xe}$ were shown in Fig. 8-36. Although the $K_\perp$ was smaller than $1.0\times10^5$ $J\cdot m^{-3}$ at $P_{Xe}$ of 0.0 mTorr, it took the maximum value of $3.2\times10^5$ $J\cdot m^{-3}$ at $P_{Xe}$ of 0.75 mTorr. This value is corresponds to the value of BaM single crystal and is a quite large value for sputter-deposited film. Their decrease at $P_{Xe}$ of 1.35 mTorr seemed to be attributed to the decrease of $4\pi M_s$ as seen in Fig. 8-34. Since $K_u$ can be calculated as $K_{u1} = K_{u\perp} + 2\pi M_s^2$, the maximum value of $K_u$ was $4.23\times10^5$ $J\cdot m^{-3}$. It was larger than that of bulk Ba ferrite of $3.30\times10^5$ $J\cdot m^{-3}$. Here, $H_k$ was calculated as $H_k = 2K_{u1}/M_s$ and it took the maximum value of 20 kOe at $P_{Xe}$ of 0.75 mTorr. This is much larger than that of the value of bulk BaM of 18.0 kOe. Although $H_k$ took extremely high value at $P_{Xe}$ of 0.75 mTorr, $H_c$ was not so high as about 2.5 kOe and it was lower than that of bulk Ba ferrite.
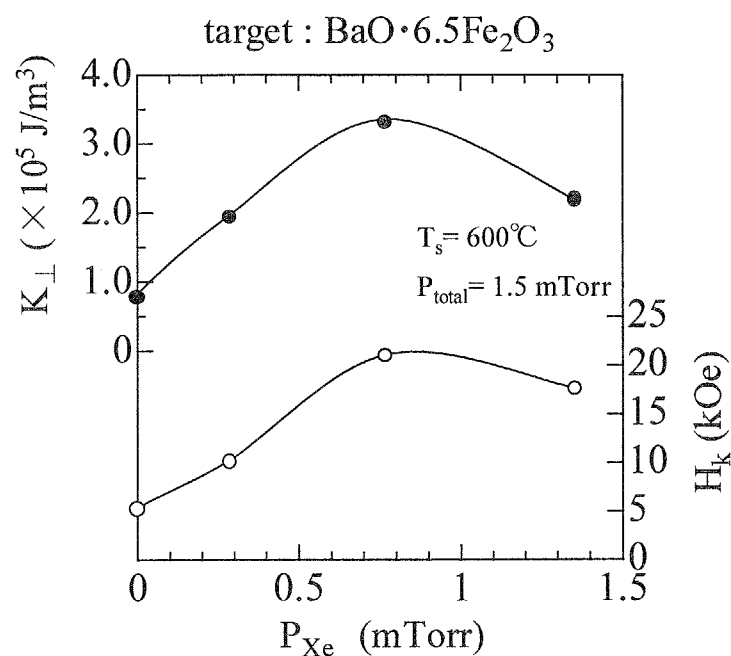
Fig. 8-36  $P_{Xe}$ dependences of anisotropy field $H_{keff}$ and perpendicular anisotropy constant $K_{\perp}$ of films deposited from BaO·6.5($Fe_2O_3$) targets.

It seemed to that strong magnetic interaction between magnetic grains in films as well as wall motion in crystallites were reasons for these results. Anyway, these values of $K_u$ and $H_k$ were much larger and higher than those of Co-Cr thin films, i.e. about 1.6 $\times 10^5$ $J\cdot m^{-3}$. Therefore, Ba ferrite films deposited using Xe mixture seems to be applicable as perpendicular recording media with high density.

Fig. 8-37 shows the relationship between saturation magnetization $4\pi M_s$ and anisotropy constant $K_{u1}$. From this figure, it was reconfirmed that both of large $4\pi M_s$ and large anisotropy constant $K_u$ were achieved for Ba ferrite films deposited from $BaFe_{13.0}O_{19.0-y}$ targets at $P_{Xe}$ of 0.75 mTorr and $T_s$ of 600℃.

Fig. 8-38 shows the relationships among Ba content x, inter-planer distance $d_{BaM(008)}$, saturation magnetization $4\pi M_s$ and the blocks structure of films deposited from BaO·6.5($Fe_2O_3$) targets at various $P_{Xe}$. Since Ba content x was smaller than stoichiometric

value and $K_{u1}$ took smaller value, spinel crystallites such as berthollide($Fe_{3-\delta}O_4$) ones seemed to be existed in films at lower $P_{Xe}$ up to 0.3 mTorr. At this range of $P_{Xe}$, non-magnetic regions were formed between magnetic grains due to bombardment from recoiled particles and therefore, $4\pi M_s$ was relatively small values. On the other hand, Ba content x was almost 1.0 and largest $4\pi M_s$ of 5.1 kG was attained at $P_{Xe}$ of 0.75 mTorr where plasma damage was mostly restricted as seen in Fig. 8-26. However, spinel(mmm) peaks were observed in XRD diagrams as seen in Fig. 8-29, and it seemed that Ba oxides, i.e. BaO, $BaO \cdot Fe_2O_3$ etc, were existed at grain boundaries between BaM and spinel crystallites. It was suggested that magnetization in spinel crystallites were coupled to those of Ba ferrite crystallites and some of spinel blocks were inserted in Ba ferrite crystallite. It was also suggested that the increase of $d_{BaM(008)}$ as seen in Fig. 8-30 was attributed to the insertion of spinel blocks to BaM ferrite crystallites. The reason $4\pi M_s$, $K_{u1}$ and $H_k$ decreased at $P_{Xe}$ higher than 1.13 mTorr was not clear. However, since Ba content x and $d_{BaM(008)}$ was slightly decreased, the growth of some kinds of berthollide($Fe_{3-\delta}O_4$) crystallites were promoted due to plasma exposure as seen in Fig. 8-26.

target: $BaO \cdot 6.5Fe_2O_3$
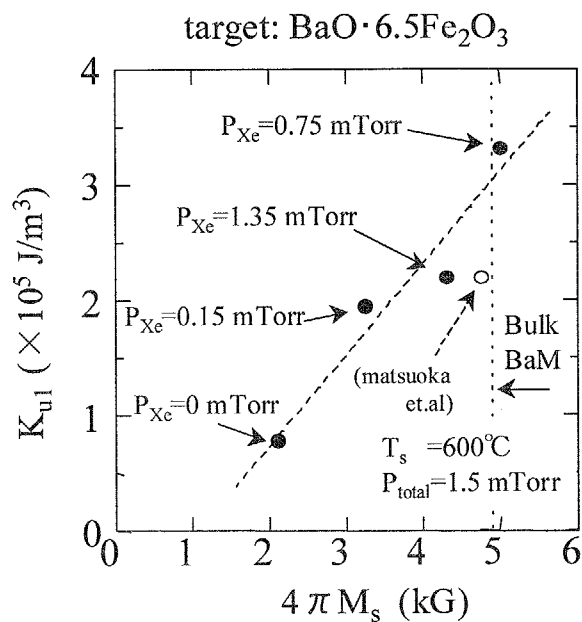
Fig. 8-37　Relationship between saturation magnetization $4\pi M_s$ and anisotropy constant $K_{u1}$.



| | Ar ————————————————— Xe | | |
|---|---|---|---|
| Partial Xe Pressure $P_{Xe}$ | 0-0.3 mTorr | 0.75 mTorr | 1.13-1.35 mTorr |
| Inter-planer distance $d_{(008)}$ | ~2.904 Å | 2.906 Å | ~2.905 Å |
| Ba content $C_{Ba}$ | ~0.8 | 1.0 | ~0.95 |
| $4\pi M_s$ | 2.1~3.4kG | 5.1kG | ~4.0kG |
| Blocks Structure | Decrease of $C_{Ba}$ Growth of Spinel Blocks | Increase of Spinel Blocks | Normal Structure ? |

Fig. 8-38　Relationships among Ba content x, inter-planer distance $d_{BaM(008)}$, saturation magnetization $4\pi M_s$ and crystallite structure of films deposited from at $BaO \cdot 6.5(Fe_2O_3)$ targets various $P_{Xe}$.

223

8-6-3 Substrate temperature dependence

From above results, largest $4\pi M_s$ of 5.1 kG and $K_{u1}$ of $4.23 \times 10^5$ J·m$^{-3}$ were attained at the optimized $P_{Xe}$ of 0.75 mTorr. In this section, therefore, Ba ferrite films were deposited at lower $T_s$ than 600 °C and their crystallographic and magnetic characteristics were investigated to confirm the critical $T_s$ for Ba ferrite films with c-axis orientation.

*8-6-3-1 Chemical compositions and surface SEM images*

Although the Ba content x of the films deposited at $T_s$ of 500, 550 and 650°C were just a little smaller than stoichiometric one, i.e. $C_{Ba}$ = 0.9-0.95, those of films deposited at $T_s$ 475 and 600°C were almost stoichiometric, i.e. $C_{Ba}$ = 1.0. It was suggested that the composition of deposited films were more strongly affected by partial Xe pressure $P_{Xe}$ than substrate temperature $T_s$.

Fig. 8-39 shows the surface and cross-sectional SEM images and center-line average roughness $R_a$ of films deposited from BaO·6.5(Fe$_2$O$_3$) targets at $T_s$ of (a)600°C, (b)550°C, (c)500°C and (d)475°C. Although it was supposed that the films deposited at $T_s$ of 475°C exhibited smaller $R_a$, the films deposited at (b)$T_s$ = 550°C and (c) $T_s$ = 500°C exhibited a little larger $R_a$ than (a)$T_s$ = 600°C. The slight increase of $R_a$ in (b) and (c) seemed to be attributed to small discrepancy in Ba content. Although their $R_a$ was not enough small for the application for contact type recording layer, it should be noted that their values are quite small for sputter-deposited Ba ferrite films.
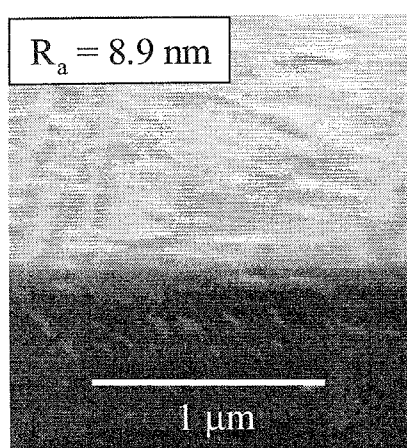
(a) $T_s = 600°C$
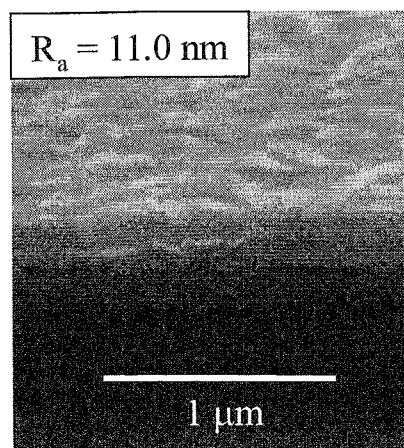


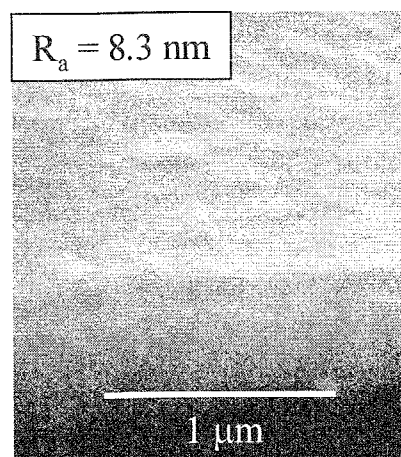(b) $T_s = 550°C$
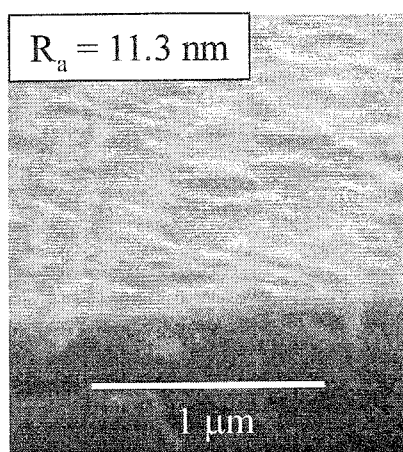


(c) $T_s = 500°C$



(d) $T_s = 475°C$

Fig. 8-39　Surface and cross-sectional SEM images of films deposited from $BaO \cdot 6.5(Fe_2O_3)$ targets at $T_s$ of (a)600°C, (b)550°C, (c)500°C and (d)475°C

*8-6-3-2 Crystallographic characteristics*

Fig. 8-40 shows X-ray diffraction diagrams of films deposited from $BaO \cdot 6.5(Fe_2O_3)$ targets at various $T_s$, where $P_{Xe}$ was set at 0.75 mTorr. It was found that Ba ferrite films composed of well crystallites with excellent c-axis orientation was obtained at even at low $T_s$ of 475°C. The decrease of critical $T_s$ for depositing the films seemed to be attributed to the damage-free deposition and moderate arrival energy of sputtered atoms at $P_{Xe}$ of 0.75 mTorr, where best crystallographic and magnetic characteristics were obtained. At lower $T_s$ of 450°C, there was no peak of BaM(001) and hallow peak which corresponds to amorphous structure was observed as well as small speaks of spinel(mmm). BaM(001) peaks became small at $P_{Xe}$ higher than 600°C. While spinel(mmm) peaks were observed at $T_s$ in the range from 500 to 600°C, only BaM(00n) peaks were observed in magnification of XRD diagram.at $T_s$ of 475°C.

Fig. 8-41 shows the $T_s$ dependence of inter-planar distance $d_{BaM(008)}$ of films deposited from $BaO \cdot 6.5(Fe_2O_3)$ targets. Although $d_{BaM(008)}$ was almost constant at $T_s$ up to 600°C, it decreased at $T_s$ of 650°C, where BaM(008) peak shifted to higher $2\theta$. Fig. 8-42 shows $T_s$ dependence of crystallite size $<D>_{BaM(008)}$ and full width at half maximum of rocking curve $\Delta\theta_{50\_BaM(008)}$ of films deposited from $BaO \cdot 6.5(Fe_2O_3)$ targets. $<D>_{BaM(008)}$ and $\Delta\theta_{50\_BaM(008)}$ took the maximum and minimum value of 28 nm and 3.4°, respectively, at $T_s$ of 600°C. They were gradually decreased and increased with the decrease of $T_s$ and 19 nm and 6.1°, respectively at $T_s$ of 475°C. Although this crystallite size is relatively large and it will have to be decreased, it was confirmed that crystallite size can be decreased by decreasing $T_s$.
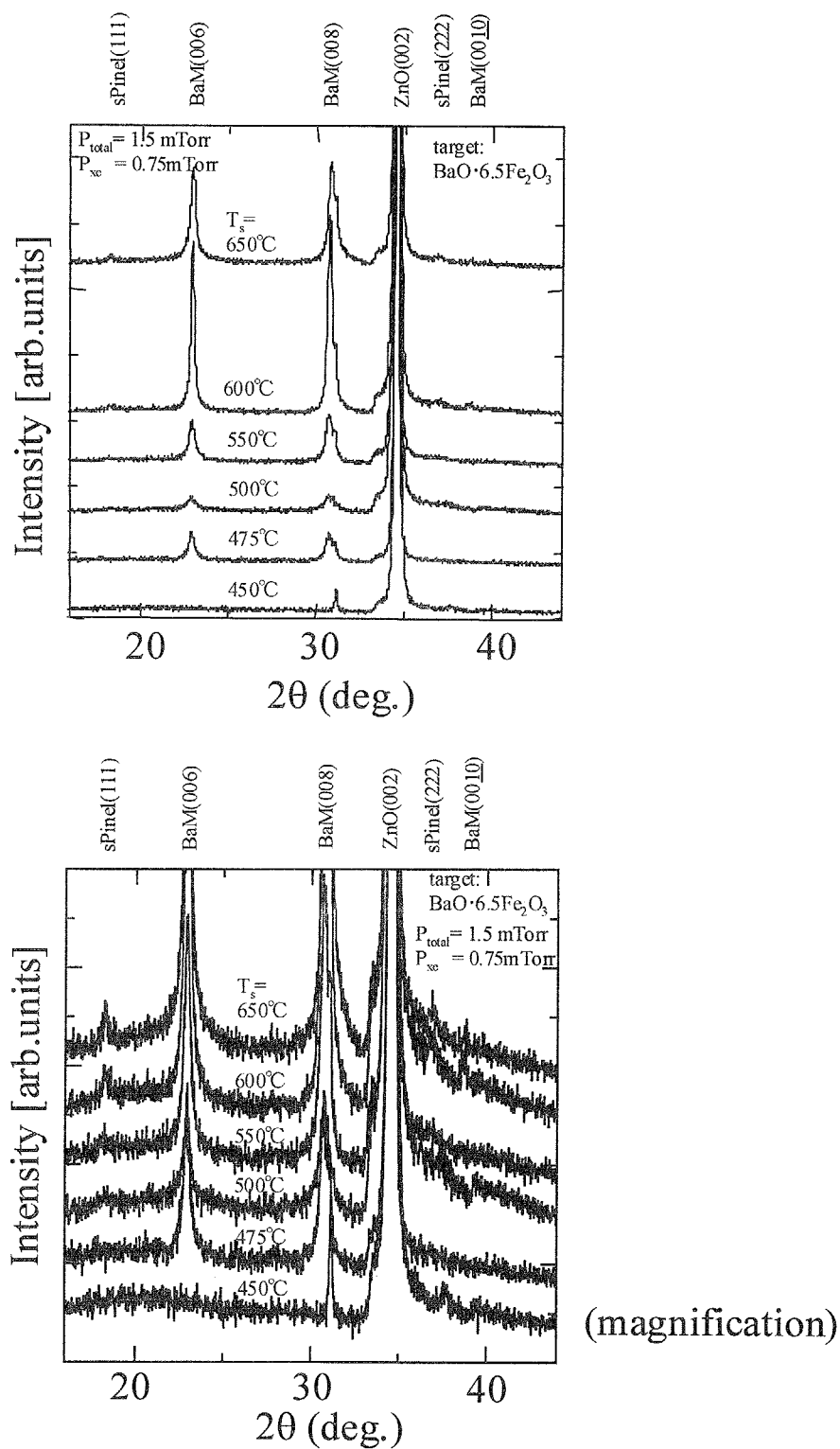
Fig. 8-40    X-ray diffraction diagrams of films deposited from BaO·
6.5($Fe_2O_3$) targets at various $T_s$. ($P_{Xe}$ of 1.35 mTorr)
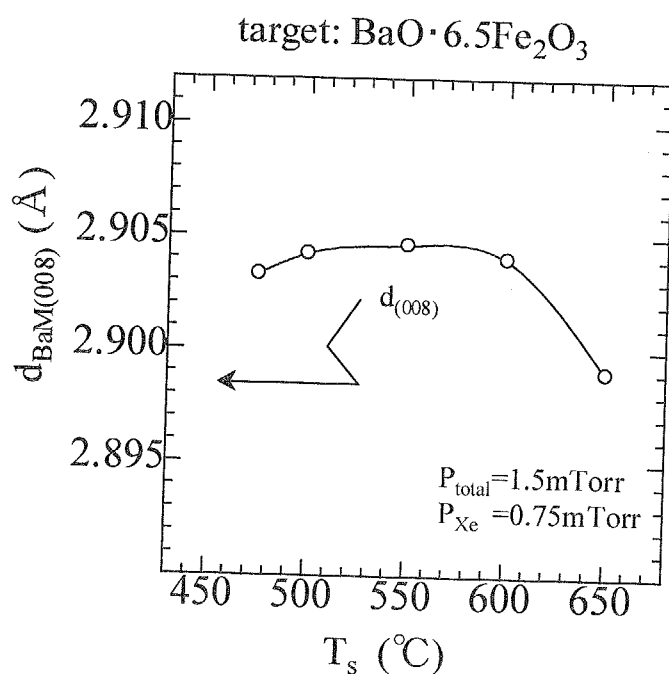
target: BaO·6.5Fe$_2$O$_3$



Fig. 8-41    $T_s$ dependence of inter-planar distance $d_{BaM(008)}$ of films deposited from BaO·6.5(Fe$_2$O$_3$) targets.
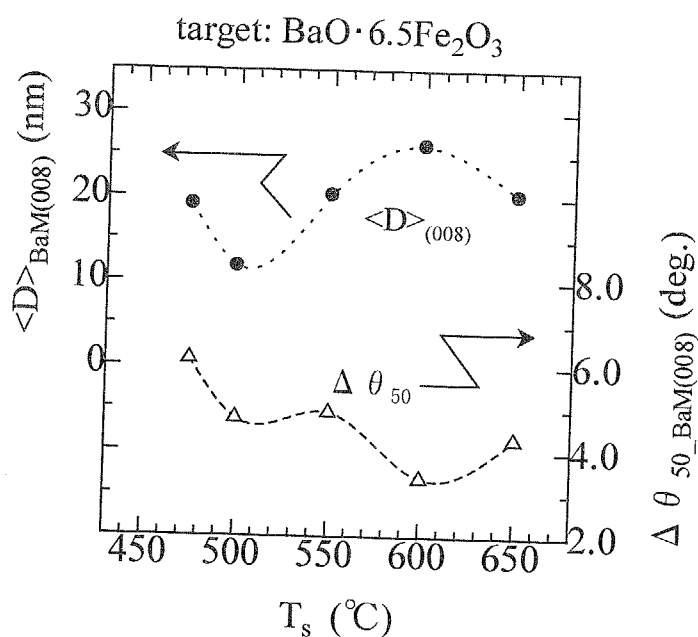
target: BaO·6.5Fe$_2$O$_3$



Fig. 8-42    $T_s$ dependence of crystallite size $<D>_{BaM(008)}$ and full width at half maximum of rocking curve $\Delta\theta_{50\_BaM(008)}$ of films deposited from BaO·6.5(Fe$_2$O$_3$) targets.

### 8-6-3-3 *Magnetic characteristics*

Fig. 8-43 shows $T_s$ dependence of saturation magnetization $4\pi M_s$ and perpendicular and in-plane coercivity, $H_{c\perp}$ and $H_{c//}$, of films deposited from $BaO \cdot 6.5(Fe_2O_3)$ targets. It was found that the deposited films possessed $4\pi M_s$ of 4.7 kG. Although this value was smaller than 5.1 kG which was attained at $T_s$ of 600°C, it was almost same value as that of BaM single crystal. Since this value was much larger than that of Ba ferrite films deposited without Xe and possessed almost same $<D>_{BaM(008)}$ and $\Delta\theta_{50\_BaM(008)}$, it seemed that the restriction of the damage from plasma or decrease of the number and energy of incorporated Ar atoms during deposition was enable to deposit Ba ferrite films with little defects. The decrease of $4\pi M_s$ at $T_s$ of 500°C seemed to be attributed to the decrease of $<D>_{BaM(008)}$.
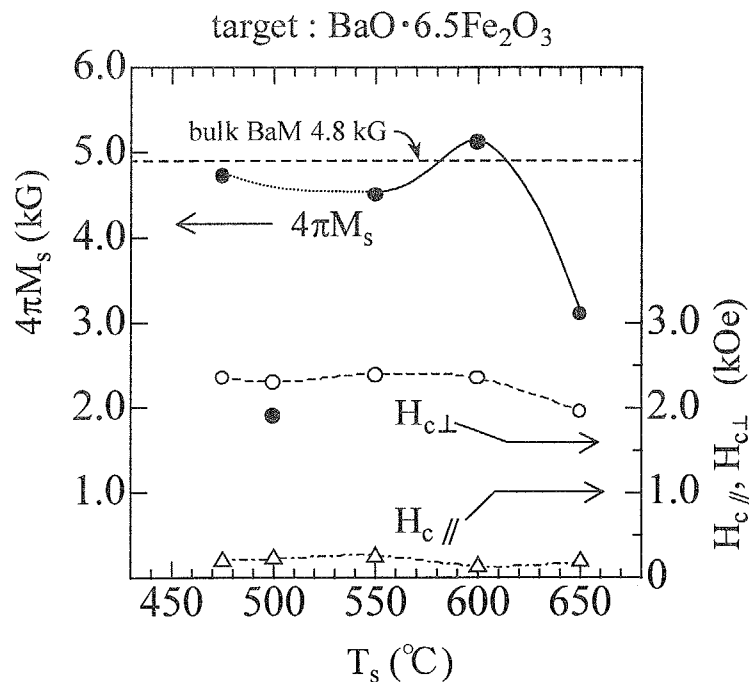


Fig. 8-43   $T_s$ dependence of saturation magnetization $4\pi M_s$ and perpendicular and in-plane coercivity $H_{c//}$ and $H_{c\perp}$ of films deposited from $BaO \cdot 6.5(Fe_2O_3)$ targets.

$H_{c\perp}$ was higher than 2.0 kOe and $H_{c//}$ was lower than 0.4 kOe in the whole rang of $T_s$, and it was confirmed that the films exhibited quite a large perpendicular anisotropy.

From these results, it was found that Ba ferrite films deposited from Fe excessive targets with composition of BaO·6.5($Fe_2O_3$), exhibited excellent c-axis orientation, large $4\pi M_s$ and well perpendicular anisotropy even at low $T_s$ of 475℃. This $T_s$ is the lowest value in the world as the substrate temperature for the sputter-deposited Ba ferrite film without post annealing process with c-axis orientation.

8-6-4    Consideration of surface smoothness and large saturation magnetization

Matsuoka et al. reported that they succeeded to obtain Ba ferrite films composed of Ba ferrite crystallites only at $T_s$ higher than critical $T_s$ of 530℃[1], and the film deposited at $T_s$ lower than 530℃ was composed of spinel crystallites and possessed magnetic characteristics almost same as those of magnetite($Fe_3O_4$). In this study, the film deposited at $T_s$ above 500℃ were composed of BaM crystallites as well as spinel crystallites and single phase of BaM crystallites was only attained at $T_s$ of 475℃. The films deposited at $T_s$ lower than critical $T_s$ of 475℃ exhibited amorphous structure in XRD diagram and possessed non spontaneous magnetization. This difference seemed to be attributed to the difference of damage from plasma during deposition.

Fig. 8-44 shows the SEM images of Ba ferrite films deposited by (a) RF diode sputtering system in Ar and $O_2$ mixture after Morisako et al., (b) Facing Targets Sputtering system in Ar and $O_2$ mixture after Matsuoka et al., (c) Facing Targets Sputtering system in Xe, Ar and $O_2$ mixture after this study, respectively, at $T_s$ of 600℃

[1] M

in which the best crystallinity and magnetic characteristics were attained and at $T_s$ of

475°C which was critical $T_s$ for c-axis orientation. In (a), both films revealed very

rough surface. Since there was serious bombardment from γ-electron and negative

oxygen ions to films during deposition, films revealed rough surface even at high $T_s$ of

670°C. In (b), while the film revealed rough surface at $T_s$ of 530°C, it was smooth at

higher $T_s$ of 600°C.

In FTS system using Ar and $O_2$ mixture, although there is damage from recoiled Ar

and therefore deterioration of grain growth and crystallite characteristics were observed
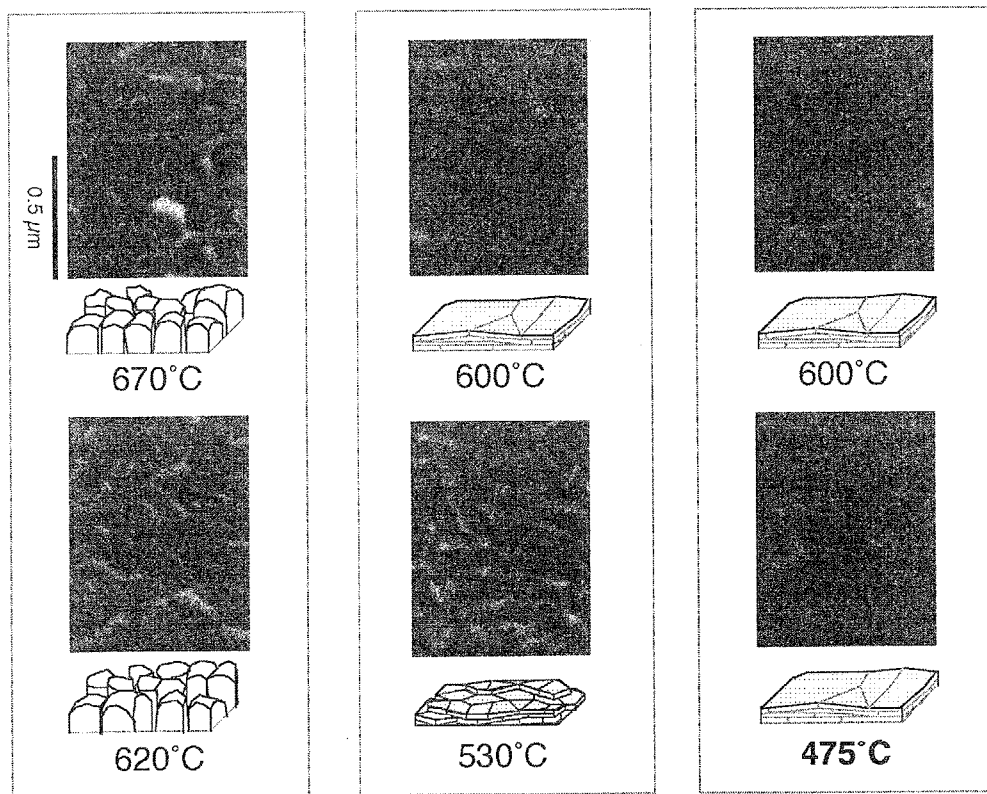


Fig. 8-44    Comparison of SEM images of Ba ferrite films deposited
by (a)RFDS in Ar+$O_2$ mixture, (b)FTS in Ar+$O_2$ mixture,
(c)FTS in Xe+Ar+$O_2$ mixture, respectively.

[1] M. Matsuoka et al. : IEEE Trans. on Magn., 18[6], pp.1119-1121 (1982)

at around critical $T_s$, these damages were compensated at higher $T_s$ around 600℃ due to surface diffusion and re-crystallization. On the other hand in (c), the both films deposited at critical $T_s$ of 475℃ and at higher $T_s$ of 600℃ revealed smooth surface. Since the damage-free deposition was attained, smooth surface was obtained even at critical $T_s$.

Crystallites which are supposed to be formed in the films deposited from Fe excessive targets are FeO with NaCl structure, $\alpha$-$Fe_2O_3$ with hexagonal collandom one, $\gamma$-$Fe_2O_3$, $Fe_3O_4$ and BaO · $Fe_2O_3$ with spinel one, and BaM and $Fe_2W$ with magnetoplumbite one. The $\gamma$-$Fe_2O_3$, $Fe_3O_4$ and BaO·$Fe_2O_3$ with spinel one, BaM and $Fe_2W$ crystallites possessed spontaneous magnetization. The low temperature phase are FeO and $\alpha$-$Fe_2O_3$ and the distance between the most close oxygen in a-axis are a = 2.155Å and a = 2.5173Å, respectively. They are smaller than those of spinel(111) and ZnO(001). Therefore, crystallites with spinel and BaM structure were easily grown on ZnO underlayer as seen in Fig. 8-29.

It is well known that there is phase change $Fe_3O_4 \rightarrow \alpha$-$Fe_2O_3$ at high temperature. The decrease of $4\pi M_s$ and perpendicular anisotorpy at $T_s$ of 650℃ in Fig. 8-43 were attributed to the formation of $\alpha$-$Fe_2O_3$ crystallites in the films. At $T_s$ in the range from 500 to 600℃, since the substrate surface was reduced atmosphere at $P_{O_2}$ of 0.15 mTorr, Fe ions were likely to be divalent. In addition to that since ZnO underlayers were used, the formation of $Fe_3O_4$ crystallites were promoted. Therefore, insertion of spinel blocks were occurred. On the other hand, since the atmosphere around substrate surface was oxidation at $T_s$ of 475℃, spinel block of $\gamma$-$Fe_2O_3$ were inserted. Since $\gamma$-$Fe_2O_3$ has a vacant in B site in its structure, there was decrease of $d_{BaM(008)}$ at $T_s$ of 475℃ in Fig.

8-41.

From above results, it was suggested that extremely large $4\pi M_s$ of 5.1 kG at $T_s$ of 600°C and at $P_{Xe}$ of 0.75 mTorr was attributed to the insertion of S-blocks with composition of $Fe_3O_4$ which has large $4\pi M_s$ of 5.8 kG and it was also magnetically coupled to the other blocks. On the other hand, the composition of the S-blocks in the films deposited at $T_s$ of 475°C was $\gamma$-$Fe_2O_3$. Since it was composed of perfect magnetoplumbite type of crystallites, it possessed $4\pi M_s$ as large as bulk value.

## 8-7    Summary

Ba ferrite films were deposited on ZnO underlayer in mixture gas of Xe(0.0-1.43 or 0.0-1.35 mTorr), Ar(1.43-0.0 or 0.0-1.35 mTorr) and $O_2$(0.07 or 0.15 mTorr) for obtaining excellent c-axis orientation and magnetic characteristics, which are equal to the bulk values, even at lower substrate temperature. Two kinds of targets with Ba contents higher and lower than stoichiometric ones, i.e. $BaFe_{11.0}Fe_{19-y}$ and $BaFe_{13.0}Fe_{19-y}$ were used for the depositions. The dependence of their magnetic characteristics such as $4\pi M_s$, $H_{c\perp}$ and perpendicular anisotropy constant $K_\perp$ on partial Xe pressure $P_{Xe}$ and substrate temperature $T_s$ were investigated, respectively.

The obtained results were as follows;

The films deposited from Ba excessive targets with composition of $BaFe_{11.0}Fe_{19-y}$ ($P_{Ar}$ = 1.43-0.0 mTorr, $P_{Xe}$ =0.0-1.43 mTorr, $T_s$ = 500-600°C)

Ba content x was changed by the change of $P_{Xe}$ and took the maximum value at $P_{Xe}$ of 0.75 mTorr, where almost the same Ar and Xe were mixed.

Crystallographic characteristics such as crystallite size $<D>_{BaM(008)}$ and the full width

at half maximum of rocking curve $\Delta\theta_{50\_BaM(008)}$ were depended on $P_{Xe}$ and the minimum and the maximum values were obtained at $P_{Xe}$ of 0.75 mTorr, where Ba content was the most far from stoichiometric one of BaM crystallites.

The largest $4\pi M_s$ of 4.9 kG, which was larger than that of bulk BaM was obtained at $P_{Xe}$ of 1.43 mTorr, where Ba content x was almost 1.0. It was suggested that this large $4\pi M_s$ was attributed to the insertion of S-blocks into block strucutre of BaM crystallites.

The critical $T_s$ for c-axis orientation was 550℃.

The films deposited from Fe excessive targets with composition of $BaFe_{13.0}Fe_{19-y}$ ($P_{Ar}$ = 1.35-0.0 mTorr, $P_{Xe}$ =0.0-1.35 mTorr, $T_s$ = 450-600℃)

It was found by plasma diagnosis using Langmuir probe that the substrate surface are free from plasma damage and free from recoiled particles at at $P_{Xe}$ of 0.75 mTorr.

The films deposited at $P_{Xe}$ of 0.75 mTorr with Ba content x of 1.0 revealed quite smooth surface and exhibited excellent c-axis orientation as well as weak spinel peaks in XRD diagram.

The maximum $4\pi M_s$ of 5.1 kG, the largest perpendicular anisotropy constant $K_{u\perp}$ of $3.3 \times 10^5$ J·m$^{-3}$ were also achieved at $P_{Xe}$ of 0.75 mTorr and these values are superior than those of bulk values. The insertion of S-blocks into block structure of BaM crystallites seemed to be one of reasons for these results.

The critical $T_s$ for c-axis orientation was decreased down to 475℃ at optimized $P_{Xe}$ of 0.75 mTorr and this is the lowest $T_s$ in the world for the sputter-deposited Ba ferrite film with c-axis orientation.

The films deposited at optimized $P_{Xe}$ of 0.75 mTorr and at critical $T_s$ of 475℃ exhibited almost same $4\pi M_s$ as that of bulk BaM.

In consequence, the critical $T_s$ for the deposition of Ba ferrite with smooth surface, well c-axis orientation, large $4\pi M_s$ and quite large perpendicular anisotropy $K_{u\perp}$ was successfully decreased down to 475°C by using Ar, Xe and $O_2$ mixture as sputtering gas. This is the lowest process temperature in the world for Ba ferrite films with almost perfect c-axis orientation. Since this temperature is in the range where glass substrate with high temperature resistance can be used as substrate, this study contributed to the practical application of Ba ferrite films as perpendicular recording layer.

# Chapter 9

# Future Prospects

In this study, Co ferrite film, Co ferrite/ZnO film, Co-Zn ferrite film and Ba ferrite/ZnO film were prepared by `damage-free` facing targets sputtering apparatus, and the chemical composition, surface structure, crystallographic and magnetic characteristics were investigated for the application of contact type of magnetic recording layer. Their future prospects will be mentioned in this chapter.

[Co ferrite film and Co ferrite/ZnO film]

Although simple Co ferrite film did not exhibit preferential orientation in XRD diagram, a moderately large saturation magnetization $4\pi M_s$ of 2.6 kG and an extremely high coercivity $H_c$ of about 4.0 kOe were attained at relatively low substrate temperature $T_s$ of 300℃. Since $H_c$ of recording layer, especially that of longitudinal magnetic recording layer, should be increased with the increase of recording density and $H_c$ higher than 3.0 kOe would be necessary to attain areal recording density over 20 Gb/inch$^2$. Therefore, although surface smoothness will have to be improved, Co ferrite film is one of candidates as a contact type of longitudinal recording layer.

On the other hand, Co ferrite layer deposited on ZnO underlayer exhibited (111) orientation even without intentional heating of substrate due to epitaxial effect between these layers. Since it exhibited almost the same and quite high in-plane and perpendicular coercivity, $H_{c//}$ and $H_{c\perp}$ of about 3.3 kOe at relatively low $T_s$ of 300℃, it seems to be applicable as a contact type of isotropic recording layer. However, the

improvement of surface smoothness would be required.

Since Co ferrite film exhibits large Faraday rotation angle and large magnetostriction, it also seems to be applicable in magneto-optical devices and SAW transducers.

[Co-Zn ferrite film]

Co-Zn ferrite films revealed quite smooth surface, i.e. $R_a$ of 1.0 nm, and had well (111) orientation. Since they exhibited relatively large $4\pi M_s$ of 3.3 kG as well as moderately high coercivity of 1.8 kOe even without intentional heating of substrate, these films could be deposited on PET tape substrate and seems to be applicable as a recording layer in data streamer with huge amount of recording capacity.

Since Co-Zn ferrite films deposited on glass ceramic disk substrates at $T_s$ of 200 and 400°C had isotropic and quasi in-plane magnetic orientation, respectively, these disks seems to be applied as isotropic and in-plane recording layer. In addition, Co-Zn ferrite disks with (111) orientation revealed smooth surface, i.e. $R_a$ of 1.2 nm. It attained relatively high linear recording density of 136 kfrpi and attained almost zero transition noise even at high linear recording density of 100 kfrpi and above. Therefore, Co-Zn ferrite disk with (111) orientation would be one of superior candidate as a contact type of recording layer in rigid disk with ultra high density.

[Ba ferrite/ZnO film]

Ba ferrite film with good surface smoothness, excellent c-axis orientation and superior magnetic characteristics were successfully prepared even without post annealing process. Therefore, Ba ferrite films prepared in this study by using the facing targets sputtering apparatus and Xe gas mixture seems to be applicable as a

perpendicular recording layer and as a material for milli-wave isolator and circulator devices.

However surface roughness is a problem for the application as a contact type recording layer. If surface smoothness $R_a$ should be improved smaller than 3 nm, it would be applied as a contact type of perpendicular recording layer with ultra high density. Since it is not so easy to sustain high substrate temperature above 500°C during deposition in an wide area, post-annealing process, which would be enable the promotion of crystallite orientation and the improvement of magnetic characteristics without excessive growth of crystallite, such as the rapid thermal annealing process, should be investigated for the mass production of Ba ferrite layers.

Ba ferrite film deposited from Fe excessive targets by using Xe gas mixture exhibited larger $4\pi M_s$ than that of bulk value and it seemed to be attributed to the insertion of spinel blocks to BaM unit cell. Therefore, the formation of W and Z type Ba ferrite, in which larger number of spinel blocks are contained and had larger saturation magnetization than BaM, would be possible by using this damage-free FTS system and Xe mixture. Especially, Z type of Ba ferrite film seems to be applicable as high frequency ferrite and magnetoelectric wave absorber.

In consequence, the deposition method of Co-Zn ferrite and Ba ferrite film at low substrate temperature were investigated in this study. Since they exhibited excellent crystallinity and magnetic characteristics, they are superior candidates as a contact type of isotropic and perpendicular recording layer with ultra high density.

# Chapter 10

# General Conclusion

Since the spacing between the head and disk media have been fairly decreasing, a contact or semi-contact type of recording layer will be certainly required in the near future. However, Co-Cr-Ta and Co-Cr-Pt layer, which are currently used in recording media, need the protective and lubricant layers on them. Moreover, the increase of media noise at high density is a serious problem for them.

On the other hand, since the sputtered ferrite media have high chemical stability and excellent corrosion resistance, they seem to be applicable as semi-contact or contact recording layer. In addition, there was a report that they exhibited much lower media noise level than the Co-based alloy media did at high recording density. Therefore, the ferrite films are drawing a lot of attention again as a contact or semi-contact type of recording layer with low noise.

In this study, therefore, a spinel type of Co-Zn ferrite film and a magnetoplumbite type of Ba ferrite films were prepared by the facing targets sputtering apparatus without post-annealing process. And their surface smoothness, crystallite orientation and magnetic characteristics were investigated to aim at the application for the contact type recording layer in rigid disks with ultra-high density.

In this section, general conclusions of this study will be described.

[Co ferrite film]

Although Co ferrite film did not exhibit a preferential orientation in XRD diagram, and the saturation magnetization $4\pi M_s$ was as small as 3.0 kG even at high substrate

temperature $T_s$ of 400℃, moderately high coercivity $H_c$ above 3.0 kOe was easily obtained for the film deposited at relatively low $T_s$ from 300 to 400℃. Since $H_c$ higher of 3.0 kOe and above will be required for recording layer with the increase of recording density, these Co ferrite films would be one of candidates as contact type longitudinal recording layer with areal density higher than 20 Gb/inch².

[Co ferrite/ZnO double layered film]

Apparent orientation of spinel (222) was observed at substrate temperature $T_s$ from 90 to 600℃ by using ZnO(001) underlayer. However, SEM images revealed that their surface were not smooth even at relatively low $T_s$ of 300℃ and large grain with diameter of several 100 nm were observed at $T_s$ of 500℃. The steep increase of crystallite size $<D>_{spinel(222)}$ of Co ferrite layer at $T_s$ of 500℃ caused the steep increase of the saturation magnetization $4\pi M_s$ and the decrease of coercivity $H_c$. Although large $4\pi M_s$ of 4.6 kG was attained at $T_s$ of 500℃, $H_c$ was smaller than 1.0 kOe. It is too small to be used as recording layer in rigid disks. However, since $H_{c//}$ and $H_{c\perp}$ of the films deposited at relatively low $T_s$ up to 400℃ took almost the same and relatively high values, these films seemed to be applicable for isotropic magnetic recording layer after the improvement of film smoothness.

[Co-Zn ferrite film]

In substrate temperature dependence $T_s$, surface and cross-sectional texture of the deposited films were quite smooth and the center-line roughness $R_a$ were 1.4 and 4.3 nm at $T_s$ of 90 and 400℃, respectively. The films deposited at $T_s$ up to 200℃ and at $T_s$

above 400℃  exhibited (111) and (311) orientation and they correspond to the formation

of the most closely packed structure of oxygen and metallic ions, respectively. The films

with (111) orientation had isotropic orientation of magnetization and they exhibited a

moderately large $4\pi M_s$ of 3.3 to 4.8 kG and high in-plane and perpendicular coercivity

$H_{c//}$ and $H_{c\perp}$ of 1.5-2.2 kOe. The films with (311) orientation had quasi in-plane

orientation of magnetization and exhibited moderately small $4\pi M_s$ of 2.2-2.7 kG and

relatively high $H_{c//}$ and $H_{c\perp}$ of about 2.0 kOe, respectively.

Since a very low temperature process has been achieved in this study, Co-Zn ferrite

films seemed to be applicable for flexible disk and tape with high recording density

even if low heat resistance sheets such as PC disks and PET tapes are used as substrates.


[Read/Write characteristics of Co-Zn ferrite disks]

The disk specimens deposited at $T_s$ of 200 and 400℃  were composed of crystallites

with excellent (111) and (311) orientation.

In read/write characteristics a merged type MR head were used, and , the isolated

waveform of both Co-Zn ferrite disk with (111) orientation, Disk(111), and that with

(311) was observed. It was suggested that Disk(111) had larger perpendicular

magnetization component. The highest $D_{50}$ for Disk(111) and Disk(311) specimens were

136 and 86 kfrpi and their thickness was 50 and 35 nm, respectively. The noise from

transition region of Disk(111) did not increase with the increase of linear recording

density. While that of Disk(311) slightly increased, it was quite small compared with

conventional longitudinal Co-Cr/Cr recording layer.

In consequence, Co-Zn ferrite disk with (111) orientation is applicable as a contact

type of recording layer at ultra-high density because of their surface smoothness and extremely low transition noise at high density. Although surface smoothness should be improved and higher coercivity is necessary, Co-Zn ferrite disk with (311) orientation also seemed to be applicable as a contact type of longitudinal recording layer.

[Ba ferrite/ZnO film]

The films deposited from $BaFe_{13}O_{19-y}$ targets at $P_{Xe}$ of 0.75 mTorr had almost stoichiometric composition, i.e. Ba content x was 1.0. They revealed quite smooth surface and exhibited excellent c-axis orientation as well as weak spinel peaks in XRD diagram. The maximum $4\pi M_s$ of 5.1 kG and the largest perpendicular anisotropy constant $K_{u\perp}$ of $3.3 \times 10^5$ $J \cdot m^{-3}$ were also achieved at $P_{Xe}$ of 0.75 mTorr and these values were superior than those of bulk values. The insertion of S-blocks into block structure of BaM crystallites seemed to be one of reasons for this larger $4\pi M_s$ than stoichiometric bulk ferrites. It was found by plasma diagnosis using Langmuir probe that the damage of substrate surface from plasma and that from recoiled particles were most efficiently restricted $P_{Xe}$ of 0.75 mTorr.

The films deposited at optimized $P_{Xe}$ of 0.75 mTorr and at critical $T_s$ of 475℃ exhibited almost same $4\pi M_s$ as that of bulk BaM. The critical $T_s$ for c-axis orientation was decreased down to 475℃ at optimized $P_{Xe}$ of 0.75 mTorr, and this is the lowest $T_s$ in the world for Ba ferrite film with excellent c-axis orientation. Since this $T_s$ of 475℃ is in the range where glass substrate with high temperature resistance, such as PIREX, can be used as substrate, this result might contribute to the realization of the application of Ba ferrite films as a contact type of recording layers.

# Acknowledgment

I would like to express my sincere appreciation to Professor Masahiko Naoe as my academic and research advisor after I joined as a stuff of Tokyo Institute of Technology. The continuous guidance, support and warm encouragement that Professor Naoe has provided me were deeply appreciated.

I am indebted to Associate Professor Shigeki Nakagawa for his continuous guidance and warm encouragement as well as various suggestions and discussions.

I would like to express my gratitude to Professor Masanori Abe, Professor Yohtaro Yamazaki, Professor Mitsumasa Iwamoto, Associate Professor Tetsuya Mizumoto of Tokyo Institute of Technology for their critical comments and discussions.

I wish to acknowledge the advice and encouragement I have received from doctoral course students of Naoe-Nakagawa Lab., Dr. Ki-Bong Song(KOLON), Dr. Kenji Noma(Fujitsu), Dr. Yasuyoshi Miyamoto(NHK), Dr. Takayuki Ichihara(Hitachi); thank is due particularly to Dr. Kenji Noma who had been a co-worker in most parts of my study from March 1992 to March 1997. His contribution in this study was very important and my study would not be successful like this without his devotion.

I wish to express special appreciation to Dr. Yoshitaka Kitamoto of T.I.T. for his suggestions and discussions concerning on read/write characteristics of recording layer. I also thank to Ms. Kumiko Kaneta for her suggestions and assistance on various clerical works.

I am looking forward to expressing acknowledges to Associate Professor Akimitsu Morisako of Shinshu University for his technical suggestions and discussions on the optimization of deposition method and read/write characteristics of ferrite rigid disks as well as warm encouragement. I would also like to express my appreciation to Associate Professor Yoichi Hoshi of Tokyo Inst. of Polytechnics for various guidance and suggestions on deposition of ferrite films. I am really appreciated Dr. Yoshio Niimura of Sumitomo-3M, Dr. Sadao Kadokura of FTS, Dr. Takakazu Takahashi of Toyama

245

*Nobuhiro Matsushita*

at O-okayama Campus of Tokyo Institute of Technology in June 1998

# List of Publications and Presentations
## (1990.10~1998.6)

[Papers and Proceedings]        57

<u>First Author</u>    (29)

1.  Nobuhiro Matsushita, Shigeki Nakagawa and Masahiko Naoe:
    "Preparation of Co Ferrite Thin Films with Large Perpendicular and In-Plane Coercivities by Facing Targets Sputtering,"
    IEEE Transactions on Magnetics, vol. 28[5], pp. 3108-3110, 1992.

2.  N. Matsushita, K. Noma, S. Nakagawa and M. Naoe:
    "Magnetic and Crystallographic Characteristics of $CoFe_2O_4$ Thin Film on ZnO Underlayer,"
    Proc. of 6th International Conference on Ferrites (ICF 6), pp. 428-431, 1992.

3.  N. Matsushita, K. Noma, S. Nakagawa and M. Naoe:
    "Preparation of Co-Zn Ferrite Thin Films for Rigid Disks with High Recording Density,"
    Proc. of 6th International Conference on Ferrites (ICF 6), pp. 1479-1482, 1992.

4.  N. Matsushita, K. Noma, S. Nakagawa and M. Naoe:
    "Magneto-optical Properties of Cobalt Ferrite Thin Films Prepared by Facing Targets Sputtering,"
    Proc. of 6th International Conference on Ferrites (ICF 6), pp. 1633-1636, 1992.

5.  N. Matsushita, K. Noma, S. Nakagawa and M. Naoe:
    "Crystallographic and Magnetic Characteristics of Co-Zn Ferrite Films Deposited at Low Substrate Temperature by Using Facing Targets Sputtering Method,"
    Proc. of 1st International Conference on Processing Materials for Properties, pp. 1169-1172, 1993.

6.  Nobuhiro Matsushita and Masahiko Naoe:
    "High Coercivity of BaM Ferrite Films Deposited by Arc Discharge Evaporation,"
    IEEE Transactions on Magnetics, vol. 29[6], pp. 4089-4091, 1993.

7.  N. Matsushita, K. Noma, S. Nakagawa And M. Naoe:
    "Preparation of Co-Zn Ferrite Films at Low Substrate Temperature by Plasma-free DC

Sputtering for Magnetic Recording Media,"
Journal of Applied Physics, vol. 75[10], pp. 5975-5977, 1994.

8. N. Matsushita, K. Noma, S. Nakagawa and M. Naoe:
"Preparation and Magnetic Properties of BaM Films with Excellent Crystallinity by Xe Sputtering,"
Journal of Applied Physics, vol. 75[10], pp. 7131-7133, 1994.

9. N. Matsushita, K. Noma and M. Naoe:
"Ba Ferrite Thin Films with Large Saturation Magnetization Deposited by Sputtering in Mixture of Xe, Ar and $O_2$,"
IEEE Transactions on Magnetics, vol. 30[6], pp. 4053-4055, 1994.

10. N. Matsushita, K. Noma, S. Nakagawa and M. Naoe:
"Structure and Magnetic Properties of a Hexagonal Type Ferrite Thin Films Prepared by Facing Targets Sputtering,"
Proc. of the 1st Magneto-Electronics International Symposium, pp. 11-14, 1994.

11. N. Matsushita, K. Noma, S. Nakagawa and M. Naoe:
"New Processes of Synthesizing Co Ferrite Films at Low Substrate Temperature by Facing Targets Sputtering,"
Proc. of IUMRS-ICA-94, pp. 671-676, 1995.

12. N. Matsushita, K. Noma, S. Nakagawa and M. Naoe:
"Co-Zn Ferrite Rigid Disks Prepared by Plasma-free Sputtering at Low Substrate Temperature,"
IEEE Transactions on Magnetics, vol. 31[6], pp. 2779-2781, 1995.

13. N. Matsushita, K. Noma, S. Nakagawa and M. Naoe:
"Control of crystallographic and magnetic characteristics in Co-Zn ferrite sputtered films,"
Journal of Magnetism and Magnetic Materials, 140-144, pp.2085-2086, 1995

14. 松下伸広, 野間賢二, 中川茂樹, 直江正彦:
『混合ガススパッタによる垂直記録媒体用 Ba フェライト膜の低温形成』
Journal of The Magnetics Society of Japan, vol. 19[S2], pp. 71-74, 1995.

15. N. Matsushita, K. Noma, S. Nakagawa and M. Naoe:

"Deposition of Ba Ferrite Films for Perpendicular Magnetic Recording Media Using Mixed Sputtering Gas of Xe, Ar and $O_2$,"
IEICE Transactions on Electronics, vol. E78-C[11], pp. 1562-1566, 1995.

16. 松下伸広, 野間賢二, 中川茂樹, 直江正彦:
『Xe を用いたスパッタリングによる大飽和磁化 Ba フェライト薄膜の作製と磁気特性』
粉体および粉末冶金, 第 43 巻 1 号, pp. 25-30, 1996.

17. N. Matsushita, K. Noma, S. Nakagawa and M. Naoe:
"Highly Crystallized (La, Sr)$MnO_3$ Films Deposited by Facing Targets Sputtering Apparatus,"
Journal of Applied Physics, vol. 79[8], pp. 5247-5249, 1996.

18. N. Matsushita, K. Noma, A. Morisako, S. Nakagawa and M. Naoe:
"Read/Write Characteristics of Co-Zn Ferrite Rigid Disks in Contact Mode Recording,"
IEEE Transactions on Magnetics., vol. 32[5], pp. 3578-3580, 1996.

19. Nobuhiro Matsushita, Kenji Noma, Shigeki Nakagawa and Masahiko Naoe: Plasma Diagnosis of Facing Targets Sputtering System for Deposition of Ba Ferrite Films in Ar, Xe and $O_2$ Gas Mixture; *J. of Korean Institute of Surface Engineering*, 29, [6], pp.834-838 (1996)

20. 松下伸広, 野間賢二, 中川茂樹, 直江正彦:
『酸化物磁性薄膜による等方性磁気ディスクの作製と記録再生特性』
日本応用磁気学会誌, Vol. 21[S1], pp.34-37, 1997.

21. N. Matsushita, K. Noma, S. Nakagawa and M. Naoe:
"Ferromagnetic Characteristics of a Perovskite Type of (La, Sr)$MnO_3$ Films Deposited by Kr Sputtering,"
Proc. of 7th International Conference on Ferrites (ICF 7), pp. 629-630, 1997.

22. N. Matsushita, K. Noma, S. Nakagawa and M. Naoe:
"Diagnosis of Mixture Gas Discharge in Damage-Free Sputtering Apparatus and Deposition of Ba Ferrite Films at Low Substrate Temperature,"
Proc. of 4th International Symposium on Sputtering and Plasma Processing (ISSP'97), pp.117-122, 1997.

23. N. Matsushita, K. Noma, S. Nakagawa and M. Naoe :
   "Excellent crystallographic and perpendicular magnetic characteristics of Ba ferrite films deposited by gas mixture of Ar, Xe and $O_2$,"
   Journal of Magnetism and Magnetic Materials, 176, pp.41-45, 1997.

24. 松下伸広、馮　　潔、塩澤友祥、渡部　康、一瀬　誠、中川茂樹、直江正彦
   『Ba フェライト磁気ディスクの低温作製と記録再生特性,』
   日本応用磁気学会誌　第 22 巻 4-2 号, pp.229-232, 1998.

25. N. Matsushita, K. Noma, S. Nakagawa and M. Naoe:
   "Control of Magnetocrystalline Anisotropy of Co-Zn Ferrite Sputtered Films,"
   Journal of the Magnetics Society of Japan, Vol. 22[S1], pp.117-119, 1998.

26. N. Matsushita, M. Ichinose, S. Nakagawa and M. Naoe:
   "Preparation and Characteristics of Co-Zn Ferrite Rigid Disks without Protective Layers for High Density Recording,"
   IEEE Transactions on Magnetics., vol. 34[4], pp. 1639-1641, 1998.

27. Nobuhiro Matsushita, Kenji Noma, Shigeki Nakagawa and Masahiko Naoe:
   "Plasma diagnosis and low-substrate-temperature deposition of Ba ferrite films in a damage-free sputtering apparatus with mixed gases,"
   to be published in "Vacuum" in 1999.

28. N. Matsushita, M. Ichinose, S. Nakagawa and M. Naoe:
   "Co-Zn Ferrite Films Prepared by Facing Targets Sputtering System for Longitudinal Recording Layer,"
   to be published in Journal of Magnetism and Magnetic Materials in 1999.

29. N. Matsushita, J. Feng, T. Siosawa, S. Nakagawa and M. Naoe:
   "Relationship between Coercivity and Deposition Conditions of Ba Ferrite Films Prepared by Facing Targets Sputtering Apparatus,"
   to be published in Journal of Magnetism and Magnetic Materials in 1999.

Co-

1.

2.

3.

4.

5.

6.

7.

8.

<u>Co-author</u> (28)

1. M. Naoe, S. Nakagawa T. Takeuchi and N. Matsushita:
   "Preparation of $BaFe_{12}O_{19}/YBa_2Cu_3O_{y-7}$ Doublelayered Films by Using Facing Targets Sputtering System,"
   Proc. $1^{st}$ Korea-Japan Joint Symposium on Dry Process Technology on New Materials, PP.147-152, 1990.

2. Masahiko Naoe, Nobuhiro Matsushita and Shigeki Nakagawa:
   "Successive Growth of Ba-ferrite Magnetic Layers on c-axis Oriented YBaCuO Superconductive Layers,"
   Journal of Applied Physics, vol.70[10], pp.6489-6491, 1991.

3. S. Akiyama, N. Matsushita, S. Nakagawa and M. Naoe:
   "2-Step Deposition at Low and High Ar Pressure for Curl-Free Co-Cr Magnetic Tape,"
   Journal of The Magnetic Society of Japan, vol.15[S2], pp.933-938, 1991.

4. S. Akiyama, N. Matsushita, S. Nakagawa and M. Naoe :
   "Very Thin Protective Film of Fe-Mo-B Based Hard Alloy for Curl-Free Magnetic Tape,"
   Materials Research Society Symposium Proceedings, vol.239, pp.641-646, 1992

5. Shigeki Nakagawa, Nobuhiro Matsushita and Masahiko Naoe:
   "Preparation of $BaFe_{12}O_{19}/YBa_2Cu_3O_x$ Bilayered Films with Well c-Axis Orientation on Amorphous Substrate,"
   Proc. of 6th International Conference on Ferrites (ICF 6), pp. 448-451, 1992.

6. Shigeki Nakagawa, Nobuhiro Matsushita and Masahiko Naoe:
   "Preparation of High $T_c$ Phase $Bi_2Sr_2Ca_2Cu_3O_x$ Films with Excellent C-Axis Orientation by Facing Targets Sputtering,"
   Proc. of 6th International Conference on Ferrites (ICF 6), pp. 612-615, 1992.

7. Masahiko Naoe and Nobuhiro Matsushita:
   "Hard Magnetism of Ultra-Fine Particles of BaM Ferrite Prepared by Arc-Discharge Evaporation at Low Gas Pressure,"
   Proc. of 6th International Conference on Ferrites (ICF 6), pp. 976-979, 1992.

8. K. Noma, N. Matsushita and M. Naoe:
   "Effects of Substrate Temperature and Input Power on Structure and Properties on Co-Zn

Ferrite Sputtered Films,"
Trans. of the Materials Research Society of Japan, vol. 15B, pp. 803-806, 1994.

9.  Masahiko Naoe, Shigeki Nakagawa and Nobuhiro Matsushita:
    "The Magnetic Multilayers Deposited by Facing Targets Sputtering for High Density Recording Media,"
    Trans. of the Materials Research Society of Japan, vol. 15B, pp. 1135-1140, 1994.

10. Masahiko Naoe, Nobuhiro Matsushita and Shigeki Nakagawa:
    "Physics and Technology of Sputtering for Depositing Magnetic Films"
    Journal of Magnetism and Magnetic Materials, 134, pp.395-402, 1994

11. Shigeki Nakagawa, Takayuki Ichihara, Nobuhiro Matsushita and Masahiko Naoe:
    "Dual Track Complimentary Type of Thin Film Recording Heads for Perpendicular Magnetic Recording,"
    Journal of The Magnetics Society of Japan, vol. 18[S1], pp. 213-216, 1994.

12. K. Noma, N. Matsushita, S. Nakagawa and M. Naoe:
    "Preparation and Recording Characteristics of Rigid Disks Using Co-Zn Ferrite Sputtered Films for High Density Magnetic Recording with Perpendicular Anisotropy,"
    Journal of The Magnetics Society of Japan, vol. 18[S1], pp. 447-450, 1994.

13. Masahiko Naoe and Nobuhiro Matsushita:
    "Deposition of $CoFe_2O_4$ Single Layer and $CoFe_2O_4/\alpha$-$Fe_2O_3$ Multilayer with Large $4\pi M_s$ and High $H_c$ using Vacuum Arc Evaporation,"
    Journal of Magnetism and Magnetic Materials, 155, pp.216-218, 1996

14. 野間賢二，松下伸広，中川茂樹，直江正彦:
    『Xe をスパッタガスとした大飽和磁化 Ba フェライト膜の作製』
    日本応用磁気学会誌, 第 20 巻 2 号, pp. 325-328, 1996.

15. 野間賢二，松下伸広，中川茂樹，直江正彦:
    『プラズマフリー・スパッタ法で作製した Co-Zn フェライト膜の結晶性と磁気特性』
    粉体および粉末冶金, 第 43 巻 1 号, pp. 46-51, 1996.

16. Takayuki Ichihara, Shigeki Nakagawa, Nobuhiro Matsushita and Masahiko Naoe :
    "Theory, Fabrication and Testing of Dual Track Complimentary Type of Thin Film

17.

18.

19.

20.

21.

22.

23

Recording Heads for Perpendicular Magnetic Recording System,"
Journal of Applied Physics, vol. 79[8], pp. 5910-5912, 1996.

17. K. Noma, N. Matsushita, S. Nakagawa and M. Naoe:
"Ba Ferrite Films with Large Saturation Magnetization and High Coercivity Prepared by Low Temperature Sputter Deposition,"
Journal of Applied Physics, vol. 79[8], pp. 5970-5972, 1996.

18. K. Noma, N. Matsushita, S. Nakagawa and M. Naoe:
"Dependence of Perpendicular Coercivity on Residual Stress of Ba Ferrite/ZnO Bilayered Films Deposited on Fused Quartz Substrate,"
IEEE Transactions on Magnetics, vol. 32[5], pp. 3822-3824, 1996.

19. K. Noma, N. Matsushita, S. Nakagawa and M. Naoe:
"Increase of Saturation Magnetization of Ba Ferrite Films Deposited by Adding Xe into Sputtering Gas Mixture,"
Proc. of 7th International Conference on Ferrites (ICF 7), pp. 487-488, 1997.

20. M. Naoe, N. Matsushita, K. Noma and S. Nakagawa:
"Sputter Deposition of Ferrite Films and Application for High Density Rigid Disk Media in Contact Mode,"
Proc. of 7th International Conference on Ferrites (ICF 7), pp. 735-738, 1997.

21. M. Naoe, K. Noma, N. Matsushita and S. Nakagawa:
"Crystallographic and Magnetic Characteristics of Ba Ferrite Sputtered Films for High Density Magnetic Recording Disks,"
Proc. of 7th International Conference on Ferrites (ICF 7), pp. 749-750, 1997.

22. K. Noma, N. Matsushita, S. Nakagawa and M. Naoe:
"Effects of composition control on crystallographic and magnetic characteristics of Ba ferrite films sputtered with the mixture of Xe, Kr, Ar and $O_2$ for recording media,"
Journal of Applied Physics, vol.81[8], pp.4377-4379, 1997.

23. K. Noma, N. Matsushita, S. Nakagawa and M. Naoe:
"Study on S- and R-block construction with additional spinel blocks in sputter-deposited Ba ferrite films,"
IEEE Transactions on Magnetics, vol. 33[5], pp. 3637-3639, 1997.

24. T. Siosawa, M. Ichinose, N. Matsushita, S. Nakagawa and M. Naoe:
"Crystallographic and Magnetic Characteristics of c-Axis Oriented Ba Ferrite Layer Deposited on Pt(111) Underlayer,"
Journal of the Magnetics Society of Japan, Vol. 21[S2], pp.73-76, 1997.

25. K. Noma, N. Matsushita, S. Nakagawa and M. Naoe:
"Control of Microcrystalline Structure of Ba Ferrite Films with Perpendicular Magnetic Anisotropy Deposited Using Plasma-free Sputtering System,"
Journal of the Magnetics Society of Japan, Vol. 22[S1], pp.120-122, 1998.

26. T. Siosawa, N. Matsushita, S. Nakagawa and M. Naoe:
"Preparation of Ba Ferrite Film with Well c-Axis Orientation using Pt Underlayer,"
Journal of the Magnetics Society of Japan, Vol. 22[S1], pp.123-125, 1998.

27. T. Namikawa, J. Feng, K. Kaneta, N. Matsushita, S. Nakagawa and M. Naoe:
"Crystal Structures and Magnetic Characteristics of $(La,Sr)MnO_3$ Films Deposited by Kr Sputtering,"
Journal of the Magnetics Society of Japan, Vol. 22[S1], pp.203-205, 1998.

28. J. Feng, N. Matsushita, T. Murakoso, S. Nakagawa and M. Naoe:
"Effect of Al Substitution for Fe in Ba Ferrite Thin Films,"
to be published in Journal of Magnetism and Magnetic Materials in 1998.

[Presentations]    61

<u>International Conferences and Symposiums</u>   (47)

(1990)
1.  M. Naoe, S. Nakagawa, T. Takeuchi and N. Matsushita:
    "Preparation of $BaFe_{12}O_{19}/YBa_2Cu_3O_{y-7}$ Doublelayered Films by Using Facing Targets Sputtering System,"
    The 1st Korea-Japan Joint Symposium on Dry Process Technology on New Materials, Oct. 21, 1990 (Seoul/Korea).

(1991)
2.  N. Matsushita, N. Ono and M. Naoe:
    "Ferromagnetic Stainless Steel Films by Facing Targets Sputtering,"
    Korean Magnetics Society 1991 Spring Conference, B-16, May 17, 1991 (Seoul/Korea).

3.  S. Akiyama, N. Matsushita, S. Nakagawa and M. Naoe:
    "2-Step Deposition at Low and High Ar Pressure for Curl-Free Co-Cr Magnetic Tape,"
    The Second Perpendicular Magnetic Recording Conference'91, 11p-10, Oct. 11, 1991 (Hachimantai Akita/Japan).

4.  S. Akiyama, N. Matsushita, S. Nakagawa and M. Naoe:
    "Very Thin Protective Film of Fe-Mo-B Based Hard Alloy for Curl-Free Magnetic Tape,"
    Materials Research Society Conference, Spring Meeting, Apr., 1991 (Anaheim/California)

(1992)
5.  Nobuhiro Matsushita and Masahiko Naoe:
    "Preparation of BaM Ferrite Films Composed of Ultra-Fine Particles by Using Arc Discharge Evaporation,"
    International Symposium on Barium Ferrite and High Density Recording, Sep. 8, 1992 (Kalamata/Greece)

6.  Shigeki Nakagawa, Nobuhiro Matsushita and Masahiko Naoe:
    "Preparation and Magnetism of Multilayers Composed of Ba and Mn-Zn Ferrite Layers,"
    International Symposium on Barium Ferrite and High Density Recording, Sep. 8, 1992 (Kalamata/Greece)

7. N. Matsushita, K. Noma, S. Nakagawa and M. Naoe:
   "Magneto-optical Properties of Cobalt Ferrite Thin Films Prepared by Facing Targets Sputtering,"
   The 6th International Conference on Ferrites (ICF 6), 29PpIII-15, Sep. 29, 1992 (Tokyo/JAPAN).

8. N. Matsushita, K. Noma, S. Nakagawa and M. Naoe:
   "Magnetic and Crystallographic Characteristics of $CoFe_2O_4$ Thin Film on ZnO underlayer,"
   The 6th International Conference on Ferrites (ICF 6), 05B1-4, Oct. 5, 1992 (Kyoto/JAPAN).

9. N. Matsushita, K. Noma, S. Nakagawa and M. Naoe:
   "Preparation of Co-Zn Ferrite Thin Films for Rigid Disks with High Recording Density,"
   The 6th International Conference on Ferrites (ICF 6), 07P2-4, Oct. 7, 1992 (Kyoto/JAPAN).

10. M. Naoe, K. Noma, S. Nakagawa and N. Matsushita:
    "The Control of Magnetic Characteristics of BaM Ferrite Thin Films by Bias Sputtering,"
    37th Annual Conference on Magnetism and Magnetic Materials (MMM '92), FZ-16, Dec. 3, 1992 (Houston/Texas).

(1993)
11. Nobuhiro Matsushita and Masahiko Naoe:
    "High Coercivity of BaM Ferrite Films Deposited by Arc Discharge Evaporation,"
    The 1993 IEEE International Magnetics Conference (INTERMAG '93), CP-08, Apr. 14, 1993 (Stockholm/Sweden).

12. K. Noma, N. Matsushita and M. Naoe:
    "Effects of Substrate Temperature and Input Power on Structure and Properties on Co-Zn Ferrite Sputtered Films,"
    The 3rd MRS International Conference on Advanced Materials/Symposium V, VFp 1.11, Sep. 2, 1993 (Tokyo/JAPAN).

13. Masahiko Naoe, Shigeki Nakagawa and Nobuhiro Matsushita:
    "The Magnetic Multilayers Deposited by Facing Targets Sputtering for High Density Recording Media,"

The 3rd MRS International Conference on Advanced Materials/Symposium V, VFp 1.11, Sep. 2, 1993 (Tokyo/JAPAN).

14. N. Matsushita, K. Noma, S. Nakagawa and M. Naoe:
"Crystallographic and Magnetic Characteristics of Co-Zn Ferrite Films Deposited at Low Substrate Temperature by Using Facing Targets Sputtering Method,"
The 1st International Conference on Processing Materials for Properties, Nov. 1993 (Hawaii).

15. N. Matsushita, K. Noma, S. Nakagawa and M. Naoe:
"Preparation of Co-Zn Ferrite Films Deposited at Low Substrate Temperature by Plasma-free DC Sputtering for Magnetic Recording Media,"
38th Annual Conference on Magnetism and Magnetic Materials (MMM '93), CB-06, Nov. 16, 1993 (Minneapolis/Minnesota).

16. N. Matsushita, K. Noma, S. Nakagawa and M. Naoe:
"Preparation and Magnetic Characteristics of BaM with excellent crystallinity by Xe Sputtering,"
38th Annual Conference on Magnetism and Magnetic Materials (MMM '93), HQ-14, Nov. 18, 1993 (Minneapolis/Minnesota).

(1994)
17. N. Matsushita, K. Noma, S. Nakagawa and M. Naoe:
"Ba Ferrite Thin Films with Large Saturation Magnetization Deposited by Sputtering in Mixture of Xe, Ar and $O_2$,"
The 6th Joint MMM-Intermag Conference, GP-16, Jun. 23, 1994 (Albuquerque/ New Mexico).

18. Masahiko Naoe and Nobuhiro Matsushita:
"Magnetic Characteristics of $CoFe_2O_4/\alpha\text{-}Fe_2O_3$ Multilayer Films Deposited by Vacuum Arc Evaporation,"
The 6th Joint MMM-INTERMAG Conference, GP-17, Jun. 23, 1994 (Albuquerque/ New Mexico).

19. N. Matsushita, K. Noma, S. Nakagawa and M. Naoe:
"Control of crystallographic and magnetic characteristics in Co-Zn ferrite sputtered films,"
International Conference on Magnetism 94, DP-219, Aug. 25, 1994 ().

20. Shigeki Nakagawa, Takayuki Ichihara, Nobuhiro Matsushita and Masahiko Naoe:
"Dual Track Complimentary Type of Thin Film Recording Heads for Perpendicular Magnetic Recording,"
The 3rd Perpendicular Magnetic Recording Conference '94 (PMRC '94), 12aB-10, Oct. 12, 1994 (Tokyo/JAPAN).

21. K. Noma, N. Matsushita, S. Nakagawa and M. Naoe:
"Preparation and Recording Characteristics of Rigid Disks Using Co-Zn Ferrite Sputtered Films for High Density Magnetic Recording with Perpendicular Anisotropy,"
The 3rd Perpendicular Magnetic Recording Conference '94 (PMRC '94), 13pA-6, Oct. 13, 1994 (Tokyo/JAPAN).

22. N. Matsushita, K. Noma, S. Nakagawa and M. Naoe:
"Structure and Magnetic Properties of a Hexagonal Type Ferrite Thin Films Prepared by Facing Targets Sputtering,"
The First Magneto-Electronics International Symposium, 9Aa I-3, Nov. 9, 1994 (Nagano/JAPAN).

23. N. Matsushita, K. Noma, S. Nakagawa and M. Naoe:
"New Processes of Synthesizing Co Ferrite Films at Low Substrate Temperature by Facing Targets Sputtering,"
IUMRS International Conference in Asia (IUMRS-ICA-'94), Dec. 1994 (Hshinchu/Taiwan).

(1995)
24. K. Noma, N. Matsushita, S. Nakagawa and M. Naoe:
"Microstructure and Magnetic Properties of Non-Stoichiometric Hexagonal Ba Ferrite Films Deposited by Using Mixture of Xe and Ar as Sputtering Gas,"
The 1995 IEEE International Magnetics Conference (INTERMAG '95), BP-04, Apr. 18, 1995 (San Antonio/Texas).

25. N. Matsushita, K. Noma, S. Nakagawa and M. Naoe:
"Co-Zn Ferrite Rigid Disks Prepared by Plasma-free Sputtering at Low Substrate Temperature,"
The 1995 IEEE International Magnetics Conference (INTERMAG '95), CQ-10, Apr. 19, 1995 (San Antonio/Texas).

26. Masahiko Naoe and Nobuhiro Matsushita:
    "Deposition of $CoFe_2O_4$ Single Layer and $CoFe_2O_4/\gamma$-$Fe_2O_3$ Multilayer with Large $4\pi M_s$ and High $H_c$ using Vacuum Arc Evaporation,"
    $6^{th}$ International Conference on Magnetic Recording Media,
    MR-0081, 1995 (Oxford, England)

27. N. Matsushita, K. Noma, S. Nakagawa and M. Naoe:
    "Highly Crystallized (La, Sr)$MnO_3$ Films Deposited by Facing Targets Sputtering Apparatus,"
    40th Annual Conference on Magnetism and Magnetic Materials (MMM '95),
    CT-01, Nov. 8, 1995 (Philadelphia/Pennsylvania).

28. T. Ichihara, S. Nakagawa, N. Matsushita and M. Naoe:
    "Fabrication of Dual Track Complimentary Type of Thin Film Recording heads for Perpendicular Magnetic Recording,"
    40th Annual Conference on Magnetism and Magnetic Materials (MMM '95), FD-13, Nov. 8, 1995 (Philadelphia/Pennsylvania).

29. K. Noma, N. Matsushita, S. Nakagawa and M. Naoe:
    "Ba Ferrite Films with Large Saturation Magnetization and High Coercivity Prepared by Low Temperature Sputter Deposition,"
    40th Annual Conference on Magnetism and Magnetic Materials (MMM '95), FF-12, Nov. 9, 1995 (Philadelphia/Pennsylvania).

(1996)
30. N. Matsushita, K. Noma, A. Morisako, S. Nakagawa and M. Naoe:
    "Read/Write Characteristics of Co-Zn Ferrite Rigid Disks in Contact Mode Recording,"
    The 1996 IEEE International Magnetics Conference (INTERMAG '96), AB-09, Apr. 9, 1996 (Seattle/Washington).

31. K. Noma, N. Matsushita, S. Nakagawa and M. Naoe:
    "Dependence of Perpendicular Coercivity on Residual Stress of Ba Ferrite/ZnO Bilayered Films Deposited on Fused Quartz Substrate,"
    The 1996 IEEE International Magnetics Conference (INTERMAG '96), GB-10, Apr. 12, 1996 (Seattle/Washington).

32. M. Naoe, N. Matsushita, K. Noma and S. Nakagawa:
    "Sputter Deposition of Ferrite Films and Application for High Density Rigid Disk Media

in Contact Mode,"

The 7th International Conference on Ferrites (ICF 7), 4-1 B 1, Sep. 4, 1996 (Bordeux/France).

33. M. Naoe, K. Noma, N. Matsushita and S. Nakagawa:

"Crystallographic and Magnetic Characteristics of Ba Ferrite Sputtered Films for High Density Magnetic Recording Disks,"

The 7th International Conference on Ferrites (ICF 7), 4-4 B 2, Sep. 4, 1996 (Bordeux/France).

34. N. Matsushita, K. Noma, S. Nakagawa and M. Naoe:

"Ferromagnetic Characteristics of a Perovskite Type of (La, Sr)$MnO_3$ Films Deposited by Kr Sputtering,"

The 7th International Conference on Ferrites (ICF 7), 5-1 A 3, Sep. 5, 1996 (Bordeux/France).

35. K. Noma, N. Matsushita, S. Nakagawa and M. Naoe:

"Increase of Saturation Magnetization of Ba Ferrite Films Deposited by Adding Xe into Sputtering Gas Mixture,"

The 7th International Conference on Ferrites (ICF 7), 6-2 A 5, Sep. 6, 1996 (Bordeux/France).

36. N. Matsushita, K. Noma, S. Nakagawa and M. Naoe:

"Plasma diagnosis of Facing Targets Sputtering system for deposition of Ba ferrite films in Ar, Xe and $O_2$ gas mixture,"

The 2nd Korea-Japan Symposium on Plasma and Thin Film Technology, 2P 27, Oct. 12, 1996 (Seoul/Korea).

37. K. Noma, N. Matsushita, S. Nakagawa and M. Naoe:

"Effects of composition control on crystallographic and magnetic characteristics of Ba ferrite films sputtered with the mixture of Xe, Kr, Ar and $O_2$ for recording media,"

41st Annual Conference on Magnetism and Magnetic Materials (MMM '96), CC-06, Nov. 13, 1996 (Atlanta/Georgia).

38. K. Noma, N. Matsushita, S. Nakagawa and M. Naoe:

"Mössbauer study of Ba ferrite sputtered films with large saturation magnetization and perpendicular anisotropy constant,"

41st Annual Conference on Magnetism and Magnetic Materials (MMM '96), FP-28,

Nov. 14, 1996 (Atlanta/Georgia).

(1997)

39. K. Noma, N. Matsushita, S. Nakagawa and M. Naoe:
"Study on S- and R-block construction with additional spinel blocks in sputter-deposited Ba ferrite films,"
The 1997 IEEE International Magnetics Conference (INTERMAG'97), FB-07, Apr. 3, 1997 (New Orleans/Louisiana).

40. N. Matsushita, K. Noma, S. Nakagawa and M. Naoe:
"Diagnosis of Mixture Gas Discharge in Damage-Free Sputtering Apparatus and Deposition of Ba Ferrite Films at Low Substrate Temperature,"
4th International Symposium on Sputtering and Plasma Processing (ISSP'97), SP1-3, June 4, 1997 (Kanazawa/Japan).

41. N. Matsushita, K. Noma, S. Nakagawa and M. Naoe:
"CONTROL OF MAGNETOCRYSTALLINE ANISOTROPY OF Co-Zn FERRITE SPUTTERED FILMS,"
International Symposium on Ferrites in Asia '97, Symposium J of IUMRS-ICA-97, J3.8, Sept.16, 1997 (Makuhari/Japan).

42. K. Noma, N. Matsushita, S. Nakagawa and M. Naoe:
"CONTROL OF MICROCRYSTAL STRUCTURE AND PERPENDICULAR MAGNETIC ANISOTROPY OF Ba FERRITE FILMS DEPOSITED USING PLASMA-FREE SPUTTERING SYSTEM,"
International Symposium on Ferrites in Asia '97, Symposium J of IUMRS-ICA-97, J4.8, Sept.16, 1997 (Makuhari/Japan).

43. T. Siosawa, N. Matsushita, S. Nakagawa and M. Naoe:
"PREPARATION OF Ba FERRITE FILM WITH WELL c-AXIS ORIENTATION USING Pt UNDERLAYER,"
International Symposium on Ferrites in Asia '97, Symposium J of IUMRS-ICA-97, J4.9, Sept.16, 1997 (Makuhari/Japan).

44. T. Namikawa, J. Feng, K. Kaneta, N. Matsushita, S. Nakagawa and M. Naoe:
"CRYSTAL STRUCTURE AND MAGNETIC CHARACTERISTICS OF $(La, Sr)MnO_3$ FILMS DEPOSITED BY Kr SPUTTERING,"
International Symposium on Ferrites in Asia '97, Symposium J of IUMRS-ICA-97,

J10.25, Sept.18, 1997 (Makuhari/Japan).

45. T. Siosawa, N. Matsushita, S. Nakagawa and M. Naoe:
"Crystallographic and Magnetic Characteristics of c-axis Oriented Ba Ferrite Layer Deposited on Pt(111) Underlayer,"
The 4th Perpendicular Magnetic Recording Conference '97 (PMRC '97), 20pB-6, Oct. 20, 1997 (Akita/JAPAN).

(1998)
46. N. Matsushita, M. Ichinose, S. Nakagawa and M. Naoe:
"Preparation and Characteristics of Co-Zn Ferrite Rigid Disks without Protective Layers for High Density Recording,"
The 7th Joint MMM-Intermag Conference, GT-05, Jan. 9, 1998 (San Francisco/California)

47. N. Matsushita, T. Siosawa, K. Watanabe, M. Ichinose, S. Nakagawa and M. Naoe:
"Improvement of Read/Write Characteristics by Excellent c-Axis Orientation in Ba Ferrite Disks,"
The 7th Joint MMM-Intermag Conference, GT-06, Jan. 9, 1998 (San Francisco/California)

Domestic Conferences and Symposiums   (14)

1. 松下伸広，中川茂樹，直江正彦 :
『対向ターゲット式スパッタ法による Bi 系酸化物超伝導薄膜の作製』
表面技術協会第 83 回講演大会, 1991 年 3 月 26 日 (埼玉).

2. 松下伸広，野間賢二，中川茂樹，直江正彦:
『低基板温度で作製した Co フェライト膜のハードディスク応用』
第 16 回 日本応用磁気学会学術講演会, 9aF-4, 1992 年 11 月 9 日 (名古屋).

3. 松下伸広，野間賢二， 中川茂樹，直江正彦:
『Xe を用いたスパッタリングによる大飽和磁化 Ba フェライト薄膜の作製と磁気特性』
粉体粉末冶金協会平成七年度春季大会, 3-18, 1995 年 6 月 28 日 (東京).

4. 野間賢二，松下伸広，中川茂樹，直江正彦:

『プラズマフリー・スパッタ法で作製したCo-Znフェライト膜の結晶性と磁気特性』
粉体粉末冶金協会平成七年度春季大会, 3-29, 1995 年 6 月 28 日 (東京).

5. 野間賢二, 松下伸広, 中川茂樹, 直江正彦:
『Xe をスパッタガスとした大飽和磁化 Ba フェライト膜の作製』
第 19 回日本応用磁気学会学術講演会, 25aG-2, 1995 年 9 月 25 日 (東京).

6. 松下伸広, 野間賢二, 中川茂樹, 直江正彦:
『低温基板上での(La, Sr)MnO$_3$薄膜の作製』
第 19 回日本応用磁気学会学術講演会, 25aG-11, 1995 年 9 月 25 日 (東京).

7. 松下伸広, 野間賢二, 中川茂樹, 直江正彦:
『混合ガススパッタによる垂直記録媒体用 Ba フェライト膜の低温形成』
第 4 回垂直磁気記録シンポジウム (PMRS'95), 1995 年 10 月 25 日 (福島県裏磐梯).

8. 野間賢二, 松下伸広, 中川茂樹, 直江正彦:
『(La, Sr)MnO$_3$膜の低温形成と磁気特性』
第 4 回垂直磁気記録シンポジウム (PMRS'95), 1995 年 10 月 25 日 (福島県裏磐梯).

9. 松下伸広, 野間賢二, 中川茂樹, 直江正彦:
『酸化物磁性薄膜による等方性磁気ディスクの作製と記録再生特性』
第 5 回垂直磁気記録シンポジウム (PMRS '96), 23p-3, 1996 年 10 月 23 日 (横浜).

10. 松下伸広, 直江正彦:
『混合希ガススパッタ法によるフェライト薄膜の低温形成と磁気特性』
表面技術協会第 95 回講演大会, PC-7, 1997 年 3 月 24 日 (東京).

11. 松下伸広, 一瀬 誠, 中川茂樹, 直江正彦:
『スパッタ法によるフェライト薄膜の低温形成と高密度磁気ディスクへの応用』
表面技術協会第 96 回講演大会, 23B-20, 1997 年 9 月 22 日 (東京).

12. 松下伸広, 野間賢二, 渡部 康, 一瀬 誠, 中川茂樹, 直江正彦:
『Ba フェライト磁気ディスクの低温作製と記録再生特性』
第 21 回日本応用磁気学会学術講演会, 4pB-4, 1997 年 10 月 4 日 (名古屋).

13. 松下伸広, 馮 潔, 塩澤友祥, 渡部 康, 中川茂樹, 直江正彦 :
『Pt 下地層上における Ba フェライト結晶子の成長と磁気特性』

表面技術協会第 97 回講演大会, 17C-10, 1998 年 3 月 17 日 (東京).

14. 松下伸広 :
『超高密度磁気記録媒体用高保磁力フェライト膜のスパッタ技術』
電気化学会講演大会, 特 1I-08, 1998 年 4 月 4 日 (東京).

[Res

1.

2.

3.

4.

5.

6.

7.

8.

[Research Meetings]　　8

1.　N. Matsushita, K. Noma, S. Nakagawa and M. Naoe:
　　"The Control of Coercivity of Co Ferrite Films for Rigid Disk Media,"
　　電子情報通信学会磁気記録研究会（第3回　日韓磁気記録シンポジウム），
　　信学技報　MR92-23, Jul.17, 1992.

2.　松下伸広，野間賢二，直江正彦:
　　『Xe を用いたスパッタにより作製した Ba フェライト薄膜の特性』
　　日本学術振興会 144 委員会資料　103-5, Jul.29, 1993.

3.　松下伸広，野間賢二，中川茂樹，直江正彦:
　　『対向ターゲット式スパッタ法による Co-Zn スピネルフェライト薄膜の低温
　　形成と磁気特性』
　　電子情報通信学会磁気記録研究会，信学技報　MR93-19, Sep.17, 1993.

4.　直江正彦，野間賢二，松下伸広:
　　『Xe, Ar, $O_2$ 混合ガスを用いた Ba フェライトスパッタ膜の構造と磁気特性』
　　日本学術振興会 144 委員会資料　105-2, Jan.27, 1994.

5.　松下伸広，野間賢二，中川茂樹，直江正彦:
　　『Co-Zn フェライト薄膜の磁気特性と記録再生特性』
　　電子情報通信学会磁気記録研究会，信学技報　MR93-73, Mar.16, 1994.

6.　野間賢二，松下伸広，中川茂樹，直江正彦:
　　『高保磁力フェライト膜の作製とリジッドディスク媒体への応用』
　　電子情報通信学会磁気記録研究会，信学技報　MR94-24, Sep.22, 1994.

7.　野間賢二，松下伸広，中川茂樹，直江正彦:
　　『非化学量論組成の Ba フェライト・スパッタ膜の結晶構造と磁気特性』
　　電子情報通信学会磁気記録研究会，信学技報　MR95-2, May16, 1995.

8.　Satoshi TANAKA, Nobuhiro Matsushita, Shigeki Nakagawa and Masahiko Naoe:
　　"Improvement of Soft Magnetism of a-Co-Zr-Ta Sputtered Films for Backlayers in
　　Perpendicular Magnetic Recording Media,"
　　電子情報通信学会磁気記録研究会（第5回　日韓磁気記録シンポジウム），
　　信学技報　MR95-45, Nov.23, 1995.